Photocatalytic system of MXene based advanced functional materials for pharmaceutical waste decontamination under visible light irradiation

Thesis Submitted for the Award of the Degree of

DOCTOR OF PHILOSOPHY

in

Chemistry

By

Upasana

Registration Number: 12108400

Supervised By

Prof. Ajit Kumar Sharma

Department of Chemistry

Lovely Professional University

LOVELY PROFESSIONAL UNIVERSITY
PUNJAB, 2026

DECLARATION

I, hereby declared that the presented work in the thesis entitled "Photocatalytic system of MXene based advanced functional materials for pharmaceutical waste decontamination under visible light irradiation" in fulfillment of degree of **Doctor of Philosophy (PhD)** is outcome of research work carried out by me under the supervision of **Dr. Ajit Kumar Sharma**, working as Professor, Department of Chemistry, School of Chemical Engineering and Physical Sciences of Lovely Professional University, Punjab, India. In keeping with general practice of reporting scientific observations, due acknowledgments have been made whenever work described here has been based on findings of other investigator. This work has not been submitted in part or full to any other University or Institute for the award of any degree.

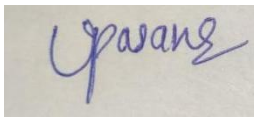

Name of the scholar: Upasana
Registration No.: 12108400
Department of Chemistry, School of Chemical Engineering and Physical Sciences of Lovely Professional University
Punjab, India

CERTIFICATE

This is to certify that the work reported in the Ph.D. thesis entitled "Photocatalytic system of MXene based advanced functional materials for pharmaceutical waste decontamination under visible light irradiation" submitted in fulfillment of the requirement for the award of degree of **Doctor of Philosophy (PhD)** in the Chemistry, School of Chemical Engineering and Physical Sciences of Lovely Professional University, Punjab, India, is a research work carried out by **Upasana**, **12108400**, is bonafide record of her original work carried out under my supervision and that no part of thesis has been submitted for any other degree, diploma or equivalent course.

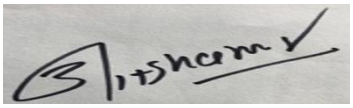

(Signature of Supervisor)
Dr. Ajit Kumar Sharma
Professor
Department of Chemistry
Lovely Professional University

Abstract

Human health and ecological balance are seriously threatened by the ongoing discharge of persistent and bioactive pollutants into aquatic habitats as a result of the growing use of pharmaceutical medications. The development of sophisticated and sustainable treatment methods is required since conventional wastewater treatment technologies frequently fail to totally eliminate such pharmaceutical residues. A promising green technology for the breakdown of resistant pharmaceutical contaminants under visible light irradiation is photocatalysis. In this study, a photocatalytic system based on two-dimensional MXene and its composite materials was created to effectively degrade pharmaceutical pharmaceuticals under visible light, including cetirizine and ciprofloxacin. Both conventional and microwave-assisted procedures were used to produce MXene ($Ti_3C_2T_x$), with the latter providing a quick, energy-efficient, and environmentally safe process. With its layered structure, high conductivity, and numerous surface terminations, the resultant MXene offered ideal locations for photocatalytic processes. Using microwave approach, composites were created by adding lanthanum and vanadium species in various molar ratios (1:1, 1:2, and 2:1) to further improve their performance.

The structural, morphological, optical, and surface characteristics of the synthesized materials were examined using a variety of characterization techniques, such as X-ray diffraction (XRD), Fourier transform infrared spectroscopy (FTIR), scanning electron microscopy (SEM), energy dispersive X-ray spectroscopy (EDX), zeta potential measurements, UV–Visible spectroscopy (UV–Vis), Electrochemical impedance spectroscopy (EIS) and photoluminescence (PL) spectroscopy. While FTIR and EDX showed the existence of surface functional groups and the successful integration of metal dopants, XRD revealed the creation of the MXene phase with distinctive (002) peaks. SEM pictures showed sheet-like and layered morphologies with better dispersion after composite synthesis.

Ciprofloxacin and cetirizine were used as model pharmaceutical pollutants in photocatalytic degradation tests conducted in visible light. Initial concentration, pH, catalyst dosage, and irradiation duration were among the parameters that were tuned.

For ciprofloxacin, the microwave-synthesised La-modified MXene (1:2) composite had the maximum degrading efficiency, whereas the V_2O_5–modified MXene (1:2) composite performed better for cetirizine. Improved light absorption, efficient charge separation, and the cooperative interaction between MXene layers and the metal oxide species were identified as the causes of the increased photocatalytic activity. According to studies, the band gap energy of the composites increased somewhat following metal insertion, enhancing visible light activation and reducing electron–hole recombination. Scavenger studies verified that hydroxyl (•OH) and superoxide ($•O_2^-$) radicals dominated the degradation process, and kinetic analysis showed that the degradation followed a pseudo-first-order model. The structural robustness of the produced composites was confirmed by the reusability investigations, which showed excellent photocatalyst stability with minimal activity loss after several cycles.

Overall, this study shows that MXene-based photocatalytic materials have the potential to be efficient, long-lasting, and visible light-responsive catalysts for the breakdown of pharmaceutical pollutants in wastewater. The results greatly advance photocatalytic technology for the treatment of pharmaceutical waste and offer important insights into the creation of next-generation MXene-based nanocomposites for sustainable environmental remediation.

Acknowledgement

I offer my deepest reverence to Almighty **God Balaji Junjharji,** whose divine blessings, strength, and protection have guided me throughout this research journey. Their grace has given me the resilience, clarity, and courage to overcome challenges and complete this thesis successfully. I extend my heartfelt gratitude to my father **Sh. Bhagwati Parsad Bagri,** my mother **Smt. Arti**, my sister Parul, my brother Jatin and my family whose unconditional love, patience, and constant encouragement have been the foundation of my academic progress. Their support has kept me motivated during the most demanding phases of my work. I would like to express my sincere gratitude to my companion in this journey, Mr. Ganesh pareek, for their constant encouragement, support, and positive influence throughout this academic journey.

I express my sincere appreciation to my supervisor **Prof. Ajit Kumar Sharma**, Department of chemistry, school of chemical engineering and physical sciences whose guidance, expertise, and constructive insights have shaped the direction and quality of this research. His support and mentorship have played an invaluable role in every stage of my study. These contributions have significantly contributed to the achievement of my proposed objectives. I express my heartfelt gratitude for his continuous support and astute insights during my academic journey. The quantification and articulation of the support and care I have gotten from his remains beyond my capacity. His unrelenting dedication to learning and teaching has always served as a perpetual wellspring of inspiration for me.

I am deeply grateful to **Dr. Ashok Mittal** (Founder Chancellor), **Mrs. Rashmi Mittal** (Pro-Chancellor), **Dr. Lovi Raj Gupta** (Pro vice chancellor) and **Monica Gulati** (Registrar) of Lovely Professional University for granting me access to exceptional infrastructure and the opportunity to conduct my research within the nurturing environment of this esteemed institution.

I would also like to extend my gratitude to the administrative and technical staff at Lovely Professional University. Your assistance and professionalism have made my research process smoother and more manageable. I am particularly grateful to **Mr.**

Manoj Kumar (Lab Technician) for your help in providing each and every required chemical and glassware for research, which are crucial to the successful completion of my research.

I am thankful to **Lovely Professional University (LPU)** and the **Centre for Research Degree Programme (CRDP)** for providing a conducive research environment, academic resources, and continuous support. My gratitude also extends to the faculty members, laboratory staff, and technical assistants of the department for their cooperation in synthesis, characterization, and experimental work.

I would also like to acknowledge my **all research colleagues and friends**, whose discussions, assistance, and companionship have been an integral part of this journey and have enriched my research experience.

Therefore, I express my sincere gratitude to all those who assisted or blessed me in achieving this significant milestone. I sincerely apologize for not mentioning these individuals.This thesis stands as a reflection of the collective support, blessings, and encouragement I have received.

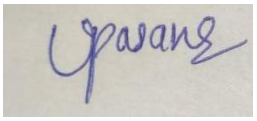

Upasana

Table of Content

4.2 Enhanced Photocatalytic Degradation of Ciprofloxacin from Pharmaceutical Wastewater Using Microwave-Synthesized Lanthanum/MXene Nanocomposites

4.2.1 Introduction

4.2.2 Materials and Methods

4.2.2.1 Chemicals Consumed

4.2.2.2 Synthesis of MXene (Ti_3C_2Tx)

4.2.2.2.1 Conventional Method

4.2.2.2.2 Microwave-Assisted method

4.2.2.3 Synthesis of Lanthanum nitrate-modified MXene (La/MX) Composites

4.2.3 Materials Characterization

4.2.4 Assessment of Photocatalytic Activity

4.2.5 Results and Discussion

4.2.5.1 Structural and Phase analysis

4.2.5.2 Surface Morphology Analysis

4.2.5.3 Elemental Analysis by EDX

4.2.5.4 FTIR Spectroscopy

4.2.5.5 Zeta Potential Measurement

4.2.5.6 Electrochemical Impedance Spectroscopy

4.2.5.7 Photoluminiscence (PL) Analysis

4.2.5.8 Optical Properties

4.2.5.9 Photocatalytic performance towards Photodegradation of Ciprofloxacin

4.2.5.10 Photocatalytic Degradation Mechanism

4.2.6 Summary

4.3 Enhanced visible light photocatalytic degradation of cetirizine in pharmaceutical liquid waste using V_2O_5-modified MXene nanocomposites prepared via microwave irradiation

4.3.1 Introduction

4.3.2 Materials and methods

4.3.3 Synthesis of MXene (Ti_3C_2Tx)

4.3.3.1 Etching method

4.3.3.2 Microwave-assisted method

4.3.3.3 Synthesis of V_2O_5 modified MXene composites

List of Figures

Fig. 23	SEM images of purchased MAX phase, La-based MAX phase and V-based MAX phase
Fig. 24	(A) Dark-phase adsorption behavior of MAX, La/MAX, and V/MAX phases towards cetirizine. (B) Photocatalytic degradation behavior of MAX, La/MAX, and V/MAX phases under visible light irradiation.
Fig. 25	Schematic illustration of the synthesis of MXene by conventional and microwave-assisted methods.
Fig. 26	Schematic diagram for the synthesis of MXene and La/MX nanocomposite by microwave method
Fig. 27	XRD analysis of (A) MAX phase, MXene (conventional) and MXene (Microwave), (B) La/MX nanocomposite synthesized by conventional method and (C) La/MX nanocomposite synthesized by microwave method
Fig. 28	SEM analyses of MAX phase(A), MXene (conventional (B), MXene (Microwave (C), La/MX nanocomposite (conventional) (D) and La/MX nanocomposite (microwave) (E)
Fig. 29	EDX analysis of MAX phase (Ti_3AlC_2) with elemental mapping of Titanium (Ti), Aluminium (Al) and Carbon (C)
Fig. 30	EDX analysis of MXene synthesized by conventional method with elemental mapping of Titanium (Ti), Oxygen (O), Carbon (C), Aluminium (Al) and Fluorine (F)
Fig. 31	EDX analysis of MXene synthesized by microwave method with elemental mapping of Titanium (Ti), Carbon (C), Oxygen (O), Fluorine (F) and Aluminium (Al)
Fig. 32	EDX analysis of La/MX nanocomposite (1:2) with elemental mapping of Titanium (Ti), Lanthanum (La), Fluorine (F), Carbon (C), Oxygen (O) and Aluminium (Al)
Fig. 33	FTIR spectra of MAX phase, MXene synthesized by conventional and microwave methods (A), La/MX composites prepared by the conventional method (B), and La/MX composites prepared by the microwave method (C).

Fig. 34	Zeta Potential of MXene (Conventional) (A), MXene (Microwave) (B) and La/MX (1:2) (C)
Fig. 35	EIS spectra of MXene (Microwave) and La/MX nanocomposite (1:2).
Fig. 36	Photoluminescence (PL) analysis of microwave-synthesized MXene (MX (MW)) and La/MX composite
Fig. 37	Tauc plots of MXene and La/MX showing absorption against energy
Fig. 38	Adsorption behavior of ciprofloxacin under dark conditions at different pH values (A–B) and effect of contact time on adsorption efficiency (C).
Fig. 39	Photocatalytic degradation of ciprofloxacin in light phase at different pH (A-C) and effect of time on degradation (D).
Fig. 40	Photocatalytic degradation of ciprofloxacin at the addition of various concentration of H_2O_2
Fig. 41	Recyclability test of synthesized La/MX nanocomposite by microwave method for photocatalytic degradation of ciprofloxacin
Fig. 42	Schematic diagram of the photocatalytic activation of La/MX nanocomposite
Fig. 43	XRD analysis of used photocatalyst La/MX (1:2) after photocatalysis
Fig. 44	FTIR spectrum of used Photocatalyst La/MX (1:2) after Photocatalysis
Fig. 45	Schematic illustration of the synthesis process for MXene and V_2O_5-modified MXene composites using the microwave-assisted method.
Fig. 46	XRD patterns of (A) Ti_3AlC_2 MAX phase, MXene synthesised via conventional (MX (Con)), and microwave-assisted method (MX (MW)) (B) XRD patterns of V_2O_5-modified MXene composites (V/MX) with varying weight ratios (1:1, 1:2, and 2:1), shows additional peaks that correspond to V_2O_5 (JCPDS card No. 41–1426).
Fig. 46C	XRD comparison of V/MX (1:2) composites prepared by conventional and microwave-assisted methods.
Fig. 47	FTIR spectra of (A) Ti_3AlC_2 MAX phase, conventionally synthesised MXene (MX (Con), and microwave-assisted MXene (MX (MW), (B) FTIR spectra of V_2O_5-modified MXene composites (V/MX) prepared via microwave synthesis with different ratios (1:1, 1:2, and 2:1).

Fig. 47C	FTIR comparison between the V/MX composites prepared using the conventional and microwave approach with ratio 1:2
Fig. 48	SEM images of (A) Ti_3AlC_2 MAX phase (B) conventionally synthesised MXene (MX (Con)) (C) microwave-assisted MXene (MX (MW)) (D) and (E) V/MX composites prepared using the conventional and microwave approach with ratio 1:2.
Fig. 49	EDX spectrum of MXene synthesised by the microwave-assisted method (MX (MW)), confirming the presence of key elements such as Titanium (Ti), Carbon (C), Flourine (F), and Oxygen (O).
Fig. 50	EDX spectrum of V_2O_5-modified MXene composite synthesised via microwave-assisted method (1:2), confirming the successful presence of Vanadium (V), Titanium (Ti), carbon (C), and oxygen (O).
Fig. 51	Zeta potential measurements of MXene synthesised by conventional and microwave (A) MX (Con), and (B) MX (MW) methods, along with the V/MX composite (C) synthesized by microwave method.
Fig. 52	EIS analysis of microwave-synthesised MXene (MX (MW)) and V_2O_5-modified MXene composite (V/MX) synthesized by microwave method.
Fig. 53	Tauc plots of MXene (MX (MW)) and V/MX (1:2) composite synthesized by microwave method used for band gap determination.
Fig. 54	Photoluminescence (PL) analysis of microwave-synthesised MXene (MX (MW)) and V_2O_5- modified MXene composite (V/MX) synthesized by microwave method.
Fig. 55	Dark-phase adsorption of cetirizine at different pH values (A–B) and effect of contact time on adsorption of cetirizine (C).
Fig. 56	Photocatalytic degradation of cetrizine at under visible light at different pH values (A-B), effect of time on degradation of cetirizine (C) and photocatalytic degradation of cetirizine in the presence of varying concentration of H_2O_2 (D).
Fig. 56E	V/MX composites synthesized by conventional method with ratio of 1:2 exhibited the high degrading efficiencies in the visible light

List of Tables

CHAPTER-1
INTRODUCTION

1. INTRODUCTION:

1.1. Background and emergence of pollution challenges

In current situation, there aren't many clean water sources, and all life on Earth depends on clean, pure water to thrive and the globe is now struggling to supply sufficient amounts of drinking water. The creation of waste in a wide variety and its unfiltered release into direct aquatic ecosystems is mostly caused by the rapid expansion of industry, which has an impact on the water's quality and aesthetic qualities. A report indicates that although water covers 71% of the earth's surface, just 2.5% of it is clean and pure [1]. A vast amount of fresh, clean water is needed, but as we all know, humans and developed industries are the main causes of the declining water quality. The world's population is steadily growing, so human activity is also growing [2]. Around the world, diseases linked to water pollution claim the lives of about 250 million people annually, and 3000 children perish from various water-related illnesses every day. About 3.5 billion people are concerned about the water problem in 2025 and are experiencing water shortages, according to a survey [3]. Variations in the chemical and physical characteristics of water that have an adverse influence on all living things are referred to as water pollution.

Water resources are primarily harmed by organic pollutants. Industrial solvents, medications, insecticides, plasticizers, phenolic compounds, and many other organic contaminants are found in water bodies [4]. Around the world, aquatic life and public health are negatively impacted by water pollution. Heavy metals, pesticides, and other harmful substances have been found in Egypt's rivers, while similar conditions have been observed in India's rivers [5]. The impacts of water pollution are so bad in China that millions of people have suffered and even died from a variety of illnesses brought on by water pollutants [6]. Only 17% of the population of the world lives in India, and as the nation moves into a new era, it also faces more and more problems in providing clean, pure water. Certain parts of India are facing water crises as a result of climate change, and even after depleting all accessible water supplies, people would still not have access to enough clean water. According to the standard restriction set by the CED water supply and sanitation sectional committee, a single person can only use 135 liters of water each day. Only 2.5 percent of the fresh water that is fit for human

consumption comes from groundwater worldwide. Since groundwater provides more than 60% of the fresh water used in agriculture and 85% of the water needed for domestic use, India needs to discover alternative sources, including rivers, which are present in approximately ninety percent of its land. Due to the nation's rapidly growing population, diminishing rivers, and a lack of technical expertise, India's water availability issue is becoming worse every day. Due to the lack of fresh water and the strain that the expanding population is placing on available water supplies, the world is currently facing a water crisis [7].

India's water supplies are either tainted with diseases and harmful materials from wastewater from industries, which comprises both inorganic as well as organic poisonous substances, or it ranks 120th worldwide in terms of the quality of water resources and quality [8]. All businesses send harmful, carcinogenic, cancer-causing, and non-sustainable substances into water bodies, but the contaminants vary greatly, and their characteristics and structures also alter as the sources of the pollutants that are produced change [9]. Everyone knows that the primary source of water contamination is industrial waste, and another important category is municipal garbage. When such polluting items are thrown directly into water sources, the environment will be left to suffer from the poisonous and destructive conditions. The emissions of chemical and pharmaceutical pollutants accounted for 20% of all pollutants [10]. Thus, one of the biggest and most serious problems of current times is water contamination, which will remain an important issue for generations into the future. There are many known pollutants in water, and some of these poisons have serious negative effects on living things, including cancer [11].

Rapid global population increase, industrialization, and agricultural development have resulted in serious environmental issues. Nowadays, there are environmental pollutants in many fields and farms all over the world, and one of the main concerns is water contamination. Since water is an essential part of every living thing. The world is 70% water, but less than 2.5% of that water is accessible as fresh water. Over time, there has been a steady rise in the need for fresh water [12]. Large volumes of wastewater are released by domestic and industrial processes, either directly or indirectly, and end up in freshwater bodies like rivers, lakes, and dams. In addition, both organic and inorganic substances contaminate the freshwater sources. Water

bodies have collected different concentrations of inorganic pollutants, including nitrates, chlorides, and heavy metals, as well as organic chemicals like pesticides and medicines [13]. The United Nations World Water Development Report from 2019 does, in fact, highlight the significance of treating contaminated water and the sources that are discharged from industrial and agricultural processes. When toxic wastes are present in water sources, the ecosystem may become toxic [14]. Aquatic life is impacted by the polluted water, which lowers their capacity for reproduction. In addition to humans, animals, as well as other living beings, are also impacted by water pollution. Several investigations and literature reviews have identified and verified that drinking water is a significant source of drug waste. The most promising strategy and environmentally friendly technology for addressing these issues is photocatalysis, which breaks down highly toxic organic and carcinogenic compounds [15]. **Fig.1**, Percentage of world water consumption and wastewater output [15].

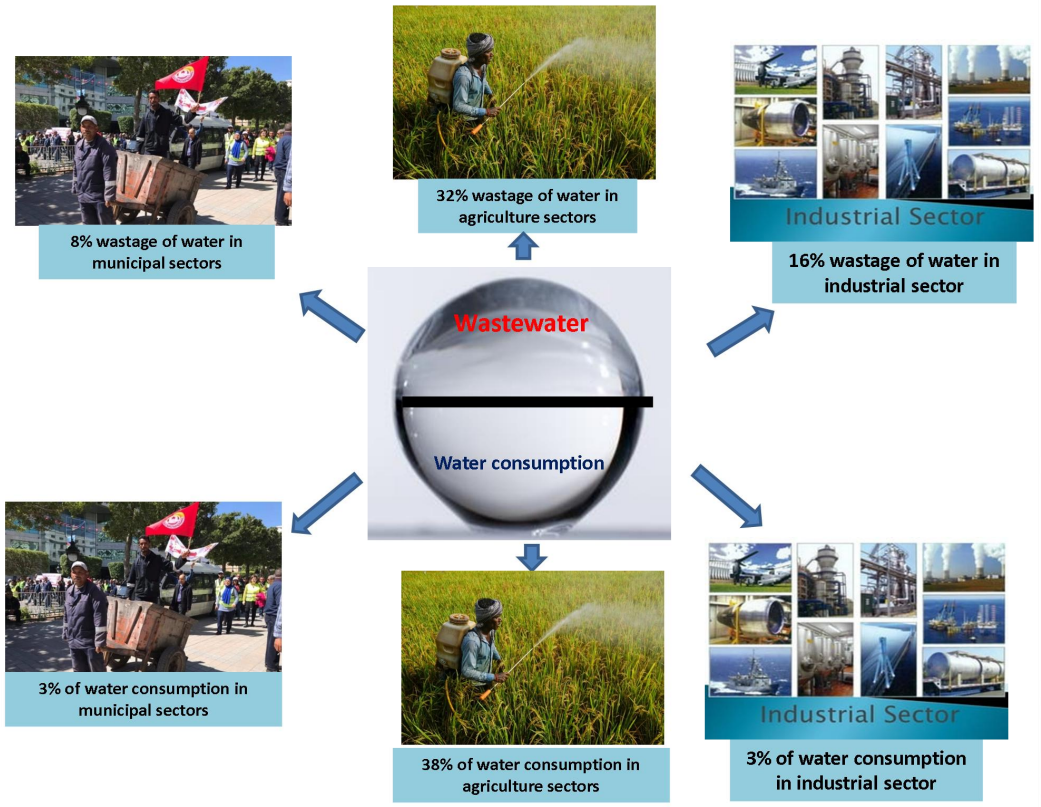

Fig. 1 Percentage of world water consumption and wastewater output.

1.1.1. Pharmaceutical drugs:

Pharmaceuticals are globally used to control the illnesses as well as to upgrade the well-being for human beings and other ecological communities. Through several pharmaceuticals, pharmaceutical drugs are extremely ingested because of their powerful effects despite of hazardous pathogens as well as microbes [16]. The advancement of medicine in recent decades has led to a sharp rise in both the manufacturing and use of pharmaceutical products. Over hundreds of tons are produced each year, with about 3,000 chemicals being employed as medications [17]. Increased research evidence of pharmaceutical products in natural aquatic systems has caused concern among those in charge of the water supply. Medicinal medications, which are supplied to living organisms through various ways (oral, skin, inhalation, injections, etc.), have been found in high concentrations in surface waters [18]. After the medicine is administered, the molecules are absorbed, dispersed, and broken down by the recipient organisms before being eliminated. Pharmaceuticals and other resistant substances primarily enter wastewater treatment facilities through excretion, unregulated drug disposal, the disposal of excess medications in homes, and veterinary uses [19]. Research conducted on these facilities' ability to remove these compounds has shown that current technologies are unable to remove enough of them [20]. This causes these substances to get into surface water, which is then utilized to make drinking water. Due to the inability of drinking water treatment facilities to eliminate these substances, extremely low levels are starting to be found in drinking water, which may eventually pose a threat to public health [21]. Pharmaceutical medications have been widely used in many fields, including farming, aquaculture, medicine, and industry, and they are very stable biologically. Pharmaceutical drugs are both synthetic and natural substances that have potent pharmacological effects. In particular, both humans and animals often and immediately dispose of prescription medications used for veterinary purposes in the environment. In addition, the production of pharmaceutical drugs continues to rise in order to prevent and cure illnesses as well as support economic expansion. Such actions allow humans and aquaculture to either directly or indirectly release pharmaceutical waste into the environment, and raise livestock [18]. Continuously releasing pharmaceutical waste into the environment without proper treatment can have a serious negative impact on

human health and ecosystems. In particular, pharmaceutical waste has grown to be a major global concern. Numerous investigations have shown that pharmaceutical waste can be discovered in groundwater and surface water at concentrations ranging from ng/L to mg/L, but this level has since increased from µg/kg. Long-term exposure to these pharmaceutical wastes in water at low concentrations could pose major dangers to aquatic, animal, and human life [22]. A variety of medications, including beta-blocking cardiac medications, analgesics, antibiotics, antiseptics, and anti-inflammatory pharmaceuticals, were discovered during the environmental experiment [23]. Antibiotics and anti-inflammatory drugs have raised the most concerns among these medications due to their widespread use worldwide.

1.1.2. Pharmaceutical pollution:

Pharmaceutical pollution, also known as drug pollution, is environmental contamination caused by pharmaceutical drugs and its metabolism products that enter the aquatic environment through wastewater and end up in groundwater, lakes, rivers, and oceans. Therefore, drug contamination is mostly another kind of water pollution. Globally, pharmaceutical contamination has been found in waterways, according to a researcher from the Cary Institute of Ecosystem Studies in Millbrook, New York. Sewage overflows, agricultural runoff, and deteriorating infrastructure are some of the causes. Pharmaceuticals cannot be removed from wastewater even when it reaches sewage treatment plants [24].

1.1.2.1. Factors and effects- The majority are only the result of the medications being eliminated through the urine. Even though the amount from expired or unnecessary medications that are flushed into the toilet is less, it is still significant, particularly in hospitals where the amount is larger than in homes. The smallest drug molecules cannot be removed by current water treatment facilities. Upgrading current facilities to employ sophisticated oxidation techniques capable of eliminating these compounds can be costly. The United States Great lakes have been shown to contain drugs like antidepressants. High levels of antidepressant residues have been discovered in fish brains by University of Buffalo researchers. Antidepressant use has been shown to have comparable effects on fish behavior, including lowering risk-avoiding behaviors and, thus, lowering the ability to survive through predators [24]. Other sources include pharmaceutical production and agricultural runoff, which is

caused by livestock using antibiotics. Water pollution has sex-related impacts that are linked to drug pollution. Aside from industrial pollution, it is thought to play a role in the deaths of fish, amphibian deaths and pathological morphology.

1.1.2.2. Water system contamination

The discovery of pharmaceuticals in the environment at the beginning of the 1990s prompted extensive scientific investigation, new laws, and public awareness [14]. It was also found in the 1990s that fifty to one hundred times as much trash was generated during the manufacturing of a kilo of an effective pharmaceutical molecule [25] and that this garbage was being dumped into the environment. Estrogens were found in wastewater in the late 1990s. This was determined to be the reason why fish became feminized. This was an additional element that led to increased environmental awareness of drugs [26]. Since at least the 1980s, reviews and data on medications found in the environment have been available [15]. Most medications are designed to have minor negative effects on the intended group [14]. Freshwater environments may be negatively impacted by low pharmacological concentration. More than 101 different medications were found in drinking water, tap water, surface water, and groundwater in the US, Spain, Germany, and the UK. The previously mentioned waters in Canada, Thailand, Australia, China, India, South Korea, Sweden, Japan, Poland, the Netherlands, Italy, Brazil, and France were found to contain between 30 and 100 various pharmaceuticals [27]. According to the most thorough investigation of the pharmaceutical contamination of the world's streams conducted in 2022, over 25% of the sites under investigation pose a risk to human health and/or the environment. It looked into 1,052 sampling locations across 258 rivers throughout 104 countries, which equates to 470 million people's exposure to river pollution. The most polluted locations were found to be in lower to moderate-income nations, and they were linked to pharmaceutical production, places with inadequate wastewater and waste treatment infrastructure, and the most commonly discovered and concentrated medicines [14-15, 25-27].

1.1.2.3. The effects of pharmaceuticals

The feminization of fish and amphibians has been brought on by the release of pills for contraception into freshwater environments [15]. About 70 years ago, antipsychotics were developed, and it wasn't until 2007 that their presence in the

environment was documented. Numerous conditions, including bipolar disorder, schizophrenia, autism, depression, and attention deficit hyperactivity disorder, are treated with them. Once a patient has eliminated antipsychotics through urine or feces, the medications and their metabolites are sent to wastewater treatment facilities, where they are not eliminated. These medications have been discovered in hospital waste, drinking water, and all kinds of water. They may go through biological concentrations and biological accumulation via the food web after entering the aquatic environment [23]. Psychiatric medications, including sertraline, citalopram, fluoxetine, oxazepam and chlorpromazine, have been shown to alter fish behavior and disturb their hormones. These medications have been shown to affect invertebrate behavior, disrupt hormones, and be hazardous to reproduction [15]. Worldwide, antineoplastic medications are used during chemotherapy. In addition to polluting water channels, they have cytostatic, ecotoxicological, and mutagenic impacts on aquatic microorganisms. Because antineoplastic medications are intractable, they cannot be eliminated by wastewater treatment. Water bodies tainted with antineoplastic medications have serious negative effects on aquatic life as well as the health of humans [28]. It has been found that chemotherapy medications such as doxorubicin, cisplatin, fluorouracil, cyclophosphamide 1, and mitomycin C can be genotoxic to aquatic life [15].

1.1.2.4. Pharmaceutical contaminants in the environment

Pharmaceutical medicines are now frequently found in a variety of water bodies due to the rising global consumption of these medications. These substances, which are referred to as personal care and pharmaceutical products, are mostly found in pharmaceutical production facilities, hospital waste and household wastewater. They can negatively affect aquatic environments and human well-being since they are biologically active and frequently persistent in the environment [29]. They can cause endocrine system disruption, resistance to antimicrobial substances, and biological accumulation in aquatic life when present in aquatic ecosystem, even at low levels.

Due to a greater understanding of their effects on water bodies, medicines' relevance for both human and veterinary usage as well as their physiologically active transformation products as environmental micropollutants, has gained increasing attention in recent years [30]. Drugs are molecules that are intended to have medicinal

effects on the body and are often active at extremely low concentrations, have the ability to cross biological membranes and remain in the body for long enough to not be inactivated before they start working. These molecules are eliminated through urine and feces as a mixture of components and metabolites, many of which remain unaltered. Wastewater from households, towns, hospitals, and businesses as well as effluents from intensive animal farming, aquaculture, and sewage treatment plants are the main sources of drug contamination. Moreover, the application of solid and liquid livestock manure and sewage sludge as fertilizers in agriculture may aid in the dispersal of pharmaceuticals into soil and, in some situations, aquatic environments, as shown in **Fig.2**. Antibiotics and anti-inflammatory medications are commonly used to treat a variety of diseases, inflammatory diseases, and allergic responses in the contemporary pharmaceutical period. However, they have become persistent environmental contaminants as a result of their frequent usage, inadequate metabolism, and poor elimination in treatment facilities for wastewater [31]. These medications, also known as emerging pollutants, are being found in groundwater, surface water, and even water used for drinking at minimal levels of nanograms to micrograms per liter [32]. Antibiotics like ciprofloxacin, amoxicillin, and tetracycline, work by interfering with vital biological processes including DNA replication, protein synthesis, and cell wall construction, in order to stop bacteria from growing [33].

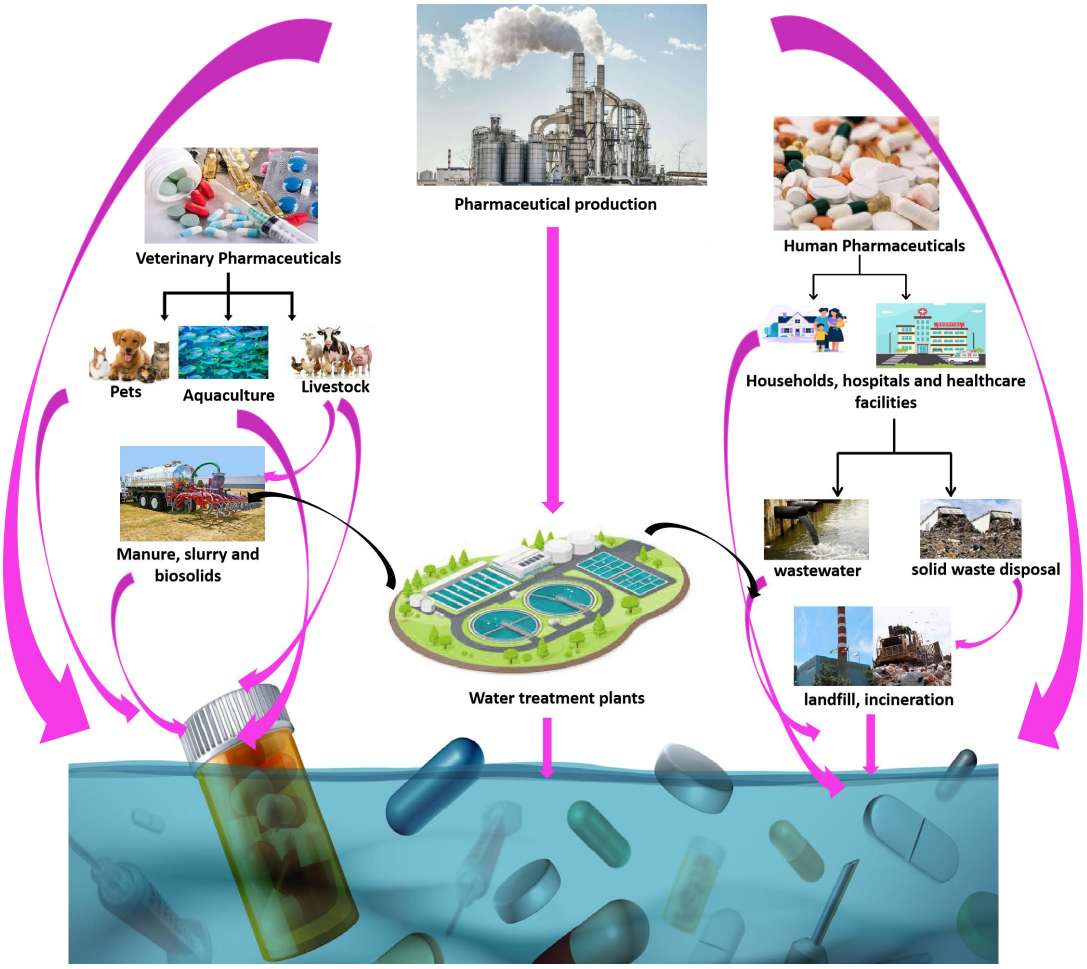

Fig.2 Movement of pharmaceuticals in the environment

1.1.2.5. Classification of pharmaceutical drugs

Based on their medicinal uses, pharmaceutical medications are generally divided into several categories, such as hormones, antidepressants, analgesics, antibiotics, and anti-inflammatory agents. Since they are among the most often prescribed and utilized antibiotics, anti-inflammatory medications are highly prevalent in the environment. Drugs, mainly antibiotics, are used to treat and prevent bacterial infections. Antibiotic-resistant bacteria are a serious worldwide health concern that are a result of their excessive use. Anti-inflammatory drugs, such as non-steroid anti-inflammatory medicines are frequently used to treat symptoms of inflammation, pain and allergies. Frequently experience in wastewater as a result of inefficient removal during conventional wastewater treatment and insufficient metabolism by humans [34-36].

1.1.2.6. Target pollutants:

Ciprofloxacin, the fluoroquinolone drug has a wide-range of antibacterial properties. It is commonly found in surface waterways, hospital waste and even water used for drinking because of its high consumption and reliability in aquatic conditions. Ciprofloxacin is persistent and has the potential to promote resistant genes to antibiotics since it is not broken down by standard wastewater treatment methods [37]. The structure of ciprofloxacin drug is shown in **Fig.3**. High biological toxicity, a wide range of water volume and concentration fluctuations, and an abundance of antibiotics are characteristics of pharmaceutical and medical wastewater [38]. Antibiotics are hard to get rid of with conventional wastewater treatment methods. Along with the treated wastewater or sludge, undegraded medicines find their way into the natural environment [39]. Additionally, one of the main causes of the high number of antibiotics that enter the ecological environment is the inappropriate disposal of expired antibiotic medications [40]. Fluoroquinolones (FQs) are novel antibacterial medications that were first developed in the 1970s and are members of the third generation of quinolones [41]. Ofloxacin, ciprofloxacin (CIP), and enrofloxacin are the most commonly used of them, which offer the widest antibacterial range have few harmful and side effects, are easy to use, and are reasonably priced [42]. Permanganate oxidation, photocatalytic oxidation, ultraviolet light together with hydrogen peroxide oxidation, chlorine oxidation, ozone oxidation, ultrasonic degradation, and many more oxidation technologies have been researched and developed in recent years to treat FQs [43]. The primary range of CIP concentrations seen in water is ng/L to μg/L. The amount of CIP observed increased over time, and it has been discovered that the range of CIP concentrations can reach up to mg/L [44]. CIP is toxic to bacteria and exhibits high chemical interference; it is also challenging for microorganisms to absorb and use. Consequently, MOF materials, activated carbon, or chitosan-synthesised adsorbent are frequently employed for CIP adsorption. Nevertheless, CIP cannot be entirely broken down and rendered harmless by the adsorption process. As a result, advanced oxidation techniques are suggested to break it down and eliminate it. Over 5340 t of CIP were utilized in China in 2013, according to the country's sewage treatment engineering network. CIP is currently the second most often used antibiotic among all fluoroquinolones, and its use is only increasing [45]. Some pathogenic bacteria become drug-resistant as a result of regular use of CIP,

endangering human health if they persist in the environment for an extended period of time. A secondary threat to human health and ecological environmental security could arise from CIP's ability to encourage the generation of resistance genes, which could then spread and diffuse and speed up the mass reproduction of resistant bacteria and pose a threat to the structure of the microbial community [46-47]. Furthermore, CIP has an enriching effect on the human body that can disrupt regular hormone secretion, lead to mental health issues, and disrupt the body's natural metabolism. Additionally, stomach cancer can result from CIP's interference with the human digestive system [48]. CIP wastewater must therefore be treated using extremely effective techniques.

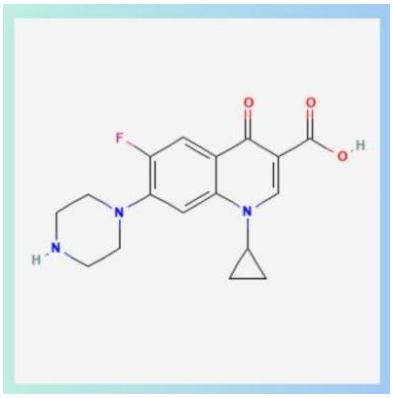

Fig.3 Structure of Ciprofloxacin

Cetirizine, a group of substances known as emerging contaminants of concern, has attracted a lot of interest lately due to its persistence and extensive occurrence in the environment [49-50]. Cetirizine, an H^1 histamine blocker, is one such contaminant in **Fig.4**. About 70-85% of cetirizine is eliminated from the human body unchanged in urine [51]. Cetirizine has been found in receiving waters, treated wastewater effluents, and wastewater influent [52-54]. The use and development of cetirizine also seem to have a seasonal component. Due to increased use to treat seasonal allergies, cetirizine content in wastewater effluent peaked in the summer and subsequently declined during the rest of the year [52]. Investigations into the presence of cetirizine in wastewater were conducted at different concentrations [53-54]. Pharmaceutical levels in the effluent of a wastewater treatment plant in India (Patancheru Enviro Tech Ltd.) near Hyderabad were extremely high; cetirizine was found in the treated effluent at

concentrations of up to 2.1 mg/L (2100 µg/L), with levels as high as 1.2 mg/L (1200 µg/L) in downstream lakes [49]. Cetirizine dihydrochloride is a second-generation antihistamine that belongs to the piperazine class and is used to treat urticaria, hay fever, allergies, and angioedema 2- (2-(4-(4-chlorophenyl) phenylmethyl) piperazin-1-yl) ethoxy) acetic acid dihydrochloride is the chemical name for cetirizine dihydrochloride [55]. Wastewater treatment is necessary for the elimination of such medications in order to avoid their harmful effects on the environment. Cetirizine is mostly eliminated by urine and undergoes very little metabolism [56-57]. Descarboxyloratadine, often known as desloratadine, is the pharmacologically active molecule that results from the metabolism of Loratadine. According to Parfitt [56], the majority of loratadine (desloratadine) is eliminated as desloratadine. Carebastine, the main detectable metabolite and which is believed to be in charge of the drug's pharmacological actions, is produced when ebastine is quickly and nearly entirely oxidized [58]. Additionally, two inactive metabolites are produced: desalkylebastine and hydroxyebastine. As parent chemicals, fexofenadine and acrivastine are eliminated [56].

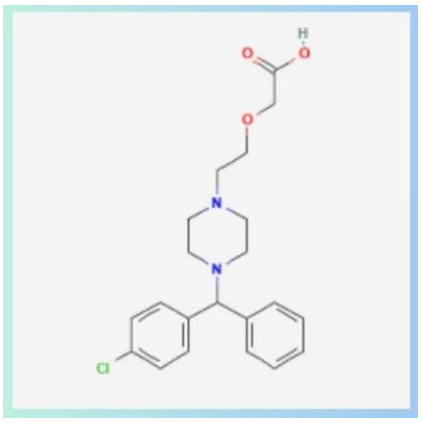

Fig. 4 Structure of Cetirizine

1.2. Challenges and motivations

1.2.1. Limitations of conventional wastewater treatment:

The main goals of conventional wastewater treatment systems are to eliminate pathogens, nutrients, and organic matter, they are not intended to remove

micropollutants like pharmaceuticals. Because of this, removal efficiency for substances such as pharmaceutical drugs and personal care products usually only varies between 50 and 90%, with results that are heavily influenced by the characteristics of the compound and its operational state . For example, with conventional treatment, the elimination efficiency of carbamazepine has been observed to be only 23% [59]. Numerous investigations have verified the continuous discharge of antibiotics, such as tetracyclines, sulfonamides, and fluoroquinolones, in wastewater treatment plants (WWTPs) effluents, occasionally at levels high enough to be hazardous to the environment [60]. This problem affects even isolated and apparently pristine environments, in England's national parks, pharmaceuticals were found in 52 out of 54 sites analyzed, possibly as a result of outdated sewage systems that are unable to remove certain micropollutant types [61-62]. The performance of tertiary procedures such as sand filtering, UV treatment, and chlorination varies. Although filtration and UV are frequently significantly less efficient than chlorination, they can lower antibiotic loads more effectively than other tertiary techniques. In certain situations, antibiotic concentrations have strangely increased after treatment possibly as a result of deconjugation or sorption effects [63]. It requires careful adjustment to maintain good performance with biological treatments like membrane bioreactors, constructed wetlands, and moving bed biofilm reactors. Although these systems can attain notable removal rates up to 95% in certain situations their effectiveness varies, even under ideal hydraulic loading circumstances, removal for some antibiotic groups (such as sulfonamides) is insufficient (< 0%) [60, 64]. These drawbacks show that traditional WWTPs are unable to adequately handle the problem of pharmaceutical pollutants, highlighting the necessity of next-generation treatment techniques capable of completely mineralizing or getting rid of these new pollutants.

1.2.2. Persistence of pharmaceutical pollutants in aquatic systems:

The chemical stability and long-term biological activity of pharmaceuticals make them particularly persistent in aquatic environments. Despite continuous natural degradation processes, numerous pharmaceuticals become pseudopersistent due to continuous inputs from human urine and medical waste [65]. Particularly resistant to microbial degradation, antibiotic categories such as cephalosporins, sulfonamides, and fluoroquinolones frequently attach to sediments and sludge, improving their

environmental retention [66]. Regarding persistence, experimental research has shown: For almost 1,000 days, quinolone antibiotics were still detectable in soils that had been biosolid-amended, significantly outperforming predicted models. Pharmaceutical half-lives in water body simulations varied from 1.5 to 82 days, highlighting the limited biodegradation [67]. In particular, fluoroquinolones have environmental half-lives of approximately 100 days, which supports their persistent presence in aquatic environments [68]. Pharmaceuticals like ciprofloxacin and sulfonamides are frequently found in treated wastewater effluent, even at trace amounts (ng/L–µg/L) [69]. Serious ecological and health issues are raised by this ongoing contamination, which can lead to bioaccumulation, ecosystem imbalances, and the spread of microorganisms resistant to antibiotics [70]. A UK study also showed that pharmaceutical levels, including antibiotics and antihistamines like cetirizine, were higher in national park waterways than in metropolitan areas [62] In order to completely eradicate new contaminants from aquatic environments, advanced degradation technologies like visible-light photocatalysis are vitally required. This is because the ecological impact, long-lasting presence, and limited removal of the pharmaceutical compounds by traditional systems.

1.2.3. Requirement of developing visible-light active photocatalysts

Visible-light-responsive materials are essential for realistic, energy-efficient applications since conventional UV-dependent photocatalysts like TiO_2 are constrained by low solar utilization, which is further hindered by the fact that UV makes up only around 5% of sunlight [71]. By using sophisticated processes including doping, heterojunction creation, and plasmonic improvements, these new photocatalysts may degrade persistent pharmaceuticals under mild ambient circumstances, which is consistent with green chemistry [72]. Therefore, integrating visible-light activation into wastewater treatment plans provides an economical and sustainable way forward, a crucial step in tackling pharmaceutical contamination in your MXene-based photocatalytic system.

1.3. Photocatalysis as a Sustainable Alternative for Water Purification

A light-driven process known as photocatalysis creates electron–hole pairs (e^-/h^+) when semiconductor materials absorb photons with energy equal to or greater than their band gap. These charge carriers move to the surface, where they start redox

processes that produce reactive species that can break down pollutants [73]. Superoxide radicals ($\bullet O_2^-$) are created when electrons in the conduction band decrease molecular oxygen, while hydroxyl radicals (•OH) are created when holes in the valence band oxidize water or hydroxide ions. Both are quite oxidative and necessary to degrade persistent contaminants [74]. Numerous studies have been conducted on the production and conversion of reactive oxygen species (ROS), such as $\bullet O_2^-$ and •OH, in photocatalysis; one noteworthy review focused on the detection techniques and reaction pathways of ROS on semiconductor surfaces [73]. The quick recombination of electrons and holes often limits photocatalytic processes, lowering overall efficiency despite their strength. To extend carrier lifetimes and improve the formation of reactive species, engineering techniques including the introduction of defect sites, heterojunctions, or coupling with conductive supports are used [75]. Degradation methods for pharmaceutical pollutants, such as cetirizine and ciprofloxacin, usually involve several steps, such as dealkylation, ring breakage, and hydroxylation, which eventually result in mineralization into harmless products like CO_2 and H_2O [76].

1.4. Advanced Oxidation Process

Over the years, a variety of techniques, including chemical, biological, and physical methods, have been employed to eliminate the contaminants. To eliminate the contaminants, physicochemical techniques such as precipitation, co-precipitation, adsorption (sorption), ion exchange, and membrane separation (reverse osmosis, electrodialysis) are widely used [77]. In addition to being expensive and producing secondary pollution, these techniques frequently fail to remove contaminants completely. Furthermore, biological techniques like aerobic and anaerobic microbial degrading procedures are used to get rid of harmful contaminants, but they have a few drawbacks, such as taking longer to complete. As a result, a more practical and effective approach is required and greatly appreciated for the elimination of harmful contaminants from the environment. One of the greatest technologies that has received a lot of attention for removing harmful contaminants from wastewater is the advanced oxidation process (AOP) [78]. An innovative and promising technique for treating a variety of harmful contaminants and getting rid of wastewater is the advanced oxidation process (AOP), which uses oxidation through a reaction with

•OH/•O_2^- radicals. The strongest oxidants that can be added to water are these reactive species, which have the ability to oxidize almost any substance that is present. As a result, the pollutants are rapidly and effectively broken down and transformed into small inorganic molecules by the reactants •OH, •O_2. The AOPs are very helpful in getting rid of biologically harmful substances, including pesticides, petroleum, aromatics, and toxic organic compounds, from wastewater. The majority of the polluted elements are transformed into stable inorganic components like carbon dioxide and water. Based on their modes of activation, such as thermal (non-photo) and photochemical reactions, the AOPs are divided into two main classes. These procedures include of electrochemical oxidation, Fenton, sonolysis, photocatalysis, and ozonation. One of these approaches is expensive and has a limited capacity to remove harmful contaminants from wastewater. The process of photocatalysis is more practical for removing pollutants and pollution remediation [79].

1.5. Photocatalysis

Photocatalysis is a good technology for identifying energy and environmental challenges and is a green strategy with many applications. An essential component of the photocatalysis process is the catalyst. When photocatalysis was first used in 1970, the term derived from Greek and was made up of the words photo (light) and catalysis (break apart). The photocatalysis process is thought to be a very successful technique that is being studied as a possible remedy for environmental and energy degradation. It is necessary to investigate new and more effective visible-light active photocatalysts in photocatalysis technologies that make use of renewable energy from the sun. The main factor that determines photocatalytic activity is the capacity of catalysts to create electron-hole pairs, which in turn produce free radicals (O_2•−, •OH) that can go through secondary reactions [80]. There are numerous uses for it, and **Fig.5,** shows the benefits of photocatalysis.

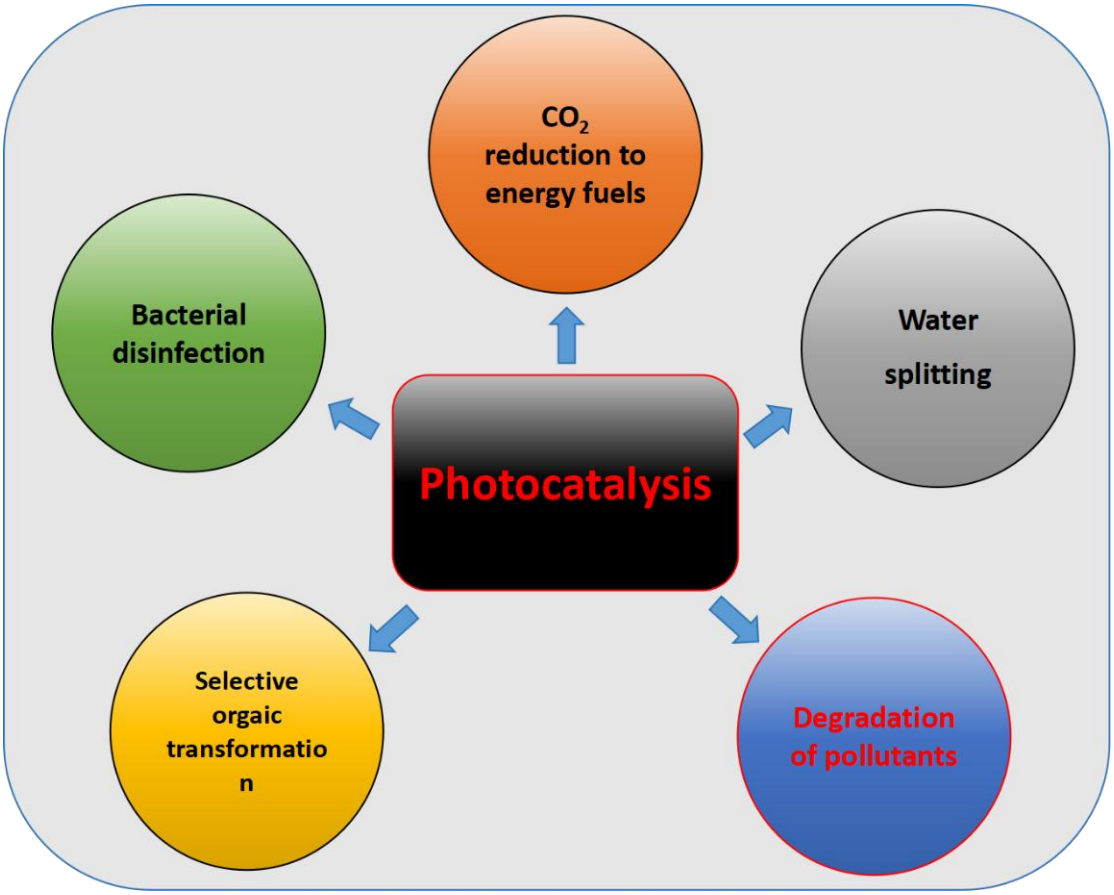

Fig. 5 Advantages of Photocatalysis

1.5.1. Types of photocatalysis

Due to its application in both homogeneous and heterogeneous photocatalysis, photocatalytic degradation was created. The catalyst and reactant are in the same phase in a homogeneous photocatalysis reaction, but in a heterogeneous reactions, they are in different phases. Technologies based on photocatalysis have recently become the most promising means of resolving the world's energy and environmental problems [81].

1.5.1.1. Homogenous photocatalysis

The catalyst and the reaction are in the same phase during homogeneous photocatalysis. Ozone and the photon-fenton reaction are found in the most widely used homogeneous photocatalyst. These reactions are followed by the Fenton process, which produces OH radicals. These processes convert solar energy into clean, readily

available fuel in the form of hydrogen molecules. These reactions have been found to be more effective than other photocatalysis methods, they have the drawback of requiring low pH values since iron behaves differently at higher pH levels and iron must be eliminated after treatment [82].

1.5.1.2. Heterogeneous photocatalysis

Heterogeneous photocatalysis is an alternative and ecologically safe method of degrading contaminants. The catalyst and reactant are in various phases when the mixture is heterogeneous. Semiconductors and transition metal oxides are the most common heterogeneous photocatalysts. While semiconductors have a void energy region, where no energy level is available to support the recombination of an electron and holes produced by photo-activation in the solid, metals contain a continuum of electron states. This method converts partially biodegradable, non-biodegradable pollutants into degradable substances, which causes organic molecules to fully mineralize. It is simple to extract heterogeneous photocatalysts from reaction mixtures. Numerous benefits of heterogeneous photocatalysis include non-toxicity, low cost, non-selectivity of catalytic activity, and chemical stability in a liquid medium. These are the primary benefits that heterogeneous photocatalysts have over their homogeneous counterparts [83].

1.6. Photocatalyst

A substance that produces a photocatalytic reaction when exposed to photo-irradiation and stays not changed throughout the reaction is called a photocatalyst. A catalyst in a chemical reaction does not undergo self-change or consumption [84].

1.7. Semiconductor photocatalyst and mechanism

Energy and environmental problems are the largest problems in the world, and semiconductor photocatalysts have been employed to help solve them. Because of its unique electrical structure, charge transport behavior, light absorption capacity, and appropriate band gap energy, it has been widely used in the photocatalytic process. A semiconductor photocatalyst produces holes in the valence band when it is exposed to light because excited electrons in the valence band migrate to the conduction band. In a very short period of time, the produced electron-hole pairs can recombine in semiconductors, releasing energy as heat. To increase the catalyst's photocatalytic activity, the recombination of these carriers must be minimized. However, these

electrons and holes become superoxide radicals ($O_2^{\bullet -}$) when they react with aqueous oxygen. OH• is created when these radicals react with water. **Fig.6** explains the fundamental mechanism underlying photocatalysis activities. Conversely, photogenerated holes interact with water's hydroxide ions to produce •OH radicals. These two processes generate hydroxyl radicals, which eventually target and break down organic molecules found in water [85, 75].

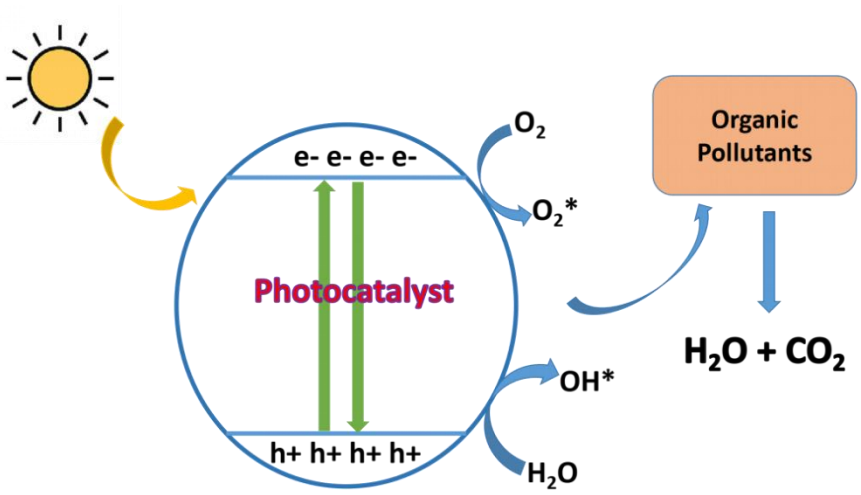

Fig. 6 Fundamental mechanism of photocatalytic activities

1.7.1. MXene as photocatalyst

Two-dimensional materials have drawn a lot of attention from researchers since they are only a few atomic layers thick and have very high aspect ratios. Since all 2D materials have been discovered, graphene is made up of a single layer of sp_2 carbon atoms that are atomically bonded in planar bonds. Graphene has been widely recognized for decades, but previous research demonstrated its single-layer isolation and associated electrical characteristics. As a result, single-layered graphene garnered a lot of attention for the synthesis of graphene-based materials. Both of them received the 2010 Nobel Prize in Physics for this enormous effort [86-87]. In general, 2D materials have found use in a wide range of applications, from reinforced composites as electrochemical energy storage electrodes to electronic devices, including sensors, super capacitors, fuel cells, batteries, transistors, etc. Compared to other 2D materials, graphene has proved more adaptable due to its flexible structure, physical

characteristics, and chemical characteristics. These characteristics, however, have turned into a double-edged sword that restricts their application in all fields. Since many compositional factors can be altered to obtain particular features, the existence of several ingredients results in new qualities [88]. Although graphene is a well-known example, there are many more that have remarkable electrical and structural characteristics. Other 2D materials have been identified in addition to graphene, including metal hydroxides and oxides, hexagonal boron nitrides, and TMDs [89]. The carbides and nitrides of transition metals are another class of two-dimensional materials. Initially, Chen et al. tried to create titanium and niobium carbide nanosheets. The combustible titanium and niobium iodides were reacted with a template composed of a few layers of graphene. The resulting nanosheets had a crystalline size of roughly 8–12 nm and were polycrystalline in nature. Therefore, rather than being a 2D transition metal carbide, it may be seen as a thin sheet [90].

1.7.1.1. MAX phase

For ternary carbides and nitrides, the $M_{n+1}AX_n$ formula is widely known, and the early transition metal (Sc to Ta), denoted by M, in order to construct layered structures with anisotropic properties, n can be 1, 2, or 3. A stands for an alkali metal (Al), silicon metal (Si), lead metal (Pb), and X for a carbon or nitrogen atom. The A-group element layers are interwoven as edge layers in the m6X octahedra. The value of n determines how thick $M_{n+1}X_n$ is n=1 produces 211 phases with a single octahedral block that is three atoms thick, whereas (n+2) produces 413 phases with three octahedral blocks. To date, over sixty distinct pure MAX phases have been identified. On the other hand, different M atom combinations, such as $(Ti_{0.5}, Nb_{0.5})AlC$, A atoms, such as $Ti_3(Al_{0.5}, Si_{0.5})C_2$, and X Sites, such as $Ti_2Al(C_{0.5}, N_{0.5})$, which have a relatively high potential number, may be used to synthesize MAX phases [91-92]. Anisotropic basal dislocations were used to balance out partial delamination in order to increase the thickness of lamellas from up to hundreds of nanometers. As a result, the MAX experienced auto-mated deformation. Phases of graphene that have significantly stronger M-A bonds are exfoliated to a few nanometers thick. By using liquid or gas phase extraction, it were the first to exfoliate the A-group layers from the MAX phases at room temperature or moderately heated. Disordered graphitic carbon, also

known as carbide-derived carbon, was demonstrated by Hofmann and colleagues. Both M and A are extracted to create carbide-derived carbon [93-94].

For the production of 2D transition metal carbides and nitrides, MAX phases are exfoliated by selectively etching A layers. The absence of the A group from MAX phases is represented by MXenes. The suffix "ene" in "MXene" denotes their 2D nature, which is comparable to the characteristics of graphene. Selective etching is used to exfoliate the A layers from the MAX phases. There are currently more than 60 MAX phases. By eliminating the A layers from the MAX structures, more than twenty pure $M_{n+1}X_n$ phases were produced. Additionally, a number of MXenes are produced from MAX solid solutions on the M and X sites. The exfoliated MAX phases are used in this work for supercapacitors, electrochemical sensors and photocatalysis [94].

1.7.1.2. Biochar as a sustainable carbon source for MAX Phase Fabrication

Carbon sources derived from biomass have received a lot of attention as a result of the ongoing search for environmentally benign and sustainable products. Among these, biochar has become a viable option because of its availability, affordability, environmental friendliness, and special physicochemical characteristics. Typically, lignocellulosic biomass is pyrolyzed under low oxygen conditions to produce biochar, which is a porous material rich in carbon. Biochar has been extensively investigated in advanced material synthesis, energy storage, environmental remediation, and catalysis due to its high surface area, thermal stability, and adjustable surface functions [95]. Biochar offers a sustainable and environmentally friendly substitute for traditional carbon sources like activated carbon or synthetic graphite. Biochar's porous shape enhances mass transfer and promotes chemical reactions, and its composition, which is often high in carbon with trace amounts of oxygen, hydrogen, and minerals makes it an appropriate precursor for the creation of carbides and nitrides. Because of these characteristics, biochar can be used as an effective carbon source to create MAX phases, which are the building blocks of MXene materials. In MAX phase synthesis, recent studies have shown that biomass-based carbons can effectively substitute costly and non-renewable graphite, providing both financial advantages and environmental sustainability [96]. By integrating advanced

nanomaterials design with waste-to-wealth principles, the use of biochar in this setting presents a novel strategy.

1.7.1.3. Pinecone-derived biochar

Pinecones are a desirable precursor for the manufacture of biochar among different biomass resources because of their high carbon content, natural abundance, and renewability. Pinecones, which are frequently thrown away as forestry waste, are mainly made up of lignin, cellulose, and hemicellulose, which are the perfect ingredients for pyrolyzing and producing stable, carbon-rich biochar. Pinecone biochar's high fixed-carbon content supplies enough carbon to promote carbide production, and its porous structure improves gas and heat transport during synthesis. Additionally, trace levels of inorganic elements (such Ca, Mg, and K) found in pinecone-derived biochar may serve as catalysts during heat processing, enhancing the final MAX phase material's crystallinity and structural integrity [97].

In the current thesis, a high-temperature heat treatment procedure has been used to fabricate La- and V-based MAX phases using pinecone-based biochar as the carbon source, as shown in **Fig.7**. This approach has two advantages that: it produces the high-quality MAX phases needed for the synthesis of MXene, and it encourages the development of sustainable materials by using biomass waste. These were then investigated as innovative photocatalysts for the degradation of pharmaceutical drugs when exposed to visible-light. This work addresses a current gap in MXene research where renewable carbon sources have received limited attention by integrating pinecone biochar into MAX phase synthesis. A novel approach for creating innovative functional materials with technological and environmental significance is provided by the combination of green chemistry concepts with the creation of extremely effective photocatalytic systems.

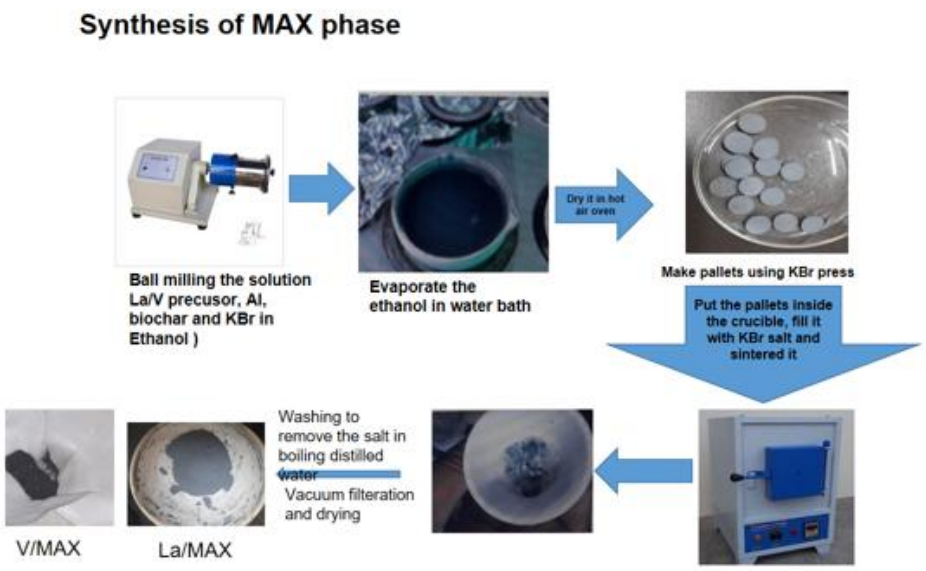

Fig. 7 Synthesis of MAX phase

1.7.1.4. MXenes

Recent studies have focused on MXenes, a novel family of 2D transition metal carbides, because of their unique characteristics, such as excellent metallic conductivity and hydrophilic surfaces that improve the stability of aqueous environments. These characteristics make 2D MXenes ideal for various kinds of uses. The M-X bond in the MAX phase is primarily covalent or metallic, and the M-A bond is metallic in nature which is why the MAX phase bond is difficult to break. However, M-A bonds are weaker since MXenes can be produced by selectively etching them with fluoride-containing water solutions. Functionalized MXenes are created with the terminal O, OH, and F atoms, abbreviated as T_x in the general formula $M_{n+1}X_nT_x$ after the Al layers are removed [98-99].

1.7.1.5. Structure and properties of MXene

Unique characteristics of MXenes include considerable surface area, significant electrical conductivity, and sufficient surface terminal groups for multilayer structures. When MXene is in its metallic, semi-metallic, or semi-conducting phases, its conductivity varies. The resulting MXenes have a symmetrical hexagonal structure that is comparable to the symmetry of MAX phases. The particle arrangement in the M layers is lamellar, with the X layers placed between them. The existence of

nitrogen or carbon atoms positioned between the M and X layers [100]. The electrical and nanostructured characteristics of the MXenes were mostly calculated using the generalized gradient approximation (GGA) methodology. However, an in-depth examination of the electronic bandgap was probably going to be accomplished using hybrid functional. The immaculate MXenes are anticipated to display metallic properties. It is anticipated that the standard MXenes will have a better charge carrier density of states (DOS) that is closer to the Fermi level than the MAX phase. Following functionalization, the semiconducting characteristics that match the arrangement of M, X, and T atoms are achieved by inhibiting the metallic behavior, improving the electrical properties of MXenes [101].

Because of their hydrophilic surfaces and metallic conductivity, which improve adsorption and photocatalytic efficiency, MXenes, a novel family of 2D materials produced by selectively etching MAX phases, have shown exceptional photocatalytic capabilities [102]. Designing complex nanostructures, heterojunctions, or composites is frequently necessary for photocatalytic processes employing 2D materials in order to maximize absorption of light, charge separation, and surface reactions. By expanding the light absorption spectrum, adding more active sites, and lowering the recombination of pairs of photogenerated electrons and holes, these modifications aim to increase the effectiveness of photocatalytic reactions. Because of their remarkable qualities, 2D materials have the potential to revolutionize the development of photocatalytic technology. Together with continuous advancements in materials engineering, their capacity to stimulate photocatalytic processes in the presence of visible-light portends a bright future for environmentally friendly energy production and cleanup. The use of 2D materials in photocatalytic systems holds potential for developing effective, environmentally responsible remedies for energy and environmental problems as research advances [103].

1.7.2. Fabrication of MXene

The main method for creating MXenes is to remove the "A" element (like Al) from their layered MAX phase precursors in a selective manner. This produces two-dimensional transition metal carbides or nitrides ($M_{n+1}X_nT_x$). The two most popular methods among the several that have been documented are microwave-assisted

synthesis and conventional hydrofluoric acid (HF) etching, as seen in **Fig.8**, each of which has unique benefits and drawbacks [104].

Conventional process, a simple displacement process, the hydrofluoric acid removes Al layers from the Ti_3AlC_2 MAX phase while producing hydrogen gas. Ti_3C_2Tx is the product of the reaction between deionized water and the HF which is strong acid, where T stands for the functionalities of MXenes oxides, fluorides, hydroxyl groups, and H_2. The hydrofluoric acid etching approach was successfully used to convert different types of MAX phases into MXenes. By treating the MAX phase (such as Ti_3AlC_2) with a concentrated HF solution, the Al layers are selectively dissolved in the traditional HF etching process, resulting in $Ti_3C_2T_x$ MXene sheets. The simplicity and reproducibility of this approach have led to its widespread use. However, a number of issues restrict its environmental acceptability and scalability. The method is time-consuming due to the lengthy reaction times (which can range from several hours to days) and the serious health and safety risks associated with the use of concentrated HF. Additionally, the MXene produced with this technique frequently has limited surface area, multilayer restacking, and partial oxidation, all of which might lessen its efficiency in catalytic applications [105].

Microwave-assisted synthesis approach, on the other hand, has become a quick, energy-efficient, and possibly safer substitute. Because microwave irradiation produces consistent, volumetric heating, the delamination process can be done in minutes as opposed to hours. In addition to speeding up the exfoliation of MXene sheets, this method reduces restacking and enhances structural homogeneity. Furthermore, surface functional groups (-O, -OH, -F) can be better controlled in microwave-assisted synthesis, which is essential for adjusting MXene's electrical, catalytic, and interfacial characteristics. Significantly, this method is ideal for creating composites based on MXene because the microwave energy strengthens the interfacial contact between MXene and other semiconductor phases, improving photocatalytic activity [106-107]. Overall, the microwave-assisted approach offers notable benefits in terms of efficiency, safety, and structural quality, even if the conventional process is still the most well-established way for preparing MXene. In light of these characteristics, both approaches are used in this work to synthesize

MXene and assess their impact on the photocatalytic degradation of pharmaceutical contaminants when exposed to visible-light [108].

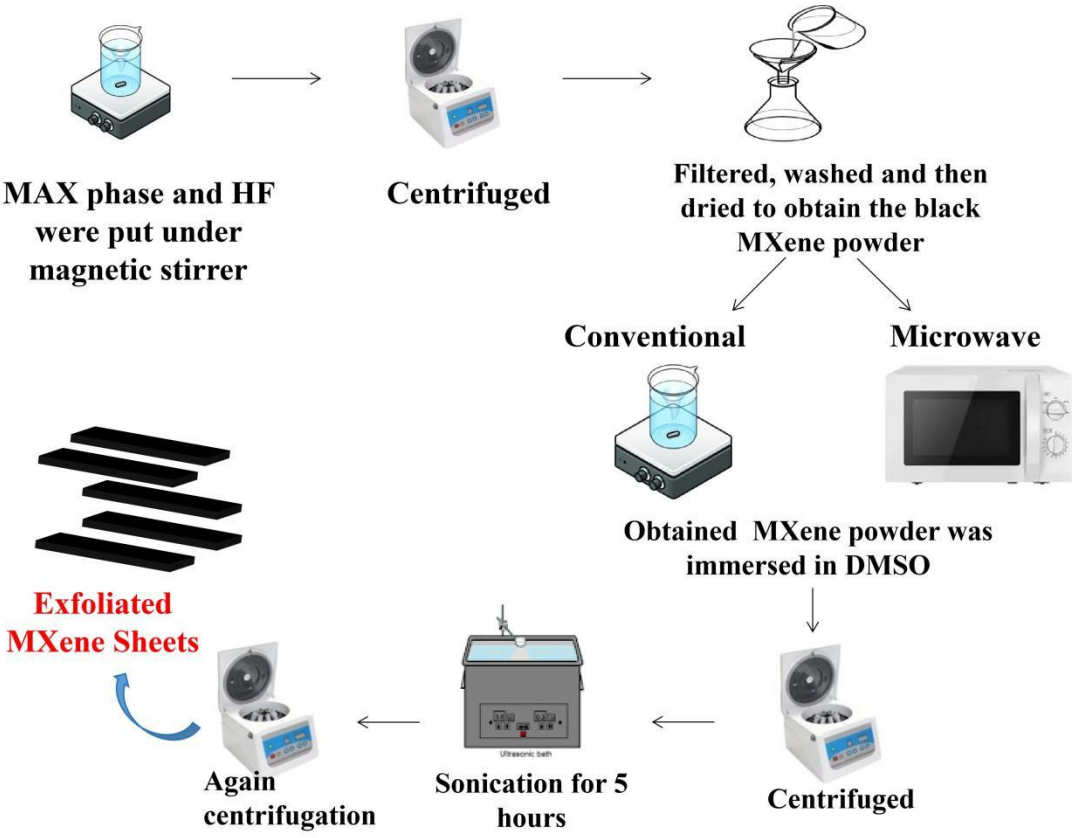

Fig. 8 Schematic Diagram for MXene synthesis from MAX phase

1.7.3. Properties of MXene relevant to photocatalysis

The distinct physicochemical characteristics of MXene-based materials set them apart from conventional semiconductors and account for their exceptional performance in photocatalytic applications. Among these, adjustable band structure, rich surface functional groups, and high electrical conductivity are essential for increasing photocatalytic efficiency [107, 111-112].

Strong M–C bonding and transition metal carbide/nitride layers give MXenes their metallic or near-metallic conductivity. Because of this characteristic, they can function as good conductive channels and electron reservoirs in photocatalytic devices. MXenes may quickly transmit photogenerated electrons when paired with semiconductor materials, which suppresses electron–hole recombination and extends

the lifespan of charge carriers. Under visible-light, this enhanced conductivity plays a crucial role in increasing the quantum efficiency of MXene-based photocatalysts [107, 111-112]. Surface functional groups like -O, -OH, and -F, together represented by the symbol T_x, are commonly used to end MXene surfaces during the etching process. MXenes are extremely dispersible in aqueous systems due to the hydrophilicity these surface terminations offer, which is beneficial for water purification applications. Functional group density and type can also improve catalytic active sites, modify interfacial interactions with adsorbed drug molecules, and affect the kinetics of charge transfer at the photocatalyst–pollutant interface. MXenes' chemical reactivity can be easily adjusted through functionalization [107, 111-112]. The band structure of MXenes can be controlled by heteroatom doping, surface termination control, or composite creation with semiconductors, despite the fact that they frequently display metallic behavior. These changes can optimize band edge positions or open band gaps to match the redox potentials needed for the photocatalytic destruction of contaminants. When MXenes are coupled with visible-light-responsive semiconductors like g-C_3N_4, $BiVO_4$, or V_2O_5, for instance, effective heterojunctions are created that promote charge separation and increase the range of light absorption. Because of its tunability, MXenes can be used in a wide range of photocatalytic devices [107, 112]. In contrast to materials like graphene, which are hydrophobic, MXenes are hydrophilic, which enables them to diffuse effectively in aqueous environments. This characteristic greatly expands their use in wastewater treatment, where effective catalyst–pollutant interaction is necessary [107, 111-112]. MXenes offer a high surface-to-volume ratio, interlayer ion transport routes, and strong interfacial interaction with other photocatalytic components because of their two-dimensional layered structure. Under visible-light, these characteristics promote both pollutant adsorption and catalytic breakdown [107].

When band structure engineering, tunable surface chemistry, and exceptional conductivity are combined, MXenes create a new class of advanced functional materials with enormous potential for environmental remediation, including the breakdown of persistent pharmaceutical pollutants when exposed to visible-light.

1.7.4. MXene-based composites for photocatalysis

Pristine MXenes have shown encouraging photocatalytic qualities because of their stacked 2D structure, metallic conductivity, and functional groups on the surface. Nevertheless, there are a number of disadvantages to using them directly in photocatalysis, such as a tendency to restack during processing, very little optical absorption in the visible spectrum, and limited long-term stability under reaction conditions. These restrictions can impair light harvesting and lower electron-hole separation efficiency, which lowers photocatalytic performance overall. Recent studies have concentrated a lot of attention on MXene-based composites, which blend MXenes with metals, metal oxides, carbonaceous materials, halide/perovskite combinations, or rare earth elements, in order to overcome these difficulties. The synergistic effects of these composites, which take advantage of the complementary qualities of MXenes and the linked materials, greatly improve photocatalytic degradation of persistent contaminants, including pharmaceuticals [109-112].

Incorporating MXenes to semiconducting metal oxides like TiO_2, ZnO, and V_2O_5 is one of the most popular methods for enhancing photocatalytic activity. MXenes serve as conductive backbones or electron mediators in these composites. Photogenerated electrons from the oxide's conduction band are quickly transported to the MXene layers upon exposure to visible-light, which inhibits electron-hole recombination. For example, compared to pristine TiO_2, Ti_3C_2Tx/TiO_2 composites have demonstrated higher degrading efficiency toward organic contaminants due to enhanced charge mobility and the formation of additional active sites. Similarly, because MXene and V_2O_5 have a favorable band alignment, V_2O_5/MXene composites can offer better visible-light absorption and increased catalytic activity [109-112]. The photocatalytic applications of MXene nanosheets are further expanded by decorating them with noble or transition metals (such as Ag, Au, Pt, or Pd). In addition to improving visible-light absorption through surface plasmon resonance (SPR) effects, metallic nanoparticles serve as effective electron sinks to promote the transfer of charge carriers at the MXene–metal interface. During multiple photocatalytic cycles, the metal nanoparticles and MXene work in concert to promote stability and redox activity. For instance, the combined effects of MXene-mediated charge transfer and SPR-driven visible-light harvesting have demonstrated increased photocatalytic degradation of antibiotics in aqueous environments in Ag-decorated MXene

composites [109-112]. Attention has also been drawn to the integration of MXenes with carbonaceous materials such as graphene, carbon nanotubes (CNTs), activated carbon, and biochar. These carbon-based supports increase surface area overall, stop MXene sheets from restacking, and offer a large number of pollutant adsorption sites. Specifically, biochar made from biomass resources like pinecones provides an environmentally benign and sustainable source of carbon. Biochar ensures effective electron-hole usage during photocatalysis by improving pollutant adsorption while retaining high conductivity when combined with MXene. These environmentally friendly composites have a lot of potential for environmental rehabilitation and are consistent with green chemistry concepts [109, 110-112]. Coupling with halide perovskites or bismuth-based compounds like $Cs_3Bi_2Br_9$, $BiVO_4$, and Bi_2O_3 results in another new family of MXene-based hybrids. Despite their great absorption of visible-light, these materials frequently have poor stability or quick charge recombination. The inclusion of MXene decreases recombination losses, increases interfacial charge transport, and strengthens its structural stability. For instance, MXene's effective electron extraction, which extends carrier lifetimes and promotes redox reactions, has allowed $Cs_3Bi_2Br_9$/MXene composites to exhibit improved degradation of pharmaceutical impurities [109, 111-112]. Doping MXenes with transition metals (such as V, Fe, and Co) or rare earth elements (like La, Ce) is another effective way to change their electrical structure. These dopants have the ability to increase the density of active sites, introduce defect states, and modify the band gap. For example, by improving band alignment and boosting drug molecule adsorption, La-doped MXene composites show increased photocatalytic activity and better visible-light responsiveness. Similarly, it has been claimed that vanadium–MXene composites offer better degrading performance because of the synergistic effects of vanadium oxide's visible-light absorption and MXene's conductivity. Although MXenes by themselves have outstanding conductivity, hydrophilicity, and active surface terminations, restacking of nanosheets, partial oxidation, and inadequate light absorption in the visible spectrum restrict their photocatalytic efficacy. Metal and metal oxide doping techniques have been used to build MXene-based composites with improved photocatalytic performance in order to overcome these obstacles. These changes improve charge carrier dynamics and light-harvesting

capacity by changing the electrical structure, band gap, and surface chemistry of MXenes [109, 111-112]. Localized electronic states brought about by rare-earth doping can improve responsiveness to visible-light and make charge separation easier. By somewhat neutralizing negatively charged functional groups, Lanthanum's inclusion into MXene modifies the surface chemistry and enhances interfacial interactions with medicinal compounds. A more advantageous band alignment for photocatalytic redox processes might also result from the modification of the band structure by La^{2+} ions. Because of these synergistic effects, prior research has demonstrated that La-modified MXene composites display improved photocatalytic degradation of antibiotics [109, 111-112].

V_2O_5 is a semiconductor with a low band-gap (about 2.3 eV) and a high absorption of visible-light. Rapid charge recombination and poor conductivity, however, restrict its use. These drawbacks are overcome by coupling V_2O_5 with MXene. V_2O_5 increases light absorption into the visible spectrum, while MXene sheets serve as electron mediators, improving charge separation and transport. According to reports, the produced MXene–V_2O_5 composites have outstanding degrading performance against persistent organic contaminants, indicating their potential for the treatment of pharmaceutical wastewater [109, 111-112]. Surface terminations (-O, -OH, and -F) and how they interact with doped species have a significant impact on the photocatalytic performance of MXene-based composites. In addition to altering the density of functional groups, metal/metal oxide doping creates defect states that customize the band gap [112]. V_2O_5 incorporation narrows the band gap, allowing for higher visible-light absorption, while La doping increases the band gap of MXene while improving charge separation [109, 112]. Doping improves the absorption of pollutants and catalytic reactivity by changing surface charge and zeta potential. For instance, electrostatic interactions with negatively charged medicinal compounds may be favored by a less negative zeta potential following La doping, increasing the effectiveness of photocatalytic breakdown [109, 112].

1.7.5. Previous research findings

Antibiotic degradation under visible-light has been shown to be enhanced by La-doped Ti_3C_2Tx MXene composites, which are ascribed to better band structure and optimized surface terminations [109,111]. The significance of interfacial charge

transfer has been confirmed by the higher ciprofloxacin degradation efficiency of V_2O_5/MXene hybrids as compared to MXene. MXene-based composites containing transition metals (Fe, Co) and rare earths (Ce, Nd) have been described in other investigations, demonstrating the wider potential of surface chemistry tailoring for environmental applications [107-109, 111-112]. One interesting way to improve photocatalytic performance is to combine metals and metal oxides, including La and V_2O_5, with MXenes. The drawbacks of pristine MXene and traditional photocatalysts are addressed by MXene-based composites through surface chemistry tailoring, band gap modification, and enhanced charge separation dynamics. Because of these characteristics, they are very useful for breaking down pharmaceutical pollutants like cetirizine and ciprofloxacin when exposed to visible-light.

1.7.6. Synergistic role of MXene-based composites

MXene-based composites are created by efficiently fusing secondary materials' light-harvesting capacity and catalytic reactivity with the conductivity, electron mobility, and hydrophilic character of MXenes. As conductive scaffolds, MXenes promote charge transfer and inhibit recombination, and the materials that are integrated increase the absorption of visible-light and offer more redox-active sites. In real environmental settings, this hybridization approach greatly improves the efficiency, stability, and recycling of photocatalysts while also overcoming the inherent drawbacks of pristine MXenes. Consequently, MXene-based composites represent a very adaptable and promising family of improved functional materials for the photocatalytic destruction of pharmaceutical pollutants under visible-light irradiation. They can be used as next-generation catalysts to solve the urgent problem of pharmaceutical pollution in aquatic ecosystems because of their special mix of characteristics [107].

1.8. Research gap

The persistence, bioaccumulation, and possible toxicity of antibiotics and anti-inflammatory medications have made pharmaceutical pollution in aquatic ecosystems a major worldwide concern. Particularly at trace amounts, conventional treatment techniques, including adsorption, membrane filtration, and biological degradation, are frequently insufficient to fully eliminate these substances. As a result, photocatalytic degradation exposed to visible-light has attracted a lot of interest as a viable and

efficient substitute [110,112]. Despite significant research, a variety of semiconductor-based photocatalysts, including TiO_2, ZnO, g-C_3N_4, and $BiVO_4$, have intrinsic disadvantages, including large band gaps, low absorption of visible light, fast electron–hole recombination, and low reusability. MXenes' hydrophilicity, vast surface area, programmable surface terminations, and metallic conductivity have made them attractive prospects in recent years. Notwithstanding these benefits, pristine MXenes have drawbacks such as layer restacking, limited light absorption, partial instability during photocatalysis, and low activity when used alone as a photocatalyst [110, 112]. Researchers have created MXene-based composites by combining MXenes with carbonaceous supports, metal oxides, noble metals, or halide perovskites in order to get around these obstacles. Even while these studies show increases in visible-light absorption and charge separation, there are still a number of gaps, such as limited investigation of rare earth doping, rare earth elements are known to enhance visible-light activity and modify surface chemistry, very few studies have examined how they can be integrated with MXenes to degrade pharmaceutical drugs. Insufficient Focus on transition metal oxide MXene systems. V_2O_5 is one of the transition metal oxides with the strongest redox activity and visible light absorption, but its low conductivity prevents it from being used alone. It is yet unknown how well V_2O_5 and MXenes work together to break down antibiotics and anti-inflammatory medications. Incomplete understanding of structure-property relationships, while prior studies have shown that MXene composites can improve photocatalysis, there is currently a lack of comprehensive knowledge regarding the ways in which doping-induced surface chemistry tuning, band gap modulation, and charge transfer dynamics lead to increased activity. Pharmaceutical-specific studies are scarce; MXene composites have been examined for dyes and general organic pollutants. There aren't many comprehensive investigations focusing on the degradation of antibiotics and anti-inflammatory drugs under visible-light [110-112].

1.9. Aim and Objectives of the Thesis

Designing, fabricating, and investigating MXene-based advanced functional materials for the effective photocatalytic degradation of pharmaceutical contaminants, specifically, antibiotics (ciprofloxacin) and anti-inflammatory medications (cetirizine) under visible-light irradiation, is the main goal of this thesis. The urgent demand for

high-performance, sustainable photocatalysts that can efficiently remove pharmaceutical contaminants from aquatic ecosystems is what drives our work [111]. In order to accomplish this goal, particular objectives as follows have been developed. (1) To produce MAX phase precursors by treating them at high temperatures with metals (La/V, Al) and a sustainable carbon source (biochar made from pinecones), and to investigate the viability of using carbon derived from biochar to replace conventional graphite/carbon sources in order to align with sustainable and environmentally friendly synthesis methods. (2) To create pristine MXene using microwave-assisted synthesis and conventional methods, and to synthesize La/V-based MXene composites via the microwave method. To examine how the synthesis process affects the final MXene materials' structural, surface, and photocatalytic characteristics. (3) To clarify the structural, morphological, optical, and electrochemical characteristics using sophisticated analytical methods (XRD, FTIR, SEM, EDX, etc.). To clearly define the links between structure and properties, with an emphasis on charge transfer kinetics, band gap manipulation, and surface chemistry tuning. (4) To evaluate the unmodified and doped MXene-based composites' photocatalytic efficacy in degrading pharmaceutical contaminants (cetirizine and ciprofloxacin), to determine the relative roles of surface adsorption and photocatalysis in degradation under dark and visible-light irradiation. to investigate how degradation efficiency is affected by important operational factors (pH, concentration, irradiation period, and reusability).

Thesis Summary

In order to provide a logical progression from the basic principles to the experimental findings and conclusions, this thesis is methodically organized into five chapters. The following is an overview of each chapter:

Chapter 1: Introduction

The background and motivation for the study are presented in this chapter, which also highlights the need for sophisticated photocatalytic materials and the environmental problems caused by pharmaceutical contaminants. MXenes are introduced, along with their characteristics, production methods, and prospective applications in environmental remediation. In addition, the chapter emphasizes the current research

gaps, talks about MXene-based composites, and describes the purpose and goals of the current study.

Chapter 2: Literature Review

This chapter provides a thorough analysis of earlier studies on photocatalysis, the treatment of pharmaceutical effluent, and the function of MXenes in advanced oxidation processes. It critically examines both established and novel approaches, the application of carbon generated from biochar, and the impact of metal/metal oxide changes on photocatalytic performance.

Chapter 3: Materials and Methods

The experimental approach used in the thesis is described in detail in this chapter. It covers the production of MXene and its composites using conventional and microwave-assisted techniques, and the construction of the MAX phase utilizing carbon generated from biochar. Additionally described are the photocatalytic testing methodologies for pharmaceutical degradation as well as the characterization methods (FTIR, SEM, EDX, Zeta potential, electrochemical investigations, etc.).

Chapter 4: Results and Discussion

The synthesis results of both MXenes and their composites are presented in this chapter, together with the results of their surface, optical, morphological, and structural characterization. The impact of synthesis techniques and their composites adjusting material properties is highlighted by a comparative analysis of materials made using various synthesis procedures (conventional vs. microwave). The degradation of antibiotics (ciprofloxacin) and anti-inflammatory drugs (cetirizine) under visible-light irradiation is discussed in this chapter, along with the impact of different operational parameters (pH, irradiation time, concentration, and reusability) on degradation efficiency and the presentation of mechanistic insights into charge transfer, band gap modification, and reactive species involvement.

Chapter 5: Conclusions and Future Perspectives

The main conclusions of the study are outlined in this chapter, with a focus on how microwave-assisted techniques and La/V incorporation can enhance photocatalytic performance. An outlook on the future advancement of MXene-based photocatalysts for environmental applications is provided at the end of the chapter, along with various possibilities for future study.

CHAPTER-2

Literature review

2.1 Overview of pharmaceutical drugs

Pharmaceutical medications are thought to be among the most revolutionary inventions of modern society. By lowering mortality, increasing life expectancy, and greatly enhancing human life quality, medications have transformed healthcare since the middle of the 20th century. Deaths from infections that had afflicted humanity for generations dramatically decreased once antibiotics were discovered in the 1940s and widely used [113]. In the same way, the development of vaccinations, anticancer medications, analgesics, anti-hypersensitivity, and psychiatric medications has been crucial to managing chronic illnesses, preventing epidemics, and reducing suffering. When taken as a whole, these pharmaceutical developments have helped societies move from periods of high mortality from communicable diseases to a time when lifestyle-related and non-communicable disorders take center stage in healthcare priorities [114]. The consumption of pharmaceuticals has increased dramatically over the last few decades, coinciding with rising urbanization, fast population expansion, and improvements in medical infrastructure. With an estimated yearly growth rate of roughly 5–6%, the global pharmaceutical market is expected to reach USD 2.5 trillion by 2030 from its 2022 valuation of USD 1.48 trillion (Fortune Business Insights, 2023). Global drug use, as measured in defined daily doses (DDDs), increased by 14% between 2017 and 2022 and is predicted to increase by an additional 400 billion DDDs by 2028, according to the IQVIA Institute (2023). The combined effects of changing demographics, rising rates of chronic diseases including diabetes, hypertension, and cancer, and easier access to necessary medications in low- and middle-income nations are responsible for this extraordinary increase [115-116]. There are clear trends in the geographic distribution of medication use. Because of their sophisticated healthcare systems and increased knowledge of sickness, developed nations like the US, Japan, and Europe consume the most medications per person (OECD, 2023). On the other hand, the fastest growth in overall consumption is occurring in emerging economies. Known as the "pharmacy of the world," India produced more than 20% of the world's generic drug supply and exported $25.3 billion worth of pharmaceuticals in 2023 [117]. Despite their critical role in public health, the widespread use of medications has led to unexpected and frequently disregarded environmental problems. Pharmaceuticals are deliberately made to target

physiological networks and are biologically active at low concentrations, in contrast to many other anthropogenic substances. After being used by humans or animals, a sizable portion of these substance is eliminated either unaltered or as active metabolites. Depending on how the medication is metabolized, 30–90% of an oral dose may be eliminated in urine or feces (Zuccato et al., 2006; Verlicchi et al., 2012). For example, the fluoroquinolone antibiotic ciprofloxacin, which is frequently administered, is excreted up to 50–70% unmetabolized and enters wastewater systems directly [118]. Pharmaceuticals were not initially intended to be removed by conventional wastewater treatment plants (WWTPs). Because of this, numerous chemicals are detected widely in aquatic habitats and go through treatment methods essentially unchanged (Larsson, 2014). Persistent substances like carbamazepine, diclofenac, and certain antibiotics have especially low removal rates, with reported clearance efficiencies ranging from 20% to 80% (Verlicchi et al., 2012). As a result, pharmaceutical residues with quantities ranging from ng/L to µg/L have been found in rivers, lakes, groundwater, and even drinking water all over the world (aus der Beek et al., 2016). For instance, ciprofloxacin and sulfamethoxazole are commonly found in Asian surface waters at comparable amounts, but diclofenac has been reported in European rivers at concentrations above 1 µg/L, above acceptable standards for aquatic life [119]. Numerous ecological and human health issues are brought up by the presence of drugs in the environment. When exposed to trace drug quantities, aquatic organisms may experience reproductive damage, behavioral changes, and endocrine disruption. For example, vultures' renal injury caused by the non-steroidal anti-inflammatory drug diclofenac has resulted in severe population reductions in South Asia (Oaks et al., 2004). Similarly, it has been demonstrated that fish exposed to psychiatric medicines change their behavior, which may upset the ecological equilibrium. However, the emergence and dissemination of antimicrobial resistance (AMR) appears to be the most urgent worldwide threat. Antibiotic residues in natural water bodies and wastewater put microbial populations under selective pressure, hastening the establishment of resistance species. According to the World Health Organization (2021), if drug-resistant infections are not adequately controlled, they may result in up to 10 million deaths per year by 2050, making AMR one of the top ten dangers to world health [120]. Because of these difficulties, pharmaceutical

pollution has emerged as a crucial topic for research and policy. Understanding the presence, fate, and consequences of medicines in the environment is important, but so is creating practical plans for getting rid of them. This issue cannot be solved by traditional wastewater treatment technologies alone, hence advanced treatment techniques such as membrane filtration, advanced oxidation processes (AOPs), and photocatalysis must be developed. Nanomaterials and newly developed functional materials, like composites based on MXene, have garnered more interest recently due to their high effectiveness in breaking down medications when exposed to visible-light (Yang et al., 2020). These strategies have the potential to reduce the environmental hazards that pharmaceuticals represent while maintaining the sustainability of the world's water supplies [121]. In conclusion, pharmaceutical medications constitute an issue in modern society: although they are essential for protecting human health and promoting medical advancement, their byproducts present serious environmental hazards that cannot be disregarded. Inadequate treatment facilities and the sharp rise in global consumption underscore how urgent it is to address these two issues. To strike a balance between the need to protect the environment and the socioeconomic advantages of pharmaceuticals, research into new catalytic materials, sustainable remediation techniques, and more robust regulatory frameworks is crucial. The very growth of pharmaceuticals has resulted in an unexpected environmental cost. Much of the medication is not completely broken down after administration and is either eliminated unaltered or as active metabolites. According to Zuccato et al. (2006) and Verlicchi et al. (2012), depending on the medicine and the patient's metabolism, 30 to 90% of the ingested amount is usually eliminated. Since wastewater treatment plants (WWTPs) are not built with the express purpose of eliminating pharmaceutical residues, many medications enter aquatic systems almost unchanged. Because of this, it is common to find antibiotics, anti-inflammatory medications, analgesics, and psychiatric medications in drinking water, groundwater, and surface water at concentrations ranging from ng/L to µg/L [122, 118].

Antibiotics are one of the most alarming categories among these. Because of its excellent chemical stability and limited biodegradability, the fluoroquinolone antibiotic ciprofloxacin, which is frequently administered, is extremely persistent in

aquatic environments. According to studies, between 50 and 70 percent of ciprofloxacin is eliminated in active form, with a significant portion going straight into sewage systems [123]. Ciprofloxacin has been found at amounts of up to 1.4 μg/L in Indian rivers close to pharmaceutical production facilities, and it has also been found in wastewater and surface water [124]. Serious ecological hazards, such as toxicity to aquatic life and, most importantly, the development of antimicrobial resistance (AMR), are presented by the constant discharge of ciprofloxacin and other antibiotics into the environment. AMR is one of the top ten worldwide public health hazards, according to WHO (2021), and if left unchecked, it is predicted to cause 10 million deaths annually by 2050. However, anti-inflammatory medications like cetirizine are frequently used to treat urticaria and rhinitis, among other allergic conditions. Cetirizine is a member of the second-generation antihistamine class, which is well-known for its extensive use and comparatively less adverse effects when compared to first-generation medications. Due to its widespread use among populations, wastewater effluents frequently contain it. Cetirizine is partially unmetabolized and resistant to biodegradation in traditional WWTPs, just like a lot of other anti-inflammatory medications. In water bodies, studies have found it to be persistent at concentrations between tens and hundreds of ng/L [124]. Long-term exposure of aquatic species to cetirizine and related medications can alter ecosystem stability by disrupting biochemical and physiological processes, even though it might not present the same AMR issues as antibiotics. Drugs like ciprofloxacin and cetirizine present a particularly concerning dual challenge: although they are essential in treating bacteria-related illnesses and allergic reactions, their buildup in the environment causes ecotoxicity, upsets the microbial balance, and poses long-term ecological risks. Furthermore, the limitations of current therapeutic approaches are highlighted by the persistence of such medications in natural waters. Only a portion of these contaminants can be eliminated by conventional treatment methods; removal efficiencies have been found to range from 20% to 80%, depending on the substance [125]. Advanced water treatment techniques are being developed in response to these worries. One of the most promising methods for breaking down persistent pharmaceutical pollutants is heterogeneous photocatalysis. Photocatalysis is a process that uses light energy to activate semiconductor catalysts, producing reactive species

(such as hydroxyl radicals) that can degrade complex pharmacological compounds into innocuous byproducts. Novel nanomaterials, particularly MXene-based photocatalysts, which have large surface area, exceptional conductivity, tunable band gaps, and visible-light responsiveness, have been the focus of recent studies [111]. These cutting-edge materials have great potential to solve the ongoing contamination of cetirizine, ciprofloxacin, and similar medications, providing a long-term remedy for the cleanup of the environment. In conclusion, pharmaceutical medications are essential to modern medicine, especially anti-inflammatory medications and antibiotics. However, their extensive use and environmental persistence point to a pressing worldwide issue. In addition to ongoing oversight and regulation, addressing this calls for the use of cutting-edge catalytic materials and treatment techniques that can efficiently break down pharmaceutical contaminants in an eco-friendly manner.

2.2 Pharmaceutical drugs consumption and production – Indian scenario

India is becoming one of the world's top producers and consumers of prescription medications. India's pharmaceutical industry is widely regarded as the "pharmacy of the world" because of its extensive manufacturing of vaccines, active pharmaceutical ingredients (APIs), and generic medications. In terms of pharmaceutical output, India now ranks third globally by volume and fourteenth by value (Kumar et al., 2021) [126]. The nation is a vital component of both national and international healthcare systems, contributing around 20% of the world's generic medication supply and meeting over 60% of the demand for vaccines worldwide (Singh and Sharma, 2020). Population expansion, urbanization, changes in lifestyle, and the increased prevalence of both infectious and non-communicable diseases have all contributed to a sharp rise in pharmaceutical medication use in recent decades on a domestic level. According to IBEF (2022), the pharmaceutical market in India was estimated to be about $42 billion in 2021 and is expected to grow to $65 billion by 2024 and $130 billion by 2030. Analgesics, anti-inflammatory medications, and antibiotics are some of the most often used drug classes; in 2019, India's antibiotic consumption was the largest in the world, surpassing 13 billion defined daily doses (DDD) (Klein et al., 2021) [127-128]. Although this expansion has greatly improved public health, it additionally created issues about the environmental damage brought on by the overuse and frequently uncontrolled use of drugs. According to Larsson et al. (2007), India is one

of the countries that contributes the most pharmaceutical residues to the aquatic environment, especially from drainage of wastewater near pharmaceutical production hubs like Hyderabad and Patancheru. Research has found that Indian rivers and lakes contain significant amounts of antibiotics, such as ciprofloxacin and ofloxacin, sometimes at levels higher than recommended by doctors (Fick et al., 2009) [129-130]. According to Laxminarayan and Chaudhury (2016), such pollution not only endangers aquatic environments but also hastens the emergence of antibiotic resistance, which has grown to be a significant public health concern in the nation. To control pharmaceutical development and its effects on the environment, the Indian govt has taken a number of steps. The legal foundation for drug approval, manufacturing, and quality control is provided by the Act on Drugs and Cosmetics (1940) and its revisions. The oversight of pharmaceutical discharges from industrial clusters has been stressed in more recent guidelines issued by the Ministry of Environment, Forests, and Climate Change (MoEFCC) and the Central Pollution Control Board (CPCB). The enormous volume of production and lax regulation in some areas, however, continue to pose implementation issues (Raghav et al., 2020) [131-132]. Pharmaceutical use in India is not just seen in hospitals and clinics; it also occurs in homes and over-the-counter. The widespread practice of self-medication, especially with regard to antibiotics and painkillers, exacerbates the issue of abuse and environmental pollution (Kotwani and Holloway, 2014). India maintains one of the highest per capita antibiotic consumption rates in the world, which is a result of both accessibility and lax prescription management. With over 3,000 pharmaceutical businesses and 10,500 production facilities, including the most USFDA-approved plants outside of the USA, India's strong manufacturing infrastructure is another factor driving the expansion (IBEF, 2023) [133]. However, a significant portion of India's Active Pharmaceutical Ingredients (APIs), particularly those from China, are imported. Chinese producers supply between 60 and 70 percent of India's bulk medication needs (DoP, 2020). In order to encourage domestic API production, legislative interventions like the Production-Linked Incentive (PLI) Scheme for APIs (2020) were implemented after the COVID-19 pandemic brought attention to the dangers of this dependency. India's pharmaceutical industry was put to the test during the COVID-19 pandemic. On the one hand, India contributed significantly to the

vaccine supply by manufacturing Covishield and Covaxin and exporting vaccinations as part of the "Vaccine Maitri" campaign. However, lockdowns and supply chain interruptions revealed India's reliance on APIs and caused brief shortages of necessary medications. Additionally, drug consumption habits changed, with a rise in the demand for steroids, antibiotics, antivirals, and supplements that increase immunity (Ghosh, 2020) [134-135]. A number of legislative measures seek to solve issues and improve India's pharmaceutical industry: Pharma Vision 2020: To establish India as a world leader in the production of complete pharmaceuticals. Pradhan Mantri Bhartiya Janaushadhi Pariyojana (PMBJP): To supply generic medications at reasonable prices via government-owned pharmacies. The 2020 PLI Scheme for APIs aims to lessen reliance on API imports. In order to reduce pollution, the Bulk Drug Parks Policy (2020) encourages cluster-based production using common effluent treatment facilities (CETPs). Green Chemistry & Sustainable Pharma: Zero-liquid discharge (ZLD) technologies and ecologically friendly medication manufacturing are receiving more attention. Therefore, India is a crucial site for pharmaceutical pollution study despite being a major producer of pharmaceuticals and a major contributor to global healthcare access due to uncontrolled medication use and environmental drug residue release. This dual function as a source of drug pollutants and a supplier of necessary medications emphasizes how urgent it is to create sustainable approaches to drug manufacturing, control, and wastewater treatment [136].

Water is an essential resource for life to exist and for the planet to be known as the "blue planet." There is no denying that water is essential to industry, aquatic life, people, and animals. This renewable energy source has seen significant contamination over the last few decades. Storm water runoff, businesses, and homes are the main sources of water pollution. Oil spills, heavy metals, chemicals, pesticides, littering, herbicides, animal waste, and other sources all emit pollutants into the environment. These industries use around one-third of the freshwater, which causes various pollutants to be released, mostly into the aquatic system [137]. The ecology and ecosystem are significantly impacted by careless disposal, inadequate or incorrect wastewater treatment, and direct material dumping. Iron (Fe), nickel (Ni), and cadmium (Cd). It is impossible to completely eliminate petroleum hydrocarbons, sulfides, arsenic (As), phenolic compounds, and other heavy metals from industrial

chemicals (S. Lokhande et al., 2012; Wang and Yang, 2016) [138]. Pharmaceutical compounds, which can save lives and heal a variety of illnesses, are composed of either natural or manufactured substances. These substances are easily absorbed, persist in the body until they reach their maximum effectiveness, and are active at lower quantities (Mezzelani et al., 2018). Two crucial prerequisites, such as biotic and abiotic variables, determine how well such pollutants may be removed. Even if these substances are found in lower concentrations, long-term exposure can have negative consequences. Thirty to ninety percent of the dosage of a medicine taken by people is excreted as active ingredients in urine [139]. Even after treatment, 90% of the active ingredients are still present in industrial effluents (Ternes, 1998). Antibiotics, NSAIDs, steroids, antidepressants, lipid regulators, hormones, and beta-blockers are among the common pharmaceutical substances found in the environment (Kaur et al., 2016). The majority of these medications end up in fresh and groundwater (Madikizela et al., 2017). In addition to these medications, dialysis centers and labs contribute equally to wastewater treatment (N. A. M.S. Khan et al., 2021) [30].

Even after 28 to 40 years from the date of creation, pharmaceutical medications including antibiotics and analgesics still exhibit up to 90% activity. The release of these medications into the environment in the next decades without adequate treatment could have dangerous consequences for people. (Madikizela and colleagues, 2017). When hospital wastewater is combined with water supplies, it can have detrimental impacts on health. Hospital wastewater treatment facilities are used to treat these effluents eliminate the water's complicated chemical components. Here, sophisticated oxidation techniques like peroxane and ozonation have been employed (Khan et al., 2020a) [140].

One of the main resources for the emergence and continuation of life is "The Water" (Singh et al., 2020). Water sources are severely polluted as a result of increasing industrialization and population growth (Edokpayi et al., 2017; Erkekoglu and Kocer-Gumusel, 2016). Wastewater is discharged from three main sectors: stormwater runoff, industrial, and residential (Kweinor Tetteh et al., 2019; Schoen and Ashbolt, 2010). Pesticides, diseases, insecticides, and other chemicals are carried away from open surfaces by stormwater runoff, which is brought on by severe rain and flooding, and then released straight into surrounding lakes, ponds, and rivers (Bani-Melhem &

Elektorowicz, 2011; Ratola et al., 2012). Cooking and cleaning are the main domestic activities that contribute to wastewater (Das and Acharya, 2003; Jonnalagadda and Mhere, 2001). Color is used to separate household wastewater (Larsen et al., 2015). Feces, detergent, food scraps, and other pollutants are all present in blackwater, the most polluted type of household wastewater. Grey water, which solely contains urine and feces, is the least contaminated type of household wastewater (Al-Jayyousi, 2003). One of the main sources of agricultural wastewater is thought to be surface irrigation (Environmental, 2020; Vymazal, 2009). Water contamination is also a result of rapid industrialization to meet rising demands (Azimi et al., 2017; Mahar and Datta, 2001; Pohl, 2020) [141]. One of the main causes of water contamination nowadays is industry, different types of contaminants distinct from the kinds of industries released in **Table 1.**

Table 1 Principal contaminants found in water from specific industries**.**

S.No.	**Areas of Production**	**Principal contaminants**	**References**
1.	Mill and Agricultural Wastes	Pesticides, fertilizers, phosphorous, nitrogen, and insecticides.	142
2.	The Metal Working Sector	Oil, grease, phenol, ammonium nitrogen cyanide, and perfluorooctane sulfonate (PFOS).	142
3.	The Dairy Sector	Suspended particles, fat, milk residues, proteins, and carbohydrates.	142
4.	Mining Sector	Suspended particles, metals, acids, and salts	142
5.	Animal and Domestic Waste	Soap, fat, detergents, chemicals, plant extracts, and microbes like protozoa.	142
6.	Electronic Sector	Organic chemicals, metals and ores of metals, and COD.	142
7.	Textile and Dye Production	Sulfides, color salts, copper, and	142

	Industries	formaldehyde. Salts, chromium, hydrogen peroxide, iron, urea, and surfactants.	
8.	Canning Sector	Proteins, carbohydrates, and suspended solids	142
9.	Paper & Pulp Sector	Lignin, AOX, Colors, Biocides, Tannins, Sterols, Suspended Solids, Chlorophenolic , and, Organic	142
10.	The petrochemical and pharmaceutical industries	Alkanes, petroleum hydrocarbons, nickel, phenolic chemicals, cadmium, nitrobenzene, and more.	142

Lakes, rivers, and ponds that are close to municipalities are frequently connected to industries. The effluents discharged by the businesses that impact aquatic, animal, and human life damage these drinkable waterways. Organic pollutants found in many of these effluents cause cancer, lung problems, reproductive disturbances, and hormonal imbalances. These pollutants also have an impact on food and the life cycle of the environment. The pharmaceutical business is one of the newer sectors that is polluting the environment [142].

In recent cycles, the level of pharmaceutical compounds in effluents has increased. Rapid contaminant leverage was generated by drug manufacture, the direct dumping of unwanted medications, veterinary care, the use of diagnostic tests, and inappropriate handling of pharmaceutical products. Pharmaceutical compounds are difficult to cure because of their longer half-life and shelf life, as well as their high water solubility. These medications frequently find their way into surface and groundwater areas, lakes, and ponds. Drinking water contains tiny levels of a wide range of pharmaceutical substances, from a few nanograms to milligrams, including hormone-balancing medications, antibiotics, and other pollutants. Recent research indicates that antineoplastic medications are being discharged into aquatic resources at an increasing rate. These medications cause cytotoxicity, mutagenicity, and ecotoxicity when they remain in water bodies [142].

One of the greatest advances in human history was the creation of drugs or medicine. Pharmaceuticals have helped to preserve millions and trillions of individual lives

worldwide, from the earliest modern treatment, morphine, to the most recent COVID medications. Pharmaceuticals are used to treat both humans and animals. The word "pharmaceuticals" refers to a broad category of medications, including prescription medications, symptomatic agents, over-the-counter medications, and nutraceuticals [142]. Now that they have been identified as "Emerging Pollutants," the success report has drawn criticism. The pharmaceutical industry is the primary source of water pollution. The **Fig.9** lists the pharmaceutical medications that are most frequently utilized and released.

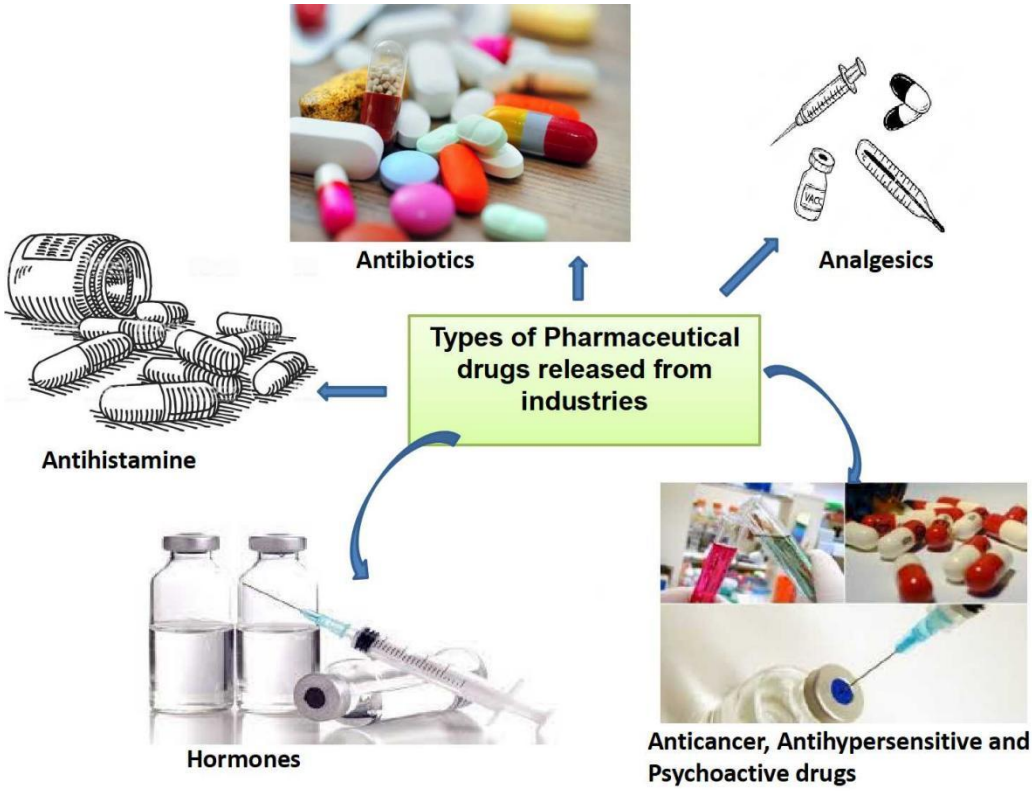

Fig. 9 Different types of pharmaceutical drugs released by the pharmaceutical industries

The range for drug detection in aquatic bodies is limited to ng/L to mg/L. The following characteristics set pharmaceutical pollutants apart from other types of pollutants: Since they are crucial to health, they cannot be limited, they have molecular masses more than 500 Da, they are complex chemical compounds in terms of molecular masses, composition, structure, and functioning, and they are polar

compounds. Properties and ionization degree vary with medium pH. Average water solubility and lipophilic qualities, not readily degradable, hence accumulating in living forms. When taken, it quickly gets absorbed by the system and changes metabolism [143]. In 1970, it was first reported that pharmaceuticals were present in aquatic systems. Due to their untraceable levels, these chemicals did not receive much attention. These substances have been found in practically every region of the world during the last three decades, including the Arctic and Antarctic regions. More than 600 pharmaceuticals are currently recognized as global pollutants [143]. According to research by the University of Gothenburg, a WWTP close to Hyderabad, India, contains about mg/L of various pharmaceutical effluents. The environmental impact of pharmaceutical effluents has not yet been proven. Non-targeted creatures exposed to these substances over an extended period of time have seen moderate side effects, such as metabolic and reproductive abnormalities. Gene-modified Salmonella typhimurium under 5 has demonstrated genotoxic effects from fluoroquinolone drugs [144]. The presence of antibiotics has reduced the capacity of benthic bacteria to nitrify sewage. Antibiotics, specifically erythromycin, amoxicillin, and clarithromycin, are the main causes of sewage system nitrification. Next to antibiotics, endocrine-disrupting chemicals (EDC) are the most widely used substances. Both humans and wildlife are negatively impacted when pharmaceutical medications are present in the environment [145]. These substances lead to cancer, diabetes, obesity, heart disease, and behavioral changes. Heavy metals and aromatic hydrocarbons make up endocrine-disrupting substances, which, when exposed over time, can cause fatal disorders. The complicated structure, function, and lifespan of pharmaceutical drugs make WWTP unprofitable to treat. Approximately 90% of anticancer medications are given to outpatients in Lisbon and Belgium. This demonstrates that domestic wastewater can also play a significant role in contaminating freshwater. Enhancing domestic wastewater treatment facilities is crucial. Numerous anti-cancer medications were found in hospital wastewater. River water samples and wastewater treatment facilities were found to have traces [146]. Pharmaceutical waste is eliminated worldwide using cutting-edge techniques such as chemical advanced oxidation processes, silica-based adsorption, carbon-based adsorption, and bioremediation [146].

2.3. Recent technology for the treatment of pharmaceutical drugs

2.3.1. Physical method

2.3.1.1. Adsorption

Adsorption is a process that primarily entails the phase transfer of chemical compounds from the fluid phase to the surface of solid or liquid surfaces. Active sites on the surface of a solid that has been involved in the adsorption process might use spatial arrangement of particular electron characteristics to create contact between the solute in the aqueous phase. Adsorbents are these kinds of solid materials that offer an absorption surface, and adsorbate is the term for the species that will be adsorbed. The type of the adsorbent and adsorbate, temperature, contact time, pollutant concentration, particle size, pH, existence of other wastes, and specific experiment circumstances are the main variables that can affect the adsorption process. Research pertaining to the application of adsorbents in the elimination of medicine waste from aqueous solutions has demonstrated that hydrophobic medicines, in contrast to those that are hydrophilic. Wastewater is treated using a variety of adsorbents, including zeolite, clays, activated carbon, and industrial wastes like sludge, fly ash, and red mud. A new coral-type MOF-derived $Co@Co_3O_4/C$ nanohybrid has been employed as the adsorbed material in this study. Their potential to treat wastewater has been demonstrated by the treatment of several antibiotics, including tetracycline, sulfonamides, and quinolones [147-149].

2.3.1.2. Carbon-based adsorbents

Adsorbent materials based on carbon include, but are not limited to graphite, activated carbon, and activated sludge charcoal. Coconut shells, lignite, coal, and peat are the sources of these commodities. Most often, activated carbon is utilized in wastewater treatment to remove pharmaceutical compounds. The reason for this is its large surface area and accessibility. Two popular forms of activated carbon are powdered activated carbon and granulated activated carbon, which can be employed in different ways. Numerous investigations have been conducted on the acquisition of activated carbon from diverse sources. Wheat agricultural wastes, olive and cherry stones, sunflower, pecan, and nut shells, corn straw, miscanthus, bagasse, birch wood, rapeseed, pinecone, cotton and olive residues, grape seeds, corn cob and hulls, rice hulls, hazelnut shells, corn stover, rice husk and straw, cotton stalk, etc. are a few examples. The precursor and preparation techniques determine the activated carbon's

properties. Drugs, including ketoprofen, diclofenac, and ibuprofen, can be absorbed from wastewater by activated carbon made from leftover olive cakes. The chemical characteristics of activated carbon determine whether nitroimidazole will adsorb on its surface. This indicates that there are non-electrostatic interactions involved in the adsorption of pharmaceutical substances [150-152].

2.3.1.3. Clays

Clays are naturally occurring materials composed of certain fine-grained minerals. The primary constituents of clays are the silicon-oxygen tetrahedron and the aluminum octahedron, which are hydrous aluminosilicate minerals. Their large specific surface area, increased cation exchange capacity, non-toxic qualities, capacity to absorb various compounds, and economic viability make them suitable for use as adsorbents for the adsorption of medicinal drugs from wastewater. It has been noted that the tricyclic antidepressant amitriptyline is absorbed in the polygonorskite clay. Montmorillonite and kaolinite are absorbed in chloramphenicol, tetracycline, and sulfamethoxazole during the clay mineral dispersion process. The capacity of ibuprofen's adsorption in goethite, kaolinite, and montmorillonite is 2.2 mg/g, 3.1 mg/g, and 6.1 mg/g, respectively. Mefenamic acid, Gemfibrozil, and naproxen absorption in exfoliated vermiculite and lightweight expanded clay aggregates is investigated [153-154].

2.3.1.4. Chitosan

Chitosan is a sugar molecule that is extracted from the tough outer shell of shellfish, including crabs, lobsters, and shrimp. They are utilized in the environmentally acceptable elimination of pharmaceutical wastes due to their unique qualities, which include biodegradability, biocompatibility, and non-toxicity with the adsorption capacity. In certain research, chitosan is grafted or altered before being utilized to adsorb drugs. N-(2-carboxybenzyl) groups are utilized to remove pramipexole dihydrochloride, while carboxyl-grafted chitosan is utilized to remove diclofenac and modify chitosan derivatives crosslinked with glutaraldehyde and grafted with sulfonate [155].

2.3.2. Biological degradation

Due to their cost-effectiveness and process efficiency, biological treatment methods can be used to treat wastewater. These systems are categorized according to the linked

organism's alive state or halted growth. Veterinary medications such as ceftiofur, tetracycline, and enrofloxacin have been eliminated using activated sludge techniques. Other uses for activated sludge include the breakdown of pharmaceutical wastes, including beta-lactam antibiotics, ibuprofen, ketoprofen, naproxen, clofibric acid, diclofenac, mefenamic acid, and others. Disc biofilm reactors, also known as rotating biological contactors, use solid media to support the growth of microorganisms in a static biofilm. A motor and air drive can rotate the disc to aid in the process of diffusion and eliminate waste. Because there is a lot of dry matter present, using this revolving biological contactor makes dehydration easier than using the activated sludge method. Additionally, it is less expensive than sophisticated oxidation or incineration practices [156-157].

2.3.2.1. Advanced chemical oxidation processes

A variety of techniques that work in the aqueous phase and aid in the breakdown of pollutants make up the advanced chemical oxidation process. Strong oxidizing chemicals, such as ozone, iron, peroxide, manganese, and titanium oxide, are employed in this procedure. These agents are frequently coupled with high-energy radiations, like UV irradiation. Subsequently, the generated hydroxyl radicals aid in the contaminants' oxidation. Photolysis, Fenton oxidation, ozonation, heterogeneous photocatalysts, wet air oxidation, catalytic wet air oxidation, electrochemical oxidation, and others are examples of sophisticated chemical oxidation processes [142]. **Fig.10.** UV light contacts with the target molecule during the process of photolysis, which can result in complete mineralization. The molecule may be degraded by a direct or indirect process. The antibacterial compounds that have been handled with the aid of the indirect photolysis technique are trimethoprim and sulfamethoxazole. Then, it was discovered in a different study that exposure to natural sunshine destroyed the sulfamethoxazole. One of the most potent oxidants that can directly or indirectly break down organic molecules is ozone. The ozonation process is the method by which contaminants are treated using ozone. Ozone-assisted pharmaceutical wastewater cleanup is the subject of several investigations. Among these are municipal wastewater, urban wastewater, and so on. The pharmaceutical pollutants such as sulfonamide, estrogen, macrolide antibiotics, and other acidic

medicines such as indomethacin, naproxen, and diclofenac have all been oxidized with the use of the ozonation process [158-160].

Fenton oxidation is a process that creates hydroxyl radicals primarily in the presence of hydrogen peroxide and ferrous or ferric ions through a free radical chain reaction. This reaction is known as a metal-catalyzed oxidation reaction. Pharmaceutical wastewater is treated using Fenton oxidation techniques, which can also be coupled with reverse osmosis, ultrafiltration, and nanofiltration. Drugs containing diclofenac sodium are eliminated via the electro-fenton method. The Fenton oxidation process is used to break down their other medications, which include metronidazole, amoxicillin, ampicillin, diclofenac, and paracetamol 64 [161-162]. The photocatalysis mechanism oxidizes the carbamazepine and ibuprofen in the aqueous solution. Clofibric acid, carbamazepine, sulfamethoxazole, diclofenac, and ofloxacin all decreased their half-lives in the photocatalysis technique in previous tests. The photocatalysis approach was used to reexamine the degradation and mineralization kinetics of carbamazepine and diclofenac. When combined with titanium oxide and cuprous oxide nanoparticles, photodegradation effectively absorbs the antibiotic tetracycline. Titanium oxide and copper-oxide nanotubes have been used to study the photodegradation of various ingested antibiotics. Those antibiotics are cefixime, ciprofloxacin, amoxicillin, and azithromycin. Pharmaceutical contaminants, namely the cytostatic chemical antibiotics, have been removed from wastewater using TiO_2-based photocatalysis, in order for wastewater to be utilized and reused [163-164].

Sulfamethoxazole can be broken down by electrochemical oxidation using the electrochemical technique. Additionally, N-(4-hydroxyphenyl) acetamide can be electrochemically degraded, and atenolol can be anodically oxidized. Wet air oxidation is an option for pharmaceutical wastes that cannot be purified by direct biological purification. Reusing it for crop cultivation and irrigation is another strategy for managing greywater that has been covered in the study [165-166]. Here, surfactant removal has been characterized as the most difficult, and substitute techniques have been suggested.

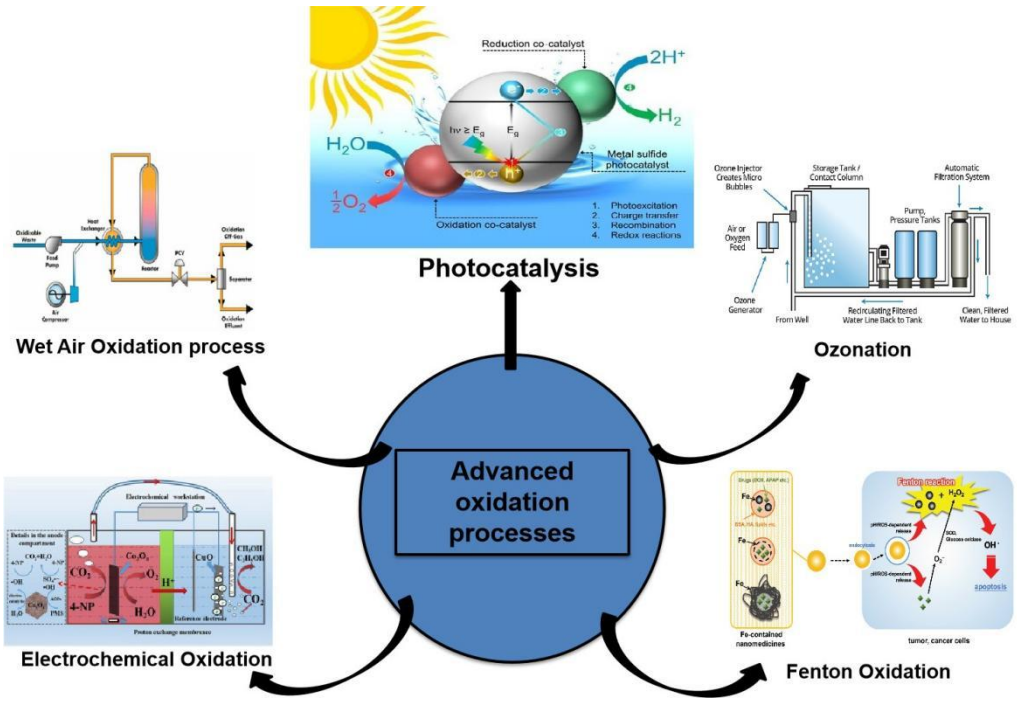

Fig. 10 Various types of Chemical advanced oxidation processes

2.3.2.2. Bioremediation of pharmaceutical wastewater

An important concern was the rising pollution brought on by fast industrialization. Microbes are increasingly being used as a means of removing these contaminants. Microbial degradation is the total breakdown or decomposition of contaminants into water, carbon dioxide, or any other non-toxic molecule. The use of bioreactors is crucial for the efficient growth of the microorganisms in microbiological remediation. The research has shown that Rhodobacter sphaeroides can cure pharmaceutical wastewater that has been supplemented with yeast extract and ammonium sulfate. The microbial consortium produces the enzyme laccase, which is utilized in the bioremediation of pharmacological treatments. Pharmaceutical wastewater from several locations in Tamil Nadu was gathered for a study, and microbial consortia comprising the following bacteria were formed and employed for treatment. The results showed a significant impact. Pseudomonas fluorescens, Bacillus subtilis, Pseudomonas putida, Bacillus megaterium, Bacillus pumilis, Aspergillus niger, Nitrobacter, Bacillus licheniformis, Nitrosomonas, and Rodococcus are among the

microorganisms. For the biodegradation of cyclophosphamide and etoposide, P. chrysosporium, G. lucidum, and T. versicolor are employed [167-168].

2.3.2.3. Mycoremediation

Mycoremediation is the term for the use of fungi to remediate wastewater. Fungi are employed in this technique to break down wastewater, and they are particularly useful in the elimination of pharmaceutical wastewater. Fungi's mycelium is essential to the mycoremediation process, which allows the fungus's mycelium to perform the breakdown process. Both filamentous and macrofungi are capable of mycoremediation. Aspergillus fumigatus, Aspergillus niger, and Aspergillus niveus are examples of fungal species that can be employed to remove pharmaceutical pollutants. The fungus Ascomycetes is capable of eliminating contaminants from industrial effluent [169]. Humic acid and tannic acid can be eliminated by the white rot fungus; filamentous fungi, such as basidiomycetes, are also utilized to cure a variety of other drug enzymatic alterations. The use of fungus to remediate pharmaceutical pollutants offers benefits over alternative techniques due to its high efficacy, affordability, and safety for the environment [170].

2.3.2.4. Phytoremediation

Phytoremediation is the process of using plants to clean up wastewater. Through processes including rhizoremediation, degradation, violation, and stabilization, the plants can eliminate the chemical pollutants; after that, mineralization may occur. Willow and alfalfa are the plants that have been utilized [171]. This method is incredibly economical and eco-friendly, as plants aid in the breakdown of harmful substances. This is mostly due to some plants' innate capacity to bioaccumulate pollutants and break them down in a way that is safe. The primary goal of phytoremediation is to rid the environment of dangerous heavy metals and organic pollutants [170]. Acetaminophen, ibuprofen, and diclofenac are among the medicinal substances that can be broken down by plants like Hordeum vulgaris, Lupinus albus, and Phragmites australis. Water hyacinth, commonly known as Eichhornia crassipes, can be utilized to remove colors used as analytical markers in the pharmaceutical business [172].

2.3.3. Other techniques

2.3.3.1. Bioventing

One technique for the biodegradation of organic contaminants from wastewater is called bioventing. This method aids in the biodegradation of hydrocarbons and increases the activity of endogenous bacteria and archaea. The process of "bioventing" uses anaerobic degradation to increase the oxidation of pesticides, organic hydrocarbons, and other contaminants [142].

2.3.3.2. Bioleaching

A technique that uses bacteria to extract low-quality minerals and ores from metals. Certain bacteria, like Thiooxidants and Thiobacillus ferrooxidans , are employed to transform insoluble metal sulfides into metal sulfates. The primary purpose of this technique is to remove heavy metals [142].

2.3.3.3. Bioaugmentation

By adding genetically modified bacteria with complex catabolic capabilities, this approach increases the effectiveness of the microorganisms and, consequently, the pace of degradation. By using a progressive approach to effectively remove contaminants, the addition of specific microbial strains to the wastewater bioreactor aids in the enhanced breakdown of particular compounds. This procedure primarily uses two strategies: bioaugmentation using both native and non-native microorganisms [142].

2.3.3.4. Biostimulation

The process by which nutrients, electron donors, or electron acceptors are spontaneously inserted into microorganisms to activate them is known as biostimulation. This procedure is mostly used to boost the bacteria's ability to degrade by adding nutrients, altering other limiting variables, or making certain alterations [142].

2.3.3.5. Biosparging

Biosparging is a technique that breaks down organic components by using microorganisms. The saturated zone has been supplied with nutrients and air to increase the bacteria's biological activity. This procedure is comparable to venting, which involves both injecting air and promoting microbial activity [142].

2.4. Pharmaceutical removal using nanotechnological methods

Pharmaceutical chemicals' persistence, capacity for bioaccumulation, and detrimental effects on the environment and human health have made their presence in aquatic

systems a major environmental problem on a global scale. Pharmaceuticals, especially analgesics, antibiotics, and anti-inflammatory medications, are commonly found in hospital effluents, municipal wastewater, and even supplies of treated drinking water. Their stable chemical structures, which are made to withstand metabolic breakdown, frequently make it difficult to remove them effectively using traditional treatment technologies such as activated carbon adsorption, coagulation–flocculation, or biological oxidation. These conventional techniques typically result in only partial removal, leaving behind quantities that could still be extremely dangerous to ecosystems and public health [173-174].

Nanotechnology has been a cutting-edge field in water treatment research in recent years, offering new possibilities for the effective elimination of drug residues. Nanomaterials are very promising for the removal of contaminants because of their remarkable physicochemical characteristics, which include high specific surface area, improved reactivity, adjustable electronic band structures, and the capacity to be functionalized with different active groups [175]. Pharmaceutical compounds can be efficiently adsorbed using nanotechnological techniques, which also facilitate catalytic and photocatalytic breakdown, leading to full mineralization into innocuous products such as water, carbon dioxide, and inorganic ions [176]. Nanotechnology-based methods offer paths for both elimination and destruction, which represents a paradigm shift in the treatment of pharmaceutical wastewater, in contrast to traditional adsorbents that mainly transfer contaminants from one medium to another.

2.4.1 Advanced oxidation process for photocatalysis

An innovative group of water and wastewater treatment methods known as advanced oxidation processes (AOPs) is intended to efficiently break down organic contaminants, refractory compounds, and various other challenging materials. At the molecular level, AOPs target and degrade complex pollutants by producing highly reactive species, especially hydroxyl radicals, which transform them into simpler, frequently less hazardous molecules. This change is accomplished by a number of processes, including Fenton's reagent, hydrogen peroxide, ozone, and UV light [177]. AOPs are known for providing high-quality water treatment in an efficient manner. They are particularly important when conventional techniques are insufficient, especially when it comes to eliminating medications, agricultural pesticides, and

various industrial pollutants. The fundamental characteristic of AOPs is their capacity to produce extremely reactive species, particularly hydroxyl radicals (•OH). These radicals provide a flexible answer to the intricate issue of industrial wastewater pollution since they can react quickly with a variety of contaminants [178]. Because of the variety and complexity of harmful substances created by the pharmaceutical, dye, and agricultural industries (such as heavy metals, bio-accumulative chemicals, and non-biodegradable compounds), AOPs are unique in their ability to handle several contaminants at once [177-178]. AOPs' applicability in several environmental conditions is demonstrated by their efficacy in addressing particular contaminants. These pollutants include pesticides, which degrade water quality and biodiversity; pharmaceutical residues, which are persistent in the ecosystem; and the colorful waste products from dye companies, which are notable for their high demand for chemical oxygen (COD) and presence of hazardous compounds and heavy metals [179]. It has been demonstrated that AOPs efficiently break down complicated dye molecules into smaller, less dangerous substances. By mineralizing organic contaminants, they can drastically lower COD and lessen the negative impacts of pesticides and pharmaceuticals on both terrestrial and aquatic ecosystems [179]. There are numerous AOP methods accessible, such as photocatalysis, Fenton's reagent, hydrogen peroxide with UV radiation, ozonation, and electrochemical oxidation **Fig.11**. These techniques can be modified to target particular pollutants in a range of environmental circumstances, and each uses a unique process to produce hydroxyl radicals. As an illustration, photocatalysis employing titanium dioxide, or TiO_2, under UV light is especially successful in eliminating pharmaceutical chemicals and organic wastewater [179]. Identifying the best AOP technique and having a thorough grasp of the chemical makeup of the pollutants are essential for effectively utilizing AOPs to reduce environmental pollution. To further move toward an environmentally friendly industrial practice, elements including the energy needs of AOP systems, operational expenses, and the environmental effects of the waste products of degradation must be carefully taken into account [179].

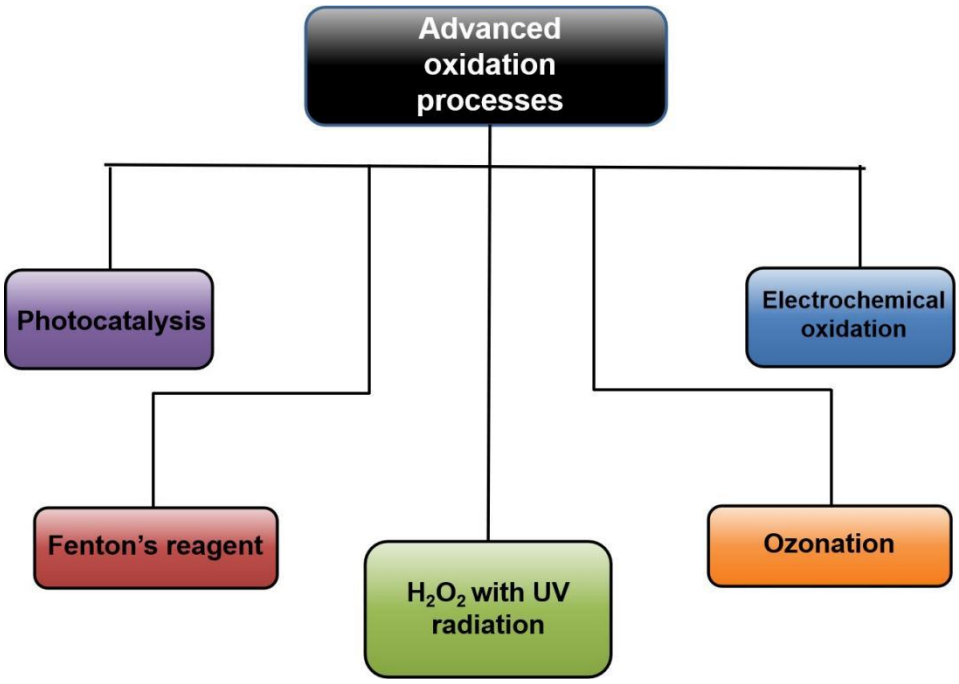

Fig. 11 Numerous AOP methods

2.4.2. Photocatalysis mechanism

As it can use light energy to break down persistent organic pollutants like pesticides, industrial effluents, and pharmaceutical residues, photocatalysis is one of the most researched advanced oxidation processes (AOPs). The fundamental idea behind photocatalysis is the special ability of semiconductor materials to produce highly reactive species that can mineralize complicated organic molecules into innocuous byproducts when activated by light. The idea of semiconductor-generated photocatalysis has been widely developed and used in environmental remediation since the important research (2017), which showed how water can photolyze on photocatalyst electrodes in **Fig.12** [180]. When photons with energies equivalent to or higher than a semiconductor material's band gap energy are absorbed, the photocatalytic process starts. A positively charged hole is left in the valence band after an electron is promoted from the valence band to the conduction band by this photoexcitation. Light energy is essentially transformed into chemical potential through the formation of electron–hole pairs, which serve as the main carriers of charge for ensuing redox processes. Because the positively charged hole in the

valence band causes oxidative reactions and the excited electron in the conduction band can engage in reductive pathways, these charge carriers are the engine of the entire photocatalytic process [181-182]. The general effectiveness of photocatalysis is determined by what happens to the electron-hole pairs after they are created. In an ideal world, these charge carriers would move to the photocatalyst's surface and engage with species that are absorbed, such as dissolved oxygen, hydroxide ions, or water molecules. Because the holes are potent oxidizers, they can draw electrons away from water or surface hydroxyl groups, producing hydroxyl radicals (•OH). In aqueous environments, hydroxyl radicals are thought to be the most potent oxidizing agents due to their high redox ability and non-selective reactivity with a wide variety of organic molecules. However, the conduction band's photogenerated electrons have the ability to decrease dissolved oxygen species, which can result in the generation of radicals of superoxide anion and, consequently, additional ROS, or reactive oxygen species, such hydroperoxyl and hydrogen peroxide radicals. These reactive species work together to create a chain reaction of oxidative agents that actively target the molecules of pollutants [183-184]. It is also important to consider how these reactive species interact with medicinal substances. Pharmaceuticals are resistant to traditional treatment methods because they frequently contain heteroatoms, halogen replacements, and aromatic rings. However, the hydroxyl radicals, as well as ROS, can hydroxylate aromatic rings, break chemical bonds, and start oxidation pathways under photocatalytic conditions, which eventually reduce the parent molecules to smaller intermediates. After undergoing additional oxidative changes, these intermediates eventually mineralize into inorganic ions, carbon dioxide, and water. Even extremely stable medications that remain in natural waters, including fluoroquinolones & non-steroidal anti-inflammatory medicines (NSAIDs), can frequently be efficiently broken down in photocatalytic AOP conditions (Ahmed & Haider, 2017) [185]. Despite its potential, photocatalysis is a dynamic interaction of excitation, charge carriers production, transfer, and surface reactions rather than a straightforward one-step procedure. The recombination of electron-hole pairs is a significant bottleneck in this mechanism. Instead of being used for chemical processes, the absorbed radiation from photons is released as heat or light when recombination takes place. The photocatalytic process's quantum efficiency is greatly reduced by this

recombination. Numerous approaches, including surface functionalization, heterojunction creation, doping with metals or nonmetals, and coupling with nanomaterials based on carbon, like graphene and MXenes, have been explored to overcome this difficulty. These changes lengthen the lifespan of photogenerated charge carriers, improve charge separation, and boost the absorption of light into the visible spectrum (Chen et al., 2010; Saafie et al., 2022) [186-187]. The function of the catalyst surface is another essential component of the photocatalytic action. Before any oxidative reaction may take place, contaminants frequently first adsorb onto the photocatalyst surface. Important factors that determine the degree of adsorption and, in turn, the degrading efficiency include a large surface area, a large number of surface functional groups, and an appropriate surface charge. For example, some anionic medications may be repelled by negatively charged photocatalyst surfaces, while electrostatic attraction may increase adsorption on positively charged surfaces. Accordingly, surface chemistry tailoring is essential to guaranteeing effective photocatalytic drug removal [184].

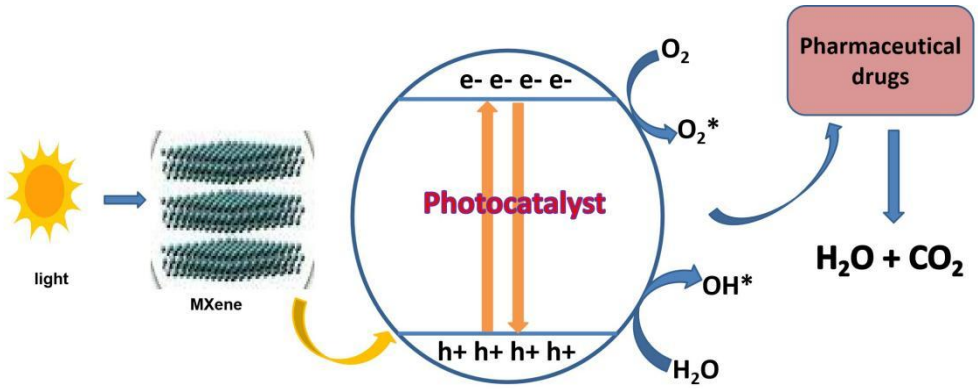

Fig. 12 General Mechanism of Photocalysis

The light source has a significant impact on the photocatalytic mechanism as well. Conventional catalysts like TiO_2 only activate when exposed to UV, which makes up just around 5% of the spectrum of sunlight, due to their broad band gap of ~3.2 eV. The practical use of photocatalysis in solar-powered environmental cleaning is

severely limited by this restriction. To get around this, visible-light-driven photocatalysts have been produced by the creation of heterostructures with comparable band alignments or the shrinking of the band gap. Examples of designed photocatalysts that exhibit high activity under visible light irradiation include ZnO, doped TiO_2, g-C_3N_4, and MXene and their composites. These materials make them more feasible for use in practical applications [186, 188]. Moreover, complicated reaction paths involving several intermediates are frequently followed in the photocatalytic breakdown of medicines. The necessity of keeping an eye on both primary deterioration and ultimate mineralization is highlighted by the fact that these intermediates might occasionally be more hazardous or persistent than the parent chemical. To identify intermediate compounds and assess the safety of photocatalytic treatment, sophisticated analytical methods like mass spectrometry with gas chromatography (GC–MS), liquid chromatography combined with mass spectrometry (LC–MS/MS), and HPLC, or high-performance liquid chromatography, are frequently used. The ecologically sustainable use of photocatalytic AOPs can only be guaranteed by full mineralization, or at the very least, conversion into non-toxic byproducts (Ahmed & Haider, 2017) [185]. In conclusion, the sequential processes of light absorption, charge carrier development, redox reactions at the catalytic surface, and the production of reactive oxygen species that target and mineralize medications comprise the mechanism of photocatalytic AOPs. The light source, surface adsorption, charge carrier recombination, and band gap energy all have a significant impact on this mechanism's efficiency. These restrictions are being addressed by ongoing developments in catalyst development and procedure optimization, which make photocatalytic AOPs is the most promising approaches for the environmentally friendly removal of pharmaceutical wastewater.

2.4.3. Properties of photocatalyst

The efficiency, stability, and general efficacy of the photocatalytic reaction for energy conversion or environmental remediation applications are all determined by the materials chosen for photocatalysts in photocatalytic processes. Using the energy of light to speed up a chemical reaction, photocatalysis has demonstrated significant potential in tackling a number of environmental issues, such as CO_2 reduction, H_2 splitting, and wastewater treatment [189]. Several essential characteristics of the

perfect photocatalyst material include high chemical stability, appropriate band gap energy, non-toxicity, cost-effectiveness, and great light absorption.

2.4.3.1. Band gap energy

The building of high-performance, effective photocatalytic systems is supported by the crucial role that band gap energy plays in the selection of photocatalyst materials. The transformation of light energy into chemical energy, which is used to catalyze a range of processes, is the fundamental component of photocatalysis, an inventive and environmentally friendly technique [190]. These reactions can break down contaminants in the environment or split water molecules to create hydrogen, a clean fuel. The idea of band gap energy is essential to comprehending the operation of photocatalysts. The energy needed to transfer an electron from the valence band to the conduction band is known as a material's band gap energy [190]. An electron must cross this gap between energy levels in order to engage in conduction. Because it establishes a material's capacity to light absorption and promote the movement of electrons and holes required for chemical processes, this characteristic is essential. The wavelength of the light that the photocatalyst can absorb is determined by the bandgap energy. The energy from the light that enters must be at least equivalent to the photocatalyst material's bandgap energy in order to stimulate the photocatalyst and initiate the photocatalytic reaction. Thus, choosing a material with the right bandgap energy is crucial to effectively using the necessary range of the solar spectrum or alternative sources of light [191-192].

2.4.3.2. Surface area

In energy and environmental applications, a photocatalyst's surface area is essential for increasing its efficacy and efficiency. More active sites, improved light absorption, efficient charge transfer, and increased photostability are all benefits of a large surface area [193]. Together, these elements enable photocatalysts with greater surface areas to catalyze reactions more successfully, making them essential for procedures like air and water purification and the generation of renewable energy. Therefore, maximizing surface area is a primary goal in the creation of photocatalytic materials.

2.4.3.3. Separation and Transfer of Charge Carriers

Crucial factors are the locations of the VB and CB in relation to the reactants' redox potential. In essence, the potential of the produced electron-hole pairs is influenced by

the bandgap energy. In order to decrease the reactant, electrons need to have enough negative potential, and in order to oxidize the reactant, holes need to have enough positive potential. Before the charge carriers may take part in the photocatalytic activity, recombination must be avoided through effective charge carrier (electron and hole) separation and conveyance. It is very desirable to have material have high charge carrier mobility and surface characteristics that are tailored to encourage charge separation [194]. The types of chemical processes that the material can catalyze are therefore greatly influenced by the bandgap energy.

2.4.3.4. Stability

For photocatalysts to be efficient and long-lasting in environmental applications, material stability is essential [194-196]. It guarantees that under a range of circumstances, including temperature changes, pH variations, and the presence of hostile chemicals, photocatalysts retain their structure and performance. Reusable materials improve sustainability and lower costs because they can be used repeatedly. A photocatalyst's chemical and structural strength under the circumstances of the photocatalytic activity is crucial to its long-term efficacy [195-196]. Over several photocatalytic cycles, materials should retain their structural integrity and be resistant to corrosion and photocorrosion. Stable photocatalysts are also necessary for the selective elimination of contaminants without the release of hazardous byproducts, improving process safety and environmental friendliness.

2.4.3.5. Economic and environmental aspects

For a photocatalytic material to be called ecologically friendly, it is vital that the materials utilized are non-toxic. This is important because the primary objective of using photocatalysts is to clean and purify the ecosystem, not to add to pollution [197]. Non-toxicity guarantees that the photocatalyst itself won't break down or release hazardous materials that could release more contaminants into the environment while the contaminants are being broken down [194-197]. This is especially important for applications that purify air and water, where the highest possible level of purification in the finished product is required. Because of their stability and non-toxicity, materials like (TiO_2) are frequently cited as the best photocatalysts [198]. On the other side, cost-effectiveness is crucial to ensuring that photocatalytic technologies are viable and accessible for broad application. It is impossible to overestimate the

importance of the economy; in order for a technology to be widely accepted, it must be within the means of small communities and developing nations, in addition to huge businesses [197-198]. Because of this accessibility, the advantages of photocatalytic technologies like cleaner air, filtered water, and the decomposition of organic pollutants are available everywhere and are not just limited to wealthier countries or organizations [197-198]. From self-cleaning surfaces to more effective water purification systems, more creative applications and solutions can result from the use of inexpensive photocatalyst materials. Photocatalyst materials must be non-toxic to prevent further environmental contamination and cost-efficient to ensure widespread accessibility and adoption if they are to be truly effective and have a positive global impact. When taken as a whole, these elements will guarantee that photocatalytic technologies can serve as a vital component in the endeavor to reduce pollution and advance a healthier, cleaner environment [197-198].

2.4.4. Common nanomaterials for pharmaceutical drug removal

Single-dimensional, two-dimensional sheets (MXenes), three-dimensional nanocomposites, and zero-dimensional nanoparticles are all included in the broad category of materials known as nanomaterials. Because of their high density of reactive sites and distinctive quantum confinement effects brought about by their nanoscale dimensions, they interact with pharmaceutical pollutants much more effectively [199]. The capacity of metal and metal oxide nanoparticles to adsorb and break down medicinal substances has been well studied. For instance, because of their potent oxidizing capacity, stability, and lack of toxicity, titanium dioxide (TiO_2) nanoparticles continue to be the most researched photocatalysts. Under UV light, TiO_2 is very effective at breaking down medications like ciprofloxacin [200-201]. TiO_2's wide band gap (~3.2 eV), which limits its activity mostly to ultraviolet light and accounts for just ~4% of solar energy, is its drawback. Its responsiveness has been extended into the visible area by modification of the surface and doping with metals (Ag, Cu) or non-metals (N, C) in order to get around this [202]. Similar to this, zinc oxide (ZnO) nanoparticles have superior photocatalytic abilities against pharmaceutical pollutants. They also have higher mobility of electrons than TiO_2 and are less expensive [203]. Non-steroidal anti-inflammatory medications (NSAIDs) like ibuprofen and diclofenac are particularly well-degraded by ZnO; nonetheless,

problems with photocorrosion and decreased stability under extended exposure to radiation must be addressed [204]. Iron-based nanomaterials, namely iron oxides and FeO_4 nanoparticles, are used extensively because of their magnetic and redox properties, which make recovery from treatment simple. Pharmaceutical pollutants have been removed using magnetic FeO_4 nanoparticles as adsorption agents and as catalysts in Fenton-like reactions [205]. Iron-based nanomaterials have been shown to have synergistic effects when added to composites containing carbon or semiconductors, increasing stability and catalytic activity [205]. Another important class of nanomaterials in the treatment of pharmaceutical wastewater is carbon-based. Pharmaceuticals like ciprofloxacin, and sulfamethoxazole have demonstrated a remarkable affinity for carbon nanotubes (CNTs) due to their high adsorption capacity and capability to be modified with carboxyl, hydroxyl, or amine groups [206]. For the adsorption of medicinal compounds, graphene oxide (GO) and reduced graphene oxide (rGO) also offer a large number of hydrogen bonding sites, electrostatic attractions, and π–π interactions [207]. Furthermore, it has been demonstrated that combining materials made from graphene with photocatalysts (such as TiO_2 and g-C_3N_4) increases electron mobility and decreases electron–hole recombination, which in turn promotes photocatalytic degradation [208]. New avenues for pharmacological elimination have been made possible by recent developments in two-dimensional (2D) nanomaterials, especially MXenes. MXenes are effective adsorption agents and co-catalysts for photocatalytic structures due to their hydrophilicity, variable interlayer spacing, and metallic conductivity [209]. They can interact strongly with medicinal compounds thanks to their termination of the surface groups (-O, -OH, and -F), and they work very well with semiconductors because they can transport electrons quickly [210]. For example, under visible light, MXene–semiconductor composites have shown improved photocatalytic degradation of antibiotics [210]. Similarly, another new material that has shown promise in visible-light-driven photocatalysis is graphitic carbon nitride (g-C_3N_4), a metal-free polymeric semiconductor with a band gap of about 2.7 eV [210].

2.4.5. MXene as a photocatalyst

Two-dimensional (2D) nanomaterials have become a more popular target in the hunt for highly effective, stable, and scalable photocatalysts for pharmaceutical elimination

and water purification because of their favorable high surface-to-volume ratio, charge transfer kinetics, and variable surface chemistry. MXenes are a class of early transition metal carbides, nitrides, and carbonitrides that have garnered a lot of interest in environmental remediation [211]. They have the general formula $M_{n+1}X_nT_x$, where M is an early transition metal like Ti, V, or Mo, X is carbon and/or nitrogen, and T_x stands for surface functional groups like –OH, –O, and –F. **Fig.13** shows that applications for MXenes in energy storage, electromagnetic shielding, catalysis, and more recently, photocatalysis, have been thoroughly investigated since their discovery in 2011 [212].

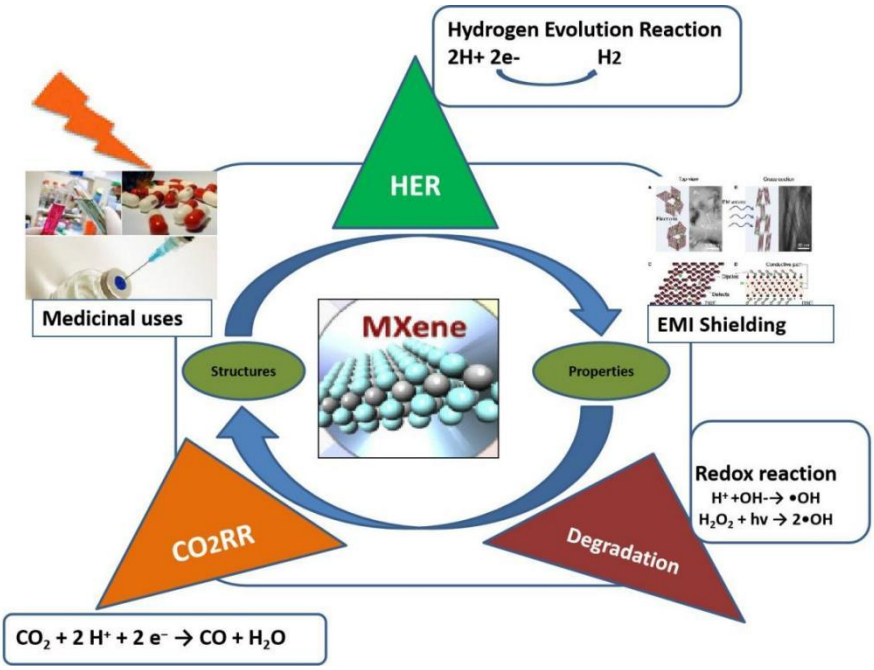

Fig. 13 Applications of MXene as a photocatalyst

2.4.5.1. Surface and structural characteristics of MXenes associated with photocatalysis

The layered 2D structure of MXenes, which is comparable to graphene and offers a significant reactive surface area for absorbing pollutants and reactivity, is one of its distinctive characteristics [213]. Additionally, the hydrophilicity introduced by surface terminations (T_x groups) improves their dispersion in aqueous solutions, which is very beneficial for photocatalytic wastewater treatment. These functional

groups operate as active sites for the production of reactive oxygen species (ROS), in photocatalysis in addition to enhancing pollutant adsorption [213]. Their metallic conductance, which is significantly higher than that of the majority of conventional semiconductors (such as TiO_2, ZnO, and g-C_3N_4), is another significant feature. By reducing the recombination of photogenerated charge carriers, a crucial bottleneck in photocatalysis, MXenes' conductivity allows them to function as superior electron mediators [214]. MXenes are reactive to visible radiation because their bandgap can be adjusted through doping, surface changes, or composite synthesis [112].

2.4.5.2. MXene-assisted photocatalysis mechanism

MXenes' partially metallic nature and adjustable bandgap allow them to function directly as photocatalysts in a stand-alone system when exposed to visible light. They more frequently act as co-catalysts in semiconductor-derived systems, creating Schottky or heterojunctions. MXenes reduce recombination and increase the lifespan of charge carriers in these situations by trapping electrons from the semiconductor's conduction band [215]. This makes it easier for ROS, such as •OH and O_2•− to form, which target and break down pharmaceutical contaminants into smaller, less dangerous intermediates and ultimately CO_2 and H_2O. Furthermore, because of their layered shape and 2D structure, MXenes offer an advantageous framework for interfacial charge transfer. For instance, it has been well documented that $Ti_3C_2T_x$ MXene may take up electrons from semiconductors such as $BiVO_4$ or g-C_3N_4, resulting in increased photocatalytic activity [216]. Furthermore, doping MXenes with rare-earth ions or transition metals (such as V, La, or Ce) increases their optical absorbance and adds more catalytically active sites, which raises their photocatalytic effectiveness even further [217].

2.4.5.3. Photocatalysts based on MXene for the degradation of pharmaceuticals

Pharmaceuticals that persist in water and have the potential to cause antimicrobial resistance, like antibiotics (like ciprofloxacin and tetracycline) and anti-inflammatory medications (like cetirizine and ibuprofen), are classified as pollutants of increasing concern. Their removal frequently requires sophisticated techniques like photocatalysis because conventional treatment methods are insufficient. Photocatalysts based on MXene have demonstrated exceptional promise in this regard. Due to MXene's strong conductivity, which encouraged charge separation and

pollutant adsorption, $Ti_3C_2/BiVO_4$ composites, for example, showed considerably improved visible-light degradation of ciprofloxacin [218, 112]. Likewise, La^{3+} ions in MXene/La composites acted as electron traps and changed the band structure to boost visible-light absorption, increasing the breakdown efficiency of tetracycline. A further study found that the synergistic effects of vanadium doping, which reduced the bandgap and enhanced ROS production, led to higher ciprofloxacin degradation performance in vanadium-modified MXene. MXene-based composites have been used to degrade dyes and endocrine-disrupting substances in addition to antibiotics, indicating their wide range of applications in environmental cleanup. $Ti_3C_2/g\text{-}C_3N_4$ nanocomposites, for instance, demonstrated enhanced degradation of rhodamine B and bisphenol A under visible light, demonstrating MXenes' ability to work well with polymeric semiconductors [219, 112].

2.4.5.4. Advantages of MXene-based photocatalysis

When compared to conventional semiconductor photocatalysts, MXenes have a number of clear benefits [220]. Better charge separation is made possible by high conductivity, which facilitates effective electron transmission and trapping. Surface functionalization, the presence of -O, -OH, and -F groups, promotes the generation of ROS and the adsorption of pollutants. Layered 2D morphology: Offers a large number of active sites and keeps composite photocatalysts from clumping together. For effective wastewater treatment, hydrophilicity is essential because it guarantees good dispersibility in watery conditions. Surface alterations, hybridization, and doping can all be used to manipulate the bandgap and catalytic activity. Because of these special qualities, MXenes are very flexible substrate for creating next-generation photocatalysts designed for the elimination of pharmaceuticals.

2.4.5.5. Outlook and challenges

MXenes have a lot of potential, but their actual use in photocatalysis is limited by a number of issues. Stability and activity may be diminished by MXene nanosheet oxidation in ambient settings. Charge transmission is hampered by MXene sheets' propensity to restack, which reduces the available surface area. Furthermore, there are safety and environmental issues with the scalability of MXene synthesis techniques, especially when using dangerous etchants like hydrofluoric acid [220].

Developing scalable and environmentally friendly synthesis methods, oxidation-resistant stabilization techniques, and creating multi-component composites (such as MXene–metal oxide–polymer hybrids) that combine the advantages of several materials are some future research avenues. Furthermore, using in situ spectroscopic methods to investigate the molecular mechanisms of photocatalysis will shed further light on MXenes' function in photocatalysis.

2.5. Modification of MXene photocatalysts

MXenes are very appealing for photocatalytic applications because of their exceptional inherent qualities, which include hydrophilicity, layered 2D shape, programmable surface terminations, and high electrical conductivity. However, pristine MXenes rarely have the full set of characteristics needed to function as long-lasting, high-performance photocatalysts in actual wastewater environments, as is the case with most emerging materials. Researchers have created a wide range of modification techniques to overcome restrictions such as surface oxidation, restacking of nanosheets, limited visible-light absorption (for specific compositions), and the requirement for efficient charge separation and stability. This section provides a thorough assessment of those modification techniques, evaluates how they affect photocatalytic behavior (particularly pharmaceutical degradation), and identifies open research questions and problems [221].

The necessity of modification must be stated before moving on to modification strategies. $Ti_3C_2T_x$ and other pristine MXenes are outstanding adsorbents and electrical conductors, but they are not well-suited as stand-alone semiconductor photocatalysts. The following factors may affect photocatalysis: some MXenes exhibit metallic or semi-metallic properties instead of the ideal semiconductor band structure. Surface oxidation (the creation of TiO_2 or other oxides) can alter active sites in an unpredictable manner. Nanosheet restacking decreases the accessible surface area, and recovery and reuse in powder form may present challenges. Thus, specific changes are intended to reduce charge recombination through heterojunctions or electron-sink, behavior enhance the surface area and active site accessibility, enhance stability towards oxidation and photocorrosion, impart functionality for realistic reactor designs (e.g., immobility on supports or membranes) and construct or adjust an appropriate band structure for visible-light activity [222]. The most

promising paths to achieving these goals are composites and manufactured heterostructures, according to reviews and experimental research.

2.5.1. Surface termination and functionalization

Surface terminations (-O, -OH, -F, and others) control the adsorption behavior, surface acidity/basicity, and hydrophilicity of MXene. Controlling terminations by means of post-synthesis procedures (chemical functionalization, alkaline washing, or thermal annealing) might affect interfacial transfer of charges to co-catalysts and customize their attraction for target pollutants. An increase in -O/-OH content, for instance, typically improves hydrophilicity and adds additional hydroxyl groups that can serve as locations for the production of hydroxyl radicals during photocatalysis. On the other hand, too many -F terminations can limit the availability of active sites and impede electron transmission. Photocatalytic interactions and adsorption affinities for medicines have been tuned using thermal or chemical treatments that substitute –F with –O/–OH or graft organic groups. Although such tuning enhances performance, stability must be balanced because harsh treatments may cause the MXene lattice to partially oxidize (produce TiO_2), which alters the behavior of the material. Pharmaceutical applications: By increasing the adsorption of polar drugs (such as cetirizine and ciprofloxacin) through hydrogen bonds and electrostatic interactions, enhanced surface -OH groups bring contaminants closer to reactive sites for effective ROS-mediated degradation [211-212].

2.5.2. Delamination and intercalation

Van der Waals forces cause MXene nanosheets to restack strongly, limiting their observable surface area and impeding mass movement. The interlayer spacing is increased, and delamination into few-layer flakes is facilitated by the intercalation of organic ions, molecules, or polymeric spacers (such as DMSO, urea, or polyvinyl alcohol). More accessible active sites and better aqueous pollutant transport are provided by wider interlayer spacing. In composite photocatalysts, intercalation can also establish ion-transport channels that facilitate charge separation. Compared to their restacked counterparts, intercalated MXenes exhibit greater adsorption capabilities and quicker photocatalytic breakdown rates for model medicines. However, because many intercalants may hinder active sites or evaporate away during long-term operation, they must be carefully chosen [219-222].

2.5.3. Fabrication of heterojunctions using semiconductors

The most common method for transforming MXenes, being passive conductors or adsorbents into extremely effective photocatalytic materials, is to form heterojunctions using conventional semiconductors (such as TiO_2, g-C_3N_4, $BiVO_4$, CdS, and V_2O_5). Numerous heterojunction architectures are employed, including: Band alignment in type-II heterojunctions encourages the spatial separation of charge carriers between two semiconductors. In order to accept electrons from the semiconductor and stop recombination, MXene frequently serves as an electron mediator. Schottky junctions, when metallic MXene and a semiconductor make a Schottky contact, electrons are trapped at the metal interface, extending the carrier lifespan [219-221]. Z-scheme and S-scheme heterojunctions are designed to preserve high-energy electrons and holes for redox processes while promoting the recombination of low-energy carriers, thus maintaining strong redox potentials. In terms of breaking down resistant organics, current MXene–semiconductor Z-scheme composites have demonstrated exceptional performance. For instance, Ti_3C_2–$BiVO_4$ and Ti_3C_2–g-C_3N_4 composites show how MXene layers move photogenerated electrons from the semiconductor to oxygen, enhancing the production of reactive oxygen species (ROS) and speeding up the breakdown of medicines like ciprofloxacin. The heterojunction method takes advantage of MXene's strong conductivity for charge transport while also extending light absorption (by the semiconductor). When treating low-concentration medications where photon consumption must be optimized, heterojunctions significantly lower bulk recombination and raise surface reaction rates [211-222].

2.5.4. Elemental substitution and doping

Doping MXenes or their companion semiconductors with nonmetals (N, S) or transition metals (V, Fe, Co, La) can produce oxygen vacancies that function as active catalytic centers, tune band energetics, and introduce mid-gap states. Vanadium-doped MXenes, for instance, boost the formation of ROS by introducing defect sites and increasing the absorption of visible light. It has been claimed that rare-earth doping (La, Ce) enhances light harvesting and creates localized energy states that promote interfacial charge transfer. Certain classes of pharmaceuticals can benefit from doping tactics that maximize photocatalytic activity; for example, dopants that

promote the generation of hydroxyl radicals tend to speed up the breakdown of electron-rich components in medications. However, optimization is required since overdoping can result in recombination centers [211-212].

2.5.5. Combining with carbonaceous supports

By using localized surface plasmon resonance (LSPR), plasmonic metal nanoparticles (Ag, Au) placed on MXene or MXene–semiconductor composites might improve photocatalysis. By enhancing specific electromagnetic fields and injecting hot electrons into the semiconductor/MXene, LSPR increases photocatalytic efficiency and expands absorbing radiation into the visible to near-infrared spectrum. Complementary advantages of carbon supports (graphene, rGO) layered with MXenes include a π–π stacking with aromatic drugs, a wide surface area, and extra electron donor/acceptor characteristics that further inhibit recombination [223].

2.5.6. Defect engineering and the creation of oxygen vacancies

Adding oxygen vacancies either in the MXene-derived oxide phases or in the linked semiconductor can boost photocatalytic activity by establishing specific states that trap electrons and allow multi-step redox processes. Vacancy engineering can boost light absorption as well as charge separation; for instance, oxygen-vacancy-rich TiO_2 produced at MXene–TiO_2 interfaces works as active sites for hydroxylation processes. However, management of vacancy concentration is crucial because too many flaws can act as recombination hotspots. Advanced synthesis processes, including such as monitored heat reduction and hydrogenation, are routinely employed to regulate defect density [219-221].

2.5.7. Composite structures

To achieve particular functional improvements, researchers employ a variety of structural motifs. Among the examples are 0D/2D composites: MXene (2D) coated with metal nanoparticles (0D) to take advantage of plasmonic hot electrons. 1D/2D heterostructures: controlled charge transfer using nanorod semiconductors on MXene sheets. Aerogels, Foams, and self-assembled scaffolds are examples of 3D macro-architectures that help immobilize continuous flow reactors, promote mass transfer, and avoid restacking. 3D macrostructures (such as MXene-based aerogels) permit immobility and reuse while preserving large surface area and fluid permeability, two

crucial factors for pharmacological treatment at the pilot scale, are especially appealing for scale-up [224].

2.5.8. Preservation against photocorrosion and oxidation

Surface oxidation to transition metal oxides during preservation or under oxidative photocatalytic conditions is a well-known problem with MXenes. Uncontrolled oxidation alters the active sites and decreases conductivity, although partial oxidation can produce advantageous oxide phases (such as TiO_2) that take part in photocatalysis. A number of tactics are employed to address this: Surface passivation using polymers or thin shells of protection (carbon, silica) that permit charge transfer but block O_2 access. Stable heterojunctions are formed in situ, where the MXene backbone is preserved, while close, catalytically active interfaces are produced via controlled oxide production. Working circumstances or antioxidant compounds that reduce oxidative deterioration while in operation. Every stabilization technique has a unique impact on catalytic processes and needs to be customized for the reactor's circumstances and the target pollutant [223-224]. Powder photocatalysts need to be immobilized or incorporated into structural supports for practical wastewater treatment applications in order to facilitate simple separation and long-term recycling. Ceramic membranes, glass beads, polymeric membranes, and electrodes have all been used to immobilize MXene composites. Size exclusion and on-surface degradation are combined in membrane-photocatalyst hybrids, which show promise in bridging the gap between lab and pilot scale transitions. MXene-coated electrodes have also been employed in photo-electrocatalytic systems, which combine light activation and bias-assisted charge separation, demonstrating improved degradation and simpler catalyst recovery [211-212].

2.5.9. Studies on pharmaceutical degradation performance

Several positive case studies for medication elimination are reported in the literature: Compared to $BiVO_4$ alone, $Ti_3C_2/BiVO_4$ exhibits improved visible-light degradation of ciprofloxacin, with faster kinetics and greater TOC elimination ascribed to better charge separation and adsorption. In lab waters, MXene/Lanthanum and MXene/V_2O_5 composites have been shown to exhibit bandgap tuning, enhanced ROS production, and enhanced tetracycline and fluoroquinolone degradation efficiency. While CdS systems need methods to stop photocorrosion and Cd^{2+} leaching, MXene–CdS and

MXene–g-C_3N_4 composites demonstrated synergistic visible-light activity and improved mineralization of model antibiotics [225].

Although most studies stay at the laboratory scale and use idealized matrices (such as spiked deionized water) instead of complex real effluents, these studies show that MXene modification through heterojunctions, doping, and structural engineering can significantly increase mineralization (TOC removal) and the degradation rates of pharmaceuticals.

2.5.10. Research Gaps and Limitations

Despite the promising catalysts created by MXene modifications, a number of crucial holes must be filled before wider adoption may occur, Validation of real effluent: The majority of research demonstrates performance at high concentrations (mg L^{-1}) in model waters. At environmentally relevant concentrations (ng–µg L^{-1}), MXene composites must be evaluated immediately in real wastewater (pharmaceutical, hospital effluent, factory effluent, and municipal WWTP effluent). Leaching and stability: There are a few prolonged cycling tests (>10–20 times) that thoroughly examine the leaching of metals and structural alterations. Leaching and ecotoxicity evaluation require standardized procedures. Quantitative investigations (time-resolution spectroscopy, charge carrier life span measurements, operando EPR) that directly connect MXene changes to charge dynamics and ROS yield are scarce, despite the qualitative invocation of heterojunctions and Schottky effects. Green and scalable manufacturing: HF or other dangerous etchants are used in a lot of MXene syntheses. More research and standardization are needed for safer, more environmentally friendly, and more scalable processes (such as electrochemical etching, molten salt pathways, or softer fluoride salt procedures). Integration into flow reactors: Most work is done on a batch scale; to understand hydraulics, fouling, and lifetime, immobilized MXene catalysts must be designed and tested in continuous reactors and membrane hybrids. Byproduct analysis and mineralization: To make sure that treatment doesn't result in the production of additional harmful species, complete mineralization (TOC/CO_2) and thorough determination of the intermediates must be documented [226].

By adjusting band topologies, improving charge separation, boosting adsorption, and strengthening stability, modification techniques turn MXenes from intriguing new

materials into useful photocatalytic substrates. Complementary techniques such as immobilization, plasmonic coupling, intercalation, doping, and heterojunction creation offer a toolkit for focused catalyst design. Under visible light, MXene composites exhibit great promise for combining adsorption and photocatalytic mineralization for the particular problem of pharmaceutical removal (such as ciprofloxacin and cetirizine). Future research must prioritize standardized, mechanistic studies, greener synthesis, pilot-scale demonstrations, and thorough safety evaluations in order to satisfy real-world expectations. If the emphasized research priorities are rigorously pursued, MXene-based photocatalysts should develop from promising lab materials into practical parts of sophisticated treatment trains in the upcoming years.

2.6. Techniques for preparation of MXene

MXenes are a class of two-dimensional transition metal carbides, nitrides, and carbonitrides that have garnered a lot of interest due to their remarkable physicochemical and structural characteristics, such as their enormous surface area, hydrophilicity, and metallic conductivity. With the successful synthesis of Ti_3C_2 from the MAX phase Ti_3AlC_2 by hydrofluoric acid (HF) etching, other synthesis techniques have been investigated to improve efficiency, control, and safety over surface terminations. MXene is normally synthesized by selectively removing the A-layer (often Al, Ga, or Si) from the MAX phase ($M_{n+1}AX_n$, where X is carbon and/or nitrogen, A is an element from groups 13–16, and M is an early transition metal). Their chemical reactivity, dispersion, and photocatalytic performance are significantly impacted by the multilayer MXene structures that are produced by this technique and terminated with functional groups like -O, -OH, and -F [211-212].

2.6.1. Conventional HF etching technique

Because of its ease of use and effectiveness in eliminating the A-layer from MAX precursors, the HF etching method continues to be the most popular and essential technique for MXene synthesis. This procedure dissolves the A element and creates multi-layered MXene by immersing the MAX phase powder in intense hydrofluoric acid for a number of hours [211-212]. The reaction can be shown as follows, Eq (1):

$$Ti_3AlC_2 + 3HF \rightarrow AlF_3 + 3/2H_2 + Ti_3C_2 \quad \text{.....(1)}$$

Repeated washing and centrifugation procedures are necessary after etching in order to eliminate unreacted precursors and bring the acidic solution's pH down to about 6. Because HF is poisonous and corrosive, this process raises serious safety issues even if it manufactures $Ti_3C_2T_x$ MXene efficiently. Additionally, partial oxidation or structural defects brought on by HF etching may compromise the homogeneity of surface terminations and restrict morphological control. However, this process yields superior MXene with outstanding electrical conductivity, setting it as a standard for alternative synthesis pathways [219-222].

2.6.2. HF formation with fluoride salts

Researchers have created in situ HF generation procedures, which combine fluoride salts (such as LiF, NaF, or NH_4HF_2) with hydrochloric acid to produce HF in controlled quantities during the etching process, in order to mitigate the dangers related to direct HF handling. This "milder" etching method gives you more control over the functional groups and morphology. For example, $Ti_3C_2T_x$ with –O, –OH, and –F surface terminations can be created by etching Ti_3AlC_2 at 35–40°C using a combination of LiF and 9 M HCl. When MXene layers are etched, the Li^+ ions intercalate between them, promoting delamination and creating single- or few-layer MXene nanosheets with better dispersion in aqueous conditions. By customizing the surface chemistry and interlayer spacing, this approach not only improves safety but also makes MXene more appropriate for photocatalytic and electrochemical uses. For instance, it found that LiF–HCl etched MXene had greater interlayer separation and fewer flaws than the traditional HF approach, resulting in a higher yield and enhanced hydrophilicity [211-222].

2.6.3. Electrochemical etching technique

By avoiding the use of dangerous acids, the electrochemical etching process provides a more environmentally responsible way to prepare MXene . This technique uses a platinum or graphite electrode as the cathode and the MAX phase as the anode in an electrolyte (such as NH_4Cl or NaCl solution). The MXene structure is left behind after the A-layer atoms are oxidized and destroyed by the application of a potential difference. By varying the electrolyte composition, applied potential, and time, this method allows for exact control over the etching procedure and surface terminations. For photocatalytic and adsorption applications, MXene with –O and –OH

terminations, as opposed to –F, is usually produced via electrochemical etching. Furthermore, the approach results in improved scalability, increased environmental compatibility, and less structural damage. Nevertheless, the procedure is often slower than chemical etching methods and could necessitate parameter tuning for every MAX phase [211-221].

2.6.4. Etching by molten salt technique

A promising fluoride-free technique for creating MXenes with distinctive surface terminations and no environmental impact is molten salt etching. By treating the MAX phase at high temperatures (400–600°C) with molten salts such as $ZnCl_2$, $CuCl_2$, or $FeCl_3$, the A-layer is selectively removed, and Cl-terminated MXene is formed. Through this approach, MXenes that would otherwise be challenging to acquire using conventional acid etching may be synthesized, and surface chemistry can be tuned. Furthermore, the resultant MXenes' stability and crystallinity are frequently improved by molten salt treatment. To prevent the production of undesirable carbide or oxide phases, this method necessitates precise temperature control. To get rid of any remaining salts, the resultant MXene could need to be post-treated or given another wash. Notwithstanding these difficulties, molten salt etching offers a more environmentally friendly and scalable method for creating MXenes with a variety of terminations appropriate for energy storage, sensing, and photocatalysis [219-221].

2.6.5. Microwave-assisted technique

It's quick, energy-efficient, and consistent heating properties, which result in quicker reaction kinetics and more precise structural control, the microwave-assisted synthesis approach has drawn a lot of interest. In this procedure, the MAX precursor is exposed to microwave radiation for a brief period of time while in an acidic medium (such as diluted HF, HCl, or NH_4HF_2). In comparison to traditional approaches, the electromagnetic field produces high-quality MXene in a substantially shorter amount of time by inducing localized heating and speeding up the etching process. By creating thinner layers with fewer structural flaws and larger active surface areas, microwave synthesis has been shown to increase MXene's exfoliation efficiency and photocatalytic activity. Additionally, microwave-assisted MXenes frequently have improved interlayer spacing and increased hydrophilicity, both of which are advantageous for visible light-driven photocatalysis. Due to improved surface

interaction and increased charge carrier mobility, studies have shown that microwave-synthesized MXene composites, perform better at degrading pharmaceutical pollutants than samples that are prepared conventionally [227].

2.6.6. Comparative analysis

Every synthesis technique has a major impact on MXene's shape, surface terminations, and photocatalytic performance. Although HF etching is still useful, there are serious safety and environmental risks. Molten salt and microwave-assisted syntheses are becoming viable and high-performing substitutes, whereas in situ fluoride salt and electrochemical techniques are safer and more adjustable. However, a significant obstacle still stands in the way of producing uniform, few-layer, defect-free MXene on a wide scale with adjustable surface chemistry. Moreover, MXene's stability during storage and use is restricted by post-synthesis oxidation and structural deterioration in ambient settings. In order to maximize MXene efficacy for photocatalytic degradation of pharmaceutical pollutants, future research should concentrate on creating scalable, environmentally safe synthesis pathways with exact control over composition, surface terminations, and layer thickness [211-227].

2.7. Preparation of MXene-based composites

One cutting-edge method to get beyond the inherent drawbacks of pristine MXenes, like restacking, oxidation susceptibility, and fast recombination of photoinduced charge carriers, is the creation of MXene-based composites. Researchers have greatly improved photocatalytic, electrochemical, and adsorption capabilities by combining MXene with a variety of functional materials, such as conducting polymers, metal oxides, metal sulfides, and carbon-based nanomaterials. MXene is a perfect substrate for creating robust interfacial interactions with other materials because of its remarkable metallic conductivity, hydrophilic properties, and abundance of surface functional groups (-OH, -O, and -F). These composites are very promising for the destruction of pharmaceutical pollutants under visible light irradiation because of their synergistic actions, which enhance charge transport, prolong visible-light absorption, and stabilize reactive sites [211-212].

2.7.1. Composite formation

Due to its limited light absorption range and potential for photogenerated electron-hole pair recombination, MXene has a low photocatalytic efficiency. MXene can

greatly improve photocatalytic activity by being included into a semiconductor framework or doped with metal cations. The high conductivity of MXene makes it easier for electrons to move from the semiconductor's conduction band to its surface, which inhibits recombination and increases the lifespan of charge carriers. Additionally, close interaction with other nanomaterials is made possible by MXene's layered structure, which results in robust heterojunction interfaces that support charge separation. Effective use of visible light is made possible by these composites' ability to control the active component's bandgap [211-212, 219-221].

2.7.2. Various routes for the synthesis of MXene-based composites

For MXene-based composites, a variety of synthesis techniques have been documented, each with unique benefits for managing interfacial chemistry, structure, and morphology. The intended use, the kind of material used in conjunction with MXene, and the operational conditions all play a significant role in the technique selection.

2.7.2.1. Hydrothermal technique

Due to its ease of use, scalability, and capacity to produce highly crystalline materials with close interfacial contact, the hydrothermal method is one of the most popular approaches for creating MXene-based composites. Typically, a precursor (such as metal nitrate, chloride, or oxide) and MXene nanosheets are disseminated in an organic or aqueous solvent. For several hours, the mixture is heated to moderate temperatures (between 120 and 200°C) while enclosed in an autoclave. A stable heterostructure is created when the secondary phase immediately nucleates and develops on the MXene surface during the reaction. Because of the effective charge transfer from TiO_2 to MXene, for example, TiO_2/MXene composites made by the hydrothermal method have demonstrated better photocatalytic performance. Similar to this, hydrothermally produced CdS/MXene and ZnO/MXene composites showed improved rates of degradation of pharmaceutical medications, including tetracycline and ciprofloxacin, which were ascribed to decreased recombination and increased absorption of visible light. In order to further alter electrical characteristics and catalytic activity, the hydrothermal technique also makes doping with transition metals or rare-earth ions easier [228].

2.7.2.2. Microwave-assisted technique

Recently, the microwave-assisted synthesis method has drawn interest due to its energy economy, homogeneous heating, and quick reaction kinetics. This method creates composites with uniform distribution and robust interfacial bonding by exposing the MXene precursor and dopant materials to microwave radiation for a few minutes. Smaller particle sizes and better crystallinity are the results of the localized microwave heating, which also improves nucleation and diffusion processes. MXene composites have been successfully created using microwave synthesis for the photocatalytic degradation of drugs in the presence of visible light. Microwave-assisted composites have more photocatalytic activity than traditional techniques because of enhanced charge transfer channels and fewer structural flaws. Furthermore, the quick synthesis reduces oxidation and maintains MXene's inherent conductivity, which is essential for electron transport [227].

2.7.2.3. In situ growth technique

A strong interfacial bond between the two materials is ensured via in situ growth, which entails the direct development of a secondary phase on MXene sheets during the synthesis process. This method avoids the secondary phase and MXene from clumping together and offers consistent coverage. For instance, tightly bonded heterojunctions that facilitate quick electron–hole separation can be formed when metal oxides (FeO_3, SnO_2, and ZnO) grow in situ on MXene sheets. Under visible light, the resultant composites frequently show improved stability and photocatalytic effectiveness. Additionally, in situ growth guarantees repeatability and consistent photocatalytic activity by providing fine control over particle morphology and dispersion [229].

2.7.2.4. Sol–gel and co-precipitation techniques

High control over the uniformity and porosity of MXene composites is possible with the sol–gel technique. This method involves mixing MXene dispersion with a sol that contains a precursor (such as a metal alkoxide) and letting it gel before drying and calcining it. MXene–ZnO and MXene–TiO_2 composites with highly interfacial contact and precisely regulated particle size have been produced using the sol–gel process extensively. In contrast, the co-precipitation approach uses pH adjustment to precipitate MXene and a metal precursor simultaneously, allowing for homogeneous loading and robust component interaction [229].

2.7.2.5. Mechanical mixing and electrostatic assembly

When high-temperature treatment is not desired, simple techniques for composite synthesis are mechanical blending and electrostatic self-assembly. Through electrostatic interactions, positively charged nanoparticles or polymers can more easily adsorb onto MXene's negatively charged surface. Metal–MXene hybrids and polymer–MXene composites with adjustable surface coverage have been effectively prepared using this method. These methods are useful for creating flexible, binder-free photocatalytic films and electrodes, despite their lack of sophistication [230].

Due to the special synergistic interactions between conductive MXene sheets and semiconductor or metallic components, MXene-based composites have enhanced photocatalytic activity. Heterojunction creation increases light absorption, speeds up charge transfer, and offers a large number of redox reaction active sites. Controlling interfacial homogeneity, avoiding oxidation during synthesis, and attaining a stable dispersion of MXene in solution are some of the remaining difficulties, though. Furthermore, maintaining structural integrity and catalytic performance during large-scale synthesis is still a crucial problem that calls for process parameter adjustment. All things considered, MXene-based composite synthesis is a flexible and promising approach to creating high-performance photocatalysts for environmental cleanup, especially for the breakdown of persistent pharmaceutical pollutants when exposed to visible light [211-212].

2.8. Pharmaceutical drug photocatalytic degradation using composites based on MXene

They are resistant to traditional wastewater treatment, and pharmaceutical substances like analgesics, antibiotics, and anti-inflammatory medications are becoming persistent organic pollutants in aquatic habitats. Aquatic ecosystems and human health may be at risk from these substances, which are frequently bioactive, stable, and present even in small amounts. Because of their strong interfacial interactions, high surface area, tunable surface functionalities, and excellent electrical conductivity, MXene-based photocatalysts have drawn a lot of attention recently for the degradation of pharmaceutical pollutants when exposed to visible light [211-222].

2.8.1. Photocatalytic degradation mechanism

The main idea of semiconductor photocatalysis, in which photo-induced electron-hole pairs take part in redox processes that result in the breakdown of pollutants, is followed in the photocatalytic degradation of pharmaceuticals utilizing MXene-based composites. When exposed to visible light, the semiconductor component's electrons (e^-) are stimulated to move from the valence band (VB) to the conduction band (CB), leaving holes (h^+) in the VB. Because of its metallic conductivity, MXene functions as both an electron sink and a co-catalyst, lowering charge recombination and promoting quick electron migration [211-212].

While holes combine with water or surface hydroxyl groups (–OH) to produce hydroxyl radicals (·OH), these photogenerated electrons can react with adsorbed molecular oxygen (O_2) to produce superoxide radicals ($\cdot O_2^-$). The oxidation and degradation of pharmaceutical compounds into innocuous byproducts, including CO_2, H_2O, and inorganic ions, is facilitated by both reactive oxygen species (ROS). Z-scheme or Schottky-type heterojunctions are frequently seen in MXene-based composites, which preserve high redox potentials while guaranteeing effective charge carrier separation (Xia et al., 2019) [211-222].

2.8.2. Pharmaceutical degradation using MXene–semiconductor composites

Composites made of MXene and semiconductors have demonstrated encouraging outcomes in the photocatalytic destruction of a variety of pharmaceutical pollutants. Ti_3C_2/TiO_2 composites, for instance, showed effective ciprofloxacin and tetracycline degradation because of the strong coupling between Ti_3C_2 and TiO_2, which improved interfacial charge transfer and absorption of visible light (Xu et al., 2023). The development of a type-II heterojunction that facilitated efficient charge separation is also responsible for the enhanced photocatalytic activity for antibiotic elimination demonstrated by Ti_3C_2/CdS composites produced by hydrothermal and microwave methods (Chen et al., 2024) [219-221]. One of the most researched MXene-based systems for drug degradation is $TiC_2/g\text{-}C_3N_4$ composites. A Z-scheme arrangement that maintains the high redox ability of charge carriers is produced by combining the conductive qualities of MXene with the visible-light absorption capacity of $g\text{-}C_3N_4$ (Yu et al., 2021) [231]. For example, (Yu et al., 2021) found that, when exposed to visible light, a 3 weight percent Ti_3C_2–$g\text{-}C_3N_4$ composite degraded tetracycline hydrochloride by more than 90% in 120 minutes. The longer light absorption range

and higher separation efficiency of photo-generated carriers were credited with the enhanced performance. The MXene–ZnO composite is another noteworthy example; it has been demonstrated to effectively break down pharmaceutical contaminants like ibuprofen and sulfamethoxazole when exposed to sunlight. The development of a Schottky barrier at the MXene–ZnO interface, which promoted electron transport and decreased recombination losses, was the main cause of the increased photocatalytic efficiency (Hannan et al., 2017) [232].

2.8.3. MXene–metal oxide and doped composite materials

MXenes are frequently combined with metal oxides like FeO_3, CuO, VO_5, and LaO_3 to create composites that have exceptional photocatalytic properties. Reactive oxygen species production is increased, and the redox potential is improved by the addition of these oxides (Zhan et al., 2020). For instance, under visible light, La-doped MXene composites showed improved ciprofloxacin degradation efficiency. This was attributed to the changed band gap and increased charge carrier mobility brought about by the insertion of La^{3+} (Zeng et al., 2019). In addition to lowering surface oxygen groups, the addition of La species to MXene surfaces suppresses electron-hole recombination and increases photocatalytic reactivity. Similarly, because of the synergistic effects of the two components, vanadium-modified MXene composites have demonstrated efficient photocatalytic degradation of medicines. Because of their varied oxidation states (V^{5+}/V^{4+}), vanadium oxides improve charge separation by facilitating effective electron transport between MXene and the semiconductor (Yang et al., 2018). Because of their enhanced light absorption capabilities and optimal band alignment, V_2O_5/MXene composites have shown notable photocatalytic degradation efficiencies for contaminants such as cetirizine and diclofenac, especially when exposed to visible light (Li et al., 2020). The degradation of antibiotics has also been investigated for other transition metal oxides, such as MnO_2–MXene and NiO–MXene. With MnO_2 functioning as a visible light absorption and MXene as a conductive support, these composites have large surface areas and excellent chemical stability (Wang et al., 2020) [211-222]. Additionally, these heterostructures have improved cycling stability, which permits reuse over several deterioration cycles with negligible activity loss.

2.8.4. Composites of MXene with carbon and MXene with metal sulphide

Due to their huge surface area and enhanced electrical conductivity, MXenes significantly enhance photocatalytic activity when combined with carbon-based materials like carbon nanotubes (CNTs) or reduced graphene oxide (rGO). The creation of MXene/rGO composites promotes quick charge transfer across the interface and improves the adsorption of medicinal compounds (Chen et al., 2022). For example, when compared to either component alone, MXene/rGO composites demonstrated exceptional tetracycline and sulfamethoxazole breakdown with greater mineralization rates. The destruction of antibiotics by visible light has also been widely documented for MXene–metal sulfide composites (e.g., MXene/CdS, MXene/MoS_2) (Zhang et al., 2024) [219-230]. CdS efficiently captures visible light due to its low band gap, while MXene offers an electron-conducting route that inhibits recombination. Because of the enhanced interfacial contact and Schottky junction formation, MXene/CdS composites have outperformed pure CdS in the degradation of ciprofloxacin, achieving over 95% degradation in 90 minutes [219-230].

2.8.5. The kinetics of degradation and contributing factors

Based on the adsorption–reaction mechanism, the degradation kinetics of medicines employing MXene-based composites often follow Langmuir–Hinshelwood or pseudo-first-order models (Zahedi et al., 2025) [231]. A number of factors, including pH, catalyst dosage, beginning contaminant concentration, and irradiation period, affect performance. Degradation efficiency is generally improved by somewhat basic conditions, which increase the production of hydroxyl radicals (·OH). Furthermore, because of the even dispersion of active sites and smaller particle sizes, composites made with microwave assistance show higher reaction rates (Zhang et al., 2024) [205]. MXene-based composites' chemical stability and reusability are essential for sustainable wastewater treatment, as evidenced by recyclability tests that show they retain high catalytic effectiveness after multiple cycles (Chen et al., 2022) [222].

2.8.6. Overview

All things considered, MXene-based composites provide a flexible and efficient method for the photocatalytic breakdown of pharmaceutical contaminants. Rapid charge transfer and enhanced visible-light utilization are made possible by their special blend of hydrophilicity, metallic conductivity, and strong interfacial interaction with semiconductors. MXene and its composites have been identified as

extremely effective photocatalysts for the degradation of antibiotics and anti-inflammatory drugs across a variety of systems. Developing multi-component MXene heterostructures with enhanced surface stability and optimal band alignments should be the main goal of future studies. Translating laboratory results into industrial-scale wastewater treatment applications would also require a focus on scalable and environmentally friendly synthesis methods (such as microwave-assisted or electrochemical approaches) [211-212]. Studies have demonstrated that under UV, visible light, or sunshine, Ti_3C_2 nanocomposites may accomplish over 90% degradation of different organic wastes, including colors and pharmaceutical pollutants. High conductivity, a huge surface area, and the capacity to alter surface functions for improved pollutant interaction are some of the main benefits. Nevertheless, issues like recyclability and environmental effect still exist. To improve performance in wastewater treatment applications, future research should tackle these problems while refining synthesis techniques and investigating novel hybrid configurations. **Table 2** lists a few of the nanomaterials based on Ti_3C_2 that are used in photocatalysis.

Table 2. Nanomaterials based on (MXene) Ti_3C_2 for photocatalytic use

S.No.	Contaminants	Photocatalyts	Degradation efficiency (%)	References
1	Methyl orange dye	N-Ti_3C_2	98.73%	235
2	Dyes like bromocresol green and methylene blue.	TMAOH MXene and MILD-MXene	100%	235
3	Bacteria	Ag_2S/Ti_3C_2	99.9%	235
4	Antacid pantoprazole	Ti_3C_2– $BiFeO_3$–ZnO	92.05%	235
5	Tetracycline	$T_{i3}C_2$/ TiO_2	96.3%	235
6	4-nitrophenol	$BaSnO_3$/MXene	98.8%	235
7	Ciprofloxacin and Congo red	BVO-BS/MXene	92.5%	235

8	Methyle Blue	Ti_3C_2Tx-$NiMnO_3/NiMn_2O_4$	100%	235
9	Methyl orange	Ti_3C_2Tx-$NiMnO_3/NiMn_2O_4$	72%	235
10	Rhodamine B	Ti_3C_2Tx-$NiMnO_3/NiMn_2O_4$	90%	235
11	Methylene Blue	SnO_2/ Ti_3C_2	70%	235
12	Benzoic acid	Ag -$LaNiO_3$/ MXene	55%	235
13	Methyl orange	Ag -$LaNiO_3$/ MXene	64%	235
14	Bromophenol blue	Ag -$LaNiO_3$/ MXene	84%	235
15	malachite green dye	$Ti_3C_2/NiTiO_3$	98.2%	235
16	crystal-violet dye	Ti_3C_2MXene/NiO/ $CsPbI_3$	92.8%	235
17	Methylene Blue	Ti_3C_2Tx/ Mn_2O_3	100%	235
18	Mixed dyes (MO, RhB and MB)	Ti_3C_2Tx/ Mn_2O_3	82% MO, 80% RhB, 96% MB	235
19	methyl orange dye	N- Ti_3C_2 MXene	98.73%	235
20	Tetracycline	TiO_2@ Ti_3C_2 MXene/Bi_2S_3	84.13%	235
21	Methylene Blue	Ag@ZnO@ Ti_3C_2	90.54%	235
22	Tetracycline	Ti_3C_2/g-C_3N_4	93.93%	235
23	Tetracycline hydrochloride	Ti_3C_2@TiO_2	90%	235

2.9. Scope and Objectives of the Current Thesis

One of the most difficult environmental problems of the twenty-first century is the ongoing presence of pharmaceutical pollutants in aquatic systems. According to [232], pharmaceuticals, especially antibiotics and antihistamines, end up in the environment due to incomplete metabolism, pharmaceutical industry effluent emissions, and inappropriate disposal of unneeded medications. Among these, medications like cetirizine and ciprofloxacin are commonly found in drinking water, groundwater, and surface water, posing health and environmental hazards. A sizable portion of these residues remains after secondary treatment since conventional wastewater treatment plants are not built to particularly remove these persistent organic pollutants [232]. The development of cutting-edge technologies that can fully degrade pharmaceutical residues instead of just moving them from one stage to another has been the subject of an increasing number of studies in recent years. Because of their capacity to produce extremely reactive hydroxyl and superoxide radicals that can mineralize organic molecules into carbon dioxide and water, advanced oxidation processes (AOPs) have garnered a lot of interest among the many strategies. Because photocatalysis may employ solar or visible light energy to drive the degradation of pollutants under mild conditions, it has become one of the most promising and sustainable strategies within AOPs. However, the photocatalyst's physicochemical characteristics, including its band structure, surface area, charge carrier mobility, and recombination rate, have a significant impact on the efficiency of photocatalytic degradation [233]. Although traditional photocatalysts like TiO_2, ZnO, and g-C_3N_4 have been investigated in great detail, their practical application is hampered by their broad band gaps and low response to visible light. Researchers have investigated a number of modification techniques to get around these limitations, such as metal or non-metal doping, heterojunction formation, and the creation of composite systems that can improve charge separation and efficiently capture visible light. The general formula for MXenes is $M_{n+1}X_nT_x$, where M is a transition metal, X is carbon or nitrogen, and T_x stands for surface terminations like –OH, –O, and –F. In this context, MXenes have emerged as a novel class of two-dimensional transition metal carbides, nitrides, and carbonitrides [211-212]. They are perfect for environmental applications because of their enormous surface area, hydrophilicity, changeable surface chemistry, and distinctive metallic conductivity. In semiconductor heterostructures, MXenes can

function as electron mediators or co-catalysts, promoting charge transfer and inhibiting electron-hole recombination to enhance photocatalytic activity in the presence of visible light. Furthermore, their optical and electrical characteristics can be readily altered or doped with metals, oxides, or sulfides to suit particular degrading requirements (Murali et al., 2022) [107].

Notwithstanding these benefits, there are still a number of obstacles to overcome before MXene-based photocatalysts can be effectively used to treat wastewater. The structural integrity and surface functionality of MXenes are significantly influenced by their synthesis techniques, which include molten salt approaches, in situ fluoride etching, and HF etching. Additionally, MXene's stability in oxidative and aqueous settings is still an issue, requiring suitable changes or the creation of composites to increase durability and recyclability. Therefore, the development of effective, stable, and sustainable photocatalytic systems for pharmaceutical degradation requires a thorough understanding of MXene production, surface modification, and photocatalytic behavior [211-221]. Therefore, the current work focuses on examining and compiling the body of research on the creation of MXene-based photocatalysts for the treatment of pharmaceutical wastewater. It focuses on comprehending how differences in synthesis techniques, composite construction, and structural modification tactics affect MXene materials' photocatalytic capabilities. The purpose of the review is to present a methodical viewpoint on how MXene's surface chemistry, band structure, and morphology relate to photocatalytic activity when exposed to visible light.

Objectives

1) Fabrication of MAX Phase using Metal (La/V, Al) and pinecone-based Biochar carbon via heat treatment process.
2) MXene (La_3C_2Tx) /(V_3C_2Tx) synthesis using MAX Phase via etching and microwave process.
3) Characteristic analysis of highly efficient photocatalytic MXene based advanced functional materials.
4) Pharmaceutical (antibiotics and anti-inflammatory) drug decontamination under dark and visible phase using MXene based advanced functional materials.

Chapter-3
Materials and Methods

3. Introduction

The production and engineering of two-dimensional (2D) materials, including MXenes, for environmental applications, specifically the photocatalytic destruction of pharmaceutical pollutants, has garnered increasing attention in recent years. Selective etching produces MXenes from MAX phase precursors, which have remarkable physicochemical characteristics such as hydrophilicity, high surface area, metallic conductivity, and adjustable surface terminations. Because of these qualities, they are ideal for building sophisticated photocatalytic systems when exposed to visible light.

In order to improve visible-light-driven degradation efficiency, the current study focuses on the synthesis of MXene via both conventional and microwave-assisted methods. La-modified and V_2O_5-modified MXene composite photocatalysts are then fabricated. The structural, morphological, optical, and surface charge characteristics of the synthesized materials were analyzed using a variety of physicochemical characterization techniques, including X-ray diffraction (XRD), Fourier transform infrared spectroscopy (FTIR), field emission scanning electron microscopy (FESEM), energy-dispersive X-ray spectroscopy (EDX), UV–visible diffuse reflectance spectroscopy (UV–Vis), and zeta potential measurements.

Additionally, the degradation of pharmaceutical compounds, such as ciprofloxacin and cetirizine, under visible light irradiation was used to systematically assess the produced materials' photocatalytic efficacy. Degradation efficiency was extensively examined in relation to compositional ratios, synthesis techniques, and solution pH. The materials, synthesis processes, characterization techniques, and photocatalytic testing protocols used in the study are all thoroughly described in this chapter. It seeks to provide a precise experimental foundation for the reported photocatalytic action and to direct the interpretation of further findings.

3.1. Materials used

All chemicals used in this work were of analytical grade and didn’t require any additional purification. Titanium aluminum carbide (Ti_3AlC_2, MAX phase) was used as the precursor material for MXene synthesis, which was purchased from Nanoshel. Hydrofluoric acid (HF, 48%), hydrochloric acid (HCl), Lanthanum nitrate hexahydrate ($La(NO_3)_3 \cdot 6H_2O$), vanadium pentoxide (V_2O_5), and other reagents were procured from Loba Chemie PVT.LTD. Ciprofloxacin ($C_{17}H_{18}FN_3O_3$) and cetirizine

($C_{21}H_{25}ClN_2O_3$) were purchased from a local medical shop, which were used as representative pharmaceutical contaminants. Distilled water was used throughout the experiments for solution preparation and washing processes.

3.2. Photocatalyst synthesis

Both conventional and microwave-assisted methods were used to synthesize MXene from the Ti_3AlC_2 MAX phase. In the conventional process, the aluminum layers were selectively removed by progressively adding 1g of MAX phase to 10 mL of 40% hydrofluoric acid (HF) and stirring it for 22-24 hours at room temperature. To obtain multilayer MXene, the etched product was repeatedly washed and centrifuged with deionized water until a neutral (6-7) pH was attained and then vacuum-dried. For the preparation of exfoliated $Ti_3C_2T_x$ nanosheets, the dried powder was intercalated in 15 mL dimethyl sulfoxide (DMSO) under continuous stirring for approximately 22 hours, followed by centrifugation, sonication in distilled water, filtration, and drying [236].

In the microwave-assisted approach, the initial HF etching procedure remained the same. After etching, the MXene powder was mixed with 15 mL DMSO and subjected to microwave irradiation using a Galanz Solo 30 L domestic microwave oven operated at 300 W for 10 min (50 Hz) to accelerate the delamination process. The irradiated material was subsequently washed, centrifuged, sonicated, filtered, and dried according to the standard procedure. This method enabled rapid and uniform heating, thereby reducing the synthesis time and enhancing the exfoliation efficiency of MXene nanosheets [237].

3.3. Synthesis of MXene-modified composites

3.3.1. La/MX Composite

In **Conventional method**, the $La(NO_3)_3 \cdot 6H_2O$ and MXene were dissolved in deionized water in molar ratios of 1:1, 1:2, and 2:1 in order to create Lanthanum-modified MXene composites. The mixture was continuously magnetically stirred for 8 hours with heating at 70-80 °C. After that the product was centrifuged, completely filtered, and dried at 60 °C. Because lanthanum incorporation introduces localized energy states into the MXene band structure, it is anticipated to increase absorption of visible light and decrease charge recombination. In **Microwave method**, Lanthanum nitrate and MXene were dissolved in deionized water in various molar ratios (1:1, 1:2, and 2:1) to create lanthanum-modified MXene composites. To ensure mixing and

interaction between La^{3+} ions and MXene layers. Controlled microwave irradiation of the solution–powder mixture allowed for quick volumetric heating and effective La^{3+} incorporation onto MXene surfaces. The La/MX (MW) composites were obtained by cooling the slurry, repeatedly washing it to a pH close to neutral, filtering it, and oven-drying it after microwave treatment. Compared to the conventional method, our approach shortened the synthesis time [237-238].

3.3.2. V/MX composites

Conventional method, For V_2O_5-modified MXene composites, V_2O_5 and MXene were taken in a weight ratio of 1:2 (V_2O_5:MXene). MXene was dispersed in 250 mL of 0.1 M HCl solution while being continuously stirred. The desired V_2O_5:MXene weight ratio was achieved by adding the required amount of V_2O_5 to the solution [366-367]. The mixture was constantly stirred with heating at 70-80 °C. After that, the solution was centrifuged, filtered, and then dried at 50 °C to obtain the green colour composites. **Microwave method**, V_2O_5-modified MXene composites were prepared in different weight ratios of V_2O_5:MXene (1:1, 1:2, and 2:1) by the microwave-assisted method. MXene was dispersed in 50 mL of 0.1 M HCl solution while being continuously stirred. The desired V_2O_5:MXene weight ratios were achieved by adding the required amount of V_2O_5 to the solution [366-367]. The mixture was subjected to 400 W of microwave radiation for 15 minutes in order to encourage uniform dispersion and interaction between MXene and V_2O_5 particles. Once the solution was thoroughly cleaned with distilled water, it was centrifuged and left to dry at 60 °C for 12 hours [237-238].

3.4. Characterization Techniques

The synthesized MXene and its composites was studied by various analytical techniques. Every approach of characterization has a different purpose in analyzing the synthesized materials. The crystalline structure and the effective conversion of the MAX phase into MXene via selective etching were determined using X-ray diffraction (XRD). Functional groups and surface terminations like -OH, -F, and -O on MXene sheets that affect photocatalytic activity were identified with the help of Fourier Transform Infrared Spectroscopy (FTIR). Detailed information on morphology, elemental composition, and dispersion of dopants or oxides on the MXene surface was obtained through investigations using Energy Dispersive X-ray

(EDX) and Field Emission Scanning Electron Microscopy (FESEM). Additionally, the band gap energy, which establishes the visible light activity of photocatalysts, was estimated, and the optical absorption behavior was examined using UV-Visible Diffuse Reflectance Spectroscopy (UV-Vis DRS). The recombination rate of photogenerated charge carriers was assessed using photoluminescence (PL) spectroscopy and electrochemical impedance spectroscopy (EIS), which provided light on how effective charge separation processes. The surface charge and colloidal stability of the samples in aqueous suspension were investigated using zeta potential analysis, which has a substantial impact on the photocatalytic degradation of pharmaceuticals by affecting the adsorption and interaction between the catalyst and pollutant molecules.

The information obtained from these characterization studies not only confirms the successful MXene synthesis and its modification. It also establishes the structural property performance, which is essential to understand the mechanism of photocatalytic degradation of pharmaceutical pollutants under visible light irradiation.

3.4.1. X-Ray Diffraction (XRD) Analysis

X-ray diffraction (XRD), one of the most popular and non-destructive methods for figuring out the crystal structure of solid materials, was used to evaluate powdered samples. Phase identification, crystallinity, lattice characteristics, and the purity of manufactured chemicals are all significantly determined by XRD (Cullity and Stock, 2014) [240]. The diffraction of monochromatic X-rays by the regularly spaced atomic planes in a crystalline solid is the basis of the basic principle of XRD. Bragg's law states that X-rays are dispersed at particular angles when they interact with the crystal lattice, which is expressed as Eq (2):

$$n\lambda = 2d \sin\theta \quad \ldots\ldots\ldots\ldots\ldots\ldots\ldots\ldots\ldots\ldots (2)$$

where d is the interplanar spacing of the crystal lattice planes, λ is the incident X-ray wavelength, θ is the angle of incidence, and n is the order of diffraction. Every crystalline substance generates a unique diffraction pattern, which is defined by a sequence of peaks that represent various lattice planes. The crystal phase and structure are determined by the positions and intensities of these peaks, which are recorded at particular 2θ values.

The crystalline phase evolution of MXene and its composites produced using both conventional and microwave-assisted techniques was investigated in this work using XRD extensively. At specific 2θ sites, the distinctive peaks that corresponded to the parent MAX phase (Ti_3AlC_2) were seen. The successful development of MXene ($Ti_3C_2T_x$) layers was confirmed by the presence of a displaced (002) reflection and the elimination of the (104) peak upon selective etching of the Al layer (Naguib et al., 2012) [94]. When functional groups (-OH, -O, -F) or intercalated ions are inserted during etching or exfoliation procedures, the (002) peak shifts toward a lower angle, signifying an increase in the interlayer gap. Additionally, additional diffraction peaks corresponding to metal oxide or dopant phases were found in the XRD patterns of doped and composite MXene samples, indicating the successful inclusion of secondary components into the MXene matrix [94]. Important information about the structural changes that take place during synthesis and doping was revealed by the XRD data. Cu Kα radiation was used to record the diffraction patterns across a particular 2θ range. Schematic diagram of XRD and Bragg's constructive diffraction is shown in **Fig.14**.

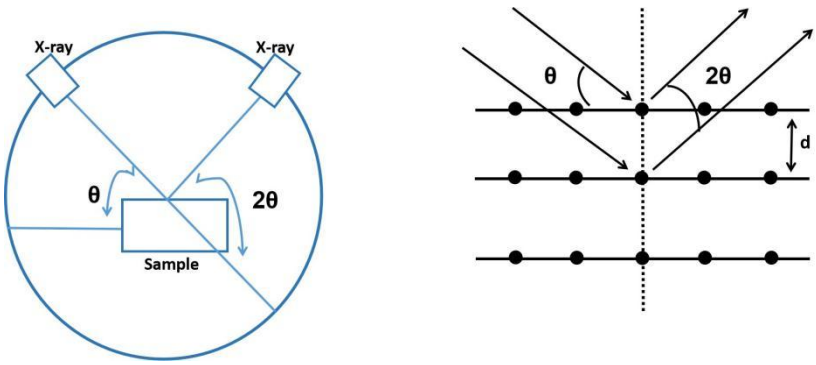

Fig. 14 Schematic diagram of XRD and Bragg's constructive diffraction

3.4.2. Fourier Transform Infrared Spectroscopy (FTIR) Analysis

A well-known analytical method for determining the functional groups and chemical bonds found in a material is Fourier Transform Infrared Spectroscopy (FTIR), which measures the absorption of infrared radiation as a function of wavelength or frequency.

The method is predicated on the basic idea that, depending on their vibrational transitions, molecules absorb particular wavelengths of infrared radiation when it travels through or is reflected from a sample. According to Smith (2011), every molecule has a particular vibrational spectrum that acts as its chemical fingerprint. An interferometer receives radiation from a broadband infrared source and modulates it into an interferogram, a composite signal that simultaneously contains information from all infrared frequencies (Griffiths & de Haseth, 2007) [241-242]. The Fourier Transform technique is then used to identify and mathematically transform the interferogram, resulting in a traditional infrared spectrum (intensity versus wavenumber, often represented in (cm^{-1}).

FTIR provides a greater signal-to-noise ratio, faster speed, and more accurate wavelengths than dispersive infrared spectrometers, which measure one wavelength at a time. The instrument's major components include an infrared source, usually a Nernst filament or Globar (silicon carbide) that emits in the mid-IR range (4000–400 cm^{-1}). By using a beam splitter to divide the beam into two directions and then recombining them after reflection from stationary and moving mirrors, an interferometer creates an interference pattern. The sample compartment is the area where the sample interacts with the modulated infrared beam in either the attenuated total reflectance (ATR) mode or transmission mode. The detector, which detects the transmitted intensity, is frequently a mercury cadmium telluride or deuterated triglycine sulfate detector.

FTIR spectroscopy was used in this study to examine the surface functional groups, verify that the MAX phase was successfully etched to create MXene, and identify the creation of new chemical bonds following lanthanum (La) and vanadium (V) modification. The synthesized materials' FTIR spectra were captured in the mid-infrared range, which is between 4000 and 400 cm^{-1}. Characteristic vibrational bands corresponding to different surface functional groups were identified by analyzing the resulting FTIR spectra. Verifying surface alterations that have a direct impact on photocatalytic performance required the use of FTIR analysis (Zhang et al., 2024) [205]. Schematic diagram of FTIR is shown in **Fig.15**.

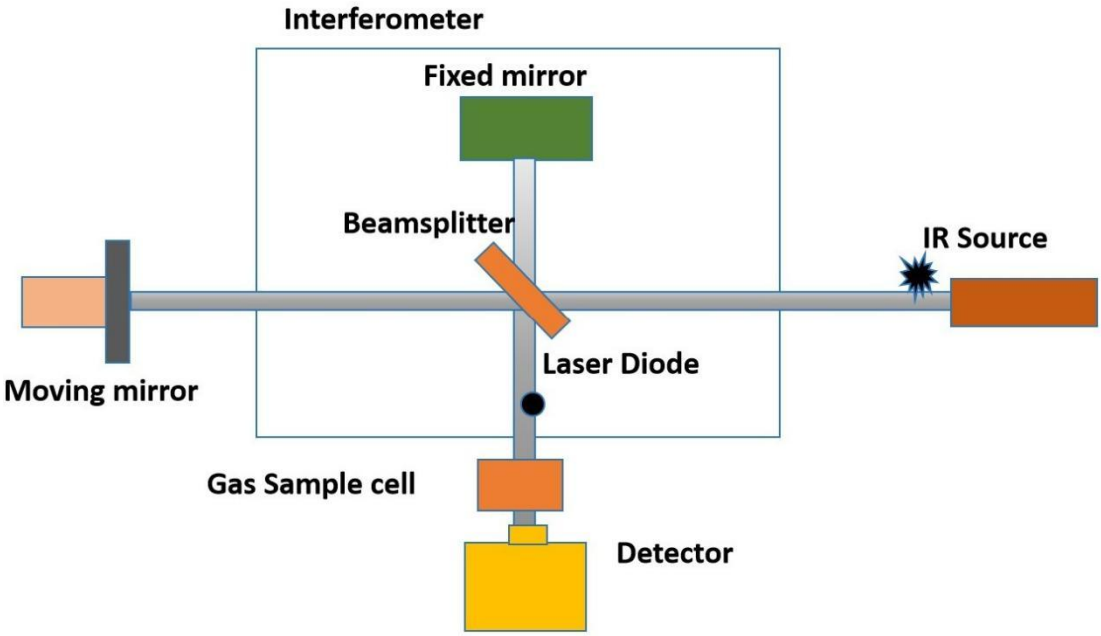

Fig. 15 Schematic diagram of FTIR

3.4.3. Scanning Electron Microscopy (SEM)

An essential analytical method for the high spatial resolution morphological and microstructural characterization of materials is scanning electron microscopy, or SEM. Understanding the physicochemical behavior and photocatalytic capabilities of synthesized nanomaterials requires the ability to visualize their surface topography, particle size, layer development, and structural homogeneity. For two-dimensional materials like MXenes, where the morphological transition from the MAX phase to few-layered structures may be immediately viewed, SEM investigation is especially important. A highly concentrated beam of high-energy electrons is employed by the SEM to scan the surface of the object. Secondary electrons (SE), backscattered electrons (BSE), and distinctive X-rays are among the signals produced when these primary electrons contact the sample's atoms. High-resolution details on morphology and surface texture are provided by secondary electrons, which come from the top few nanometers of the sample surface. The principle diagram of scanning electron microscopy is shown in **Fig.16**. Since heavier elements backscatter more effectively, backscattered electrons, which are produced by elastic scattering processes, are employed to identify compositional contrast. When combined with Energy-Dispersive

X-ray spectroscopy, characteristic X-rays are released when inner-shell electrons are displaced, offering elemental information (Reimer 2000) [243]. A set of electromagnetic condensers and objective lenses is used to concentrate the primary electron beam. To prevent charging effects, the sample needs to be electrically conductive. For this reason, non-conductive materials are frequently coated with a thin layer of conductive metal ,i.e, gold (Au), using a sputter coater before imaging. The surface morphology and microstructural evolution of MXene and its modified composites were examined in this study using SEM analysis. Double-sided carbon tape was used to mount powdered samples on aluminum stubs, and gold was then sputter-coated to improve electrical conductivity. A field-emission scanning electron microscope running under high vacuum conditions was used to record the micrographs at different magnifications.

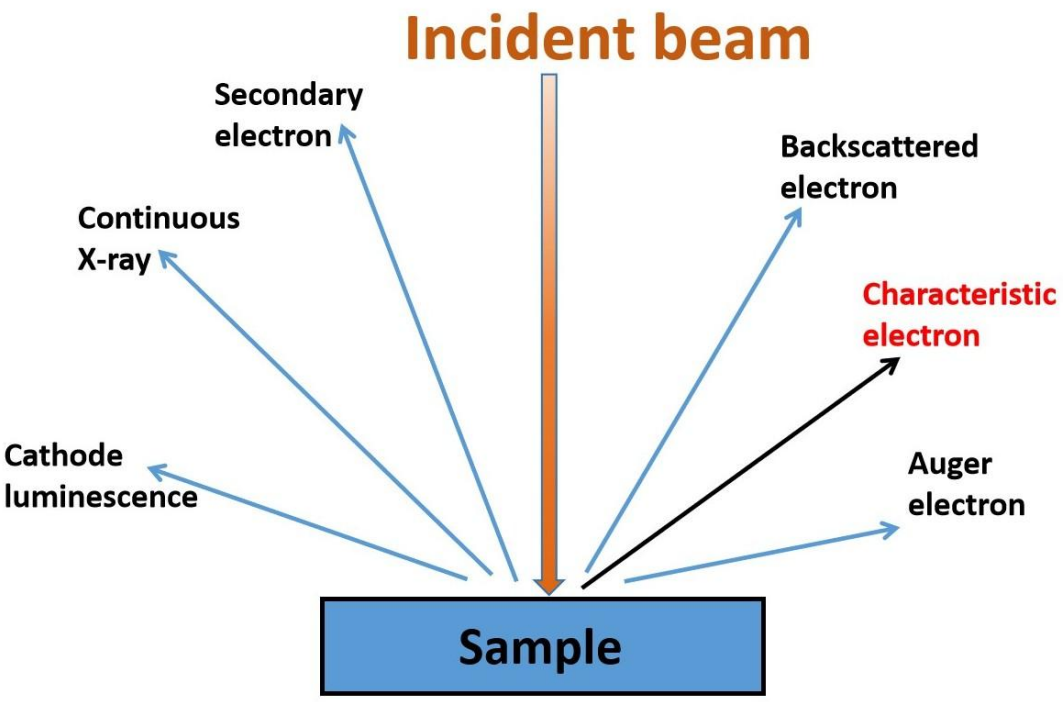

Fig. 16 Principle diagram of Scanning electron microscopy

3.4.4. Energy Dispersive X-ray (EDX) Spectroscopy Analysis

An effective microanalytical method for figuring out the fundamental composition and chemical distribution of materials is energy dispersive X-ray spectroscopy, which is frequently used with scanning electron microscopy (SEM). The effective synthesis of MXene, the removal of the Al layer from the MAX phase, and the inclusion of dopants like La and V into the MXene lattice were all confirmed in this study using EDX analysis. The method allows for the testing of material homogeneity and purity by offering both qualitative and semi-quantitative elemental information (Goldstein Newbury & Ritchie, et al., 2018) [244]. Electron vacancies are created when inner-shell electrons, often from the K or L shell, are expelled from the specimen's atoms by the high-energy primary electron beam in a scanning electron microscope. Electrons from higher energy levels go downward to fill these vacancies and restore electronic stability, producing element-specific X-ray photons. The energy of these released X-rays is equal to the difference in the binding energies of the two shells engaged in the

transition. The elemental makeup of the sample can be determined by employing a silicon drift detector to detect the unique energy values of the X-rays that each element emits. Peak positions correspond to particular elements, and peak intensities relate to their relative abundances. The resulting EDX spectrum shows the energy on the x-axis and the X-ray counts on the y-axis. The depth of analysis is contingent upon the material's density, atomic number, and accelerating voltage (Williams & Carter, 2009) [245]. The compositional and structural integrity of the synthesized materials was crucially confirmed by the EDX results.

3.4.5. Zeta potential analysis

The electrical potential at the plane surrounding a particle scattered in a liquid medium is described by the zeta potential (ζ-potential), a crucial physicochemical characteristic. Surface charge, colloidal stability, and interparticle electrostatic interactions in nanomaterial suspensions are frequently assessed using it (Hunter, 2013) [246]. Ions adsorb onto the surface of a solid particle in an aqueous environment, creating an electrical double layer. The zeta potential is defined as the potential at the sliding plane, which is the border between the main liquid and the immobilized layer of ions. Electrophoresis is the foundation of the zeta potential measurement method. Charged particles move in the direction of the electrode with the opposite charge when an external electric field is introduced across a colloidal dispersion. This movement's speed, known as electrophoretic mobility, is directly correlated with the particles' surface potential. Laser Doppler velocimetry, which measures the frequency shift of scattered light from moving particles, is used by devices like the Malvern Zetasizer to calculate electrophoretic mobility. The Smoluchowski equation and other theoretical models are then used to derive the zeta potential from the mobility (Delgado et al., 2007) [247].

3.4.6. UV–Visible Spectroscopy (UV–Vis) Analysis

A potent analytical method for examining the optical absorption behavior, electronic transitions, and band structure of solid photocatalytic materials is UV–Visible Diffuse Reflectance Spectroscopy (UV–Vis DRS). Understanding how photocatalysts interact with ultraviolet and visible light is crucial for assessing photocatalytic performance since photocatalysts function by producing electron–hole pairs upon light irradiation (Tauc, 1968; Kubelka & Munk, 1931) [248-249]. Because UV-Vis DRS analyzes

diffuse reflection rather than transmission, it is very useful for powdered or opaque samples, which makes it perfect for MXene-based materials and their composites.

A portion of incident light is absorbed, scattered, and diffusely reflected when it hits a powdered sample. An integrating sphere is used to gather the reflected component and send the diffuse reflectance signal to the detector. The Kubelka-Munk function can be used to transform the resulting reflectance spectrum, which is usually recorded in the wavelength range of 200–800 nm, in order to extract information relating to absorption. This enables accurate determination of the optical band gap energy (Eg), which controls the material's capacity to capture visible light and start electronic transitions. A Shimadzu UV-2600 spectrophotometer with an integrating sphere attachment was used in this investigation to quantify UV–Vis DRS. The reference standard was a BaSO4 plate. At room temperature, reflectance spectra were captured across the 200–800 nm wavelength range. Tauc plots obtained from the Kubelka–Munk transformed reflectance data were then used to determine the band gap energy of each material. A schematic diagram of UV-Vis Spectroscopy is shown in **Fig.17**.

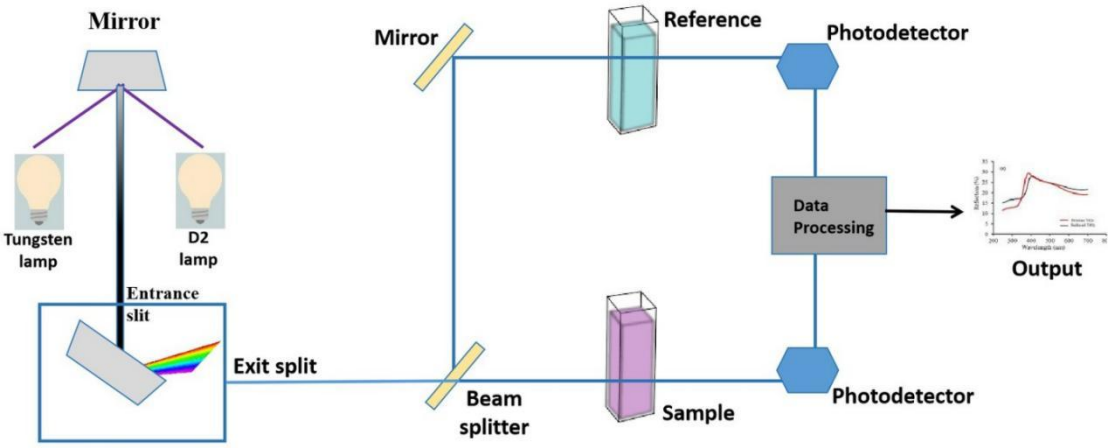

Fig. 17 Schematic diagram of UV-Vis Spectroscopy

3.4.7. Photoluminescence (PL) Spectroscopy Analysis

An important optical characterisation method for examining the recombination behavior of photogenerated charge carriers in semiconductor materials which has a

direct impact on their photocatalytic performance is photoluminescence (PL) spectroscopy. By measuring the light released when electrons recombine with holes following photoexcitation, PL spectroscopy offers crucial insights into these charge dynamics (Wang et al., 2020) [250]. When a material absorbs photons with enough energy to excite electrons from the valence band (VB) to the conduction band (CB), holes are left in the VB. This is the usual process that causes PL emission. These electrons recombine to release energy in the form of photons, which produces an emission spectrum that is indicative of the material's electrical structure. A lower PL emission intensity generally denotes effective charge separation and less recombination, which are associated with increased photocatalytic effectiveness for photocatalytic materials such MXene-based composites (Yuan et al., 2021) [145]. Enhanced separation efficiency of photoinduced carriers is confirmed by this impact, which shows up as a quenching (reduction) in PL intensity. Therefore, in order to clarify the photophysical characteristics of MXene-based photocatalysts, PL spectroscopy is an essential characterization method.

3.4.8. Electrochemical impedance spectroscopy

EIS is an effective method for evaluating the behavior of electron migration and recombination at the electrode–electrolyte interface, which has a direct impact on photocatalytic efficiency. A typical three-electrode electrochemical cell with a working electrode coated in the photocatalyst material, a platinum wire as the counter electrode, and Ag/AgCl as the reference electrode was used to conduct the tests. A homogeneous slurry of the photocatalyst was drop-cast onto a clean fluorine-doped tin oxide substrate to create the catalyst-coated working electrode, which was then allowed to cure at room temperature to adherence [251]. A sinusoidal alternating current (AC) voltage was applied to the working electrode in order to gather impedance data. In order to record both high-frequency and low-frequency electrochemical processes, the excitation signal was usually swept throughout a broad frequency range (10^5 to 10^{-2}Hz) with an amplitude of 5–10 mV. By modulating the amplitude and phase of the generated current, the applied AC voltage makes it possible to determine the impedance components using complicated impedance modeling and Ohm's law [252]. Nyquist plots, which show the relationship between

the real (Z') and imaginary (Z'') components of the impedance, were used to record the resulting impedance spectra. Electrolyte resistance, charge-transfer resistance (Rct), double-layer capacitance, and Warburg impedance related to ion diffusion are frequently calculated using these graphs. **Fig.18** displays a schematic representation of typical EIS spectra [253]. The charge-transfer resistance, which gives information on the rate of electron transport across the catalyst electrolyte interface, was calculated for each sample using the diameter of the semicircular region in the high-frequency domain. Faster charge transfer and reduced recombination losses are associated with a smaller semicircle. [253].

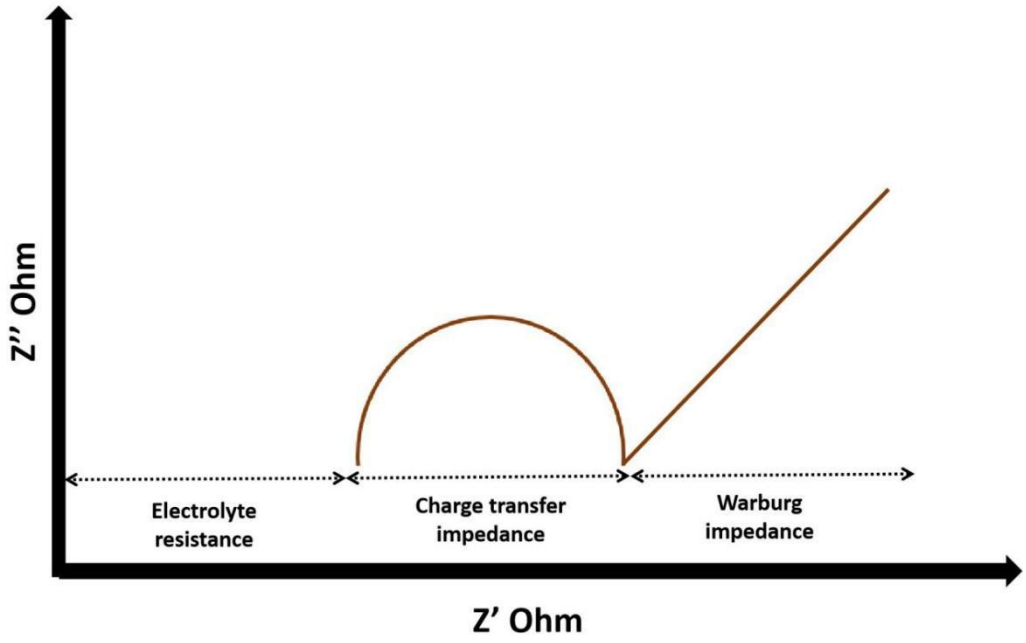

Fig. 18 Schematic representation of Electrochemical impedance spectroscopy

3.4.9.1. Photocatalytic activity tests

The efficiency of the photocatalyst in breaking down organic pollutants or transforming light energy into chemical energy is directly determined by photocatalytic activity tests, which are among the most important assessments in the study of semiconductor-based materials. These experiments offer useful information about the stability, surface reactivity, charge carrier dynamics, and light-harvesting

capacity of photocatalysts under light (Fujishima & Honda, 1972; Herrmann, 1999) [254-255]. Complex organic molecules are mineralized during photocatalytic breakdown to produce simpler, less dangerous substances like CO_2, H_2O, and inorganic ions. When photons with energy equal to or more than the photocatalyst's band gap energy are absorbed, a series of photophysical and photochemical reactions usually takes place. Electrons in the photocatalyst's valence band (VB) are stimulated to the conduction band (CB) by illumination, creating electron–hole pairs (Zhang et al., 2016) [75]. While electrons reduce dissolved O_2 to form superoxide radicals ($\bullet O_2^-$), photogenerated holes oxidize organic molecules or water to produce reactive oxygen species (ROS) like •OH radicals. These charge carriers migrate to the catalyst surface and engage in redox reactions with adsorbed species (He,S., et al., 2022) [256]. The oxidative breakdown of pharmaceutical contaminants is driven by the combined action of these reactive radicals (Wang et al., 2021) [45]. An aqueous solution of the target pharmaceutical pollutant is created at a specified beginning concentration, often in the range of 100 mg/L, in a typical photocatalytic experiment. To uniform suspension, a predetermined quantity of photocatalyst is distributed throughout the solution while being continuously stirred. To create an adsorption–desorption equilibrium between the pollutant molecules and the photocatalyst surface, the suspension is magnetically agitated in the dark for 30 minutes before irradiation. A high-intensity white LED bulb was used to provide visible light irradiation, which contributes to the photocatalytic reaction. Samples are taken out of the reaction vessel at regular intervals (5 to 180 minutes) while it is kept at room temperature. After the photocatalyst is removed from each aliquot by centrifugation, the remaining pollutant concentration is measured spectrophotometrically at the drug's characteristic wavelength using a UV-Vis spectrophotometer [185, 257-258]. Eq (3**)** is used to determine the pollutant's degradation efficiency (η,%).

$$\eta(\%)=\frac{Ca-Ct}{Ca}*100\ldots\ldots\ldots\ldots\ldots\ldots\ldots\ldots..(3)$$

Where, Ca and Ct indicate the pollutant's initial and residual concentrations at time t, respectively.

3.4.9.2. Photocatalyst Stability and Reusability

For real-world uses, the photocatalyst's stability and reusability are essential characteristics. The photocatalyst is recovered by centrifugation following each degradation cycle, cleaned with ethanol and distilled water, dried, and then utilized again for further cycles. Good stability and photocorrosion resistance are indicated by a modest decrease in degradation efficiency across several cycles. Because of their strong layered structure and durable metal–carbon bonding, MXene-based composites have demonstrated exceptional endurance (Kuang et al., 2020) [258]. In general, measurements of photocatalytic activity offer a quantitative and mechanistic knowledge of the behavior of MXene and MXene-based composites when exposed to visible light. These investigations show the promise of materials formed from MXene for environmental remediation, particularly in the destruction of persistent pharmaceutical pollutants, by connecting structural and electrical features determined from characterization techniques to actual photocatalytic efficacy.

Chapter 4
Results and Discussion

Introduction

MXenes are a family of 2D transition metal carbides and nitrides that are well-known for their superior electron mobility, hydrophilicity, tunable surface terminations, and metallic conductivity, which make them perfect for environmental and photocatalytic applications (Naguib et al., 2012; Gogotsi & Anasori, 2023) [94, 212]. Their electrical structure, band gap, charge separation effectiveness, and surface reactivity are all improved by doping and composite creation [104, 212].Due to their chemical stability, partial metabolism, and resistance to biodegradation, pharmaceutical pollutants like cetirizine and ciprofloxacin endure in water bodies. Because of their large surface area, defect-rich structure, and responsiveness to visible light, MXene-based photocatalysts are showing promise as materials to solve this problem [211-212]. This chapter establishes the link between structure, property, and activity by correlating the structural, optical, and surface characteristics of Lanthanum nitrate and V_2O_5-modified MXenes with their photocatalytic performance. Every discussion has been supported with appropriate research.

Section-1

4.1. Fabrication of MAX Phase Using La/V Precursors and Pinecone Biochar Carbon

A reactive carbon source that can take part in high-temperature carbide production with metal precursors is necessary for the creation of MAX phases. Biochar synthesized from pinecone powder was used in this project as a cheap, carbon-rich, and sustainable feedstock. When it reacts with La/V and Al metals, its amorphous nature and high defect density make it ideal for carbide production. The production of biochar and its subsequent transformation into the MAX phase via regulated heat treatment are described in this section [259-260].

4.1.1. Synthesis of pinecone biochar

The raw pinecones were cleaned thoroughly to get rid of any dirt, they were dried for 24 hours at 80°C. After being dried, the material was crushed and moved to an alumina crucible under nitrogen atmosphere while heating. The biomass was heated to 650°C at a rate of 5°C per minute in a muffle furnace, where it was carbonized for 2.5 hours under a nitrogen atmosphere (oxygen-limited conditions) [369]. Hemicellulose, cellulose, and lignin break down in turn during pyrolysis, releasing volatiles and creating a stable aromatic carbon structure. To create a consistent powder of biochar, the carbonized material was ground and sieved after cooling [261].

4.1.1.1. FTIR analysis of Biochar

The synthesized pinecone-based biochar's FTIR spectrum **Fig.19** shows the presence of several surface functional groups that are essential to the biochar's reactivity, adsorption capability, and suitability for MAX phase synthesis. The spectra shows a number of distinctive absorption bands in the 4000–400 cm^{-1} range, which is in line with biochars that have been previously described. The stretching vibrations of hydroxyl (–OH) groups found in alcohols, phenols, and adsorbed water are represented by a wide absorption band seen at about 3662 cm^{-1}. This suggests that hydrophilic surface groups are somewhat retained even after pyrolysis. Biochars made from biomass and pinecone have been shown to exhibit similar O-H vibration. The asymmetric stretching of aliphatic C–H bonds, usually from $–CH_2$ and $–CH_3$ groups, is represented by a strong peak around 2987 cm^{-1}. These bands' existence indicates to the persistence of some aliphatic structures following carbonization. Biochars made

from lignocellulosic precursors frequently exhibit similar characteristics. The band observed at 1393 cm^{-1} may be attributed to the bending vibration of O–H groups in phenolic functionalities and the deformation vibration of aliphatic C–H groups. A contribution from carboxylate ($–COO^-$) groups may also be possible; however, the absence of a distinct C=O stretching band near 1700 cm^{-1} suggests that such functionalities are present only in limited amounts. The absorption bands observed at 1250 and 1066 cm^{-1} are attributed to C–O stretching vibrations of phenolic, alcoholic, and ether functional groups present on the biochar surface. These bands indicate the partial retention of oxygen-containing surface functionalities after pyrolysis and have been widely reported in biomass-derived biochar. The presence of polyaromatic rings created during pyrolysis is confirmed by the sharp band seen around 891 cm^{-1}, which corresponds to aromatic C–H out-of-plane bending. Carbonized biomass materials often have this characteristic [262-264].

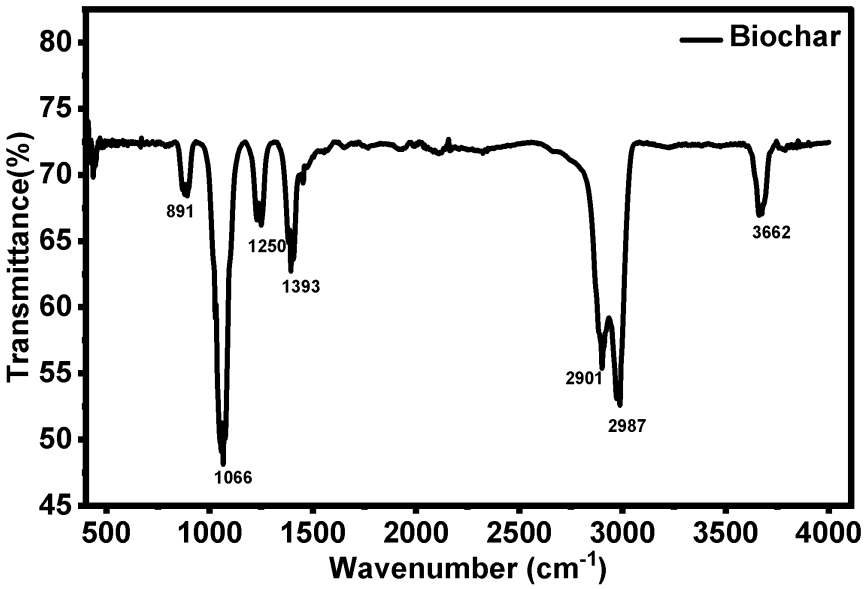

Fig. 19 FTIR spectrum of synthesized pinecone biochar

4.1.1.2. XRD analysis of synthesized Biochar

The synthesized pinecone-based biochar's XRD pattern **Fig.20** shows both partially crystalline and amorphous characteristics, which are typical of lignocellulosic biomass carbonized at moderate pyrolysis temperatures. Disordered turbostratic carbon structures are indicated by a amorphous hump that dominates the diffraction

profile and is centered in the region of 22–25° (2θ). The random stacking and poor ordering of carbon layers created during the thermal breakdown of cellulose, hemicellulose, and lignin are the cause of these wide properties. A weak diffraction feature observed at 28.27° (2θ) may be associated with partially ordered carbon domains; however, because of its low intensity and broad nature, this assignment remains tentative and may also include contributions from mineral phases present in the biochar. The relatively low intensity and broad nature of this diffraction feature indicate that the biochar remains predominantly non-graphitized and contains only small and imperfect aromatic domains. When biomass-derived char is produced at 650 °C, aromatic clusters start to form but do not completely align into graphitic layers, which is a typical structural feature. The amorphous background is contrasted with a prominent sharp diffraction peak at 29.34° (2θ), which may be attributed to the (104) plane of calcite ($CaCO_3$). Such sharp reflections in biochars are generally associated with mineral (ash) components remaining after pyrolysis. Thus, a crystalline inorganic phase (such as calcite or carbonate/salt residue) present as ash in the pinecone feedstock is most likely responsible for the steep 29.34° peak. A few weaker peaks between 30° and 50° (2θ) indicate the presence of mineral impurities, which may be caused by naturally occurring ash components found in pinecone biomass, such as silica, calcium carbonate, and metal oxides. According to previous research, these mineral-associated peaks have been extensively observed in lignocellulosic biochars [265-270].

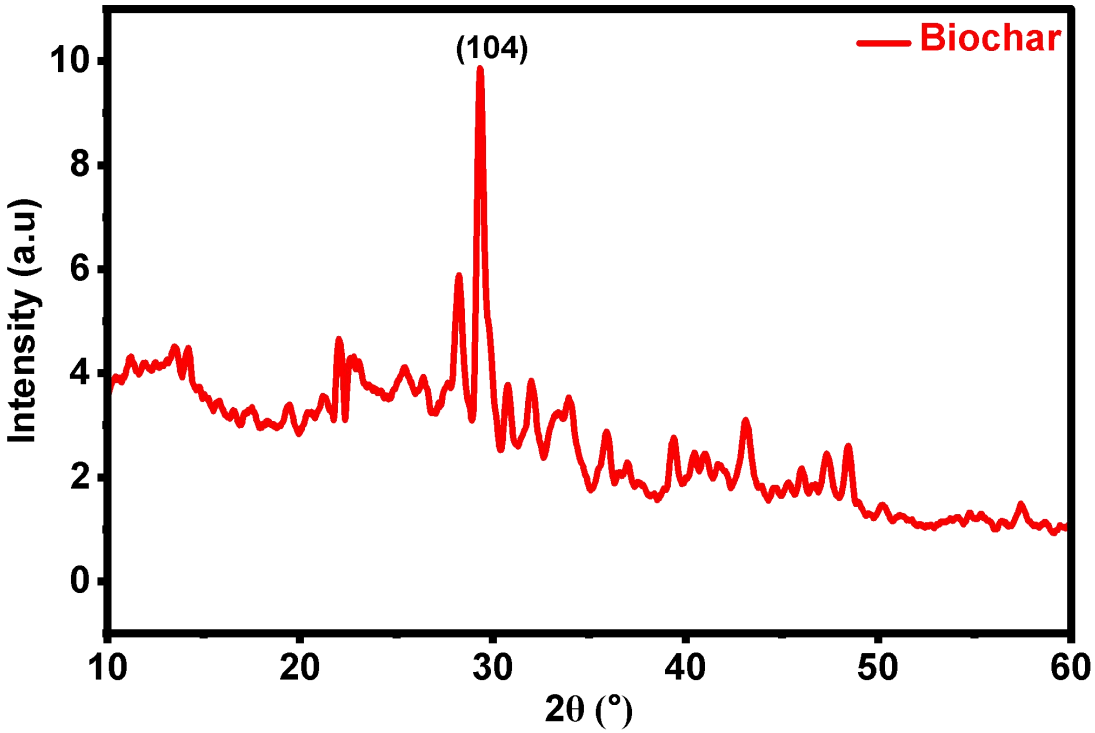

Fig. 20 XRD analysis of pinecone-biochar

4.1.2. Synthesis of MAX phase by using La/V Precursors and pinecone biochar

MAX phase was synthesized by molten-salt technique. Synthesis of MAX phase was performed at high temperature. The stoichiometric proportions of the La/V metal powders, aluminum and synthesized biochar carbon were thoroughly combined to create MAX phases in the ratio of 3:2:1 by using a mortar and pestle. After that ball milling process was performed for 24 hr, the mixed powder was combined with potassium bromide (KBr) in a 1:1 weight ratio in ethanol as a dispersion solvent to promote this process. Ethanol should be evaporated in a water bath and then dried in a hot air oven. Pellets are made with a KBr press, placed within a crucible, and sintered for 8 hours at 1200 ºC. MAX phase powder is obtained by washing in boiling distilled water to remove the salt. After that the obtained powder was dried in hot-air oven at 60 ºC for 5 hours [271].

4.1.2.1. XRD analysis of synthesized MAX phases

Fig.21 shows the XRD patterns of MAX phase (MAX), Lanthanum nitrate based MAX phase (La/MAX) and V_2O_5 based MAX phase (V/MAX) reveals a diffraction

peaks at around 39.46º corresponding to the (104) plane, indicating the presence of aluminum layers. The intense diffraction peak observed at around 9.45° corresponds to the (002) plane of Ti_3AlC_2 MAX phase, confirming its layered structure. In La/MAX and V/MAX, the intensity of this peak decreases significantly, indicating structural distortion and reduced crystallinity caused by the presence of lanthanum and V_2O_5 species. The peak at 60.62º corresponds to (110) plane also indicates the formation of MAX phase. The weak intensity of the (002) peak in La/MAX suggests reduced crystallinity and structural distortion due to the larger ionic radius of lanthanum species. Additional diffraction features observed between 27° and 32° may be associated with lanthanum-containing phases, such as lanthanum oxides, lanthanum titanate, or lanthanum aluminate [272–273] The reduced intensity of the (002) peak in V/MAX also suggests decreased crystallinity and modification of the layered structure due to the presence of V_2O_5. A weak diffraction peak at 13.03º in V/MAX may be associated with V-containing phases and structural modification of the MAX phase[272-273].

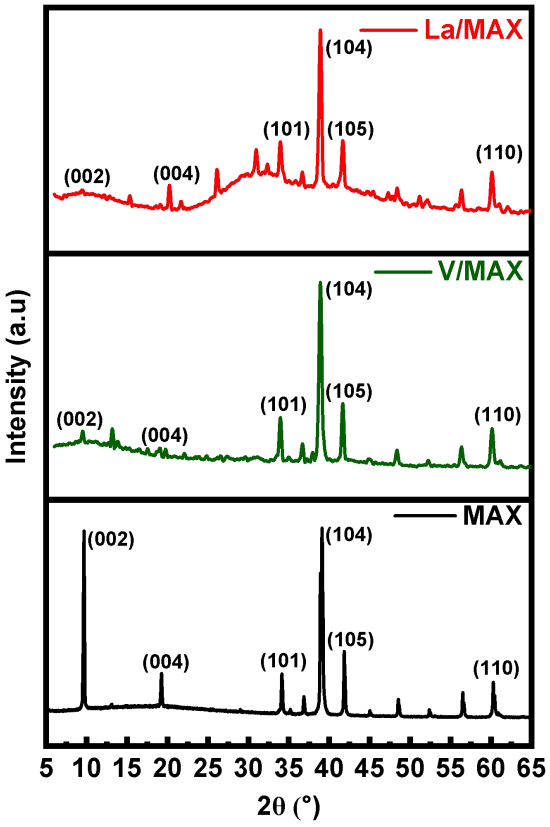

Fig. 21 XRD patterns of MAX phase (Ti_3AlC_2), V_2O_5-based MAX phase (V/MAX), Lanthanum nitrate based MAX phase (La/MAX).

4.1.2.2. FTIR analysis of synthesized MAX phases

FTIR spectrum of MAX phase, La-based MAX phase (La/MAX) and V-based MAX phase (V/MAX) shows in **Fig.22** shows characteristic absorption bands corresponding to Ti–O, Al–O, La–O–Al, V–O and oxygen-containing surface groups at around 482, 541, 800, 1005, 1295, 1433, 1553 and 3580 cm^{-1}. The Broad O–H stretching of $La(OH)_3$ due to adsorbed water at around 3580cm^{-1}. The stronger peaks at 1005 cm^{-1} and 1295 cm^{-1} shows the La–O–Al networks. The peak at 1433 cm^{-1} indicates the presence of residual NO_3^- from $La(NO_3)_3$ not fully decomposed. The bands around 482 cm^{-1} and 541 cm^{-1} are attributed to Ti–O and Ti–C related vibrations, whereas the appearance of a band near 800 cm^{-1} corresponds to V–O stretching due to V_2O_5 formation. The appearance of the band at around 800 cm^{-1} is attributed to V–O stretching, confirming the presence of V_2O_5 species. The sharp band at around 1005 cm^{-1} is assigned to the V=O stretching vibration of V_2O. The band at 1433 cm^{-1} may be associated with carbonate species (COO^-) or residual nitrate groups from incompletely decomposed $La(NO_3)_3$. The weak band around 1553 cm^{-1} could arise from oxygen-containing surface functionalities [272–274]. The difference between the FTIR spectra of MAX and V/MAX is attributed to the incorporation of V_2O_5, which introduces additional V–O and V=O vibrational bands and modifies the local chemical environment of the MAX phase. These changes confirm the successful incorporation of vanadium species into the MAX structure.

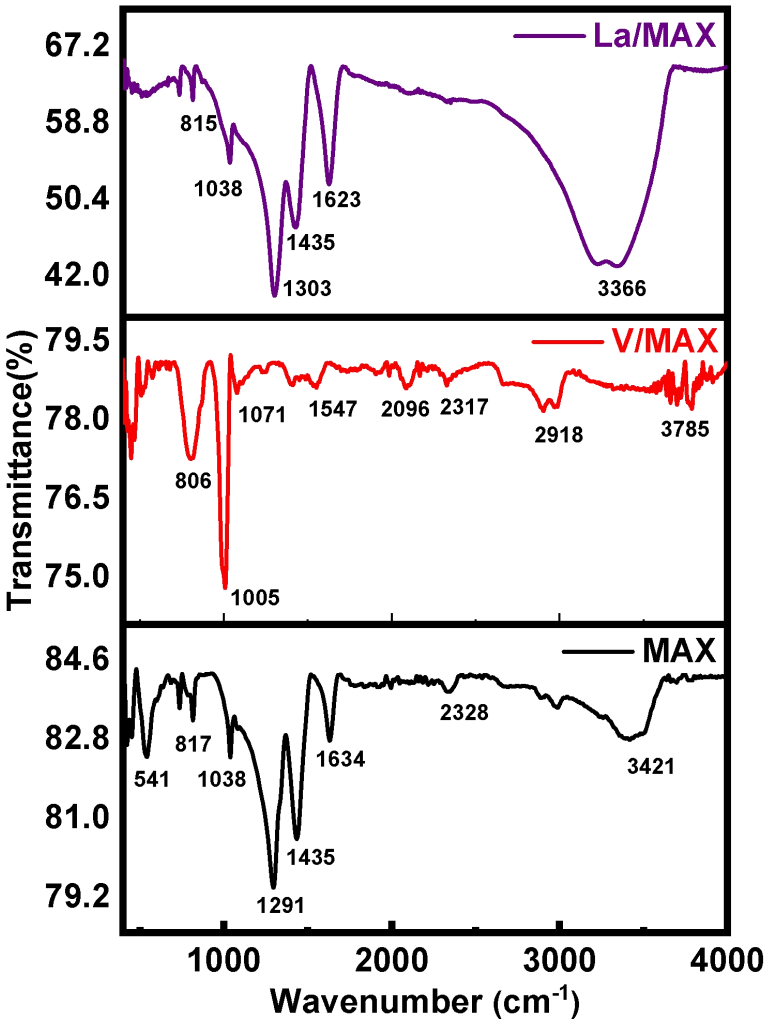

Fig. 22 FTIR spectrum of MAX phase, La-based MAX phase and V-based MAX phase

4.1.2.3. SEM analysis of MAX phases

The SEM picture of MAX phase, La/MAX and V/MAX materials shows the appearance of being thick, compact and densely packed structure because the layers are strongly bonded with each other [272-275]. **Figure 23** illustrates the uneven surface and densely packed structure of all the MAX phases.

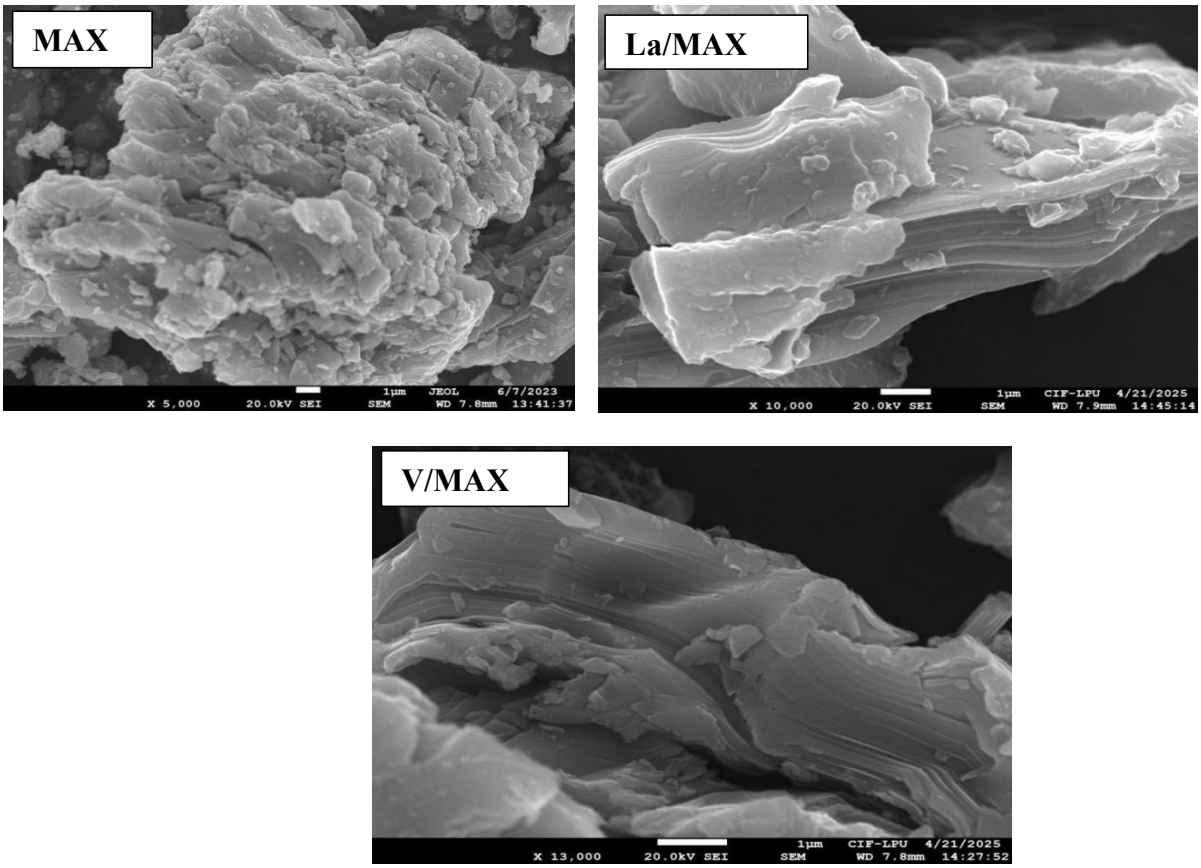

Fig. 23 SEM images of MAX phase, La-based MAX phase and V-based MAX phase

4.1.3. Performance of MAX, La/MAX, and V/MAX Phases in Photocatalytic and Dark-Phase Decontamination

The adsorption behaviour of MAX, La/MAX, and V/MAX phases towards cetirizine was examined under dark conditions, while photocatalytic degradation was investigated under visible light irradiation at different pH values (2, 4, 6, 7, 8, and 10) to evaluate the drug removal capability of the synthesized precursor materials. Prior to visible light irradiation, the catalyst suspension was stirred in the dark for 120 minutes to attain adsorption–desorption equilibrium. Both the La/MAX and V/MAX phases exhibited low adsorption under dark conditions **(Fig.24A)** and moderate photocatalytic degradation under visible light irradiation **(Fig.24B)**, with V/MAX exhibiting comparatively better performance. These findings validate the necessity of etching into MXene and confirming that MAX phases alone are not responsible for

high photocatalytic performance. This behavior is in line with previous findings that MAX phases have low specific surface area, thick lamellar structures, and a restricted supply of active sites needed for catalytic or adsorption reactions [272-276]. The low pollutant removal observed under dark conditions indicates that adsorption contributes only marginally to cetirizine removal. Therefore, the enhanced removal under visible light can mainly be attributed to photocatalytic degradation rather than adsorption.

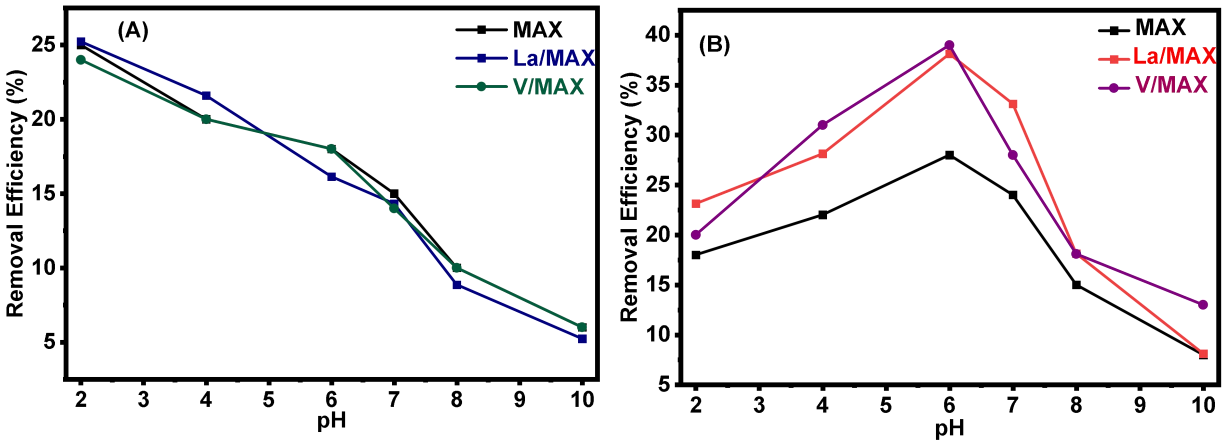

Fig. 24 (A) Dark-phase adsorption behavior of MAX, La/MAX, and V/MAX phases towards cetirizine. (B) Photocatalytic degradation behavior of MAX, La/MAX, and V/MAX phases under visible light irradiation.

Section-2

4.2. Enhanced Photocatalytic Degradation of Ciprofloxacin from Pharmaceutical Wastewater Using Microwave-Synthesized Lanthanum/MXene Nanocomposites

4.2.1. Introduction

Water contamination can arise from various sources such as pharmaceutical companies, textiles, municipal sectors, homes, companies that create agricultural chemicals, beverages, food factories, medical facilities, and oil refineries. Due to their widespread use, pharmaceuticals are released into the ecosystem in their unused form or as their metabolites. Since a majority of drugs are extremely polar and not so volatile that's why they have a higher tendency to remain in water. Some pharmaceutical drugs have pharmacological properties and can be found in non-prescription, prescription, and animal medicine drugs. Therefore, pharmaceuticals tend to be found in industrial wastewater pollutants that may have some of their constituents partially eliminated [277]. The contaminants include antibiotics, which are widely employed in treating infections by bacteria in animals, plants, and humans. These drugs are usually released into aquatic environments without restriction, resulting in the development of antibiotic resistance that danger the ecosystem and human health. Because of extremely high chemical stability, ciprofloxacin, one of the fluoroquinolone antibacterial drugs that are most commonly found in aquatic habitats, is typically not biodegradable and is difficult to remove using traditional water treatment methods [278].

Advanced oxidation processes have been recognized as an effective tactic for removing ciprofloxacin from water, and they can convert organic pollutants that are harmful to less harmful or not hazardous compounds. For example, typical oxidizing agents for the formation of reactive species by different activation techniques like UV and ultrasonic are ozone, hydrogen peroxide, chlorine as well as sulfates [279]. A lot of focus has been placed on photocatalysis, which uses solar radiation to produce active species that help antibiotic drugs break down into less harmful compounds in the environment. It is a procedure in which radiation of light generates positive and negative charge carriers, which then take part in the redox processes that are necessary for degradation by sunlight. The redox reaction capability of the

photocatalytic material is determined by the valence band and conduction band potentials. However, several photocatalytic materials that are based upon semiconductors particularly those that have high bandgap frequently exhibit poor photocatalytic efficacy because of their limited range for light response and fast recombination of charge carriers. Numerous approaches have been utilized so far to solve this problem, such as heterogeneous structure creation, doping of metals, morphological changes, and exposure of crystal facets, which can all help to simplify the separation of charge carriers in order to increase photocatalytic capabilities [280].

Two-dimensional materials are widely used because of their great electronic conductivity, huge surface area, and active sites which are exposed to combine with a wide range of semiconductor photocatalytic materials to generate established heterostructures [281]. When paired with semiconductor photocatalysts, MXenes ($Ti_3C_2T_x$ and their corresponding structures) are a class of two-dimensional materials composed of carbonitrides, carbides, or nitrides of transition metals. Their low Fermi energy level and superior electrical conductivity make them efficient electron sinks. MXene has hydrophilic nature is demonstrated by a double nature that exhibits semiconductor and metallic properties as well as strong mechanical and chemical durability, improving the application significance of MXene in the fields of co-catalyst, photocatalysis, and filtration of water [282].

For the degradation of Ciprofloxacin (CIP), a variety of MXene-based structures were used such as CXB, Ti_3C_2-Bi/ BiOCl, and TiO_2/g–C_3N_4. When CIP was exposed to visible light, CXB (carbon nitride/Ti_3C_2 MXene/black phosphorus) synthesized by calcination achieved exceptional photodegradation efficiency (less than 99% in 60 min). Bi/BiOCl was incorporated into MXene nanosheets to create outstanding Ti_3C_2-Bi/BiOCl photocatalysts, which demonstrated a high degrading efficiency (89%) for CIP. The rapid degradation of CIP is caused by the stimulation of photogenerated charge separation performance by heterojunction creation and Ti_3C_2 MXene's greater electrical conductivity. TiO_2/g–C_3N_4 photocatalyst anchored in graphene layers demonstrated superior catalytic activity for CIP degradation. Rare-earth elements typically have a significant impact on the development of a material's many features, including improvements in electrical, optical, and magnetic capabilities. Pharmaceutical drugs almost entirely mineralize (97.5%) into CO_2 and H_2O by nano

hetero-structures MXene/$La_{0.5}Sr_{0.5}CoO_3$, all without producing hazardous environmental byproducts. Pharmaceutical drugs, particularly tetracycline hydrochloride in the visible region, can be degraded extremely effectively by MXene/$La_{0.5}Sr_{0.5}CoO_3$ [283].

The proposed work successfully synthesized the MXene and Lanthanum nitrate-modified MXene composites (La/MX) by microwave technique to reduce the time in the synthesis process, which was then utilized to degrade the ciprofloxacin drug from an aqueous medium. The photocatalytic uses of MXene-based photocatalysts have been well explored. But, this study offers a novel comparison between synthesis methods, examines the impacts of La incorporation, and examines effectiveness for ciprofloxacin degradation under visible light conditions, all of which are supported by charge transfer and surface feature analysis, despite the fact that MXene-based photocatalysts have been thoroughly studied [284]. This study presents a novel La/MX photocatalysts synthesized via microwave-assisted method for the photocatalytic degradation of ciprofloxacin under visible light irradiation. Microwave-assisted synthesis, antibiotics degradation, and lanthanum doping have all been studied in previous reports [285]. This work introduces a novel material with improved photocatalytic effectiveness and recyclability that was created using a quick microwave-assisted process.

Rapid and volumetric heating from microwave irradiation leads to faster development and crystal growth, improved reaction kinetics because of localized superheating and better ion dispersion (e.g., La^{3+} ions) [286], and shorter synthesis times than traditional heating techniques [287]. These elements result in increased surface area, enhanced material homogeneity, and better crystallinity, all of which have a direct impact on photocatalytic performance [287]. Photocatalysis has emerged as a viable and efficient technique for environmental cleanup, particularly for the removal of pharmaceutical contaminants, when exposed to sunlight or visible light. Complex drug molecules are broken down into less dangerous byproducts by this process, which generates reactive oxygen species (ROS) like superoxide ions and hydroxyl radicals [288]. All the utilized photocatalytic materials were characterized by SEM, XRD, FTIR, and EDX techniques. Furthermore, all the as-prepared La/MXene composites showed enhanced photocatalytic performance in the elimination of

ciprofloxacin. The most significant reactive species are hydroxyl radicals in the photocatalytic reaction, according to the results of the radical trapping experiment. Furthermore, the possible mechanism and reusability were also examined.

4.2.2. Materials and Methods

4.2.2.1. Chemicals Consumed

MAX phase (Ti_3AlC_2) was purchased from Nanoshel, Lanthanum nitrate, hydrofluoric acid (40%), sodium hydroxide, and dimethyl sulphoxide (DMSO) was purchased from Loba Chemie Pvt.Ltd, India. All chemical reagents were used without any additional purification. Solutions are prepared using distilled water. Ciprofloxacin drug was bought from a local medical shop in Punjab, India.

4.2.2.2. Synthesis of MXene (Ti_3C_2Tx)

4.2.2.2.1. Conventional Method

MXene was synthesized via the HF etching process by dispersing 1 g of Ti_3AlC_2 MAX phase powder into 10 mL of hydrofluoric acid, followed by continuous magnetic stirring for 22 h. After that, the suspension was centrifuged at 4500 r/min for 20 min then washed several times with distilled water and dried at 60 °C to obtain the black (Ti_3C_2Tx) MXene powder. After that for delamination and intercalation, the obtained powder was immersed in 15 ml DMSO at room temperature with magnetic stirring for 22 h and then centrifuged at 4000 r/min for 20 min. The obtained material was dispersed in 300 ml distilled water under sonication for 5 h and then again centrifuged at 4000 r/min for 20 min and then dried at 60–70°C for 24 h to obtain the exfoliated sheets of **MXene (conventional)** [289] as shown in **Fig.25**.

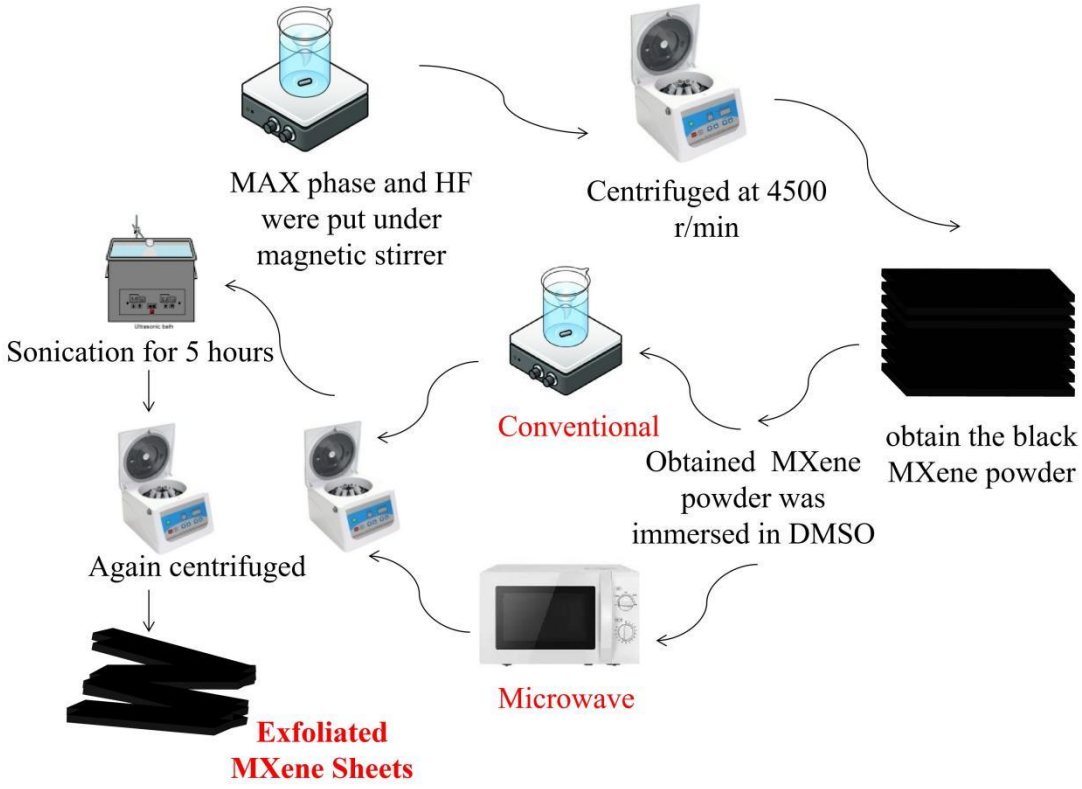

Fig. 25 Schematic illustration of the synthesis of MXene by conventional and microwave-assisted methods.

4.2.2.2.2. Microwave-Assisted method

The synthesis of MXene using the microwave-assisted (MW) method followed the same procedure as the previously described process up to the etching of the aluminum layer from the MAX phase, as shown in **Fig.25.** After that for delamination and intercalation, to reduce the time from many hours to few minutes the obtained powder was microwave heated at 300W for 10 min with 15 ml of DMSO and then centrifuged at 4000r/min for 10 min and then the material with distilled water was sonicated in for 5 h. Again, centrifuged at 4000 r/min and then dried at 60°C for 24 h [290].

4.2.2.3. Synthesis of Lanthanum nitrate-modified MXene (La/MX) Composites

The conventional process for synthesizing La/MX was carried out using a co-precipitation approach. The precursor ratios and reaction conditions were optimized in the present study. First of all, lanthanum nitrate solution was prepared by adding the lanthanum nitrate in 250 mL distilled water and stirred for one hour on magnetic stirrer. For the 1:1 ratio, 500 mg lanthanum nitrate and 500 mg MXene were used. For

the 1:2 ratio, 250 mg lanthanum nitrate and 500 mg MXene were used, while for the 2:1 ratio, 500 mg lanthanum nitrate and 250 mg MXene were used. After that, the as-prepared MXene (conventional) powder was added in to Lanthanum nitrate solution and again stirred for 5 hours at 60 to 80 degree Celsius as shown in **Fig.26.** After that, the prepared mixture was cooled at room temperature and filtered. The prepared sample was washed many times with distilled water to maintain the pH 6-8 and then dried in oven at 60 ºC to make powder for further characterization. In this way, we prepared three different concentrations of Lanthanum nitrate and MXene samples with the ratios of 1:1, 1:2, and 2:1[291].

For the synthesis of La/MX by microwave method (La/MX (MW)), again we prepared three lanthanum nitrate solutions by adding lanthanum nitrate in 50 mL distilled water and then the synthesized MXene powder was added in to lanthanum nitrate solution with three different ratios (1:1, 1:2 and 2:1) and heated in microwave for 10min at 200W. The quantities of lanthanum nitrate and MXene used were the same as those employed in the conventional method. Then the mixture was cooled at room temperature, filtered and washed many times with distilled water for maintained the pH 6-8. After that, the material was dried in oven at 60 degree celsius [291].

4.2.3. Materials Characterization

The spectral variations in the 200–700 nm wavelength range were analyzed using a UV-1700 Shimadzu UV spectrophotometer, while the functional groups of the materials were identified through Perkin Elmer Fourier Transform Infrared Spectroscopy (FTIR). The crystallinity was examined using X-ray diffraction (XRD, Bruker) at the 2θ range of 6°–80°. The surface morphology and elemental content of all the materials were examined using an energy-dispersive X-ray (EDX) spectrometer and a scanning electron microscope (SEM).

4.2.4. Assessment of Photocatalytic Activity

The degradation of 100 mg/L of ciprofloxacin was used to assess the photocatalytic activity under visible light. 100 mg of ciprofloxacin was dissolved in 10 mL of 40% HCl to create a stock solution, which was subsequently diluted with 1000 mL of distilled water. 30 mL of ciprofloxacin solution was mixed with 10 mg of photocatalyst for each test, and the pH was changed with either 0.1 M HCl or NaOH. Under visible light, the reaction was conducted at room temperature. A preset volume

of solution were centrifuged and filtered using Whatman paper for analysis at regular intervals. To determine the maximum absorbance wavelength (λmax) of ciprofloxacin, absorption spectra in the 200–700 nm range were recorded using a UV–Vis spectrophotometer. The distinctive absorption of ciprofloxacin was detected at 278 nm, when a high absorption peak was seen. In order to determine the degradation efficiency for each photocatalytic degradation experiment, the filtrates were analyzed with a UV–Vis spectrometer at 278 nm. Investigations were conducted on the effects of pH, exposure time, and H_2O_2 [292]. Photocatalytic degradation tests were conducted with a 60W white LED bulb (operating at 220 V, 50 Hz) under visible light. According to the manufacturer's specifications, the light source generates slightly less UV light and mostly in the range of visible light (400–700 nm). To confirm uniform irradiation, the reactor was positioned at a predetermined distance (about 15 cm) from the bulb; throughout the experiments, no natural sunlight was used. The quantity of ciprofloxacin degradation caused by photocatalysis was calculated using Eq.(4) as follows:

$$\text{Photo-degradation (\%)} = \frac{(Ca-Cb)}{Ca} X 100 \ldots\ldots\ldots\ldots\ldots\ldots (4)$$

Where, Ca and Cb are the initial and final concentrations (mg/L) of pharmaceutical drugs, respectively.

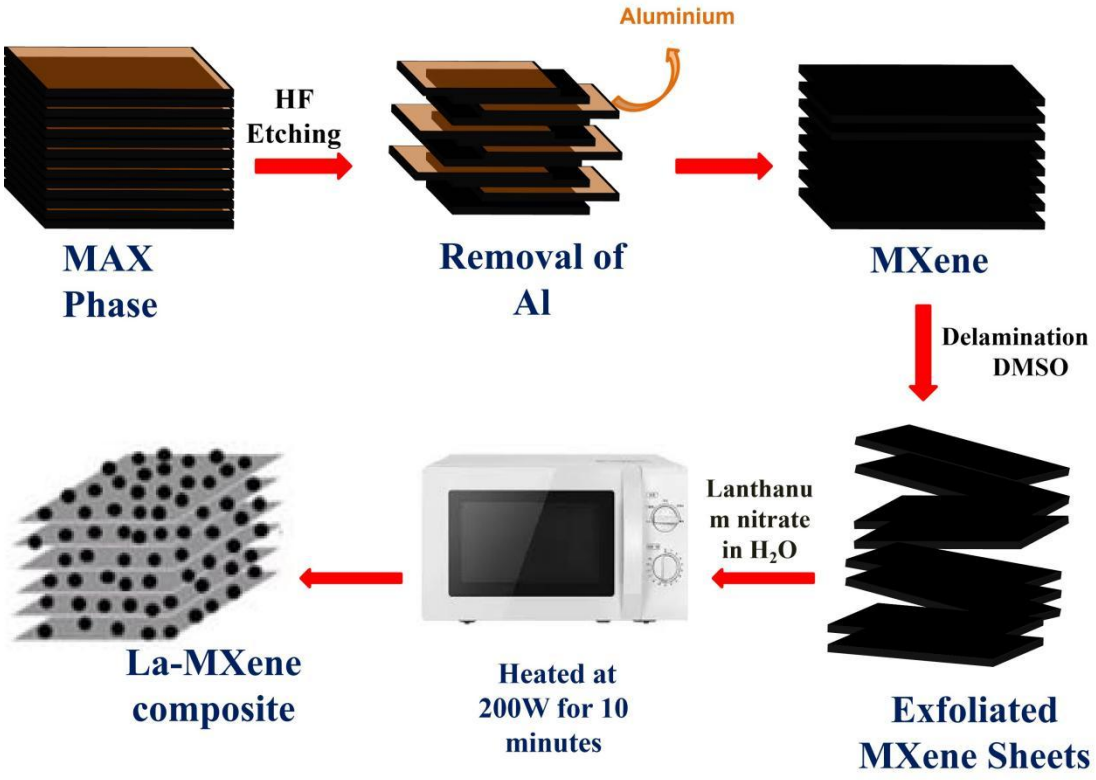

Fig. 26 Schematic diagram for the synthesis of MXene and La/MX nanocomposite by microwave method**.**

4.2.5. Results and Discussion

4.2.5.1. Structural and Phase analysis

In **Fig.27,** XRD was used to assess the phase of MAX phase, MXene prepared from conventional and from microwave method **(A)** and the La/MX composite prepared from both conventional **(B)** and microwave method **(C)** with three different ratios (1:1, 1:2 and 2:1). In Fig.27 **(A),** the XRD analysis confirms the successful synthesis of MXene by conventional and microwave method from MAX phase. The XRD peaks of MAX phase shows at 9.45°, 19.21°, 33.76°, 39.09°, 35.39°, 56.44°, 41.64°, and 60.39° represents (002), (004), (101), (104), (103), (109), (105) and (110). The reflection (002), which relates to the MXenes basal planes, shows shifts from higher to lower (9.68° to 6.25° in MXene (conventional) and 9.68° to 6.44° and 9.03° in MXene (Microwave) 2θ values), indicates the rise of interlayer space [293]. The two peaks splitting in MXene (Microwave) from initial single (002) peak of MAX phase due to the layer stacking variations and distortions might result from the etching step and

afterward the addition of surface terminations. The sharp peak (104) at 2θ=39.09° can be seen in MAX phase (Ti_3AlC_2) corresponds to aluminium, and this almost disappeared in both cases of MXene (conventional and microwave) that confirms transformation of MXene from MAX phase and successful removal of Al layers. In MXene (conventional), the peaks at 25.23° and small peaks at 27.13° and 28.76° might shows the extra reflections or interferences from molecules that have intercalated or residualized in the MXene structure. Also, the small peaks at 35.53° and 41.24° corresponds to (103) and (105) planes represents TiC impurities. In MXene (microwave), the peak at 19.21° represents (004) of MAX phase shifts towards lower angle 18.48° corresponds to (004), shows rise in the interplanar distance. In addition, the (006) reflection peak at 27.48° were also observed. The diffraction peaks at (103) and (105) at the position of 35.30° and 41.16° due to the impurities of TiC. In both MXenes, during the etching of Al layer, there was little amount of titanium dioxide was formed which was visible in the 40–45° 2θ range. The difference between MXenes (conventional and microwave) is that the peak intensity of MXene (microwave) has high intensity of those peaks which shifts from max phase due to the increase of interlayer space than MXene (conventional) [293-298].

Fig.27**(B)**, represents the XRD of La/MX synthesized by conventional method (La/MX), the diffraction peaks (002) and (102) at 25.42°, 27.70°, 39.15° are belongs to Lanthanum on the surface of MXene. The comparison between the XRD results showed the (002) peak show shifting from MXene (conventional) 6.25° to 5.79° in (1:1) where both MXene and lanthanum content are equal, 5.94° in (1:2) where lanthanum content was less than MXene and 5.52° in (2:1) where lanthanum content was more than MXene in synthesized composites. The significant shifts in the (002) peak to lower angles may be due to the successful intercalation of lanthanum ions which was maximum in (2:1), where lanthanum content was more relative to Mxene. The MXene related peaks have less intensity in (2:1), whereas in (1:2) and (1:1) have higher intensity of MXene peaks [293-298].

Fig.27 **(C)**, represents the XRD of La/MX synthesized by microwave method (La/MX (MW)), the diffraction peaks (002) was found at position 9.07° in (1:1) where both lanthanum and MXene are in equal amount, 8.80° in (1:2) where MXene content was more than lanthanum and 9.03° in (2:1) where Lanthanum content was more than

MXene. An indication of little intercalation caused by the introduction of lanthanum ions due to the splitting of MXene peaks in the composites with ratio (1:1) and (2:1). Grain size increase, MXene stacks and the basal plane are all indicated by the sharpness with minor shifts at 60.88° in all composites. The peaks appears in all composites 73.27° confirmed the lanthanum presence in the surface of MXene. These results indicates the presence of lanthanum on MXene's surface in all La/MX composites (conventional and microwave) [293-298]. **Table 3** provides a summary of the XRD results for MAX phase, MXene synthesized by conventional and microwave method and Lanthanum based MXene composites synthesized by microwave method.

Table 3 A tabular data for XRD peak evaluation

Peak position (°)						
MAX phase	**MXene (conventional)**	**MXene (microwave)**	**La/MX (1:1)**	**La/MX (1:2)**	**La/MX (2:1)**	**hkl**
9.45°	6.25°	6.44° 9.03°	9.07°	8.80°	9.03°	002
19.21°	25.23° 27.13° 28.76°	18.48° 27.48°	18.31° 27.59°	18.31° 27.59°	18.31° 27.59°	004
33.76°						101
39.09°						104
35.39°	35.53°	35.30°	35.16° 37.03°	35.16° 37.03°	35.16° 37.03°	103
41.64°	41.24°	41.16°	41.51°	41.51°	41.51°	105
56.44°						109
60.39°			60.88° 73.27°	60.88° 73.27°	60.88° 73.27°	110

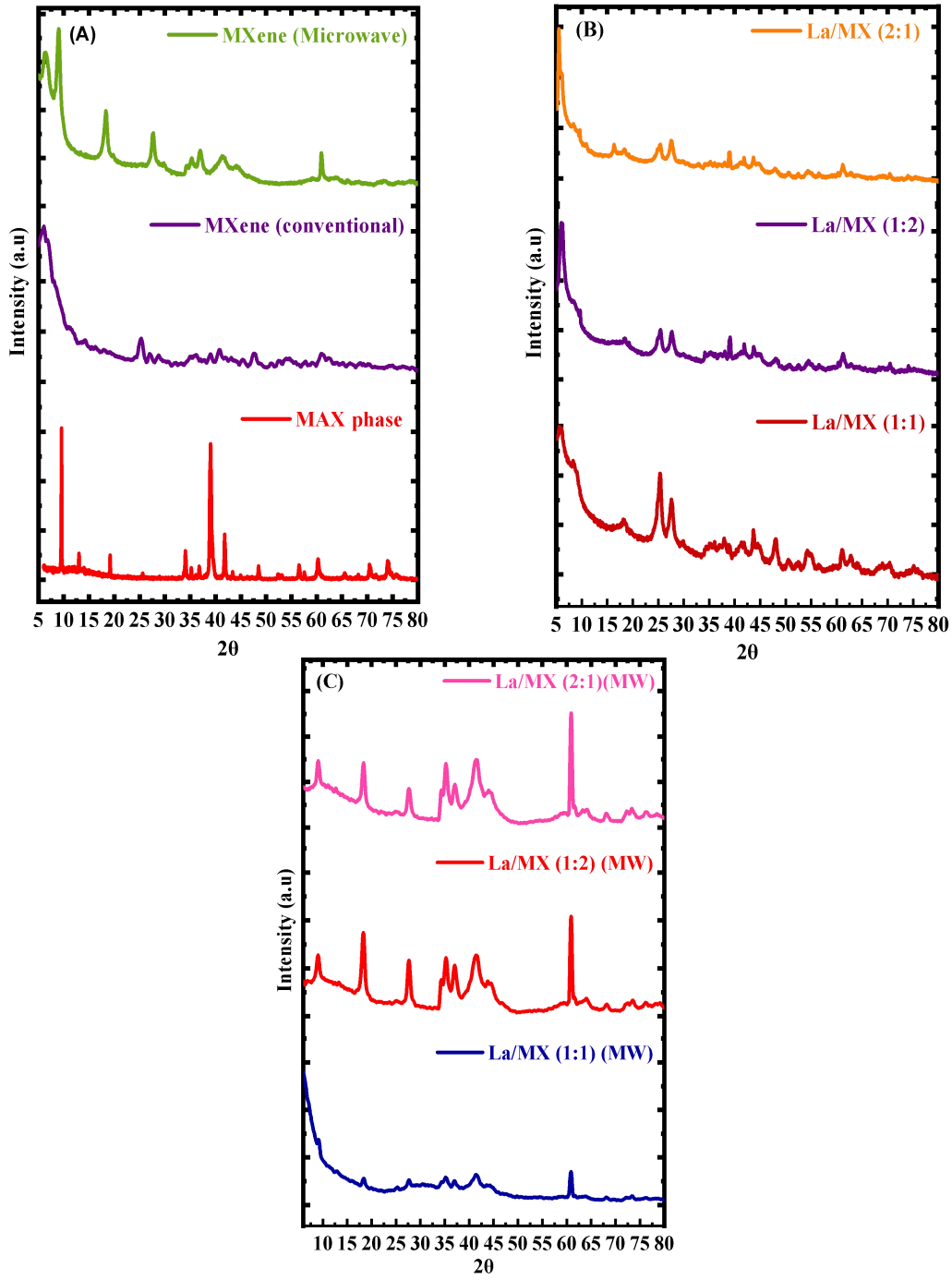

Fig. 27 XRD analysis of (A) MAX phase, MXene (conventional) and MXene (Microwave), (B) La/MX composite synthesized by conventional method and (C) La/MX composite synthesized by microwave method

4.2.5.2. Surface Morphology Analysis

The SEM characterization was carried out to analyze the surface morphology of MAX phase, MXene prepared by HF etching method, MXene prepared by microwave method, La/MX composite synthesized by conventional method in ratio (1:2) and La/MX composite prepared by microwave method with ratio (1:2) as shown in **Fig.28 [A, B, C, D and E].** In **[A],** the SEM images of MAX phase material shows the layered structure which appears dense, compact and tightly together due to strong bonding between the layers. Overall, there is not much exfoliation and the substance appears continuous. But after the treatment with hydrofluoric acid, the MAX phase exfoliates in two dimensional sheets MXene due to the removal of aluminium layer. It is possible that the exothermic reaction between the MAX phase and hydrofluoric acid. In **[B],** the MXene synthesized by conventional method looks the less compact and more open and thinner layered structure compared to the MAX phase images. The porosity and gaps presence appears increased between the layers of MXene due to the removal of aluminum layer. The MXene delaminated by microwave method may have lesser defects and more uniform compared to conventionally synthesized MXene. The layers of MXene prepared by microwave method appear more exfoliated and more loosely stacked than conventionally synthesized MXene as shown in **[C].** The SEM images of both La/MX synthesized by conventional and microwave method in **[D]** and **[E]** shows the MXene surface loaded with majority of Lanthanum nanoparticles which confirms the synthesis of La/MX composite and **[E]** shows, small amount of lanthanum nanoparticles are injected in the MXene layers which prevents the restacking of MXene [297-300].

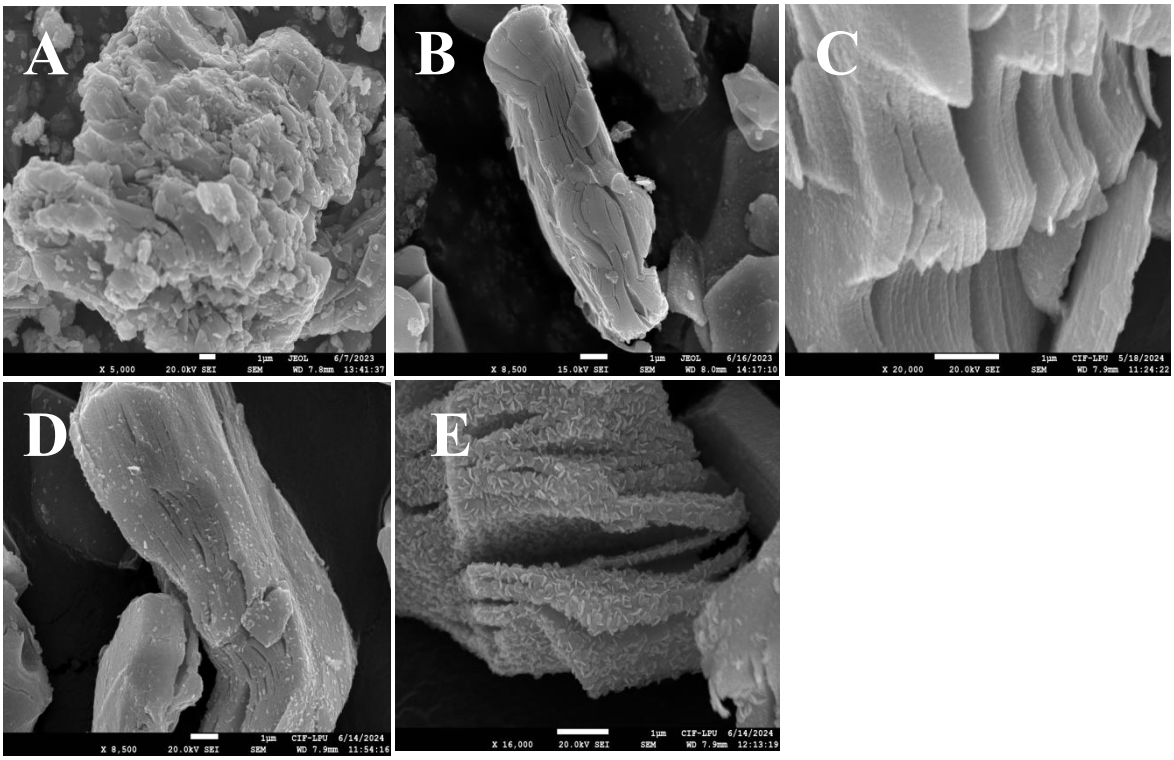

Fig. 28 SEM analyses of MAX phase(A), MXene (conventional (B), MXene (Microwave (C), La/MX nanocomposite (conventional) (D) and La/MX nanocomposite (microwave) (E)

4.2.5.3. Elemental Analysis by EDX

EDX elemental analysis (**Fig.29, 30, 31, 32**) validates composition shifts from MAX to MXene and La/MX composites synthesized by microwave method. Ti, Al, and C peaks in the MAX phase are displayed in **Fig.29**, with Al at 20.05%. Effective Al removal is indicated by the peaks for Ti, C, O, F, and traces of Al (0.26% and 0.13%) that MXene (conventional) in **Fig.30** and MXene (microwave) in **Fig.31** shows after etching. Variations in the peak intensities of Ti and C indicate changes in the chemistry and stoichiometry at the surface [301]. La presence is confirmed by **Fig.32**, which displays peaks for La, Ti, C, O, F, and residual Al in the La/MX (1:2) composite [302, 290]. HF utilized in MXene production is the reason fluorine occurs

in EDX, with –F terminations probably still present on the surface. Surface characteristics, zeta potential, charge behavior, and photocatalytic activity can all be influenced by these, which may improve photocatalytic performance. **Table 4**, shows the atomic percentages of all elements by EDX analysis of all materials. Energy-dispersive X-ray spectroscopy (EDX) was used to evaluate the synthetic materials' elemental composition. Ti, C, O, and La are confirmed by the EDX spectra shows that the etching and subsequent Lanthanum loading were successful. Table 4 provides a summary of the quantitative elemental composition to go along with the qualitative spectra. The table offers accurate atomic and weight percentages, providing a better understanding of loading efficiency and elemental distribution, while the spectrum visually validates the elemental profile.

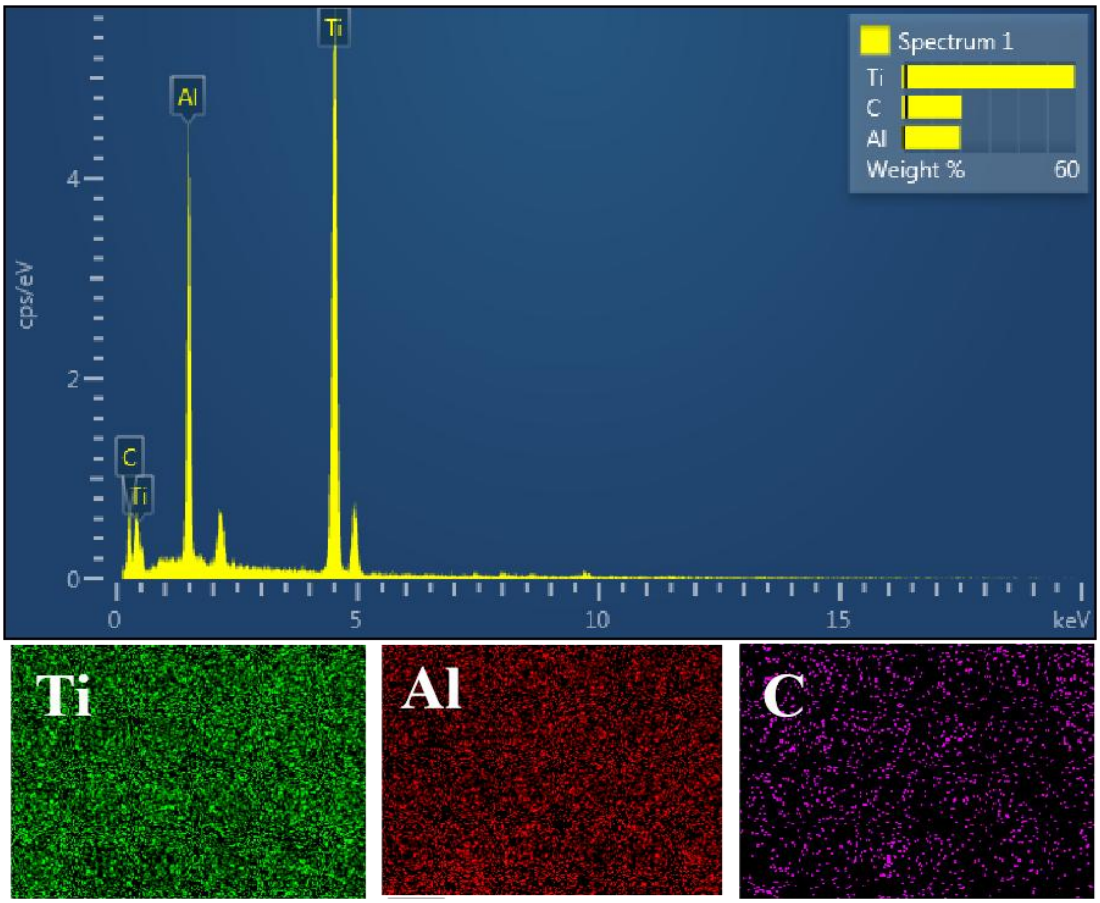

Fig. 29 EDX analysis of MAX phase (Ti_3AlC_2) with elemental mapping of Titanium (Ti), Aluminium (Al) and Carbon (C)

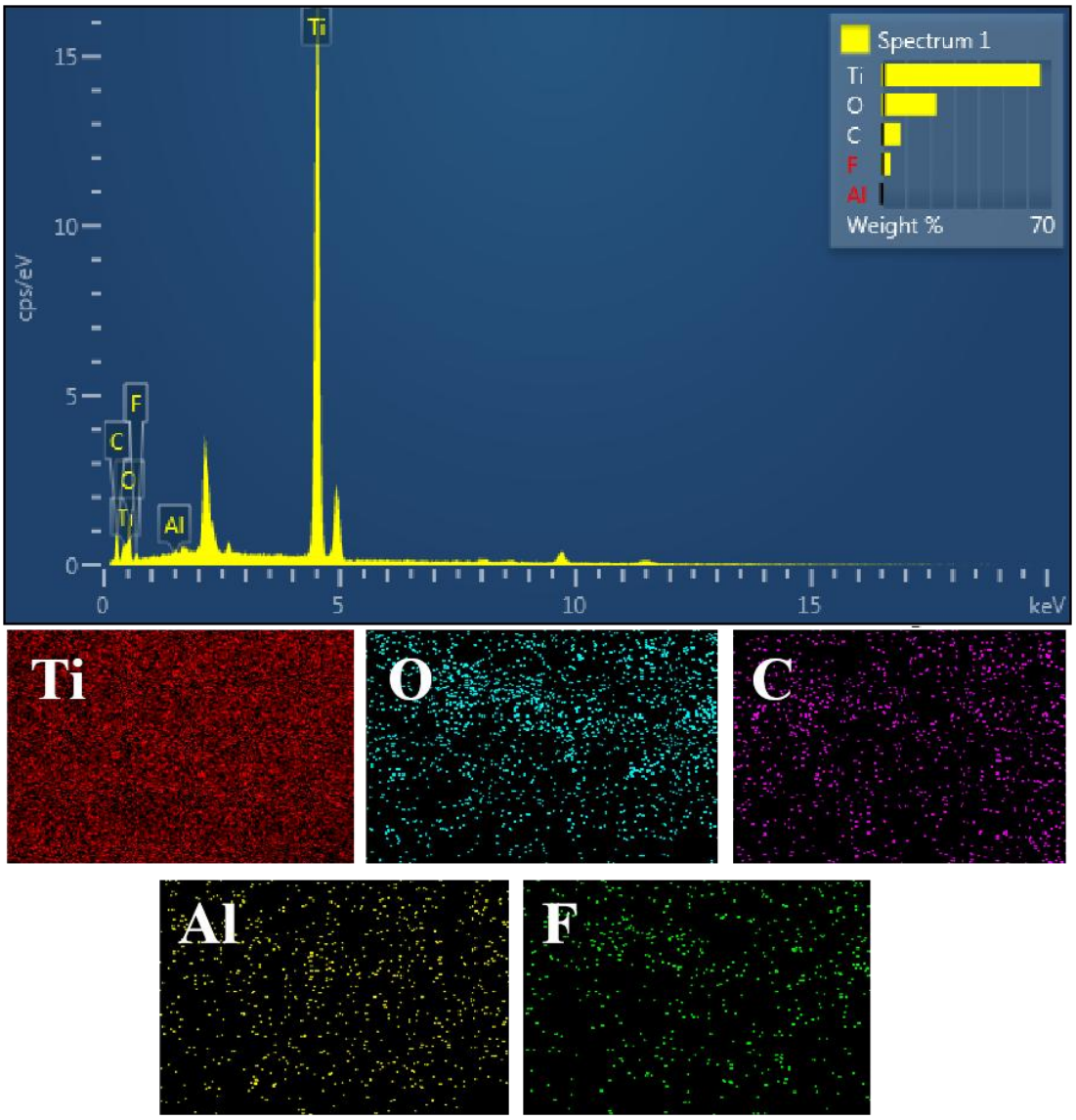

Fig. 30 EDX analysis of MXene synthesized by conventional method with elemental mapping of Titanium (Ti), Oxygen (O), Carbon (C), Aluminium (Al) and Fluorine (F)

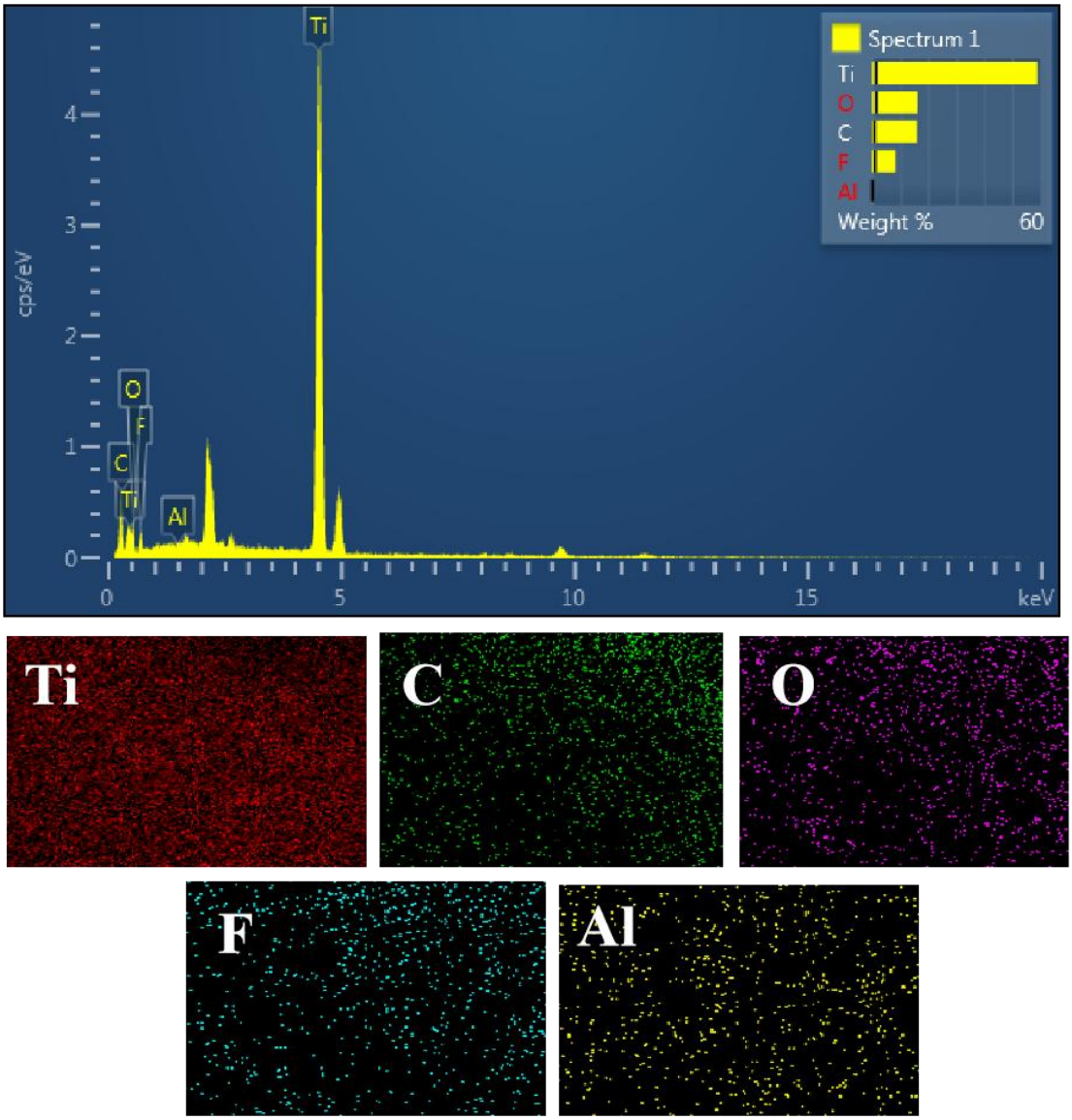

Fig. 31 EDX analysis of MXene synthesized by microwave method with elemental mapping of Titanium (Ti), Carbon (C), Oxygen (O), Fluorine (F) and Aluminium (Al)

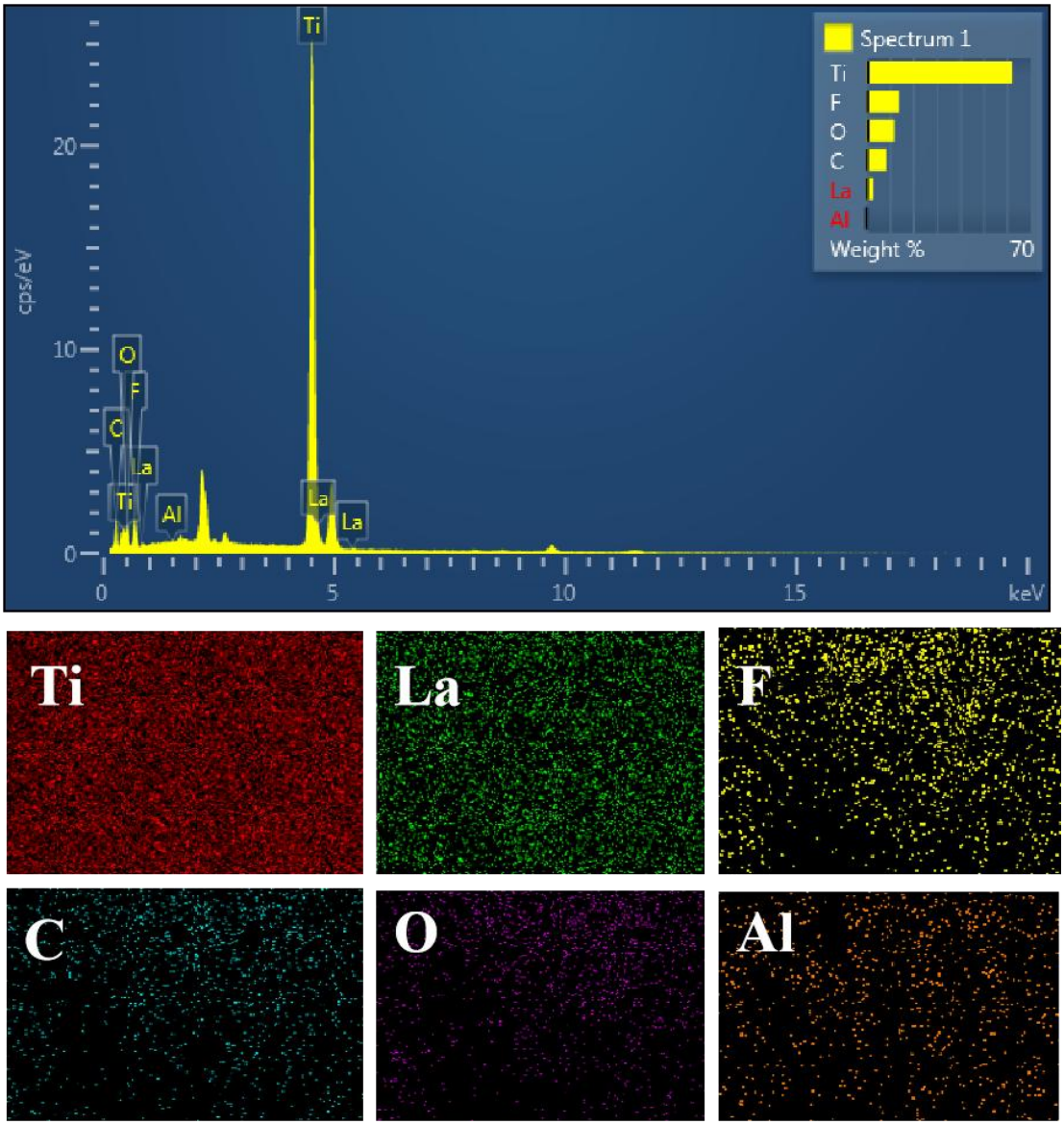

Fig. 32 EDX analysis of La/MX composite (1:2) with elemental mapping of Titanium (Ti), Lanthanum (La), Fluorine (F), Carbon (C), Oxygen (O) and Aluminium (Al)

Table 4 A tabular data for atomic percentage by EDX spectrum

	Atomic percentage (%)					
Elements	**Carbon**	**Aluminium**	**Titanium**	**Oxygen**	**Fluorine**	**Lanthanum**
MAX phase	46.26	20.05	33.69			
MXene (conventional)	17.99	0.26	37.58	38.98	5.19	
MXene (Microwave)	33.00	0.13	30.65	25.20	11.02	
La/MX (1:2)	20.65	0.08	36.77	21.05	20.84	0.61

4.2.5.4. FTIR Spectroscopy

In **Fig.33** shows the FTIR spectrum of MAX phase, MXene (conventional) and MXene (microwave) [**A**], all La/MX composites by conventional method [**B**] and all composites of lanthanum and MXene synthesized by microwave method [**C**]. The composition and surface functionalities of the synthesized material are revealed by FTIR analysis. The FTIR spectrum [A] of MAX phase exhibits bands at 543, 1030, 1430 and 2350 cm^{-1} corresponding to Ti–O, Al–O and surface functional groups. In the FTIR spectrum of conventionally synthesized MXene, a broad absorption band observed in the 3000–3500 cm^{-1} region and a weak band around 1686 cm^{-1} may be attributed to O–H stretching and H–O–H bending vibrations of adsorbed water molecules and surface hydroxyl groups, reflecting the hydrophilic nature of MXene. Peaks around 843 and 1064 cm^{-1} may be associated with surface functional groups introduced during the etching process. In microwave-synthesized MXene, bands around 486 and 606 cm^{-1} are attributed to Ti–O and Ti–C vibrations, respectively. The FTIR spectra of La/MX composites prepared by conventional and microwave methods show characteristic bands around 597–608 cm^{-1}, which may be assigned to La–O vibrations, suggesting the incorporation of lanthanum species and interaction with the MXene surface. The Ti-O peak may distort between 550 and 750 cm^{-1} [303-305].

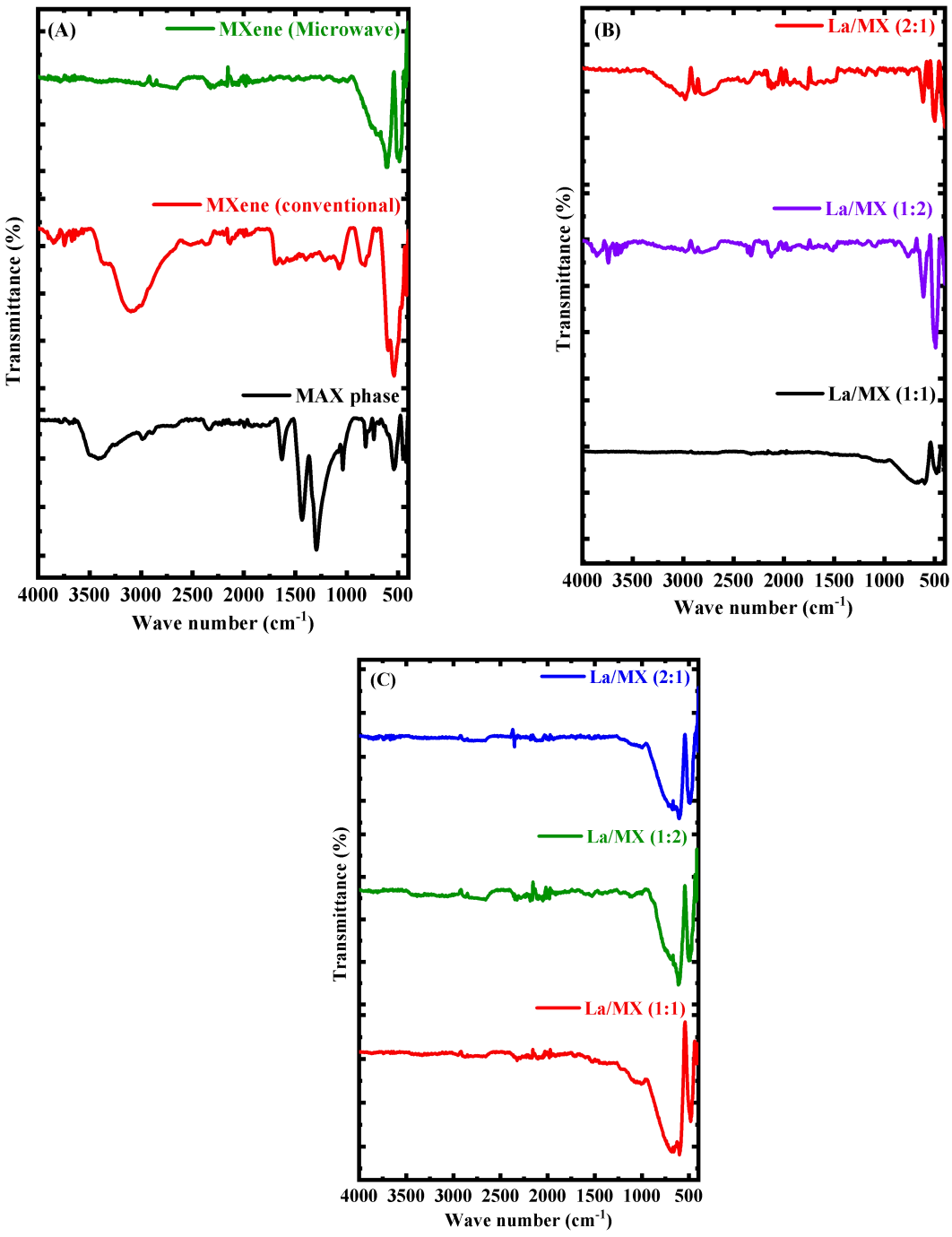

Fig. 33 FTIR spectra of MAX phase, MXene synthesized by conventional and microwave methods (A), La/MX composites prepared by the conventional method (B), and La/MX composites prepared by the microwave method (C).

4.2.5.5. Zeta Potential Measurement

The zeta potential (ζ) is associated with the surface charge of materials, which has a substantial impact on the material's stability in suspension, photocatalytic activity, and interactions with contaminants such as ciprofloxacin. **Fig.34**, shows the zeta potential values of MXene (conventional) **(A)**, MXene (microwave) **(B)**, and La/MX prepared by microwave (1:2) **(C)** are −13.0 mV, −10.5 mV, and−5.39 mV respectively. The zeta potential reflects nanosuspension stability through electrostatic repulsion. In **Fig.34A** and **Fig.34B**, MXene (conventional) and MXene (microwave) shows strong negative zeta potential, indicating high surface charge and good colloidal stability due to abundant –OH or –F groups [306-307]. After La incorporation in **Fig.34C**, the zeta potential shifts closer to neutral, suggesting reduced surface charge. This is likely due to La^{3+} interacting with and partially neutralizing the negatively charged functional groups on the MXene surface [307].

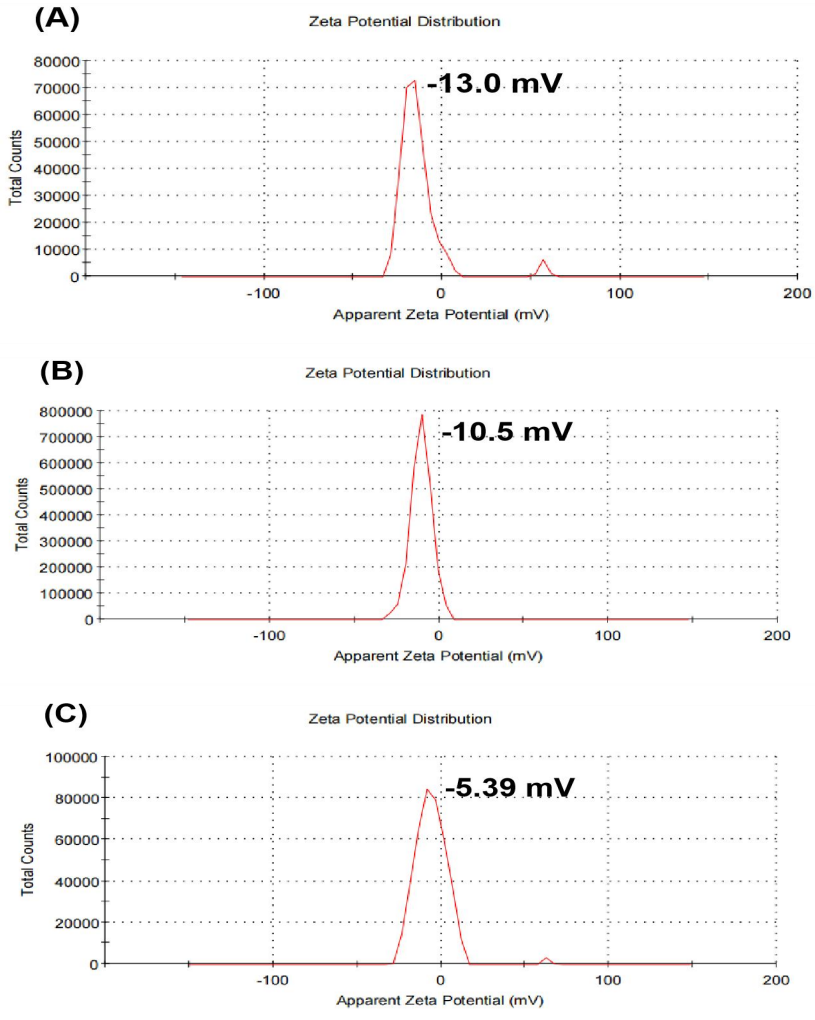

Fig. 34 Zeta Potential of MXene (Conventional) (A), MXene (Microwave) (B) and La/MX (1:2) (C)

4.2.5.6. Electrochemical Impedance Spectroscopy

The charge carrier recombination or transfer behavior of MXene and La/MX with ratio (1:2) prepared by microwave method was examined using electrochemical impedance spectroscopy EIS (10 MHz~100 kHz). The characteristics of the electrode surface and the size of the semicircle determine the charge transfer resistance [308]. In **Fig.35**, on the Nyquist curve, the Rs value (solution transfer resistance) for MXene (MW) is 10.45Ω whereas for La/ MXene (MW) is 8.59Ω and the La/MX (MW) showed the shorter arc size showing higher conductivity that makes electron migration easier. On the other hand, MXene (MW) showed a wider arc radius, which may indicate higher carrier transfer impedance. The impedance value in the Nyquist diagram represents the resistance to the charge transfer. A lower impedance value of the test sample is correlated with a smaller arc radius, suggesting a higher probability of photocatalytic reaction occurrence [309].

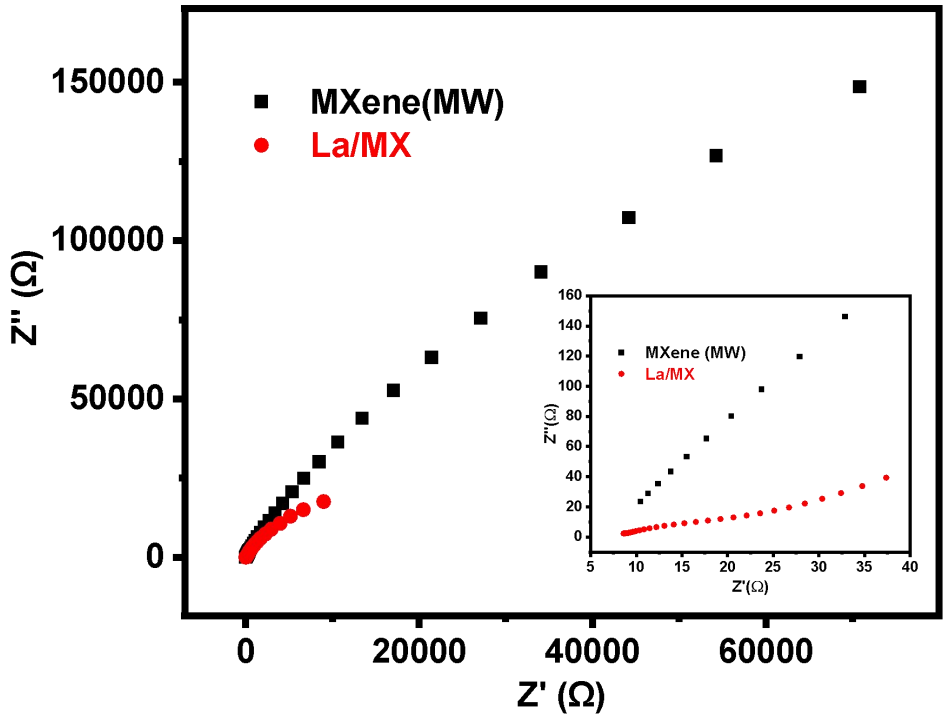

Fig. 35 EIS spectra of MXene (Microwave) and La/MX nanocomposite (1:2).

4.2.5.7. Photoluminiscence (PL) Analysis

The charge carrier dynamics of the synthesized photocatalysts were investigated by using photoluminescence (PL) spectroscopy. Strong photoluminescence (PL) signals in semiconductors indicate fast recombination by radiation of photogenerated electron-hole pairs, which is harmful to photocatalytic activity because it decreases the amount of charge carriers available for surface redox reactions [325-326]. To improve photocatalytic performance, on the other hand, a suppressed PL signal signifies a longer carrier existence and more efficient charge separation [327]. The PL spectra of the MXene (MW) and the La/MX composite with ratio (1:2) synthesized by microwave method are presented in **Fig.36**. The intrinsic radiation recombination of electron-hole pairs inside the structure of MXene (MW) is characterized by a high-intensity emission peak in its spectra. On the other hand, the PL spectrum of La/MX composite shows a significant decrease in intensity, indicating a considerable quenching of photoluminescence. Strong spectroscopic convincing evidence for the reduction of the recombination of electron-hole pairs in the composite is provided by this significant quenching. By spatially isolating the electrons and holes and limiting their recombination, the MXene and the La^{3+} component facilitates to efficiently transmit photogenerated charge carriers. One of the main causes of the increased photocatalytic activity of La/MX composite is greater charge separation.

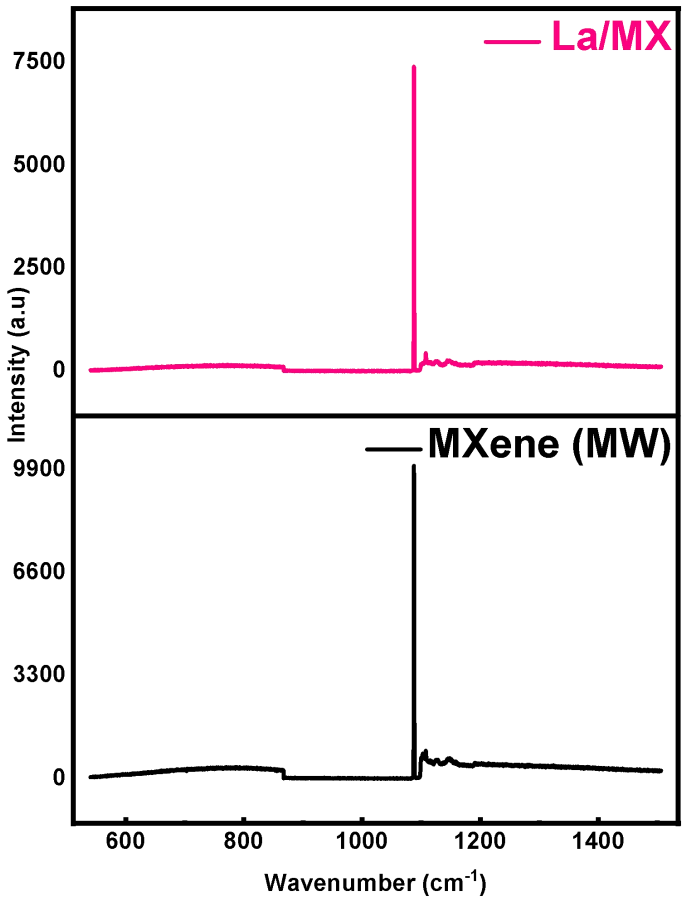

Fig. 36 Photoluminescence (PL) analysis of microwave-synthesized MXene (MX (MW)) and La/MX composite

4.2.5.8. Optical Properties

The optical properties of MXene and La/MX (1:2) synthesized using microwave technology were analyzed using a UV–vis spectrophotometer. Tauc's plot was used to calculate the band gap for both samples. Plotting $(\alpha hv)^2$ against band gap energy Eg allowed for the determination of the band gap of hybrid samples. It was discovered that the band gaps of MXene and La/MX were 1.27 and 1.58 eV, respectively in **Fig.37**. Changes in the electrical structure, defect development, decreased oxygen content, strain effects, charge transfer, and perhaps the production of new phases are the likely causes of the increased band gap in La/MX [310]. An increasing band gap is the result of the material's energy levels changing due to each of these above variables. In comparison to pure MXene, which has a 1.27 eV band gap, the La/MXene composite with a 1.58 eV band gap, performs better in the photocatalytic

degradation of ciprofloxacin under visible light. MXene (1.27 eV) absorbs light with a wavelength of about 976.38 nm, which is in the near infrared region. But La/MX composite (1.58 eV) absorbs light with a wavelength of about 821.19 nm, which is closer to the visible spectrum. Therefore, the La/MX composite with a 1.58 eV band gap will absorb more visible light than the MXene with a 1.27 eV band gap, making it more suitable for photocatalytic degradation of ciprofloxacin under visible light. Its higher performance can be attributed to its enhanced absorption of visible light and possibly to improved charge carrier dynamics brought about by creating composites [311]. The optical band gap values were estimated from Tauc plots derived from UV–visible absorption measurements. The corresponding UV–visible absorption spectra were used for band gap calculations.

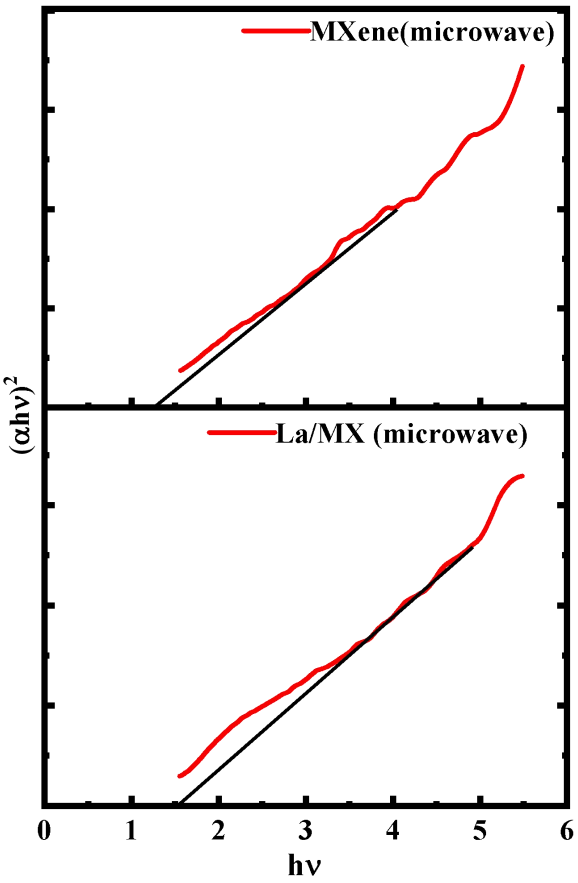

Fig. 37 Tauc plots of MXene and La/MX showing absorption against energy

4.2.5.9. Photocatalytic performance towards Photodegradation of Ciprofloxacin

4.2.5.9.1. In Dark Phase

4.2.5.9.1.1. pH Effect: To confirm the photocatalytic nature of the degradation process, we conducted a set of control experiments under dark conditions for all prepared catalysts, using ciprofloxacin solution at different pH values optimized for each material. The adsorption efficiencies were recorded after 120 min in the absence of light. In **Fig. 38A**, the adsorption efficiencies of MAX phase, MXene (conventional), and MXene (microwave-assisted) were 7.7% (pH 7), 9.8% (pH 8), and 9.9% (pH 8), respectively. Similarly, the adsorption efficiencies of La/MX (microwave) composites with ratios 1:1, 1:2, and 2:1 were 15.9%, 21.0%, and 16.8%, respectively, at pH 6, as shown in **Fig. 38B**. These results demonstrate that no actual photodegradation occurs in the absence of light.

4.2.5.9.1.2. Effect of Contact Time: In **Fig. 38C**, the adsorption efficiencies after 180 min under dark conditions were 9.7% for MXene (conventional), 10.1% for MXene (microwave), and 22.0% for La/MX (1:2). These results indicate that only limited adsorption occurs in the absence of light, confirming that significant ciprofloxacin removal is mainly due to photocatalytic degradation under irradiation.

The minor reduction in ciprofloxacin concentration under dark conditions is attributed to physical adsorption onto the catalyst surface, which may be influenced by surface chemistry. The higher adsorption observed for La/MX composites (particularly the 1:2 ratio) may be attributed to a combination of factors. One possible reason is the improved structural and surface characteristics achieved through microwave synthesis, which has been reported in literature to enhance surface area and porosity [312]. Additionally, the La^{3+} doping might introduce more surface-active sites, facilitating interaction with ciprofloxacin molecules. No noticeable degradation was observed in the absence of visible light.

4.2.5.9.2. In light phase

4.2.5.9.2.1. pH Effect: In **Fig.39**, shows the findings of a study that how pH affects on all photocatalytic materials [MAX phase, MXene (conventional) and MXene (microwave) [**A**], all La/MX prepared by conventional [**B**] and all La/MX synthesized by microwave [**C**]] ability to photocatalytic degrade ciprofloxacin in the presence of visible light. In (**A**), Max phase material shows very less degradation due to its stable structure. It was less reactive in basic and acidic medium because it has fewer active sites compared to other photocatalytic materials but it showed moderate degradation

efficiency (36.8%) at neutral pH was 7.0. The stable structure of MAX phase interacts with ciprofloxacin but not as much as MXenes because of their surface terminations. With MXene photocatalytic materials synthesized by conventional and microwave, the removal efficiency of ciprofloxacin increased with increasing pH range from 2 to 8 but after that decreased when pH was raised to 10. A slightly basic pH of 8.0 was found to be the optimal value for both MXene materials. In the visible region, the ciprofloxacin removal efficiencies achieved with MXene (conventional) is 77.8%, MXene (microwave) is 86.8%, because there are less H^+ ions present when the pH is raised to an acidic level, the degradation percentage decreased. The number of H radicals in solution will decrease as a result of a lesser number of H^+ ions, which will lower the removal percentage. While a rise in pH will result in an increase in OH ions, it will also increase the quantity of OH radicals. Since OH radicals generate more quickly than H radicals, ciprofloxacin degrade more quickly in alkaline environments than in acidic ones [313, 272]. Whereas, the maximum degradation efficiencies in the visible light region was achieved with all La/MX composites (conventional) (**B**) with ratios 1:1, 1:2 and 2:1 is (89.1%, 95.4% and 91.3%) and Lanthanum and MXene composites (microwave) in (**C**) with ratios 1:1, 1:2 and 2:1 is 91.4%, 97.8% and 93.2%. But with all La/MX composites synthesized by conventional and microwave, the degradation of ciprofloxacin was comparatively less in acidic medium but it becomes very high when the pH range was increased to slightly acidic to neutral medium but after that it was decreased when pH rose to basic medium. So, a slightly acidic pH of 5.0 was found to the optimal value for all La/MX composites. The ciprofloxacin removal was maximized with the La/MX (microwave) with ratio (1:2).

4.2.5.9.2.2. Effect of Contact Time: The effect of contact (irradiation) time is shown in **Fig.39** (**D**), where the elimination efficiency of ciprofloxacin raised with irradiation time with MXene (conventional), MXene (microwave), La/MX (conventional with ratio 1:2) and La/MX (microwave with ratio 1:2). Figure (D) illustrates how the percentage of degradation for the MXene (conventional) getting from 24.5% to 78.0%, MXene (microwave) getting 29.6% to 87.9%, for La/MX (1:2) Conventional from 54.1% to 95.8% and for the La/MX with ratio (1:2) Microwave getting from 57.3% to 98.0%, when the irradiation time interval was increased from 5 to 180 min. It is because more OH radicals will be produced if irradiation is provided for longer

periods of time which increases the removal percentage by accelerating the photocatalytic process [314]. Figure (D), shows that La/MX prepared by Microwave shows highest degradation efficiency than other photocatalyst in the visible region. Doping of MXene with lanthanum produces the vacancy of oxygen and defects on surface which may trap the electrons from conduction band and reduced the rate of recombination of charge carriers. These surface defects also help in the adsorption for the reactant. When the oxygen was adsorbed at defects then electrons from conduction band are trapped by the surface imperfections, reducing the oxygen molecules to superoxide radicals, which then transforms in to hydroxyl radicals. Defects sites formed in La/MX hence improve the ciprofloxacin degradation efficiency [315].

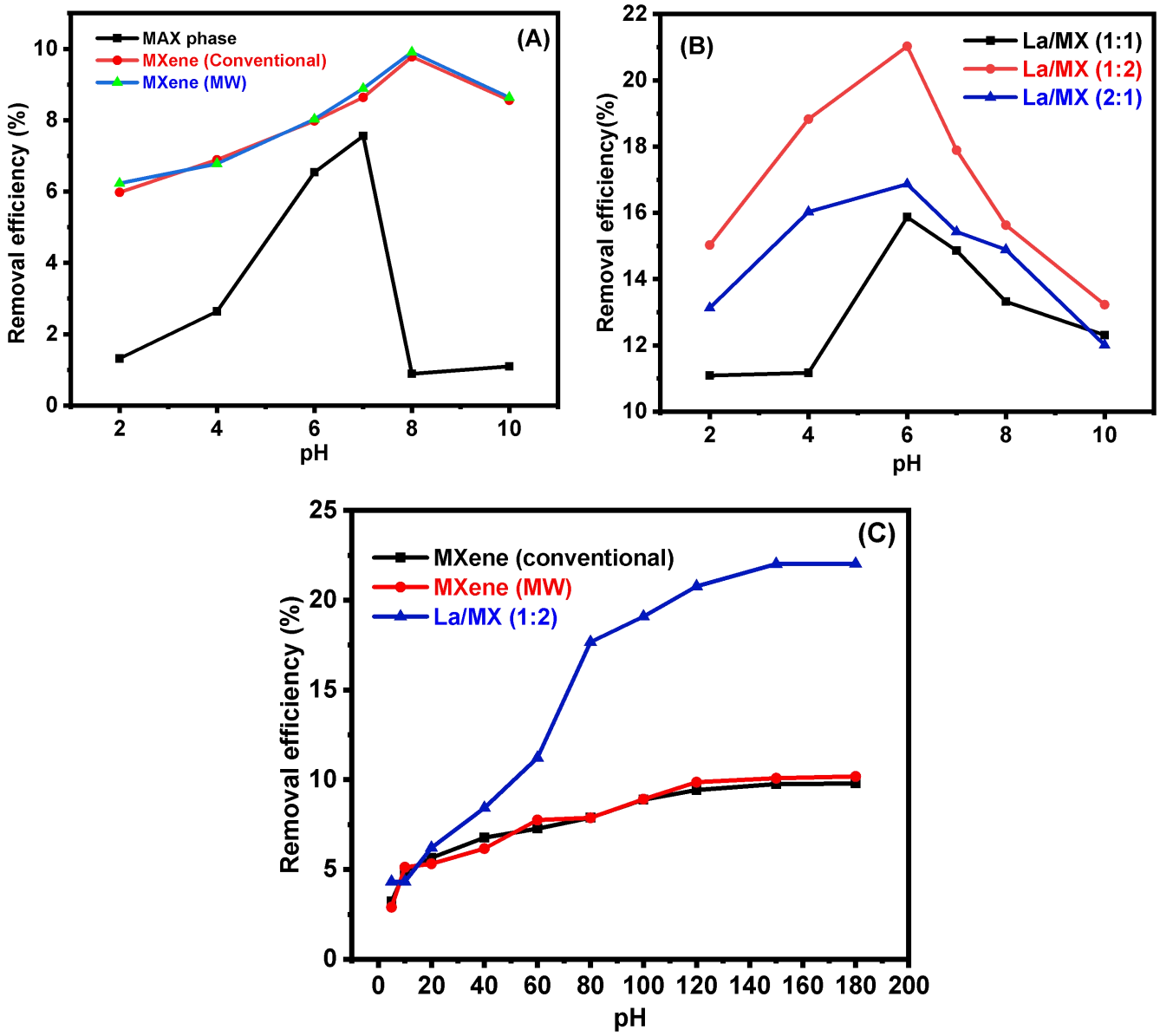

Fig. 38 Adsorption behavior of ciprofloxacin under dark conditions at different pH values (A–B) and effect of contact time on adsorption efficiency (C).

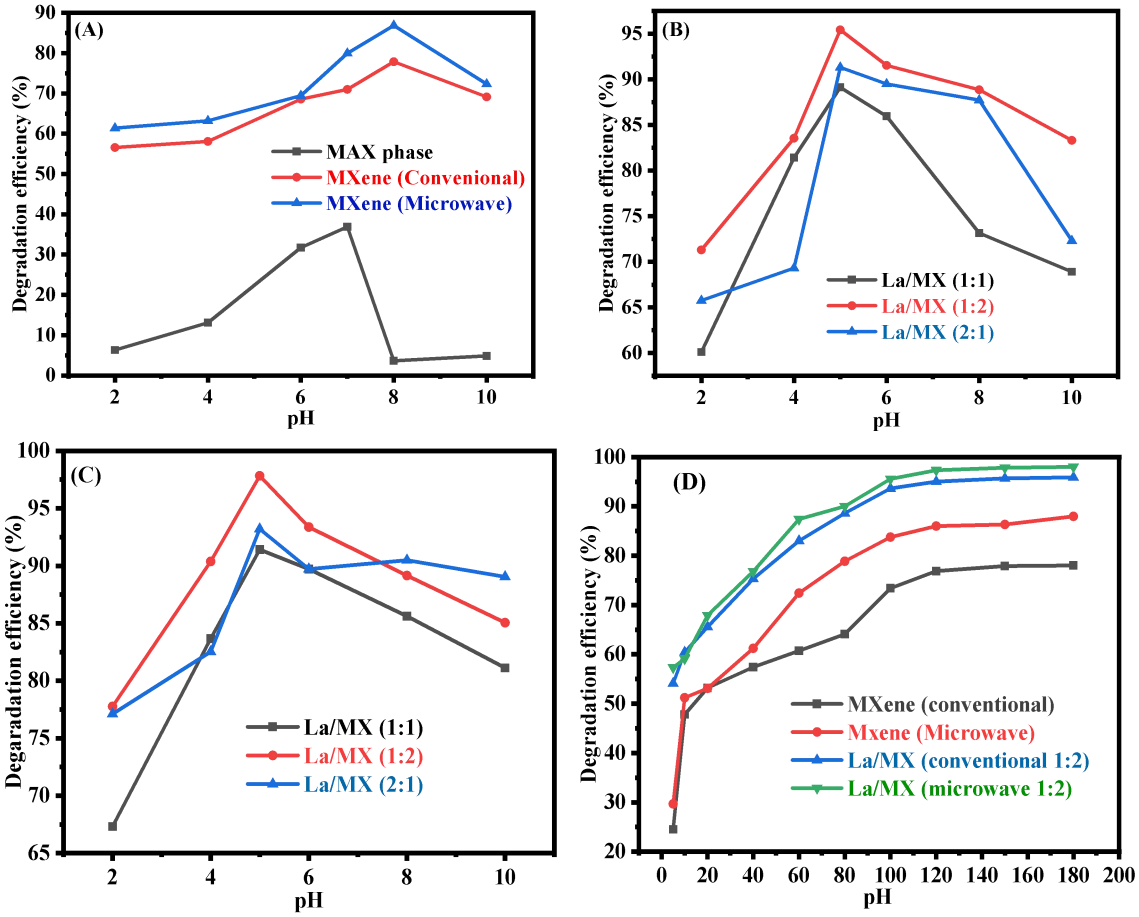

Fig. 39 Photocatalytic degradation of ciprofloxacin in light phase at different pH (A-C) and effect of time on degradation (D).

4.2.5.9.2.3. H_2O_2 effect:

H_2O_2 was used as an oxidizing agent in advanced oxidation process to OH− (hydroxyl) radicals, which are highly reactive and can improve the photocatalytic degradation. As we can see from above results in Fig.39D, the MXene and La/MX (1:2) composite synthesized by microwave method achieved degradation efficiency 87.9% and 98.0%. This high efficiency shows that composite was already very effective. The H_2O_2 effect on the elimination of ciprofloxacin drugs by MXene (MW) and La/MX (1:2) is seen in **Fig.40**, where the hydrogen peroxide was raised from 0.01 to 1%. In case of MXene (MW), as the concentration of H_2O_2 increasing from 0.01 to 0.5%, it enhanced the photocatalytic degradation of ciprofloxacin from 87.9 to 97.8%, but

after 0.5%, as the H_2O_2 concentration was increased to higher to 1%, the rate of degradation was decreased to 78%. Whereas, in the case of Lanthanum and MXene composite, the photocatalytic degradation was increased from 98.01 to 99.05% with the H_2O_2 concentration from 0.01 to 0.05%, after that the concentration of H_2O_2 was increased then removal rate was decreased to 81%. This drop in removal efficiency was due to the excess of H_2O_2 which acts as scavenger for hydroxyl radicals, forming less reactive species like oxygen and water which decreases the degradation efficiency of photocatalytic materials. Trapping photogenerated electrons in hydrogen peroxide can stabilize the coupled charge carriers. The OH radicals can be produced by the reaction of H_2O_2 with e− or oxygen. Although the addition of H_2O_2 slightly improved the degradation efficiency, the photocatalytic activity of the synthesized materials was already high in the absence of H_2O_2. Therefore, H_2O_2 acted only as a supplementary oxidizing agent, and excessive H_2O_2 concentration adversely affected degradation due to scavenging of hydroxyl radicals [316].

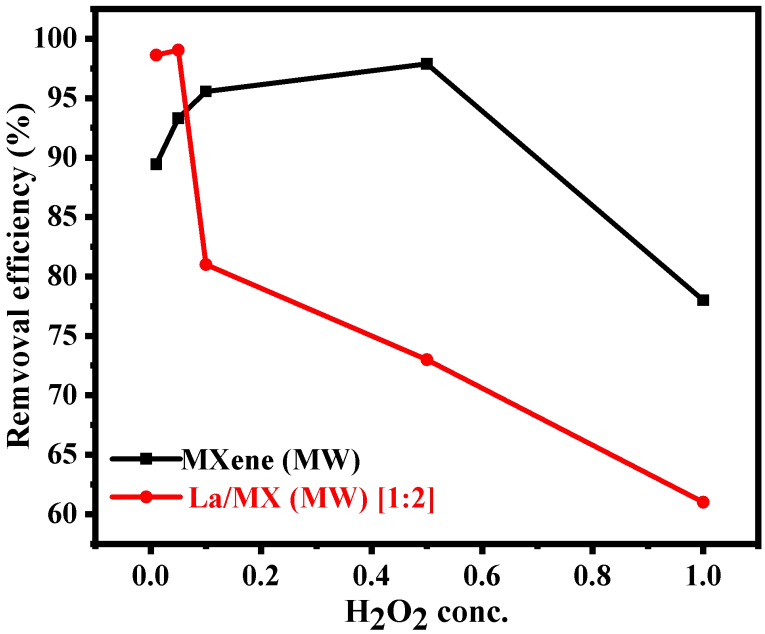

Fig. 40 Photocatalytic degradation of ciprofloxacin at the addition of various concentration of H_2O_2

4.2.5.9.2.4. Regeneration of Photocatalyst:

For the catalyst to be more economically viable, the synthesized composite material needs to be recycled 'n' times. To determine the stability, the composite was recovered from resulting ciprofloxacin aqueous solution by process of centrifugation and reutilized for the following reactions. For regeneration, the recovered photocatalyst was treated with 0.1 g/10 mL H_2O_2 solution and stirred for 1 h before being reused in subsequent cycles. Recyclability was investigated by the degradation efficiency of ciprofloxacin **Fig.41**. As shown in **Fig. 41**, the degradation efficiency gradually decreased with increasing regeneration cycles and reached nearly 60% after the ninth cycle. Despite this decline, the La/MX composite retained appreciable photocatalytic activity, demonstrating good stability and reusability. These results indicate that the synthesized La/MX composite possesses good recyclability with gradual performance loss after prolonged use [317-318]. The gradual decrease in degradation efficiency may be attributed to catalyst loss during recovery, surface fouling, or photocorrosion during repeated photocatalytic cycles. The utilized catalyst's FTIR and XRD revealed no significant structural alterations, indicating structural stability [319].

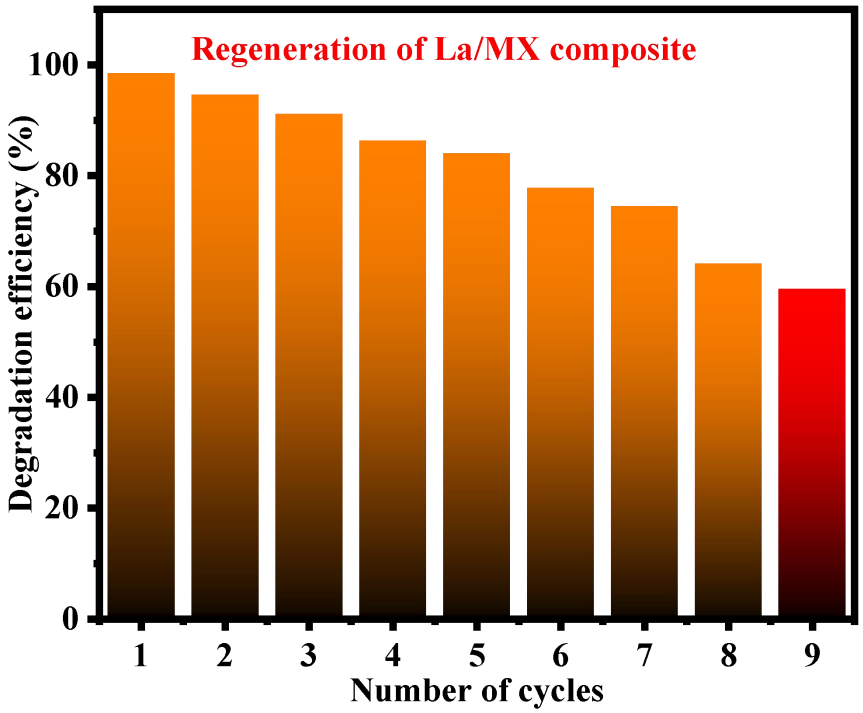

Fig. 41 Recyclability test of synthesized La/MX nanocomposite by microwave method for photocatalytic degradation of ciprofloxacin

4.2.5.10. Photocatalytic Degradation Mechanism

Adsorption, the production of reactive oxygen species (ROS), and electron transfer are all involved in the photocatalytic breakdown of ciprofloxacin by (Ti_3C_2) MXene. Ciprofloxacin is effectively adsorbed by MXene due to its wide surface area, hydrophilicity, and negatively charged surface. Upon exposure to visible light, MXene produces electron-hole pairs that react with oxygen and water to form ROS, including hydrogen peroxide (H_2O_2), superoxide (O_2^{-}*), and hydroxyl radicals (OH*), which degrade ciprofloxacin into smaller components **Fig.42**. The deterioration is also facilitated by direct redox reactions at the MXene surface. By adding additional active sites and altering its electrical structure, lanthanum incorporation further increases MXene's photocatalytic activity. This promotes faster electron transfer, enhances charge separation, and raises ROS production. Because ciprofloxacin is more efficiently oxidized and eventually mineralized into CO_2, H_2O, and mineral ions, La/MX composites exhibit better degrading efficiency [317]. According to earlier research, ciprofloxacin breaks down through piperazine ring cleavage, hydroxylation, and decarboxylation, producing less hazardous byproducts such as CO_2 and H_2O [320]. Using UV–Vis spectroscopy, degradation was observed at 278 nm in this investigation, demonstrating the photocatalyst's capacity for effective drug removal in the presence of visible light. La-incorporated MXene composites were efficiently created, and their photocatalytic activity was assessed. While residual –F terminations boost hydrophilic properties and pollutant interaction [321], La improves performance by encouraging charge separation and lowering recombination [322]. Due to its synthetic origin, fluorine concentration was not independently controlled, and particle size measurement was irrelevant because La exists in either ionic or clustered form. Performance gains with La incorporation are the main focus of the study, and future research will try to correlate structure and activity. The proposed photocatalytic degradation mechanism is supported by the XRD, FTIR, UV–Vis, PL, and EIS

characterization results obtained in this study. The reduced arc radius observed in the EIS Nyquist plot and the PL quenching effect of the La/MX composite indicate improved charge transfer and suppressed electron–hole recombination, which contribute to its enhanced photocatalytic performance.

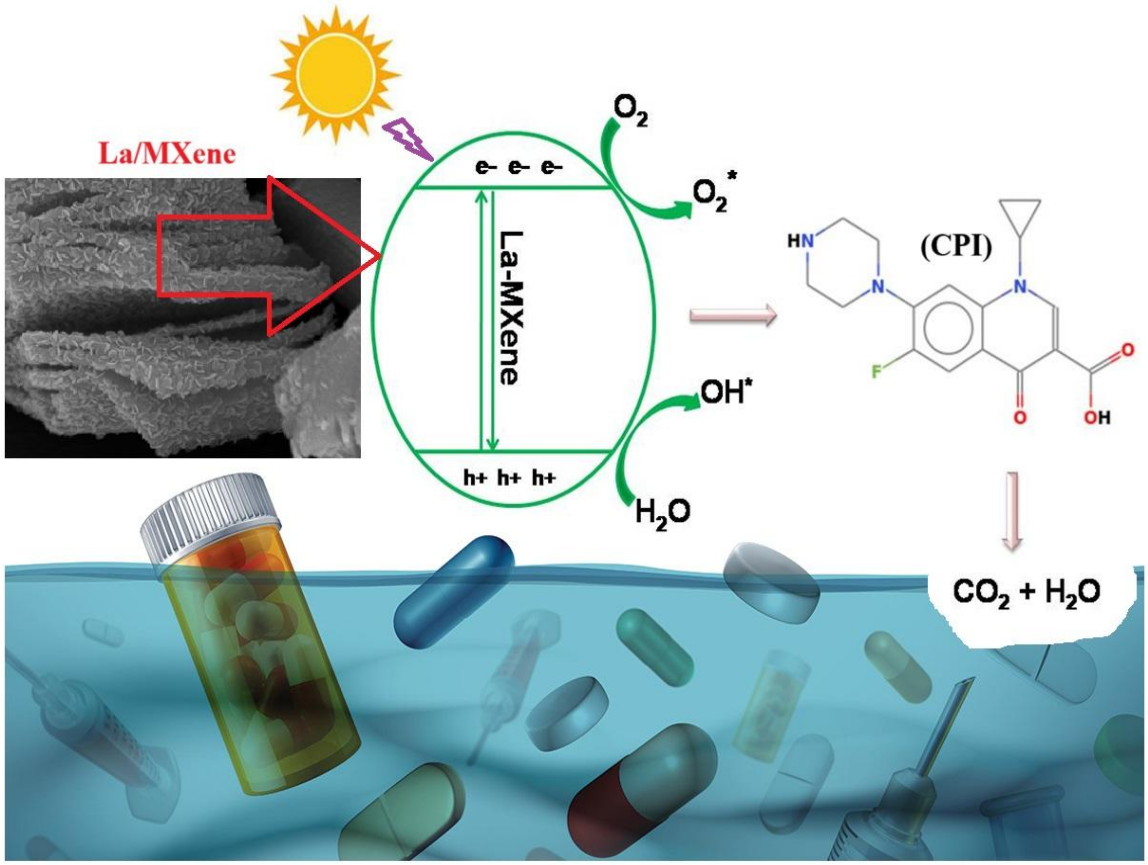

Fig. 42 Schematic diagram of the photocatalytic activation of La/MX nanocomposite

To confirm any structural changes and to assess whether any residues of ciprofloxacin to intermediate compounds remained on the catalyst surface. We characterized the spent photocatalyst after the photocatalytic degradation experiments using **FTIR and XRD**. The **FTIR spectrum** of the used photocatalyst in **Fig.44** showed, no extra peaks corresponding to ciprofloxacin functional groups (such as C=O from carboxylic acid or quinolone ring vibrations) were visible in the FTIR spectrum of the employed

photocatalyst, suggesting that no appreciable quantity of the parent medication or stable intermediate products were adsorbed or remained on the surface following photocatalysis [323]. Similarly, the **XRD pattern** of comparing the used catalyst's XRD pattern to that of the new catalyst in **Fig.43**, it was also mostly unchanged, showing not any additional crystalline phases that would indicate the creation of additional crystalline intermediates or the deposition of stable byproducts. This demonstrates that the breakdown products did not build up on the surface in crystalline form and that the catalyst maintained its structure [324].

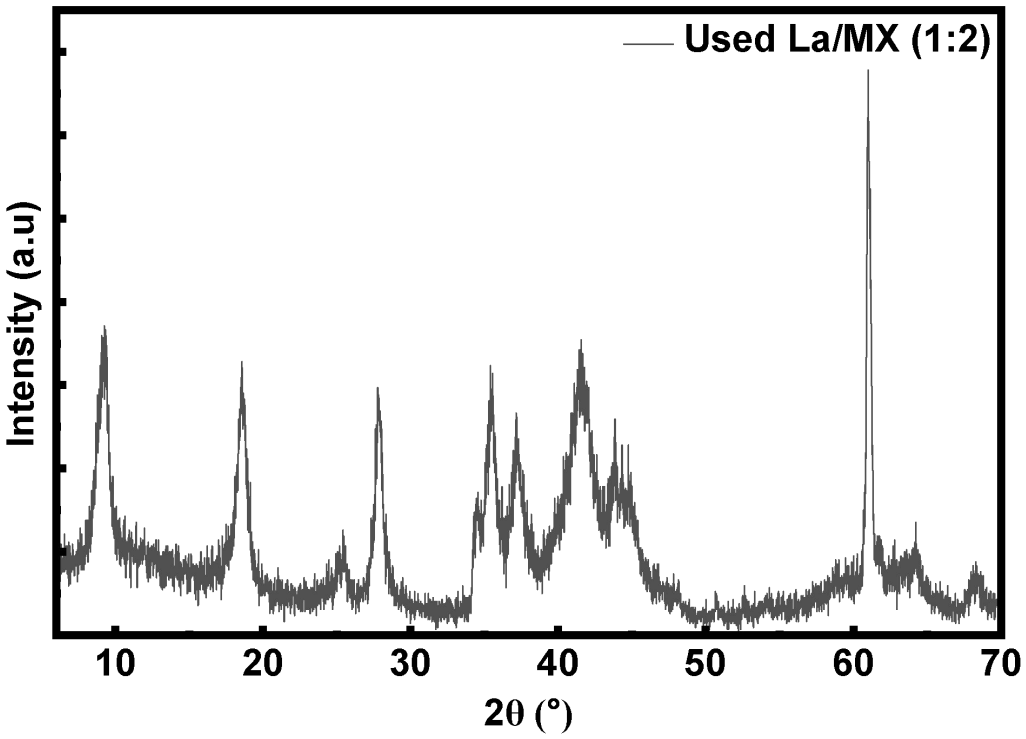

Fig. 43 XRD analysis of used photocatalyst La/MX (1:2) after photocatalysis

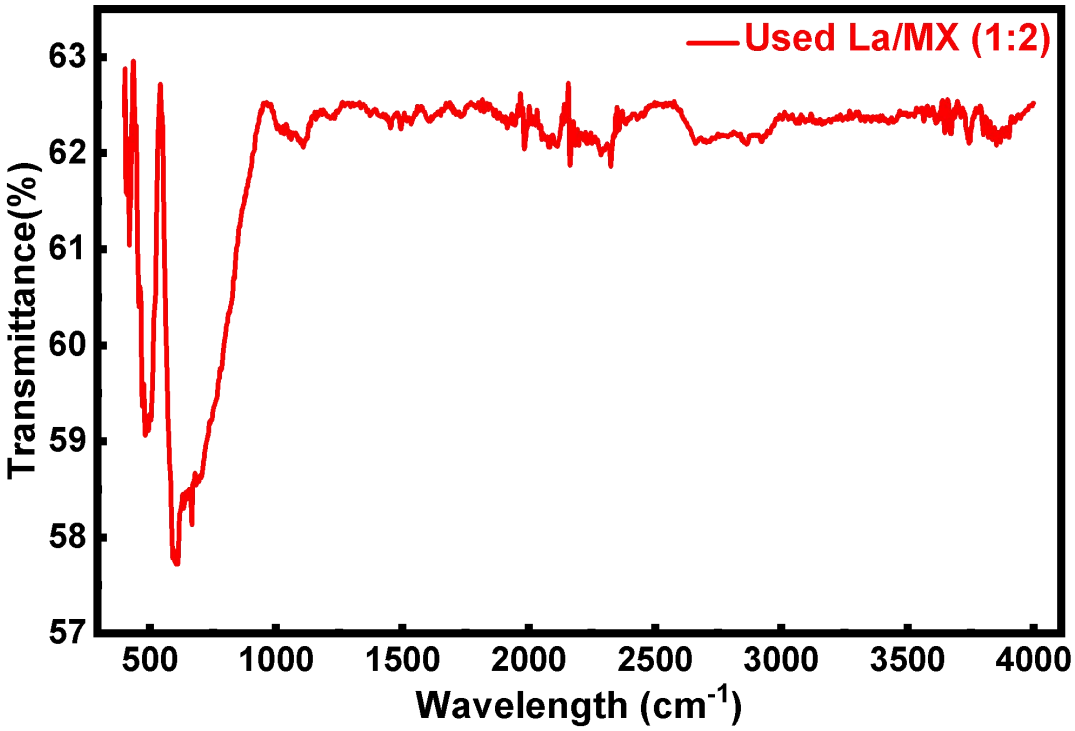

Fig. 44 FTIR spectrum of used Photocatalyst La/MX (1:2) after Photocatalysis

4.2.6. Summary

MXene and La/MX photocatalytic materials were used in a comparative photo-degradation investigation of Ciprofloxacin. MXene and La/MX materials were synthesized by both conventional and microwave process. The microwave technique was used for synthesize the materials because to reduce the time from many hours to few minutes. Microwave-assisted synthesis enables rapid volumetric heating, promoting uniform La incorporation, reduced synthesis time, and enhanced surface features, which are essential for efficient photocatalytic activity. These advantages are consistent with prior reports on microwave-based nanomaterial preparation. SEM pictures revealed improved intercalation and delamination in materials produced in a microwave. Lanthanum on MXene surfaces was verified by SEM–EDX. The results of optimization showed that MXene worked best at pH 8 while La/MX composites worked best at pH 5. La addition promoted visible-light deterioration by increasing hydroxyl radical production, decreasing charge recombination, and increasing oxygen

vacancies. Under ideal circumstances (pH 5, 10 mg catalyst, 180 min), La/MX composites degradation efficiency was 97.83%. EIS findings and zeta potential (–5.39 mV) verified improved conductivity and quicker electron transport in La/MX. The best photocatalytic efficiency was demonstrated by the La/MX (1:2) composite that was microwave-synthesised. Its improved zeta potential and reduced impedance suggest improved surface characteristics and charge transfer, most likely as a result of the uniform La incorporation made possible by the microwave method. While energy utilization outside the visible spectrum remains a challenge, La/MX demonstrates exceptional photocatalytic potential for Ciprofloxacin degradation under visible light conditions. According to the EIS Nyquist plot, La/MX (MW) exhibits superior conductivity and charge transfer due to its smaller semicircle (Rs=10.45 Ω) and lower resistance (Rs=8.59 Ω) than MXene (MW). In keeping with its enhanced photocatalytic efficacy, La^{3+} inclusion improves electron mobility and charge separation. By adding –F terminations to MXene, HF etching raised the negative zeta potential and changed the charge-transfer resistance. Although the activity may be limited by these terminations, the inclusion of La^{2+} enhanced charge separation and increased photocatalytic efficacy. Post-treatments to improve surface chemistry and efficiency will be investigated in future research. After photocatalysis XRD and FTIR analyses of La/MX (1:2) revealed no drug residue and confirmed structural stability. However, these techniques cannot be fully confirmed to prove complete mineralization to CO_2 and H_2O. Future research will use advanced techniques like LC–MS or TOC to gain a deeper understanding of degradation routes and byproducts.

Section-3

4.3. Enhanced visible light photocatalytic degradation of cetirizine in pharmaceutical liquid waste using V_2O_5-modified MXene nanocomposites prepared via microwave irradiation

4.3.1. Introduction

Emerging pollutants cause concern are a group of substances that have attracted a lot of interest lately due to their persistence and broad presence in the environment [328]. Cetirizine, an H^1 histamine blocker, is one such newly discovered contaminant. Cetirizine has a poor metabolism and is eliminated from the body in about 80% [329]. Cetirizine has been found in receiving waters, wastewater influent as well as treated wastewater effluents. Cetirizine consumption and occurrence seem to have a seasonal component as well. Due to increased use to treat seasonal allergies, the concentration of cetirizine in wastewater effluent peaked in the summer and subsequently declined the rest of the year. Cetirizine persists in water bodies due to their recalcitrant nature and low biodegradability, leading to potential ecological toxicity and bioaccumulation in aquatic organisms [173]. Although they are widely used, conventional water-treatment techniques such as membrane filtration, coagulation, adsorption, biological degradation and chemical oxidation frequently have low efficiency, high operating costs, or produce hazardous byproducts. In contrast, photocatalysis offers total breakdown without the production of secondary pollutants when exposed to light. In order to overcome the drawbacks of traditional techniques and improve activity-selectivity performance under visible light, advanced research is increasingly concentrating on creating heterojunctions and composite catalysts [300]. . In addition to photocatalysis, a number of conventional methods, such as the Fenton process, are employed to remove pollutants. Despite their effectiveness, these techniques frequently have drawbacks such as restricted reusability, sludge production, and a narrow pH range. To get around these limitations, recent research has looked into better Fenton-like catalysts [330]. That is why, it is necessitating the development of innovative and efficient remediation technologies. In addition to its application in pollutant degradation, photocatalysis is essential for organic synthesis, ammonia decomposition and hydrogen production. Interfacial charge separation is crucial, as evidenced by a recent study that showed a Z-scheme heterojunction enabling effective

photocatalytic H_2 generation under visible light [331]. Additionally, photocatalysis is often used to remove harmful heavy metals from water. Reactive species produced by light-activated catalysts in this method convert metal ions (such as Cr(VI), Pb(II), and Hg(II)) into less hazardous or insoluble forms that are easily separated. Adsorption and photocatalytic redox reactions are combined in this dual action to provide a sustainable and effective heavy metal removal method [332]. Through the production of reactive species (such as ·OH and $\cdot O_2^-$) that harm cell walls of microbes and genetic material, photocatalysis is also successful in deactivating pathogens in wastewater. Effective photocatalytic removal of bacteria and viruses has been shown in recent research, highlighting its potential for tertiary treatment applications and safe water reuse [333].

MXenes, a 2D-transition metal carbides and nitrides attracted a lot of interest due to their remarkable physicochemical characteristics, which include variable surface chemistry, high surface area, and superior electrical conductivity. MXenes are intriguing prospects for environmental applications due to their unique structure and adaptability, especially in photocatalysis and adsorption processes. The ability of MXenes to be functionalised or doped with different metals to increase their photocatalytic activity under visible light has been shown in recent investigations [334].

Doping of vanadium is especially attractive since it can create new electronic states and increase charge separation for photocatalytic efficiency. Additionally, vanadium promotes redox processes, which improves the material's capability to break down persistent organic contaminants. Vanadium pentoxide is the most stable of the several vanadium oxides and has remarkable applications in the field such as Li-ion batteries, chemical or gas sensors, photocatalysis and photoluminescence. Vanadium pentoxide is a visible light photocatalyst and doping can further adjust its band gap. When exposed to visible light for 300 min, it was found that vanadium pentoxide degraded methylene blue, methyl orange, and rhodamine B by 85%, 45% and 24%, respectively [335]. The visible-light-responsive metal oxide vanadium pentoxide (V_2O_5) has effective photocatalytic capabilities but is hampered by fast electron–hole recombination. MXene promotes better charge separation and surface interaction because of its excellent electrical conductivity and high surface area. Through

synergistic effects, their combination in various ratios (1:1, 1:2, and 2:1) is intended to increase photocatalytic efficiency. Such heterostructures are an emerging trend in visible-light-active photocatalysis, already discussed in recent studies [336].

Since heterogeneous photocatalysis relies on surface phenomena, 2D materials have been used extensively in photocatalysis lately because of their huge surface area. For instance, it was reported using a V_2O_5/Pt/rGO composite to effectively degrade oxytetracycline, the V_2O_5/rGO composite had better photocatalytic effectiveness for the photodegradation of methylene blue dye, and ZnO/RGO, and ZnO/GO nanocomposites were created to improve the breakdown of industrial effluents [292]. In an effort to broaden the scope of photocatalysis, researchers have also experimented with different types of 2D materials, because of its extremely conductive, and semi-conductive qualities, MXene is regarded as a more effective 2D material than graphene. Among the many benefits of the microwave-assisted method are its quick crystallisation, affordability, simplicity of use, phase selectivity, regulated material size, quick heating, high reaction rates, and control over morphology [337]. Recent research has shown that chemical activation, such as the use of sodium borohydride ($NaBH_4$), can further increase photocatalytic effectiveness by providing extra electrons to speed up pollutant destruction. Similarly, it has been demonstrated that activation by peroxymonosulfate (PMS) produces reactive sulphur-based radicals when exposed to visible light, greatly accelerating the rate of degradation in wastewater applications [294].

Motivated by this, MXene was synthesised using both conventional MX (Con) and microwave assisted MX (MW) methods. Subsequently, V_2O_5-modified MXene composites (V/MX) were prepared via microwave synthesis with different ratios (1:1, 1:2, and 2:1). The resulting materials were thoroughly characterised using various physicochemical techniques to investigate their optical, morphological, and structural properties. The photocatalytic performance was then evaluated through the degradation of cetirizine under visible light irradiation. MXene and its composites with V_2O_5 are synthesised in this work utilising both conventional and microwave-assisted techniques, and their photocatalytic efficacy for visible light-driven degradation of pharmaceutical contaminants is assessed.

4.3.2. Materials and methods

4.3.2.1. Chemicals consumed

Sodium hydroxide, vanadium pentoxide, hydrofluoric acid (40%) and dimethyl sulphoxide (DMSO) (99%) were purchased from Loba Chemie Pvt. Ltd, India, while the MAX phase (Ti_3AlC_2) (99%) was acquired from Nanoshel. All chemical reagents were used without any further purification. Distilled water was used, for solution preparation. Cetirizine drug was bought from a local medical shop in Punjab, India.

4.3.3. Synthesis of MXene (Ti_3C_2Tx)

4.3.3.1. Etching method

MXene was created using the HF etching method, by dispersing 1 g of Ti_3AlC_2 MAX phase powder into 10 mL of hydrofluoric acid and continuously stirring with a magnetic stirrer for 24 h. The resulting black sediment was centrifuged for 20 min at 4500 rpm and then repeatedly washed with Distilled water. It was then dried at 60°C to produce Ti_3C_2Tx MXene. The powder was submerged in 15 mL of DMSO and agitated for 22 h at room temperature in order to promote delamination. Exfoliated MXene sheets MX (Con) were obtained by centrifuging the material again, sonicating it for 5 h in 300 mL distilled water, and then centrifuging and drying it [237].

4.3.3.2. Microwave-assisted method

The microwave-assisted technique for synthesis of MXene MX (MW) followed the same steps as the process mentioned before process until the aluminium layer from the MAX phase was etched. Following that, the resulting powder was microwave heated at 300 W for 10 min with 15 mL of DMSO to shorten the time needed for delamination and intercalation from several hours to just a couple of minutes [305, 310]. The final exfoliated MXene was obtained by centrifuging the product for 10 min at 4000 rpm, sonicating it for 5 h in distilled water, centrifuging it once more, and then drying it for 24 h at 60°C [338].

4.3.3.3. Synthesis of V_2O_5 modified MXene composites

V_2O_5-modified MXene composite was synthesized by the conventional method using V_2O_5 and MXene in a weight ratio of 1:2 (V_2O_5:MXene). The prepared MXene (Ti_3C_2Tx) material and V_2O_5 were dispersed in 0.1 M HCl solution. The solution was stirred for 7 hours at 70-80 degrees Celsius. The obtained mixture was cooled down, filtered and washed many times and then dried at 50°C.

Microwave-assisted technique was used for V_2O_5 modified MXene composites. V_2O_5-modified MXene composites were synthesized in different weight ratios of V_2O_5:MXene (1:1, 1:2, and 2:1), as shown in **Fig. 45**. MXene was dispersed in a 0.1 M HCl solution while being continuously stirred. The required amount of V_2O_5 was then added to obtain the desired V_2O_5:MXene weight ratios. To promote even dispersion and interaction between MXene and V_2O_5 particles, the mixture was exposed to 400 W of microwave radiation for 15 min [300, 339]. After a thorough washing with distilled water, the resultant suspension was centrifuged and allowed to dry for 12 h at 60°C. Rapid and consistent heating provided by the microwave treatment shortens the synthesis time and improves the crystallinity of the material. By enhancing the particle dispersion and promoting improved MXene and V_2O_5 interaction, this technique increases photocatalytic efficiency.

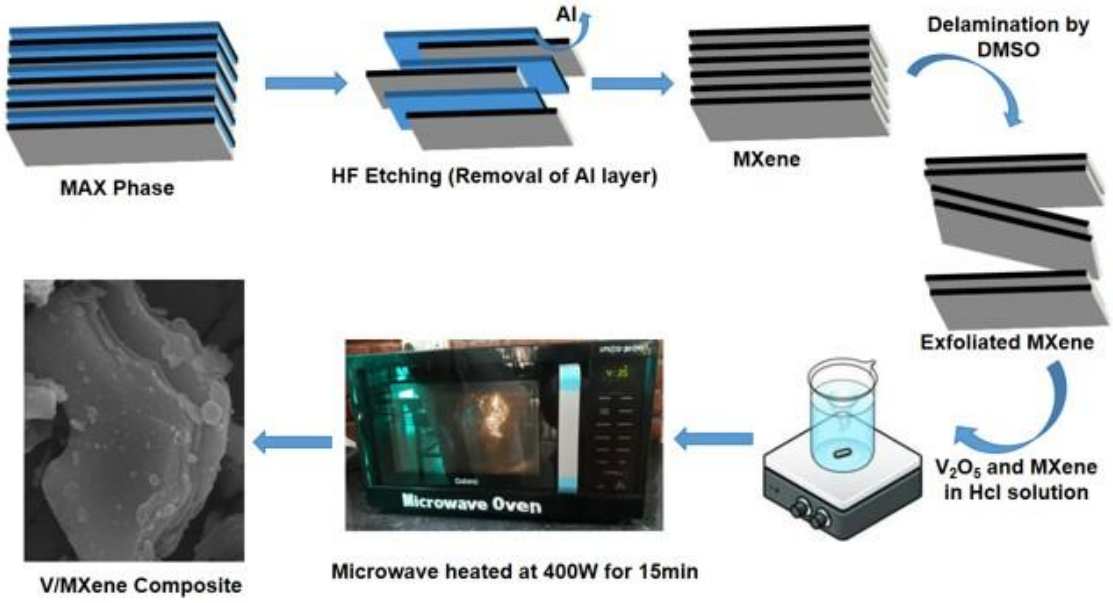

Fig. 45 Schematic illustration of the synthesis process for MXene and V_2O_5-modified MXene composites using the microwave-assisted method.

4.3.4. Materials characterisation

Perkin Elmer Fourier Transform Infrared Spectroscopy (FTIR) was used to determine the chemical bonds and functional groups of the produced materials in the 400–4000 cm^{-1} range. The UV-1700 Shimadzu UV spectrophotometer was used to investigate

the spectral fluctuations in the 200–700 nm wavelength range in order to evaluate the optical characteristics and use Tauc plots to calculate the band gap. X-ray diffraction (XRD, Bruker) was used in the 2θ range of 6°–80° to examine the crystalline structure and phase composition. A scanning electron microscope (SEM) was used to observe the particle distribution and surface morphology. An Energy Dispersive X-ray (EDX) detector connected to the SEM was used for elemental analysis and mapping. Prior to SEM measurement, all samples were gold-coated to increase conductivity. The characterisation section by including Photoluminescence (PL) analysis to evaluate the charge carrier recombination behaviour in section. The XRD data has been updated with JCPDS reference patterns for V_2O_5 to better confirm crystallinity.

4.3.5. Assessment of photocatalytic activity

The photocatalytic activity of the synthesised nanocomposites was assessed by degrading 100 mg/L of cetirizine in the presence of visible light. In a volumetric flask, 100 mg of cetirizine was dissolved in 10 mL of 40% HCl to create a stock solution, which was then diluted to 1000 mL with distilled water. Photocatalytic experiments were conducted at room temperature in a batch reactor that was exposed to visible light. About 10 mg of the photocatalyst was mixed with 30 mL of the cetirizine solution for each experiment. The pH was adjusted with either 0.1 M HCl or NaOH. The solution was exposed to visible light at a room temperature just before the reaction start. A predetermined amount of the solution was centrifuged and filtered through Whatman filter paper at regular intervals during the light exposure. The UV-Vis spectrophotometer (λ = 230 nm) was used to measure the cetirizine concentration. The effects of various parameters, such as pH, irradiation time and the presence of H_2O_2, were evaluated. To study photocatalytic degradation in visible light, a 60 W LED bulb operating at 220 V and 50 Hz was used. According to the manufacturer's specifications, the bulb emits visible light (400–700 nm) and relatively less UV radiation. The reactor was set up at a distance of around 15 cm from the source of light to provide uniform irradiation; sunlight was not used throughout the experiments. Using Eq.(5), the amount of cetirizine degradation brought on by photocatalysis was determined as follows:

$$\text{Photo-degradation (\%)} = \frac{(Aa-Ab)}{Aa} X 100 \ldots\ldots\ldots\ldots\ldots (5)$$

where, Aa and Ab are the initial and final concentrations (mg/L) of pharmaceutical drugs, respectively.

4.3.6. Results and discussion

4.3.6.1. Structural and phase analysis (XRD)

In **Fig.46**, the MAX phase, MXene created using the conventional and microwave methods (A), the V/MX composites prepared using the microwave approach (B) in three different ratios (1:1, 1:2, and 2:1) were assessed using XRD and (C) shows the comparison between the MAX phase, MXene created using the conventional and microwave methods, and the V/MX composites prepared using the conventional and microwave approach with 1:2. **Fig.46A** shows the distinct diffraction peak pattern of MAX powder (Ti_3AlC_2) and MXene that matches with the JCPDS card No. 52–0875 and 04–004–2919 [340]. Ti_3AlC_2 exhibits the distinctive sharp peak of 'Al' (104) at $2\theta = 39.09°$. To get good-quality MXene with more layer separation, this 'Al' must be entirely etched out of Ti_3AlC_2 [94]. The TiC impurity is represented by the diffraction peaks (101), (103) and (105) at positions 33.76°, 35.39° and 41.64°, respectively [341]. When Ti_3AlC_2 is treated with HF, the resulting peaks become rougher, weaker and broader. This shows a level of disorderly behaviour of the planes, the formation of new structures of layered material and the disappearance of the crystalline structure of MAX phase. Furthermore, in both the case of MX (Con) and MX (MW), the distinctive (104) peak of 'Al' in Ti_3AlC_2 has almost disappeared [94]. The backwards shifting of the (002) peak, which is another intriguing alteration seen in the MXene spectra, is also shown magnified in Fig.46A to demonstrate the shift [301]. These modifications confirm that MXene flakes were successfully synthesised. MX (MW) differs from MX (Con), in that its peak intensity is higher than that of conventional MXene, which changes from MAX phase due to expanding interlayer space.

Fig.46B represents the XRD of V/MX composites synthesised by microwave method, the existence of V_2O_5 in all produced V/MX composites is shown by the diffraction peaks at $2\theta = 15.42°$, 20.31°, 26.19°, 31.07°, and 34.30°, which correspond to the (200), (001), (110), (301), and (310) planes [298]. The further exfoliation of MXene to a few layered structure is demonstrated by the formation of a new peak at $2\theta = 12.21°$, which corresponds to the (004) plane. Another additional peak appears at

25.8° at high doping levels, which is in a good match with the position of the (101) diffraction peak of TiO_2 [306]. The XRD results suggest the successful incorporation of crystalline V_2O_5 within the exfoliated MXene structure. The noticeable diffraction peaks at 2θ values match standard JCPDS cards very well. In particular, the orthorhombic phase of V_2O_5 is confirmed by the peaks ascribed to it matching that of JCPDS card No. 41–1426 [342]. These results confirm the successful incorporation of V_2O_5 into the MXene matrix in all V/MX composites.

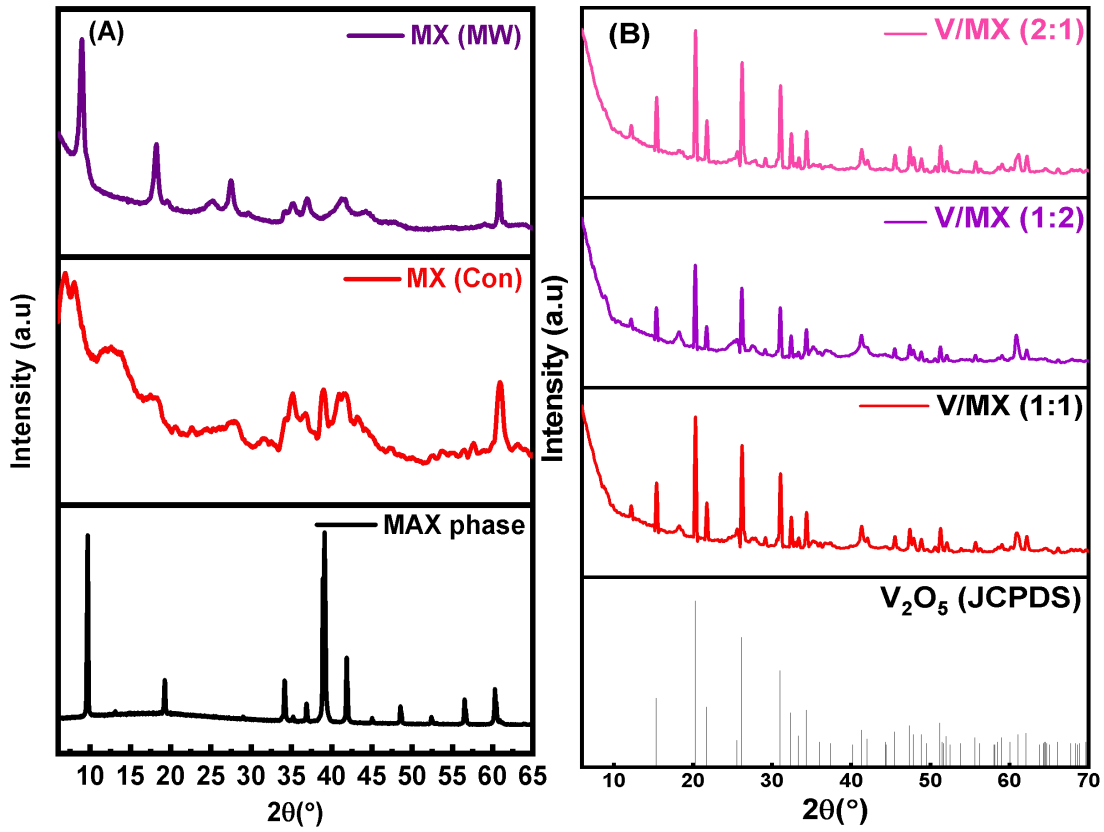

Fig. 46 XRD patterns of (A) Ti_3AlC_2 MAX phase, MXene synthesised via conventional (MX (Con)), and microwave-assisted method (MX (MW)) (B) XRD patterns of V_2O_5-modified MXene composites (V/MX) with varying weight ratios (1:1, 1:2, and 2:1), shows additional peaks that correspond to V_2O_5 (JCPDS card No. 41–1426).

Fig.46C represents the XRD comparison of the V/MX composites prepared using the conventional and microwave method with ratio of 1:2. The diffraction peaks at 2θ=15.42°, 20.31°, 26.19°, 31.07° and 34.30° corresponding to the (200), (001), (110), (301) and (310) planes indicates the presence of V_2O_5 in Vanadium and MXene composites. The (002) peak shift diminished may indicating a slight contraction in d-spacing. This may be due to the excessive vanadium doping that has now covered the entire surface of DMSO-treated MXene thus decreasing the space between different MX layers. A new peak of 2θ=12.21° corresponds to (004) plane arises, showing the further exfoliation of MXene to a fewer-layered structure. At high doping level another new peak evolves at 25.8° which matches well with the (101) diffraction peak position of TiO_2 [94, 301, 298, 306, 340-342].

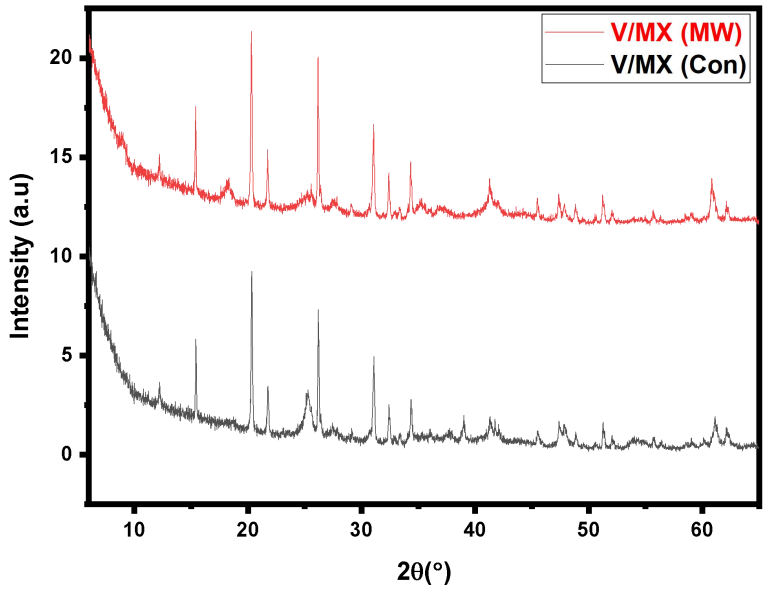

Fig. 46C XRD comparison of V/MX (1:2) composites prepared by conventional and microwave-assisted methods.

4.3.6.2. FTIR spectroscopy

Fig.47 shows the FTIR spectrum of MAX phase, MX (Con) and MX (MW) **Fig.47A**, all V/MX composites synthesized by microwave method **Fig.47B** and **Fig.47C** shows the FTIR comparison between the V/MX composites prepared using the conventional and microwave approach with ratio 1:2. Through FTIR analysis, the synthesized material's composition and surface functionalities can be determined. In the FTIR

spectrum Fig.47A of the MAX phase, the bands of the Ti-O, Al-O, CH_2, and C-H groups are located at 543, 1030, 1430, and 2350 cm^{-1}, respectively [313]. The band at around 606 cm^{-1} in the MX (Con) and MX (MW) FTIR spectra represents the out-of-plane vibrations of Ti–C. Moreover, the peak at 486 cm^{-1} was probably generated by the deformation vibration of the Ti–O bond. The weak bands observed at 2356 and 2662 cm^{-1} may be associated with atmospheric CO_2 adsorption and/or combination bands. Therefore, a definitive assignment of these bands to CH and CH_2 groups could not be established from the present FTIR data[341]. Fig.47B shows the FTIR spectrum of V/MX composites, highly adsorbed hydrogen-bonded external molecules of water to the −OH groups on the V/MX composite surface are responsible for the peaks observed at around 3138 cm^{-1} and 1616 cm^{-1} [341]. The small peak at 1406 cm^{-1} can also be used to identify the distinctive bond vibration of C-H, while the small peak detected at 2330 cm^{-1} is associated with the CH_2 groups of MXene. The V=O stretching mode of V_2O_5 may have been connected to the peak at 1005 cm^{-1}. The O-V-O symmetric stretching vibration modes have been identified by the peak observed at 511 cm^{-1} [272]. The V-C stretching is associated with the peak at 659 cm^{-1} [341]. The successful etching of the MAX phase and the creation of V/MX composites are confirmed by the FTIR spectra. Complete Al elimination is shown by the disappearance of the Al–O and Ti–Al peaks in etched MXene (Con and MW). The presence of V=O and V–O–V bonds in V/MX composites, showing successful V_2O_5 incorporation. Improved photocatalytic activity is a result of these chemical interactions, which also improve active sites. The XRD and FTIR results indicate the successful incorporation of V_2O_5 into the MXene structure while preserving its layered nature. However, during V_2O_5 incorporation, MXene may partially oxidise to TiO_2, which could lead to a hybrid structure of MXene–TiO_2–V_2O_5. This is consistent with earlier studies that emphasise how easily MXene surfaces can oxidise in oxidative or heat environments [343]. **Table 5**, shows the FTIR results of all materials. **Fig.47C**, The peaks observed at 3138 and 1616 cm^{-1} are due to the strongly adsorbed hydrogen-bonded external water molecules to the −OH groups present on the surface of V/MXene composite. The small observed at 2330 cm^{-1} related to the CH_2 groups of MXene and the characteristic bond vibration of C-H can also be identified by peak at 1406 cm^{-1}. The peaks observed at 1286 cm^{-1} is C-F related band. The peak at 1005

cm^{-1} could be related with V=O stretching mode of V_2O_5. The peak obtained at 511 cm^{-1} has been attributed to the O-V-O symmetric stretching vibration modes. The peak at 659 cm^{-1} is related to V-C stretching [272, 341-343].

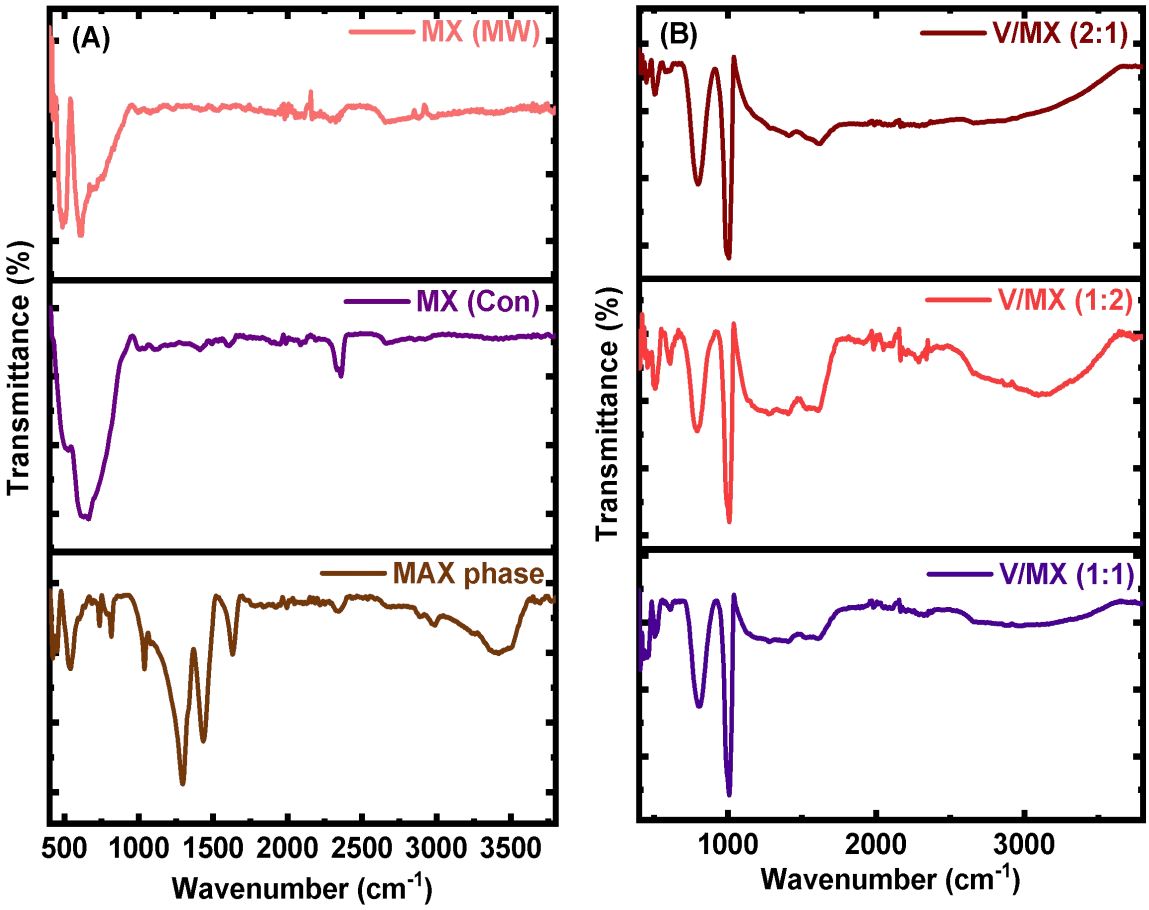

Fig. 47 FTIR spectra of (A) Ti_3AlC_2 MAX phase, conventionally synthesised MXene (MX (Con), and microwave-assisted MXene (MX (MW), (B) FTIR spectra of V_2O_5-modified MXene composites (V/MX) prepared via microwave synthesis with different ratios (1:1, 1:2, and 2:1).

Table 5 A tabular data for synthesized materials by FTIR spectrum

Materials	**Wavenumber (cm^{-1})**	**Functional group**
MAX phase	543	Ti-O
	1030	Al-O
	1430	CH
	2350	CH_2

MX (Con) and MX (MX)	606	Ti-C
	486	Ti-O
	2356	CH
	2662	CH_2
V/MX (1:1), V/MX (1:2) and V/MX (2:1)	3138	OH
	1616	OH
	1406	CH
	2330	CH_2
	1005	V=O
	511	O-V-O
	659	V-C

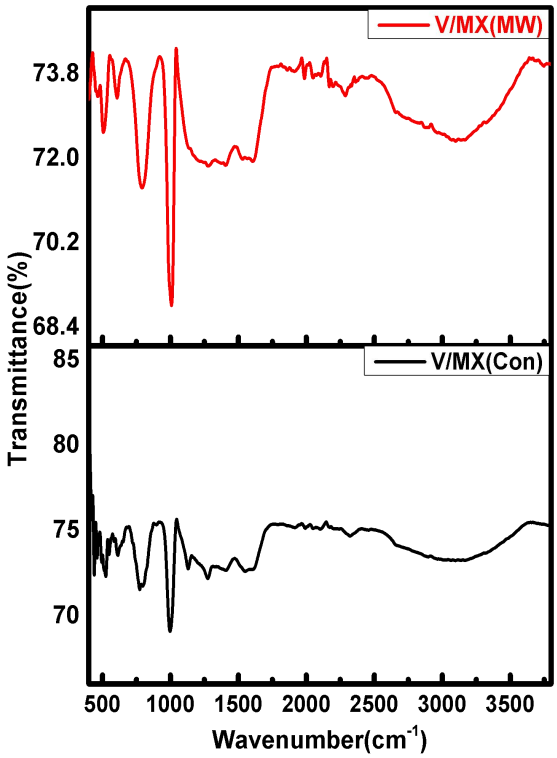

Fig. 47C FTIR comparison between the V/MX composites prepared using the conventional and microwave approach with ratio 1:2

4.3.6.3. Surface morphology analysis

As seen in **Fig.48**, the surface morphology of the MAX phase, MX (Con), MX (MW) and V/MX composites (1:2) synthesized by conventional and microwave method was analysed using SEM analysis. Strong bonding among the layers gives the layered

structure in **Fig.48A**, SEM picture of MAX phase material, the appearance of being thick, compact and densely packed. The substance looks continuous and there is not much exfoliation overall. However, the removal of the aluminium layer causes the MAX phase to exfoliate in two-dimensional sheets of MXene following hydrofluoric acid treatment. Hydrofluoric acid and the MAX phase may undergo an exothermic reaction [314]. Comparing the MXene produced by the conventional approach to the MAX phase pictures, **Fig.48B** shows a less compact and less thick layered structure. The elimination of the aluminium layer appears to enhance the porosity and spaces between the MXene layers. Whereas, in **Fig.48C**, the layers of MXene made using the microwave approach appear more loosely stacked and exfoliated than those made using a normal conventionally synthesis process. Compared to MX (Con), the MX (MW) may have fewer defects and be more consistent [344]. The SEM images of V/MX [1:2] **Fig.48D** and **Fig.48E** shows that when the vanadium and MXene composite synthesised, the MXene surface turns rough, which is a sign that the surface is being influenced by vanadium ions. Furthermore, MXene's structure remains intact and exhibits layered morphology [345].

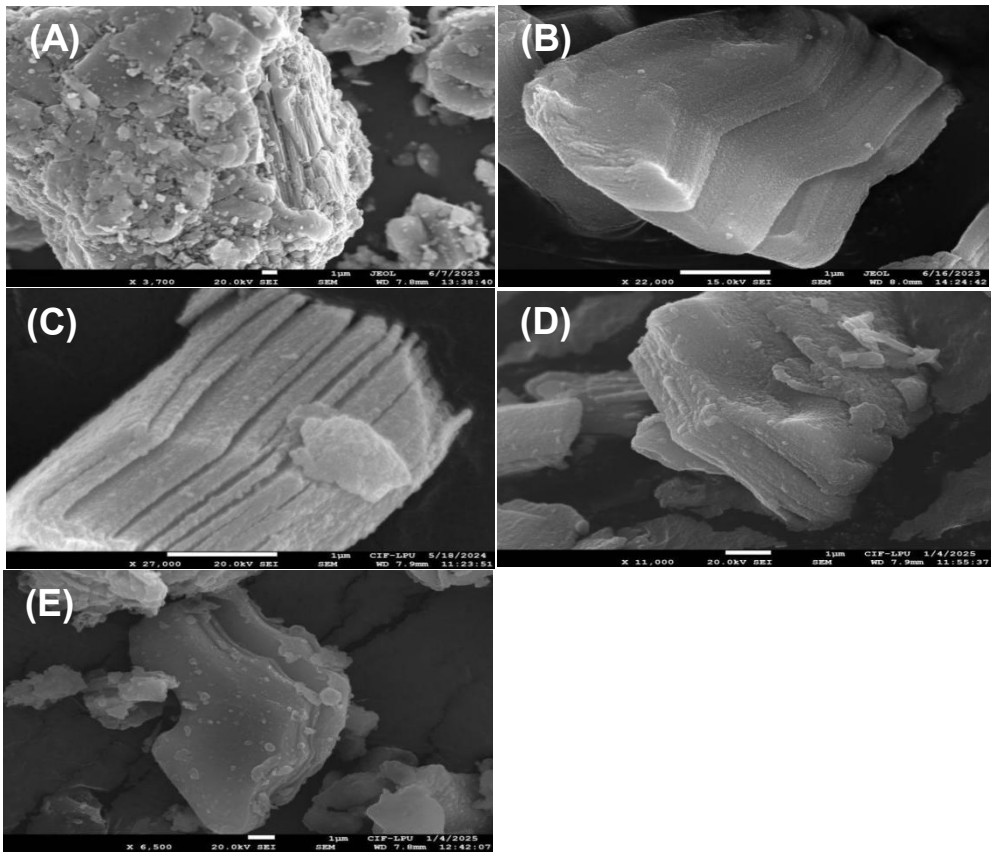

Fig. 48 SEM images of (A) Ti_3AlC_2 MAX phase (B) conventionally synthesised MXene (MX (Con)) (C) microwave-assisted MXene (MX (MW)) (D) and V/MX composites prepared using the conventional and microwave approach with ratio 1:2.

4.3.6.4. Elemental analysis by EDX

Fig.49 shows the elemental analysis of MX (MW), and as-prepared V/MX composite (1:2) was examined from EDX analysis shown in **Fig.50**. The EDX results of MX (MW) Fig.49 shows the presence of elements Ti, C, O and F that clearly show the HF-etching of MAX phase. The atomic percentage of these elements in **Table 6,** shows titanium, oxygen and carbon as the major elements [316]. In Fig.50, the EDX spectrum of V/MX (1:2) confirms the presence of V along with Ti, C, O, F, and trace amounts of Al, indicating the successful formation of the V_2O_5-MXene composite. The elemental composition obtained from EDX analysis supports the successful formation of the composite system. The atomic percentage showing extremely low Al content suggests effective etching of the MAX phase and conversion to MXene. The residual Al signal may arise from traces of unetched Al-containing phases[111].

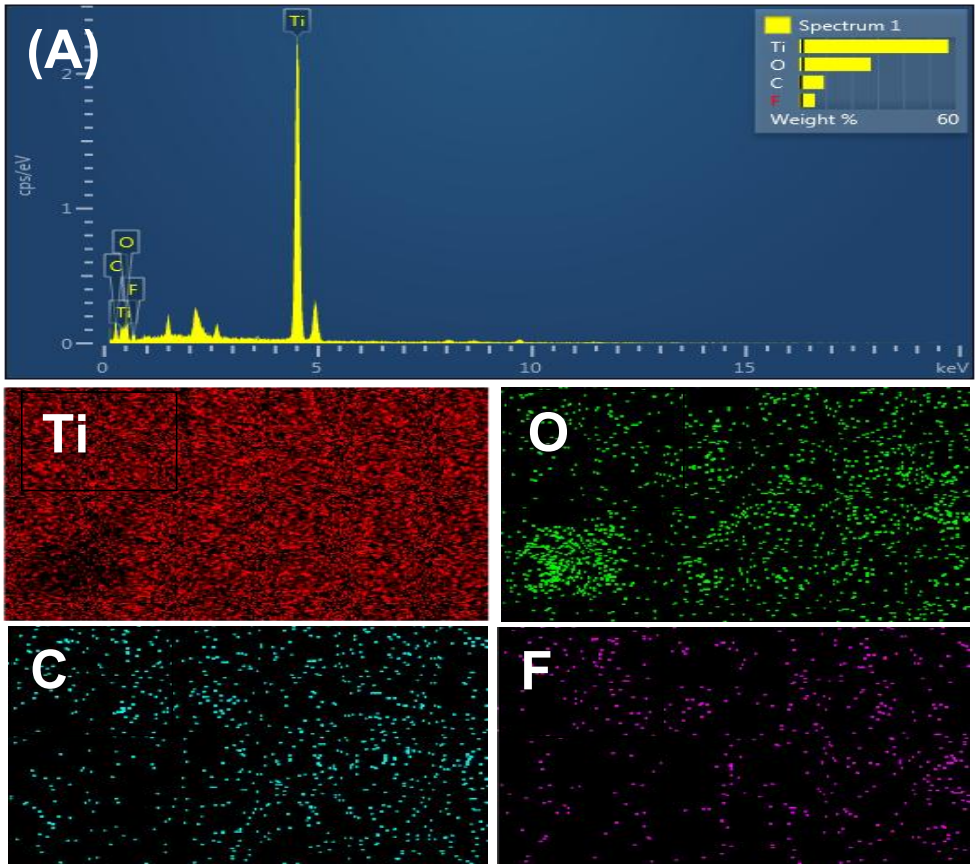

Fig. 49 EDX spectrum of MXene synthesised by the microwave-assisted method (MX (MW)), confirming the presence of key elements such as Titanium (Ti), Carbon (C), Flourine (F), and Oxygen (O).

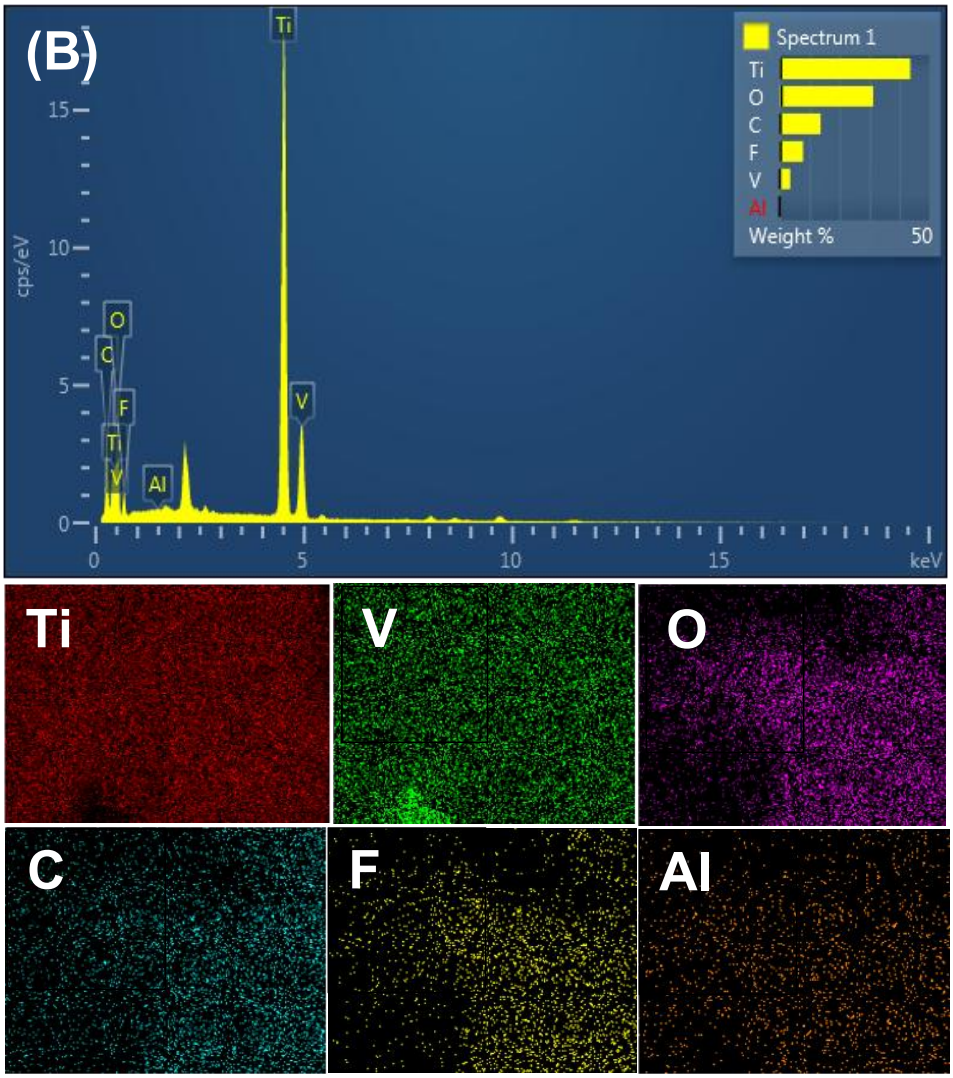

Fig. 50 EDX spectrum of V_2O_5-modified MXene composite synthesised via microwave-assisted method (1:2), confirming the successful presence of Vanadium (V), Titanium (Ti), carbon (C), and oxygen (O).

Table 6 A tabular data for atomic percentage by EDX spectrum

	Atomic percentage (%)					
Elements	**Carbon**	**Titanium**	**Oxygen**	**Fluorine**	**Vanadium**	**Aluminium**
MX (MW)	19.51	29.85	42.80	7.84		

V/MX (1:2)	25.41	20.30	43.56	9.14	1.55	0.05

4.3.6.5. Zeta potential measurement

The surface charge of materials is linked to their zeta potential (ζ), which significantly affects their stability in suspension, photocatalytic capability and interactions with pollutants like cetirizine. Zeta potential values of MX (Con), MX (MW) and V/MX (MW) (1:2) are −8.70 mV, −11.0 mV and −21.4 mV, respectively, as shown in **Fig.51**. A higher negative zeta potential in MX (Con) and MX (MW) indicates a higher surface charge and improved electrostatic stability in colloidal suspensions. The increased negative charge in MX (MW) is likely due to the presence of more surface functionalities on the MXene sheets [341-345]. However, after vanadium introducing on MXene, more negative zeta potential was observed because of that enhanced surface charge density generated by the vanadium, the colloidal stability and distribution in aqueous solutions are improved. The adherence of hydroxyl groups to the surface of the V/MX particles caused a considerable increase in their zeta potential, which also reveals that the surface contains an abundance of polar functional groups [346]. This increased negative surface charge promotes more effective adsorption and speeds up the photocatalytic degradation process by strengthening electrostatic interaction with positively charged cetirizine molecules and improving colloidal stability.

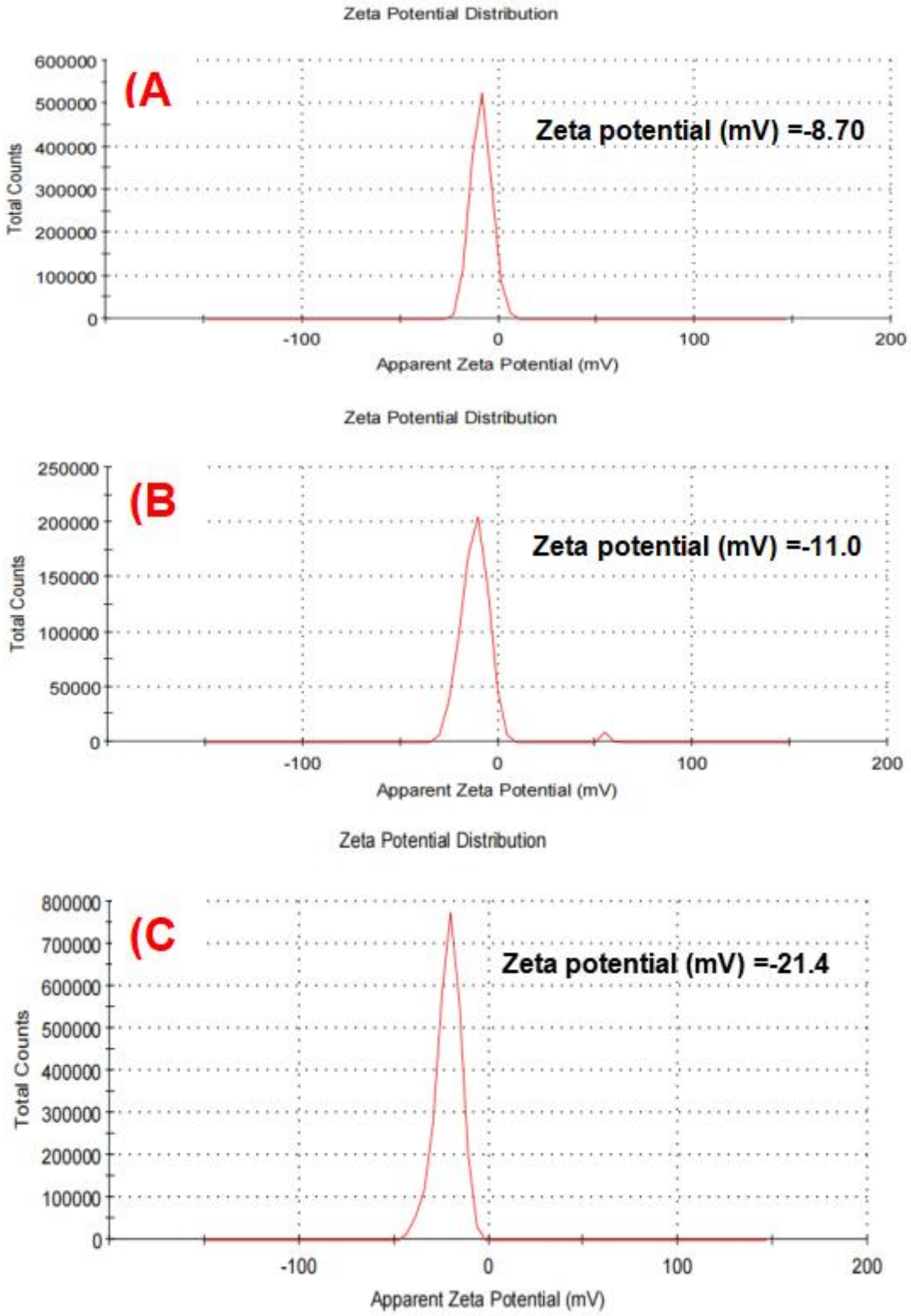

Fig. 51 Zeta potential measurements of MXene synthesised by conventional and microwave (A) MX (Con), and (B) MX (MW) methods, along with the V/MX composite (C) synthesized by microwave method.

4.3.6.6. Electrochemical impedance spectroscopy

The charge transfer properties of the synthesised materials, which are essential in determining photocatalytic efficiency, were examined using EIS analysis shown in **Fig.52**. The resistance that photogenerated charge carriers encounter as they transfer over the catalyst interaction is revealed by the Nyquist plots that are acquired from EIS. The charge transfer resistance (Rct), which is related to the resistance to electron transfer at the photocatalyst surface, and the equivalent series resistance (Rs), which represents the resistance of the electrolyte and contacts, are two important characteristics that were determined from EIS [333]. The V/MX composite in this investigation demonstrated effective charge transfer at the catalyst–electrolyte interface with an Rs value of 6.7433 Ω and a relatively low Rct value of 36.144 Ω. On the other hand, the MX (MW) sample has Rs value of 7.455 Ω and a significantly larger semicircle in the Nyquist plot, which is indicative of a far stronger resistance to charge transfer and reflected poor interfacial charge transfer dynamics. This significant variation in Rct values indicates that the addition of vanadium to MXene efficiently lowers the charge transfer resistance, allowing photogenerated electrons and holes to separate and migrate more quickly [333, 346]. Because it inhibits electron–hole pair recombination and encourages their involvement in surface redox processes, lower charge transfer resistance is associated with increased photocatalytic activity. Therefore, the EIS results suggest that the improved charge transport and reduced charge transfer resistance of the V/MX composite may contribute to its enhanced photocatalytic activity. The lower charge transfer resistance observed in EIS, together with the reduced PL intensity, indicates more efficient charge separation and suppressed electron–hole recombination in the V/MX composite.

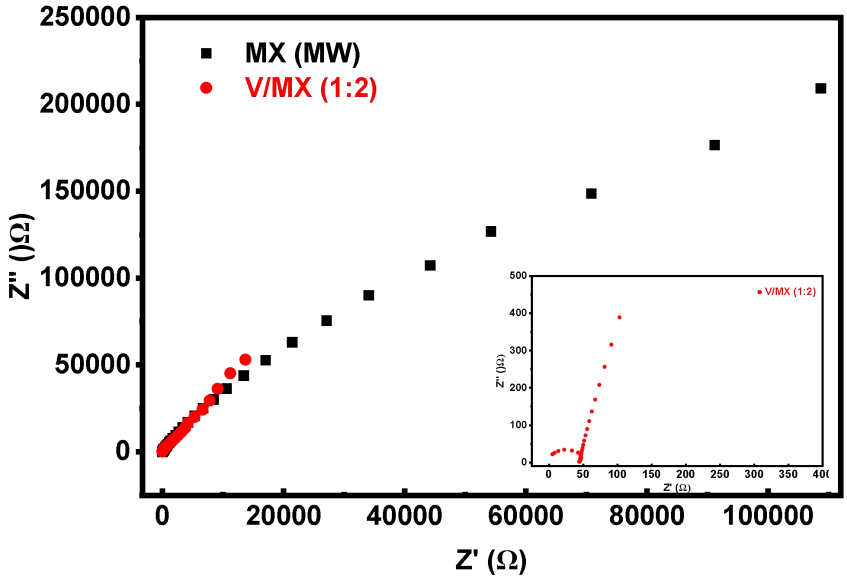

Fig. 52 EIS analysis of microwave-synthesised MXene (MX (MW)) and V_2O_5-modified MXene composite (V/MX) synthesized by microwave method.

4.3.6.7. Band gap energy

A UV-vis spectrophotometer was used to examine the optical characteristics of MXene and V/MX (1:2) that were synthesised using microwave technology. The band gap for both samples was determined using Tauc's plot. The band gap of these samples was determined by plotting $(\alpha hv)^2$ versus band gap energy Eg. In **Fig.53**, the band gaps of MXene and V/MX were found to be around 1.34 and 1.68 eV, respectively. The observed increase in band gap after V_2O_5 incorporation may influence charge separation behaviour and redox properties, thereby contributing to enhanced photocatalytic performance. While the increased valence band edge promotes stronger oxidation processes, the rise in conduction band energy improves the reduction capacity of photogenerated electrons. As a result, the breakdown of cetirizine molecules is facilitated by the more efficient generation of reactive oxygen species (ROS), including hydroxyl radicals (•OH) and superoxide radicals (O_2^-)• [347-349]. This band gap modulation brought about by the incorporation of V_2O_5 can be understood as a type of bandgap engineering, which is important for increasing photocatalytic efficiency. The recombination of photogenerated charge carriers can be inhibited and greater redox potentials can be obtained by modifying the band structure.

Pharmaceutical pollutants like cetirizine degrade more quickly as a result of these modifications, which also improve visible light absorption and enable more efficient reactive oxygen species formation [346].

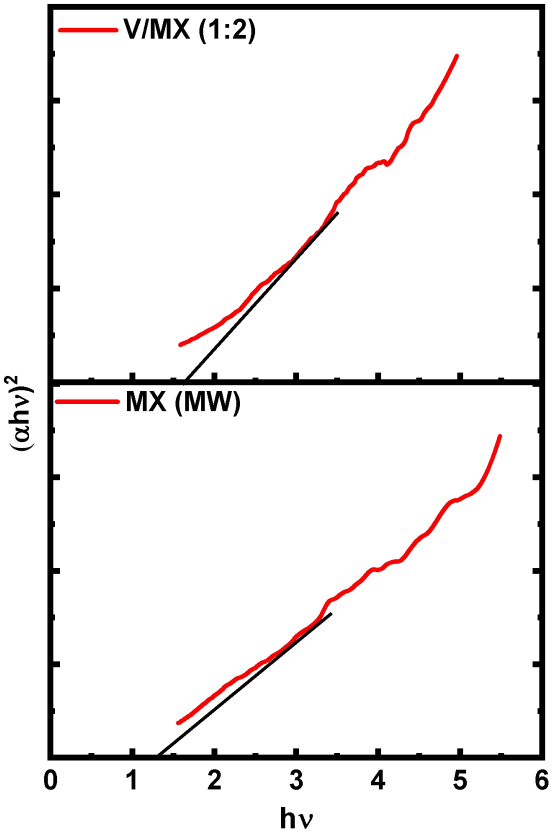

Fig. 53 Tauc plots of MXene (MX (MW)) and V/MX (1:2) composite synthesized by microwave method used for band gap determination.

4.3.6.8. Photoluminescence (PL) spectroscopy

PL spectroscopy was used to examine the charge carrier dynamics of the synthesised photocatalysts. Because it decreases the quantity of charge carriers available for surface redox reactions, a high PL intensity is an indication of a rapid radiative recombination of photogenerated electron–hole pairs, which is harmful to photocatalytic activity [350]. Thus, a suppressed PL signal is an important characteristic since it indicates a longer carrier lifetime and more effective charge separation, both of these contribute essentially for improving photocatalytic performance [350]. Analysis of electron–hole pair recombination by PL is important for understanding photocatalysis [351]. The V/MX composite PL spectrum, in

comparison, demonstrates significant quenching of the PL signal. By facilitating the rapid transfer of photogenerated electrons from the MXene to the V_2O_5 component, the connection between the two materials spatially separates the electrons from the holes and stops recombination [352]. **Fig.54** shows the PL spectra of the V/MX composite and MX (MW). A comparatively lower PL intensity was observed for the V/MX composite than for MX (MW), suggesting reduced electron–hole recombination and improved charge separation. The interaction between MXene and V_2O_5 may facilitate charge transfer and contribute to enhanced photocatalytic performance. Therefore, the PL results qualitatively support the improved photocatalytic activity of the V/MX composite [350-352].

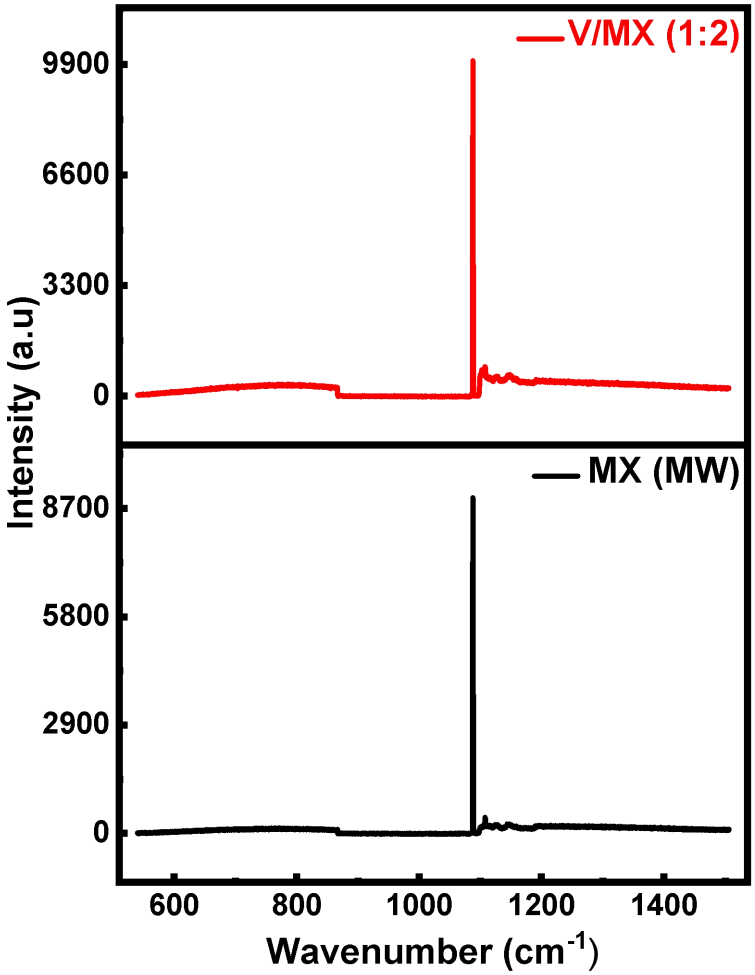

Fig. 54 Photoluminescence (PL) analysis of microwave-synthesised MXene (MX (MW)) and V_2O_5- modified MXene composite (V/MX) synthesized by microwave method.

4.3.6.9. Photocatalytic performance towards photodegradation of citerizine

4.3.6.9.1. Dark phase

4.3.6.9.1.1. pH effect

The dark-phase adsorption behavior of the MAX phase, conventionally synthesized MXene (**MX Con**), and microwave-assisted MXene (**MX MW**) was assessed at pH 2, 4, 6, 8, and 10 in **Fig.55A**. With a removal efficiency of about 20% at pH 2, the MAX phase demonstrated extremely poor adsorption performance. The dense layered structure of MAX phases and their restricted surface terminations are likely to cause such poor adsorption. Due to the development of functional groups, the (MX Con) exhibited somewhat better adsorption following etching; nonetheless, the dark-phase adsorption efficiency remained low, reaching about 36% at pH 4. Due to increased defect concentration and greater interlayer opening resulting from rapid microwave heating, the microwave-synthesised MXene showed somewhat higher adsorption across all pH levels, showing an adsorption efficiency of about 32% at pH 4[303]. The overall adsorption remained low despite this improvement, indicating that none of the compounds showed appreciable pollutant removal in the absence of irradiation. These findings suggest that the degradation observed under visible light is predominantly governed by photocatalytic processes rather than dark-phase adsorption [90].

In order to determine the vanadium-based MXene composites capacity to remove pollutants in the absence of light and to verify that any resulting degradation under visible irradiation is photocatalytic rather than adsorption-driven, the dark-phase adsorption behavior of the materials was also investigated. At pH 8, all V/MX composites synthesised by the microwave method showed moderate adsorption behaviour. The adsorption efficiencies of V/MX (1:1), V/MX (1:2), and V/MX (2:1) were 44.4%, 47.0%, and 40.0%, respectively, as shown in **Fig.55B**. All three of the vanadium-based composites had higher adsorption efficiencies than the Ti-based MAX/MXene systems, but the values were still insufficient to account for significant degradation, suggesting that these materials are ineffective at removing drugs in the dark. Where V/MX exhibit improved conductivity and surface chemistry but still need light activation to start catalytic processes [189, 349]

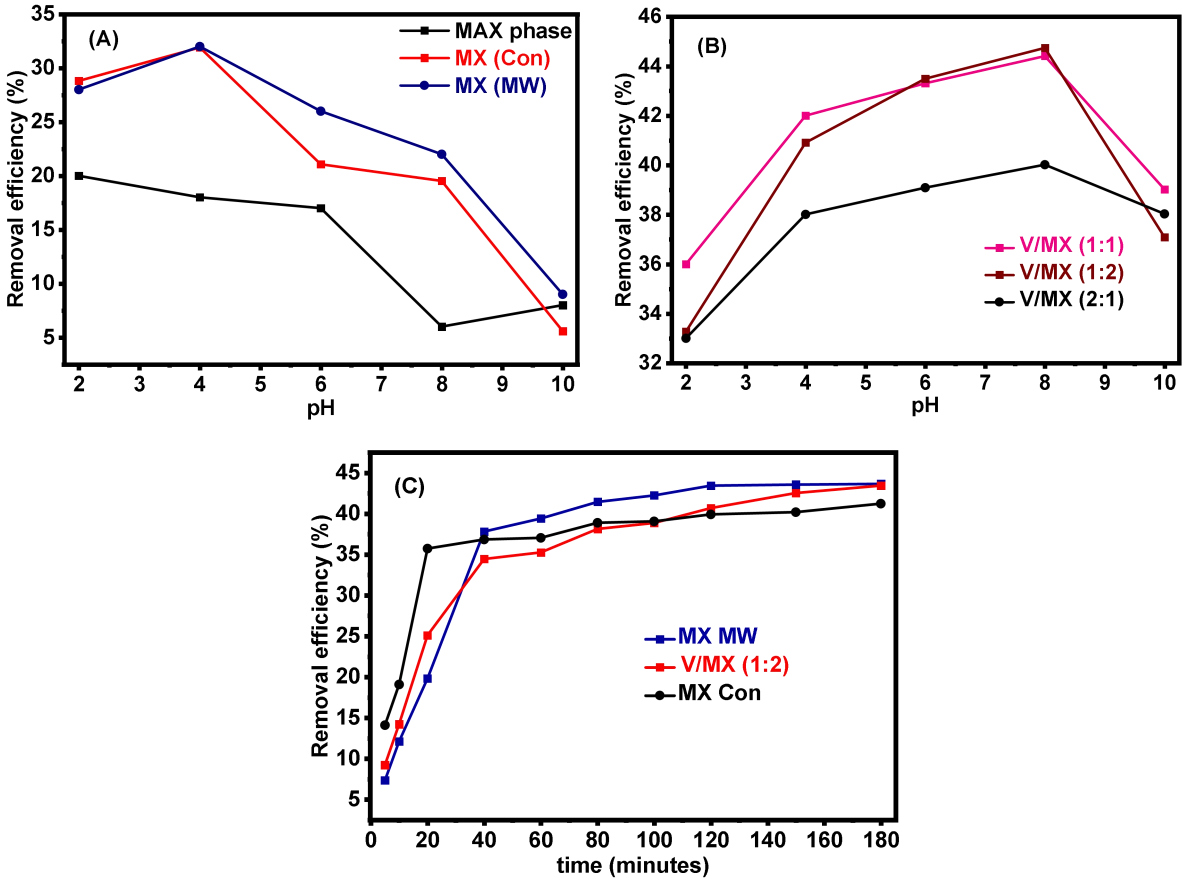

Fig. 55 Dark-phase adsorption of cetirizine at different pH values (A–B) and effect of contact time on adsorption of cetirizine (C).

4.3.6.9.1.2. Effect of time

The purpose of the dark-phase tests was to identify the synthetic materials' pure adsorption contribution prior to photocatalytic degradation. The time-dependent adsorption behavior of conventional MXene, microwave MXene, and V/MX (1:2) over a 180-minute period is displayed in **Fig.55C**. Every sample showed a steady rise in adsorption over time, indicating that accessible surface sites were gradually occupied. The adsorption increased rapidly during the initial stage due to the availability of a large number of active sites on the MXene surface, which facilitated interactions with the drug molecules. The majority of easily accessible surface sites

were occupied after 120 minutes, as indicated by the adsorption curves toward equilibrium. The synergistic interaction between V_2O_5 and MXene layers is responsible for the higher adsorption efficiency (50.0%) observed for the V/MX (1:2) composite. This interaction may promote stronger adsorption of drug molecules. The presence of V_2O_5 in the composite may contribute to improved dark-phase adsorption by providing additional defect sites and oxygen-containing surface functionalities [359-360].

4.3.6.9.2. Light phase

4.3.6.9.2.1. pH effect

Fig.56 represents the results of a study that examined the effects of pH on the photocatalytic degradation of cetirizine in the presence of visible light for all photocatalytic materials [MAX phase, MX (Con) and MX (MW), all V/MX composites synthesized by microwave (A) and (B), and V/MX composites synthesized by conventional method with ratio [1:2] (E)]. Because of the stable structure of MAX phase material in **Fig.56A** exhibits less degradation. It had less active sites than other photocatalytic materials so it showed less reactivity in basic and acidic media. At slightly basic pH of 8.0, it demonstrated a moderate degradation efficiency of 67.83%. In the case of MXenes, there are functional groups present on the surface, that is why they are that much compact and rigid like MAX phase. So, MXene interacts more with cetirizine as compared to MAX phase. The elimination ability of cetirizine using MX (Con) and MX (MW) materials increased from 2 to 8 pH but then dropped at 10 pH which determined that the ideal pH for both MXene compounds was slightly basic at 8.0. The cetirizine degradation efficiency obtained with MX (Con) and MX (MW) in the visible area are 84.5% and 87.6%, respectively. The lower degradation efficiency observed under acidic conditions may be attributed to reduced generation of reactive oxygen species and less favourable interactions between the catalyst surface and cetirizine molecules. Although more OH^- ions will be present when the pH rises, there will also be more OH radicals. Cetirizine breaks down more rapidly in alkaline conditions than in acidic medium because of the fast generation of OH radicals than H radicals [353-355]. On the other hand, all V/MX composites **Fig.56B** with ratios of 1:1, 1:2, and 2:1 exhibited the highest degrading efficiencies in the visible light band, which are 93.2%, 94.6%, and 90.1%,

respectively. With all V/MX composites, the degradation of cetirizine was comparably lower in acidic environment, but it turns very high when the pH value range has been raised to slightly basic medium but after that it lowered at pH 10 [349]. The pH of the solution, which affects the pollutant's ionization state as well as the catalyst's surface charge, has a significant impact on the photocatalytic degradation efficiency. The pKa values of cetirizine, a triprotic compound, are roughly 1.52, 2.92, and 8.27. Because of this, it is mostly protonated (cationic or zwitterionic) at pH values below ~2.9 and mostly resides in its deprotonated (anionic) form above ~2.9 [356-357]. Both zwitterionic and anionic forms of cetirizine are present at pH 8, and zeta potential studies reveal that the V/MX composite has a noticeably negative surface charge. As a result, adsorption is improved by electrostatic interactions. Furthermore, the production of reactive oxygen species, especially hydroxyl (·OH) and superoxide (O_2^{-}•) radicals, is encouraged in slightly alkaline environments, which increases the oxidative destruction of cetirizine molecules [358]. These two factors clarify the enhanced degradation performance observed in these conditions: increased ROS generation under pH 8 and improved adsorption through advantageous electrostatic interactions. Therefore, the ideal pH for all composites was also determined to be 8, which is somewhat basic. The V/MXene ratio (1:2) was used to optimize the elimination of cetirizine.

Fig.56E shows the photocatalytic degradation of cetirizine by the conventionally synthesized V/MX (1:2) composite at different pH values. The maximum degradation efficiency of approximately 91.2% was achieved at pH 8, indicating that a slightly basic medium is also favourable for the conventionally synthesized composite. With V/MX composites synthesized by conventional method, the degradation of cetirizine was comparably lower in acidic environment, but it turns very high when the pH value range has been raised to slightly basic medium but after that it lowered at pH 10 [349].

4.3.6.9.2.2. Effect of contact time

Fig.56C illustrates the impact of contact (irradiation) time. Utilising MX (Con), MX (MW) and V/MX composite (1:2), the degradation efficiency of cetirizine increased with the duration of irradiation. The percentages of degradation for MX (Con) went from 7.3 to 87.1%, MX (MW) went from 8.8 to 90.6% and V/MX (1:2) increased

from 16.63 to 95.36% when the irradiation time interval was extended from 5 to 180 min. The reason for this is that longer durations of irradiation will result in more OH• radicals, which speeds up the photocatalytic process and raises the elimination percentage. Compared to other photocatalysts in the visible spectrum, the composite exhibits the best degrading efficiency. **Table 7**, presents a comparison with previously published photocatalysts for pharmaceutical degradation in order to assess the photocatalytic performance of the various materials. Different materials, target medications, degradation circumstances, and efficiency are all included in the comparison. Vanadium introducing on MXene results in surface defects and oxygen vacancies that may gather electrons in the conduction band and slow down the rate at which charge carriers recombine. The adsorption of the reactant is also aided by these surface imperfections. The oxygen molecules are reduced to superoxide radicals, which then change into hydroxyl radicals, when the oxygen is adsorbed at defects and electrons from the conduction band are trapped by the surface imperfections [359-360].

Table 7 A tabular data presents a comparison with previously published photocatalysts for pharmaceutical degradation in order to assess the photocatalytic performance of the various materials .

S. No.	Photocatalyst	Drug	Source of light	Degradation efficiency (%)	References
1	TiO_2/Ti_3C_2Tx	Carbamazepine	UV light	~98.6%	111
2	Carbon nitride coupled with Ti_3C_2-Mxene	Rhodamine B	Visible light	~97.22%	111
3	Carbon nitride coupled with Ti_3C_2-Mxene	Tetracycline	Visible light	~86.34%	111

4	Nb_2O_5/Nb_2CT_x	Tetracycline	Visible light	~91.2%	111
5	Nb_2O_5/Nb_2CT_x	Rhodamine B	Visible light	~98.5%	111
6	**V_2O_5/MXene composite (this work)**	**Cetirizine**	**LED (Visible light)**	**94.66%**	**Present study**

4.3.6.9.2.3. H_2O_2 effect

Hydrogen peroxide (H_2O_2), when added to photocatalyst, can greatly increase its photocatalytic degradation activity by functioning as an electron acceptor, efficiently splitting photogenerated electron–hole pairs, and producing highly reactive hydroxyl radicals (OH•) that can more effectively degrade organic pollutants; in simply increasing the oxidation process power of system [361]. **Fig.56D** shows the impact of increasing the hydrogen peroxide from 0.01 to 1% on the removal of cetirizine by MX (MW) and V/MX (1:2) synthesized by microwave method. When H_2O_2 concentration increased from 0.01 to 0.5%, it improved the photocatalytic degradation of cetirizine from 62.2 to 79.3% in case of MX (MW) and whereas in the case of V/MX (1:2) from 72.3 to 94.8% but when the H_2O_2 concentration increased to 1%, the rate of degradation dropped in both MX (MW) to 58.9% and V/MX (1:2) to 79.4%. The extra H_2O_2 was the cause of this decrease in removal effectiveness because it scavenges hydroxyl radicals and forms less reactive species like water and oxygen, which lowers the rate of degradation [362]. It is possible to stabilise the linked charge carriers by capturing photogenerated electrons in hydrogen peroxide. When H_2O_2 reacts with oxygen or e^-, OH• radicals can be created. Therefore, the addition of an optimum concentration of H_2O_2 enhanced cetirizine degradation by promoting the generation of hydroxyl radicals and improving charge separation.

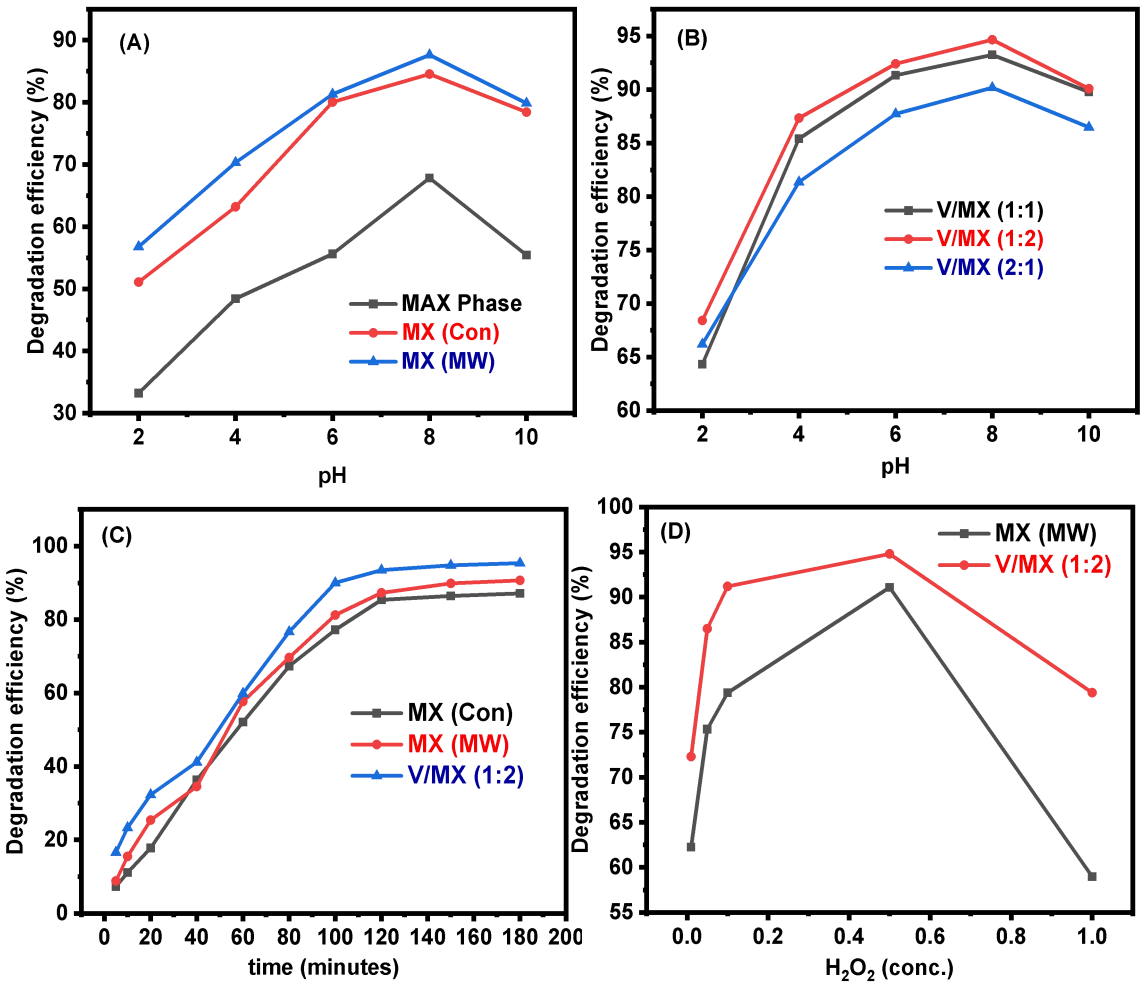

Fig. 56 Photocatalytic degradation of cetirizine at under visible light at different pH values (A-B), effect of time on degradation of cetirizine (C) and photocatalytic degradation of cetirizine in the presence of varying concentration of H_2O_2 (D).

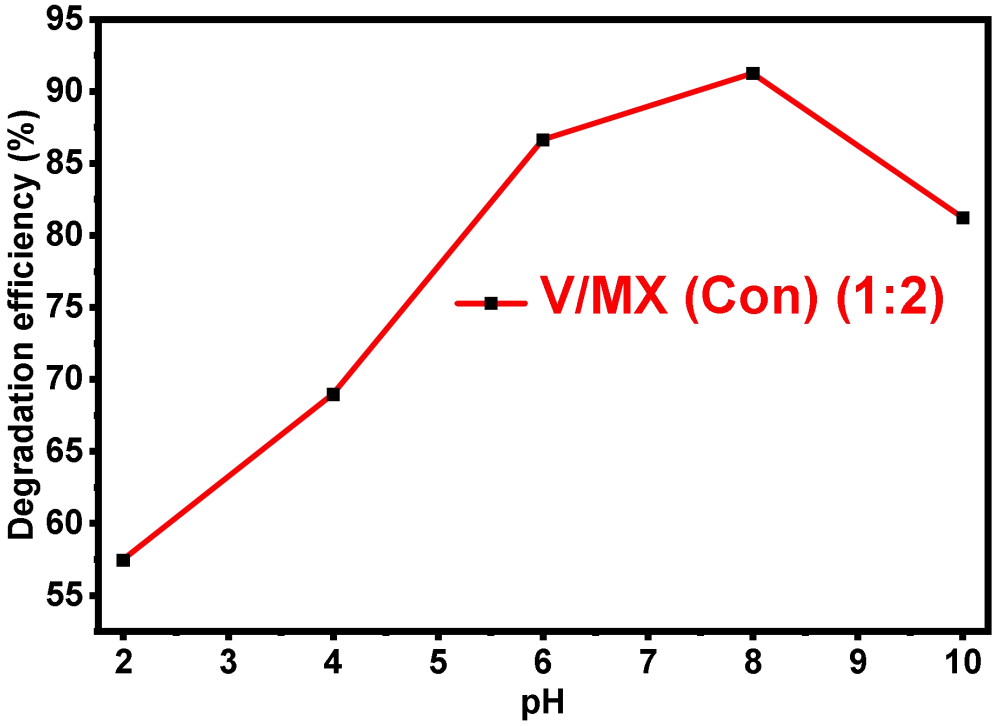

Fig. 56E V/MX composites synthesized by conventional method with ratio of 1:2 exhibited the high degrading efficiencies in the visible light

4.3.6.9.3. Recyclability of photocatalytic materials

The produced composite material must be recycled 'n' times in order for the catalyst to be more economically feasible. In order to evaluate the recyclability of the vanadium-based MXene synthesized by microwave method, five successive degradation cycles of cetirizine were carried out under visible light irradiation with an ideal concentration of 0.1 g/10 ml of H_2O_2 solution and stirred for 1 hr. The catalyst was filtered and cleaned with distilled water, dried at 60°C and then reused again for the next cycle. The degradation efficiency for each cycle is presented in **Fig.57**. As shown in Fig.57, the degradation efficiency gradually decreased with increasing regeneration cycles and reached approximately 64.5% after the fifth cycle. Despite the decrease in efficiency, the V/MX (1:2) composite retained appreciable photocatalytic activity after five cycles, indicating good stability and reusability. The gradual decrease in activity may be attributed to catalyst loss during recovery, surface fouling,

leaching of active sites, or partial oxidation of vanadium species during repeated photocatalytic cycles. [363-364].

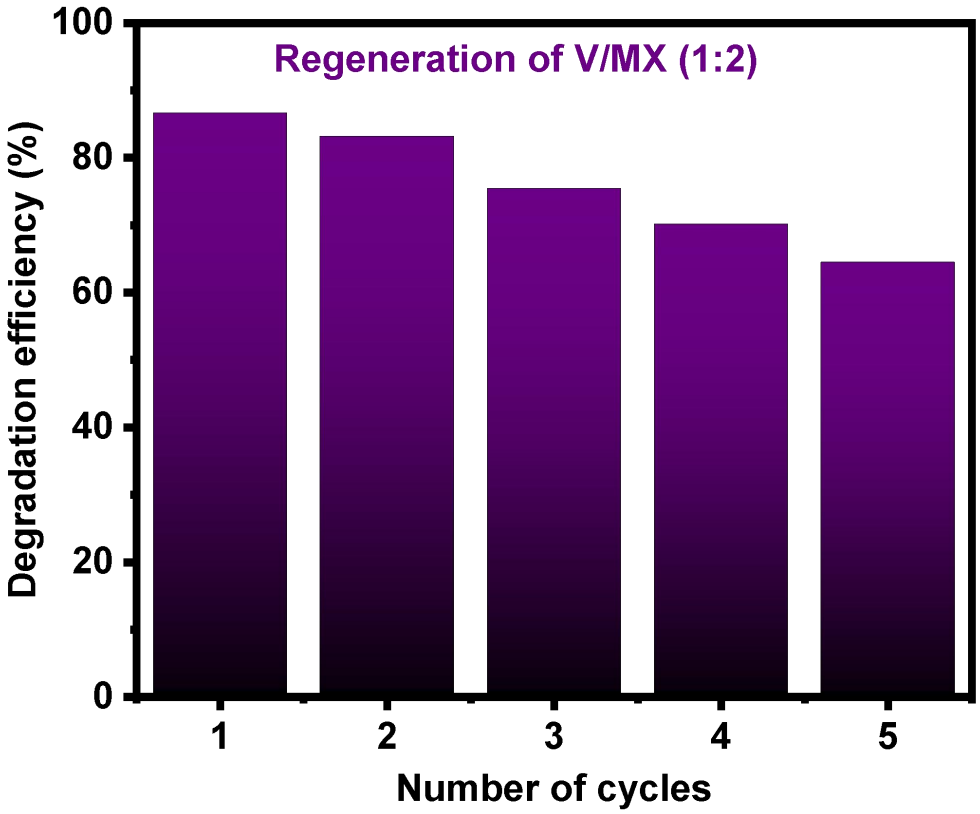

Fig. 57 Recyclability test of V_2O_5-modified MXene (V/MX) composite with ratio (1:2) synthesised by the microwave-assisted method for photocatalytic degradation of cetirizine under visible light.

4.3.6.10. Mechanism of photocatalytic degradation

MXene-based materials have drawn a lot of interest as photocatalysts because of their metallic conductivity, huge surface area, and adjustable band structure. But under visible light, pristine MXene frequently shows low charge carrier separation and low photocatalytic effectiveness because of photogenerated charge carrier recombination. Vanadium addition to MXene improves charge transfer kinetics and promotes the production of reactive oxygen species (ROS) for effective pollutant degradation in order to get over these limitations [347-348]. Vanadium is proposed to facilitate electron transfer and improve charge separation in the V/MX composite. The interface

between V_2O_5 and MXene may promote charge separation and suppress electron–hole recombination. Defect sites generated during synthesis may contribute to improved charge separation and photocatalytic activity. Furthermore, through modification of the band structure, these inherent defects might increase the absorption of visible light. According to earlier research, when exposed to visible light, designed voids greatly increase the breakdown efficiency of pharmaceutical pollutants [365]. Defect structures created during the synthesis procedures are partly responsible for the produced composite photocatalysts' higher performance in this context, and they probably help to increase photocatalytic efficiency. The photo-excited electrons (e^-) and holes (h^+) in **Fig.58** can interact with oxygen and water molecules to create reactive oxygen species (ROS), including hydrogen peroxide (H_2O_2), superoxide radicals ($O_2^{-}\bullet$), and hydroxyl radicals ($OH\bullet$) [347]. These extremely reactive ROS have the ability to target cetirizine molecules resulting in degradation. A ROS-driven oxidative route drives the photocatalytic degradation of cetirizine by MXene and V/MX composites, where vanadium introduction greatly improves charge separation, encourages the production of hydroxyl radicals and speeds up the full mineralisation of cetirizine. The 2D structure of MXene and the incorporation of vanadium are suggested to contribute to the improved photocatalytic performance of the composite. [349]. The photocatalytic degradation pathway of cetirizine utilising V_2O_5-modified MXene in the presence of visible light is depicted in Fig.58. Holes (h^+) are left behind when electrons (e^-) are excited by light and move from the valence band to the conduction band. The presence of vanadium may enhance charge separation and suppress electron–hole recombination. Superoxide radicals ($O_2^{-}\bullet$) are created when electrons decrease O_2, and hydroxyl radicals ($\bullet OH$) are created when holes oxidise H_2O. Cetirizine is broken down by these reactive oxygen species into non-toxic byproducts (CO_2 and H_2O). The background image connects the catalyst's activity to environmental remediation by highlighting actual pharmaceutical contamination. The proposed mechanism is supported by the EIS results, which showed a lower charge-transfer resistance for the V/MX composite compared with pristine MXene, indicating improved charge transport and reduced recombination of photogenerated charge carriers.

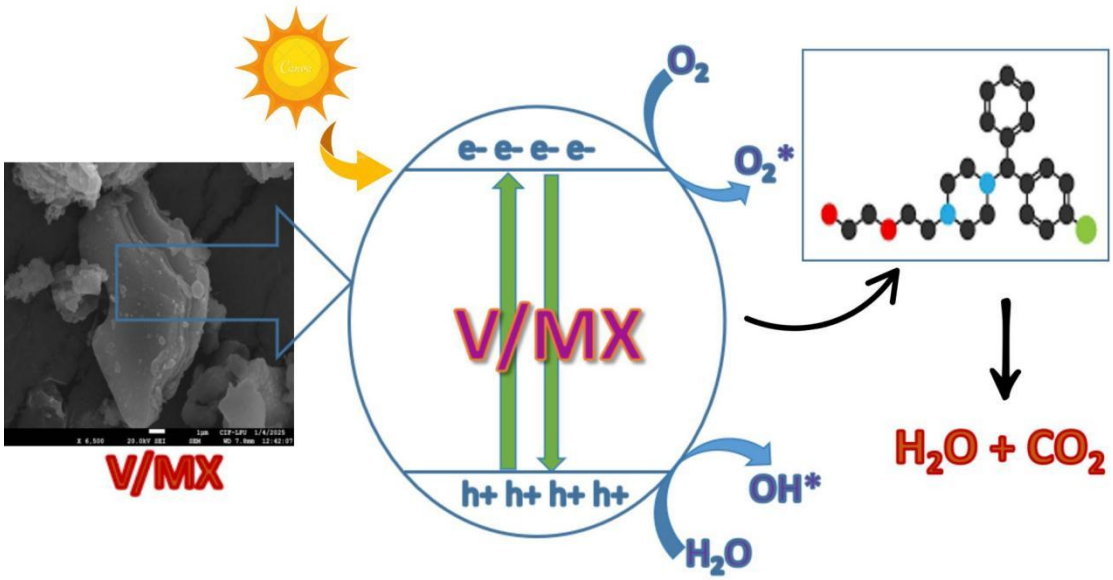

Fig. 58 Schematic mechanism for photocatalytic degradation of cetirizine drug from pharmaceutical aquatic waste by activation of V_2O_5-modified MXene nanocomposite.

X-ray diffraction (XRD) analysis of the used material was performed to assess the stability of the structure of the photocatalysts following degradation resulting from visible light in **Fig.59**. When compared to the fresh photocatalyst, the diffraction patterns obtained during photocatalysis showed no significant changes in peak positions. This demonstrates that the material's structural integrity and resistance to photocorrosion under the applied circumstances were confirmed by the crystalline structure's stability throughout the degradation process. For metal-based photocatalysts, comparable stability has been documented in the literature. For example, examined a dual Z-scheme Ag@ZnO/Ag/SnO_2 heterostructure and found that, following several photocatalytic cycles, there were no structural alterations in the XRD patterns. Additionally, their XPS investigation demonstrated significant surface and bulk stability during visible-light irradiation, further confirming the conservation of chemical states [366]. These results indicate that the synthesised photocatalyst is structurally stable and sustains its performance under photocatalytic conditions, which is consistent with the current findings.

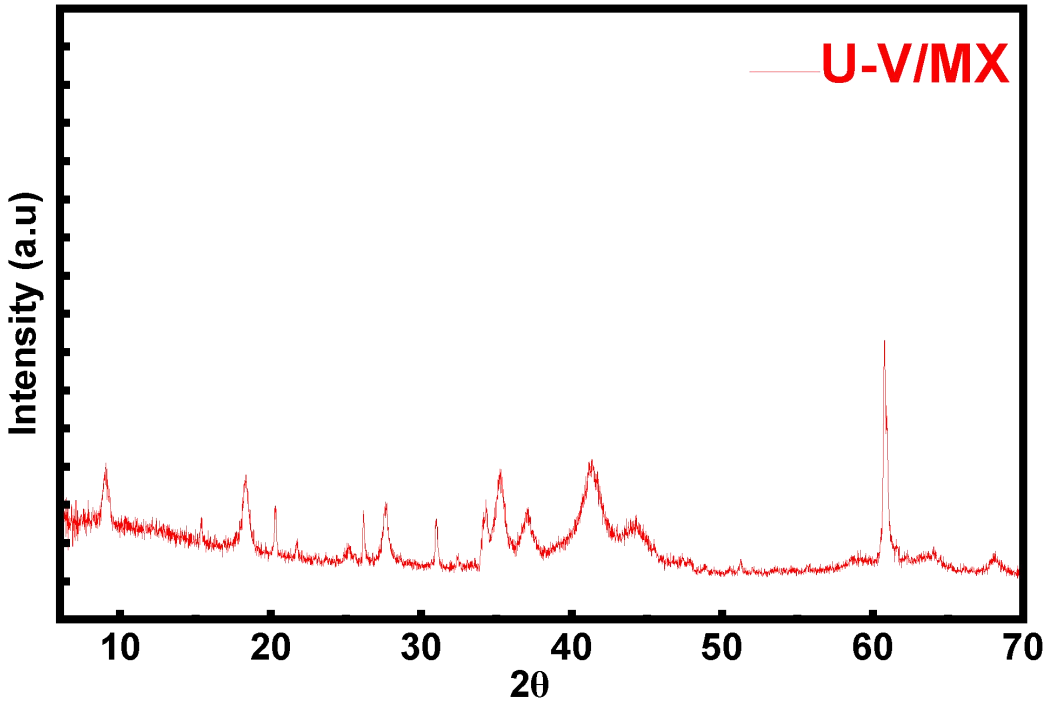

Fig. 59 XRD analysis of V_2O_5-modified MXene composite with ratio 1:2 (U-V/MX) after photocatalytic degradation of cetirizine.

4.3.7. Summary

This study presents a comparative investigation of MXene and V_2O_5-modified MXene photocatalytic materials for the degradation of cetirizine under visible light. To optimise synthesis, MXene was prepared using both conventional and microwave-assisted methods, with the latter significantly reducing synthesis time from hours to minutes. Our results demonstrate that the synthesis method and V_2O_5-to-MXene ratio play crucial roles in determining photocatalytic performance. Notably, the V_2O_5-MXene composite with a 1:2 ratio achieved the highest degradation efficiency of 94.66%, underscoring the importance of MXene in enhancing photocatalytic activity. Zeta potential analysis revealed that the incorporation of vanadium alters the surface charge of the catalyst, affecting its adsorption and charge transfer properties. Furthermore, the observed reduction in band gap energy suggests that vanadium enhances visible light absorption, thereby improving degradation efficiency. The impact of pH on degradation efficiency was also evaluated, with optimal performance

observed at pH 8. This finding highlights the significance of reactive oxygen species in the photocatalytic mechanism. In order to minimize the requirement for pH correction, photocatalytic degradation was carried out at pH 8, which is close to natural wastewater conditions. H_2O_2 was added to promote degradation, although in small amounts. Creating catalysts that function well without the use of additional chemicals would save costs and increase sustainability for large-scale applications. The oxidation states and phase composition will be confirmed by additional thorough surface characterisations using techniques like Raman spectroscopy and XPS. Overall, our study highlights the potential of V_2O_5 enabled MXene composites as efficient photocatalysts for the degradation of pharmaceutical pollutants under visible light, offering promising prospects for wastewater treatment applications.

CHAPTER-5

Conclusion

Conclusion

The main goal of the current study was to create and investigate MXene-based improved functional materials for the photocatalytic destruction of pharmaceutical pollutants under visible light irradiation, with a particular focus on the antibiotics and anti-inflammatory drugs. The synthesis, structural, optical, and surface characteristics of pure MXene and its composite forms, as well as their relationship to photocatalytic efficiency, were all methodically examined in this study.

Both standard conventional and microwave-assisted techniques were used to manufacture MXene ($Ti_3C_2T_x$), which allowed for a comparison of the effects of the synthesis pathway on physicochemical properties and photocatalytic activity. Because of its uniform and quick heating mechanism, the microwave-assisted approach showed a notable improvement in surface morphology, crystallinity, and electron mobility, resulting in higher photocatalytic degradation efficiencies of 97.83% for ciprofloxacin (La/MX 1:2) and 94.66% for cetirizine (V/MX 1:2) under visible light irradiation.

Lanthanum nitrate and Vanadium pentoxide were then added to MXene in different molar ratios (1:1, 1:2, and 2:1) to create La–modified MXene and V_2O_5-modified MXene composites, respectively. The surface charge, band structure, and defect sites of MXene were successfully modified by the addition of metal species, which improved charge separation and increased absorption of visible light.

XRD, FTIR, SEM, EDX, zeta potential, UV–Vis spectroscopy, PL, and EIS analyses were used for comprehensive characterization of the synthesized materials.

- XRD verified the development of multilayer MXene structures with noticeable shifts and widening, indicating effective intercalation and exfoliation after metal doping.
- Surface terminations such –OH, –F, and –O, which are essential to photocatalysis by trapping charge carriers, were identified by FTIR spectra.
- While composites displayed surface roughness and partial restacking, which helped with effective light scattering and active site production, SEM images of MXene revealed a typical 2D layered structure.
- The elemental composition and successful doping of La and V elements were confirmed by EDX analysis.

- Measurements of zeta potential revealed modified surface chemistry and increased interaction with cationic contaminants.
- PL analyses revealed lower emission intensities for the synthesized composites, indicating enhanced charge transfer and suppressed electron–hole recombination, which contributed to the observed high degradation efficiencies.
- UV–Vis spectroscopy revealed band gap values of 1.27–1.58 eV for La/MX systems and 1.34–1.68 eV for V/MX systems, indicating enhanced visible-light response after metal incorporation.

The V_2O_2–modied MXene (1:2) composite demonstrated the highest efficiency (94.66%) for cetirizine degradation. The composite also maintained approximately 64% degradation efficiency after five regeneration cycles, demonstrating reasonable stability and reusability. Zeta potential tests showed that the modification changed surface charge, resulting in better absorption of visible light. The catalyst's significance in actual wastewater environments is highlighted by its optimal performance at pH 8, which is near to natural water conditions. Degradation was further accelerated by the addition of small amounts H_2O_2, however in order to improve sustainability, future designs should concentrate on catalysts that can operate without external oxidants. Whereas,the La/MX (1:2) composite made using the microwave technique had the highest degrading efficiency (97.83%) for ciprofloxacin. The composite retained nearly 60% degradation efficiency after nine regeneration cycles, indicating good long-term stability. Increasing oxygen vacancies, producing more hydroxyl radicals, and improving the visible-light sensitivity were all made possible by La incorporation. Superior electron transport kinetics were confirmed by EIS, where the charge-transfer resistance decreased from 10.45 Ω for MXene (MW) to 8.59 Ω for La/MX (MW), which showed considerably reduced charge-transfer resistance and enhanced conductivity for La/MX (MW). In comparison to MXene, the zeta potential (-5.39 mV) also showed favorable surface interactions.

Overall, the study shows that MXene-based photocatalysts with superior structural and electrical properties gets effectively modified using microwave-assisted synthesis. By modifying the surface potential, enhancing charge carrier dynamics, and extending light absorption into the visible range, the La and V ions greatly improved the photocatalytic activity. The results of this study show that MXene and its metal-doped

composites are viable options for the effective and sustainable elimination of pharmaceutical pollutants from aquatic environments when exposed to visible light. In addition to providing a basis for future research including multi-metallic or heterojunction MXene composites for wider wastewater treatment applications, the study advances MXene-based photocatalytic systems as next-generation materials for environmental remediation.

Future Scope

Even though the current study shows that MXene-based and metal-modified MXene composites have good photocatalytic performance for the degradation of pharmaceutical contaminants like cetirizine and ciprofloxacin under visible light, there are still a of research directions that could be pursued.

- To advance this area of research, it will be essential to increase the scientific understanding of MXene photocatalysts and improve their practical applicability. To monitor changes in oxidation states, bonding environments, and surface terminations in modified MXene composites during photocatalysis, additional characterization using X-ray photoelectron spectroscopy XPS is significant.
- In order to customize visible-light absorption, maximize band alignment, and improve interfacial electron transport, future research may investigate hybridization of MXene with other high-performance semiconductors (such as g-C_3N_4, ZnO, Bi-based oxides, and metal sulfides) and newly developed plasmonic or perovskite materials.
- For large-scale production, the development of HF-free, low-temperature, and energy-efficient preparation techniques for MXene and MXene composites such as electrochemical etching, molten salt etching, and sophisticated microwave–hydrothermal hybrid systems would improve sustainability and safety.

Overall, developing MXene-based photocatalysts will necessitate better material stability, a deeper understanding of mechanics, and the building of multifunctional composites that can produce high photocatalytic efficiency under visible light with little chemical assistance. Future developments could turn materials produced from MXene into reliable, scalable, and ecologically friendly photocatalysts for the cleanup of pharmaceutical effluent.

Topics in Catalysis
https://doi.org/10.1007/s11244-025-02214-9

ORIGINAL PAPER

Enhanced Photocatalytic Degradation of Ciprofloxacin from Pharmaceutical Wastewater Using Microwave-Synthesized Lanthanum/MXene Nanocomposites

Upasana Bagri[1] · Saima Jan[1] · Ajit Sharma[1] · Prabal Pratap Singh[2]

Accepted: 11 September 2025

Abstract
The rampant misuse of pharmaceuticals, including ciprofloxacin, has severely harmed ecosystems. Although oxidative degradation of ciprofloxacin shows promise, it often requires substantial energy consumption. Therefore, developing an eco-friendly and efficient degradation method is crucial. This study investigates the degradation of ciprofloxacin using MXene (Ti_3C_2) synthesized via conventional and microwave-assisted (MW) methods. To enhance photocatalytic activity, La/MXene nanocomposites were synthesized using the MW method with three different ratios (1:1, 1:2, and 2:1). Characterization techniques, including FTIR, XRD, SEM, and EDX analysis, confirmed the development of MXene and La/MXene nanocomposites. SEM images revealed lanthanum nanoparticles attached to the surface of MXene layers. The effects of pH, time, and hydrogen peroxide concentration on ciprofloxacin removal were examined. Photocatalytic investigations showed that La/MXene nanocomposites significantly outperformed pure MXene in ciprofloxacin removal. Notably, the La/MXene nanocomposite (1:2) achieved a remarkable removal efficiency of 97.83% within 120 min. Adding 0.05% H_2O_2 further enhanced degradation to 99.05%. The La/MXene nanocomposite demonstrated good recyclability and stability.

✉ Ajit Sharma
ajitsharma2003@gmail.com

[1] Department of Chemistry, School of Chemical Engineering and Physical Sciences, Lovely Professional University, Phagwara, Punjab 144411, India

[2] Department of Chemistry, GLA University, Mathura, UP 281406, India

Published online: 10 October 2025

INTERNATIONAL JOURNAL OF ENVIRONMENTAL ANALYTICAL CHEMISTRY
https://doi.org/10.1080/03067319.2025.2550655

Enhanced visible light photocatalytic degradation of cetirizine in pharmaceutical liquid waste using V_2O_5-modified MXene nanocomposites prepared via microwave irradiation

Upasana Bagri[a], Ashima Thakur[a], Ajit Sharma[a], Dai-Viet N. Vo[b,c] and Prabal Pratap Singh[d]

[a]Department of Chemistry, School of Chemical Engineering and Physical Sciences, Lovely Professional University, Phagwara, India; [b]Institute of Applied Technology and Sustainable Development, Nguyen Tat Thanh University, Ho Chi Minh City, Viet Nam; [c]Graduate School of Energy and Environment, Korea University, Seoul, Republic of Korea; [d]Department of Chemistry, GLA University, Mathura, India

ABSTRACT

The pervasive presence of pharmaceutical pollutants like cetirizine in water sources poses significant environmental concerns due to their persistence and potential ecological impacts. This study investigates the enhanced photocatalytic degradation of cetirizine under visible light irradiation using MXene synthesised via conventional (MX (Con)) and microwave-assisted techniques (MX (MW)), as well as its V_2O_5-modified MXene nanocomposites. MXene was prepared by selectively etching Ti_3AlC_2, while V_2O_5-modified MXene nanocomposites (V/MX) were fabricated using microwave techniques with varying MXene-to-V_2O_5 ratios (1:1, 1:2, and 2:1). The synthesised materials were thoroughly characterised using XRD, FTIR, SEM, EDX, zeta potential, and band gap measurements to examine their surface, morphological, and structural properties. Photocatalytic studies were conducted at different pH values (2, 4, 6, 8 and 10) with a constant cetirizine concentration of 10 ppm to assess degradation efficiency over time. The results indicate that microwave-synthesised MXene exhibits superior photocatalytic activity compared to conventionally prepared MXene, and modification with V_2O_5 further enhances degradation performance. Notably, the microwave-synthesised V_2O_5-modified MXene (V/MX) composite with a 1:2 ratio demonstrates the highest degradation efficiency among the composites. This research highlights the potential of MXene-based photocatalysts for effectively removing pharmaceutical contaminants from wastewater, offering a sustainable approach to environmental remediation.

ARTICLE HISTORY
Received 26 May 2025
Accepted 14 August 2025

KEYWORDS
Photocatalysis; microwave-assisted synthesis; cetirizine; degradation; visible light irradiation; MXene

1. Introduction

Emerging pollutants cause concern are a group of substances that have attracted a lot of interest lately due to their persistence and broad presence in the environment [1]. Cetirizine, an H_1 histamine blocker, is one such newly discovered contaminant. Cetirizine has a poor metabolism and is eliminated from the body in about 80% [2]. Cetirizine has been found in receiving waters, wastewater influent as well as treated

CONTACT Ajit Sharma ajitsharma2003@gmail.com

MXene-Based Two-Dimensional (2D) Hybrid Materials and Their Applications Towards an Environment

Upasana Bagri, Vijaykumar Patel, Ajit Kumar Sharma, Tim Tim Mashangva, Mukesh Kumar, Ashima Thakur, and Harmanjit Singh

Abstract MXenes have obtained noticeable interest cause of their unique features (physical and chemical features). MXenes are considered auspicious applicants considering the resolution of ecological and energy issues because of their distinctive stacked nanostructure, multiple functionalities at the surface, the excess of these compounds on earth, and their appealing optical, electrical, and thermal properties. Due to its large area, flexible chemical composition, and readily modifiable compositions of elements, MXenes need to become a viable choice to enhance photocatalytic efficiency in renewable energy and ecological treatment applications. Cause of their layered nanostructure with an abundance of functionality, they are with outstanding adjustable performance and are simple to mix with other materials, like metallic oxides, polymers, organic hybrids, and carbonaceous materials, to satisfy the demands of high-performance applications. MXenes are excellent catalysts because of their multiple interlayer groups, surface group activities, and adaptable layer spacing. The MXenes family contains more than 30 distinct members, all of which have been investigated and effectively used as catalysts. The fabrication, mechanism at the surface, and uses of MXenes with associated nanocomposites are covered in this chapter. We also discuss MXenes principles and their respective manufacturing methods, such as exfoliation delamination, HF etching, hydrothermal, polymerization, etc., to better understand. MXenes have excelled as photocatalysts for photochemical degradation, carbon dioxide reduction, hydrogen evolution, and nitrogen fixation. Moreover, surface flaws of MXenes offer lots of CO_2 adsorption sites. Also, these materials' superior 2D-nanomaterial structure and fast electron transport pathways contribute to their extremely effective oxidation reaction activity. The effectiveness of heterostructures based on MXene and their nanocomposite photocatalysts for removing organic pollutants is also thoroughly analyzed in

U. Bagri · V. Patel · A. K. Sharma (✉) · T. T. Mashangva · M. Kumar · A. Thakur · H. Singh (✉)
School of Chemical Engineering and Physical Sciences, Lovely Professional University, Jalandhar, Punjab, India
e-mail: ajitsharma2003@gmail.com

H. Singh
e-mail: harmanjit.singh@lpu.co.in

N. Talreja et al. (eds.), *Two-dimensional Hybrid Composites*, Engineering Materials,
https://doi.org/10.1007/978-981-99-8010-9_4

Applied Materials Today 38 (2024) 102163

Contents lists available at ScienceDirect

Applied Materials Today

journal homepage: www.elsevier.com/locate/apmt

Frontiers in MXene research: Pioneering synthesis, unveiled properties, and emerging applications in VOC detection

Tim Tim Mashangva [a], Anshika Goel [a], Upasana Bagri [b], Sangeeta Prasher [c], Ajit Sharma [b,*], Mukesh Kumar [a,*], Pravin Kumar Singh [d,*]

[a] Department of Physics, Lovely Professional University, Phagwara 144411, India
[b] Department of Chemistry, Lovely Professional University, Phagwara 144411, India
[c] Department of Physics, Kanya Maha Vidyalaya, Jalandhar, Punjab 144004, India
[d] Institute of Advanced Materials, IAAM, Gammalkilsvägen 18, Ulrika 590 53, Sweden

ARTICLE INFO

Keywords:
MXene
Synthesis methods
2D materials
VOC sensor
Gas sensitivity
Sensing mechanism
Limit of detection

ABSTRACT

Throughout history, numerous incidents involving harmful gas leaks have been documented, highlighting a clear and pressing vulnerability in safety protocols. These events underscore the critical need for materials capable of proactively detecting dangerous gases before they reach perilous concentrations. With the rapid evolution of technology, the emerging material 'MXene' stands out due to its unique properties, including the presence of abundant and tunable surface functional groups, high conductivity, good stability under a wide range of environmental conditions, exceptional chemical and thermal stability, and a high surface area. These attributes make MXene a promising candidate for advancing gas detection capabilities. This review delves into MXene-based sensors, highlighting their potential to detect various volatile organic gases at very low concentrations, measured in parts per million. To provide a comprehensive overview, we also explore the intricate structure and synthesis methods of MXene, shedding light on its unique properties and operational dynamics. We assess the synergy of MXene with substrates such as metal oxides, conducting polymers, 2D materials, and noble metals, focusing on their enhanced sensitivity, target specificity, and optimal response times. Additionally, we examine the fascinating mechanisms behind MXene's gas-sensing capabilities. Our objective is clear: to pave the way for the development of next-generation gas sensors capable of detecting minute traces of gases down to parts per billion levels under ambient conditions. By achieving this goal, we aim to establish an advanced gas sensor that offers outstanding sensitivity and energy-efficient gas sensing technologies.

1. Introduction

Industrialization and the expansion of human activities release toxic and harmful gases, posing significant threats to both human health and the environment [1,2]. Amongst all the toxic gases, Volatile organic compounds (VOCs) that are commonly used as a solvent in the industry are a large contribution to the threat. It is a vital hazardous air pollutant usually found in the environment because of various industrial and human activities. Some of the identified VOCs found in the exhaled breath are used as an active-biomarkers for early diagnosis of diseases such as lung infection [3], acetone for diagnosing diabetes mellitus [4], toluene used as a biomarker for identifying smokers and non-smokers [5], etc. Methanol, although the fuel is considered to be a proficient option for power generation, on the other hand, it is highly flammable and can undergo slow oxidation and accumulation inside the human body [6]. Formaldehyde, a colourless and odourless gas found in new furniture at a certain concentration can damage our eyes [7]. Ammonia is an air pollutant largely produced from chemical industries combustion, automobiles, agriculture, and livestock farming [8]. It is also used as an active biomarker for clinical diagnoses such as kidney disorders and as an indicator to monitor spoiled food [9]. Developing a VOC gas sensor is needed not only for the purpose of environmental and industrial safety but also to diagnose diseases. Thus, it is essential to develop a gas sensor that is of low production cost, high selectivity, and chemical stability, small dimension, room temperature (RT) operating device and has the potential to integrate with various circuit technologies for identifying and quantifying the toxic and harmful gases to monitor the air quality, human health, and industrial safety. The source, type, and a

* Corresponding authors.
E-mail addresses: ajitsharma2003@gmail.com (A. Sharma), moka.esh9@gmail.com (M. Kumar), pravin.singh@iaam.se (P.K. Singh).

https://doi.org/10.1016/j.apmt.2024.102163
Received 14 December 2023; Received in revised form 6 March 2024; Accepted 10 March 2024
Available online 23 March 2024

Chemical Physics Impact 9 (2024) 100751

Contents lists available at ScienceDirect

Chemical Physics Impact

journal homepage: www.sciencedirect.com/journal/chemical-physics-impact

Visible light-induced continuous process for photodegradation of chlorpyrifos using g-C_3N_4/GO/La_2O_3 photocatalyst from agricultural aquatic waste

Sahima Tabasum [a,b], Ajit Sharma [b,c,*], Nandini Dhupar [b], Upasana Bagri [b], Souheen Yousuf [b], Vibha Kumar [d], Atheesha Singh [e], Sudheesh K. Shukla [b,c,f]

[a] Department of Chemistry, School of Climate Change and Sustainability, Institution of Eminence, University of Delhi, Delhi, India
[b] Department of Chemistry, School of Chemical Engineering and Physical Sciences, Lovely Professional University, Phagwara, Punjab, 144411, India
[c] Centre for Nanoscience and Nano Biotechnics, School of Chemical Engineering and Physical Sciences, Lovely Professional University, Phagwara, Punjab, 144411, India
[d] Department of Chemistry, PLMS Campus, Sri Dev Suman Uttarakhand University, UK, 249199, India
[e] Water and Health Research Centre, Faculty of Health Sciences, University of Johannesburg, Doornfontein, 2028, South Africa
[f] Department of Chemical Sciences, University of Johannesburg, Doornfontein Campus, P.O. Box 17011, Johannesburg, 2028, South Africa

ARTICLE INFO

Keywords:
Photocatalyst
Chlorpyrifos
Visible light
Continuous process
Lanthanum oxide

ABSTRACT

The widespread use of pesticides and the formation of by-products on the gradual decomposition of these pesticides have led to environmental pollution, which in turn has caused harm to both human and ecosystem health. Pesticides have been found in water bodies worldwide and are a cause of concern. Photocatalytic reactions have received significant attention in the past few decades for the breakdown of pesticides. Different parameters were studied, including the effects of pH, kinetics, dose, and regeneration. The UV–vis spectroscopy results suggest that the g-C_3N_4/GO/La_2O_3 nanocomposite is a superior reusable photocatalyst for the degradation of chlorpyrifos (CPF) compared to pure g-C_3N_4 and GO/ g-C_3N_4. This is demonstrated by the fact that the g-C_3N_4/GO/La_2O_3 nanocomposite outperforms both of these materials. The increased photocatalytic performance may be attributed to a balance between the band gap, morphology, crystalline quality, and surface area, all of which may be slowing down the electron-hole recombination rates. This may be due to the enhanced photocatalytic performance. In addition, the feasible processes were outlined from radical quenching studies, and the results clearly indicate that the presence of more OH radicals plays an essential role in the process of efficient photodegradation using novel g-C_3N_4/GO/La_2O_3 nanocomposites.

1. Introduction

A substantial increase in pesticide use has been observed in recent years [1–2]. The main reason for this surge is the increased need to safeguard crops, fruits, vegetables, cereal, pasture, and fiber against harmful pests. Due to their solubility or miscibility in water, most pesticides tend to leach from the soil and accumulate in groundwater, resulting in a substantial concentration of these chemicals [3]. According to Saw et al. [4], pesticides are the second-largest contaminants found in drinking water sources. Even though they are present at low concentrations, many concentrations of these pesticides have been shown to create mutations in DNA cells, which can ultimately lead to cancer. Furthermore, these pesticides have been shown to cause damage to the neurological and endocrine systems of the human body.

Organophosphate pesticides, such as Chlorpyrifos (CPF), are used in agriculture for crops, including cotton, maize, and fruit trees. They have also been applied to wood in large quantities to prevent termites. Chlorpyrifos is one of the most commonly used pesticides, not only for crops but also for household purposes to kill insects and mites. According to several studies, agricultural fields are the most significant contributor to water pollution. In these areas, pesticides are used to keep pest populations under control for crops such as cotton, vegetables, and other horticultural commodities [5]. Lakes in the state of Karnataka, India were found to have extremely high levels of CPF pollution in water [6–7]. As a direct consequence, CPF is present in high concentrations in the runoff from agricultural land and urban streams [8, 9]. Chlorpyrifos,

* Corresponding author.
E-mail address: ajitsharma0003@gmail.com (A. Sharma).

https://doi.org/10.1016/j.chphi.2024.100751
Received 29 June 2024; Received in revised form 15 September 2024; Accepted 1 October 2024
Available online 2 October 2024

Topics in Catalysis (2024) 67:725–736
https://doi.org/10.1007/s11244-023-01865-w

ORIGINAL PAPER

Efficient Photocatalytic Degradation of Chlorpyrifos Pesticide from Aquatic Agricultural Waste Using g-C_3N_4 Decorated Graphene Oxide/V_2O_5 Nanocomposite

Sahima Tabasum[1] · Suman Rani[1] · Ajit Sharma[1,2] · Nandini Dhupar[1] · Prabal Pratap Singh[3] · Upasana Bagri[1] · Deepak Kumar[1]

Accepted: 22 August 2023 / Published online: 16 September 2023

Abstract
In the present work, graphitic carbon nitride/GO/V_2O_5 nanocomposite was synthesized via a single stage and utilized this photocatalyst for the degradation of the pesticide Chlorpyrifos. The nanocomposite was prepared using the hydrothermal method. The crystal structure was determined using powder X-ray diffraction of ternary nanocomposite material crystallite size, phase, and defects. Scanning electron microscopy (SEM) and FT-IR evaluated surface morphologies and functional groups. FTIR heterocycle C–N and C=N stretching modes due to bands of 1200–1650 cm^{-1} During the course of the experiment, the impacts of the experimental parameters (such as pH, time, H_2O_2 concentration, and Catalyst Dose) on the degradation of Chlorpyrifos were investigated. The photocatalytic studies indicated that the graphitic carbon nitride/GO/V_2O_5 composites significantly outperformed the pure versions of g-C_3N_4 in photocatalytic degradation of Chlorpyrifos. The excellent photocatalytic removal efficiency of more than 88% in 120 min obtained using a graphitic carbon nitride/GO/V_2O_5 catalyst pointed toward a great alternative catalyst for the treatment of Chlorpyrifos and other hazardous pesticides from wastewater. By using 0.1% H_2O_2, the photocatalytic elimination of Chlorpyrifos was further increased from 88 to 90.5%. The g-C_3N_4/GO/V_2O_5 catalyst has outstanding recycling performance and a high level of stability.

Keywords Photo-catalyst · Mineralization · g-C_3N_4 · Pesticide · Aquatic

1 Introduction

Pesticides are synthetic compounds or mixtures that are intended to prevent, eliminate, or manage pests such as disease vectors, unwanted plant and animal species, and animals that cause damage during the manufacturing, storage, distribution, transportation, or sale of food or agricultural farming produce [1].

Pesticides containing organophosphorus are widely used across the world. These insecticides are commonly used in agriculture to boost yields and satisfy nutritional requirements. Carbon, nitrogen, oxygen, and sulphur are also bonded to a central phosphorus atom in organophosphorus insecticides. Organophosphorus insecticides have also attracted attention because of their great efficacy and limited stability [2]. Besides their increasing worldwide utilization, water pollution arising from these agro-pesticides is one of the most pressing environmental concerns due to their potential toxicity and bioaccumulation [3]. Pesticide residue is ubiquitous in stream, river, and groundwater sources, and their presence corresponds to the region's geographic and seasonal insecticide consumption trends [4].

They get into water supplies through a variety of routes, including industrial effluent, agricultural runoff, and chemical usage. Pesticide concentrations in drinking water are capped at 0.1 µg/l by the European economic community.

✉ Ajit Sharma
ajitsharma2003@gmail.com

✉ Deepak Kumar
deepak.sharma99967@gmail.com

[1] Department of Chemistry, School of Chemical Engineering and Physical Sciences, Lovely Professional University, Jalandhar, Punjab 144001, India

[2] Institute of Advanced Materials, IAAM, Gammalkilsvägen 18, 590 53 Ulrika, Sweden

[3] Department of Chemistry, GLA University, Mathura, UP 281406, India

CHAPTER FOUR

Hydrogen production scale-up

Vijaykumar Patel[1,2], Rajesh K. Sani[1], Ajit Kumar Sharma[2], Upasana Bagri[2]

[1]Department of Chemical and Biological Engineering, South Dakota School of Mines and Technology, Rapid City, SD, United States
[2]School of Chemical Engineering and Physical Science, Lovely Professional University, Phagwara, Punjab, India

4.1 Introduction

The rise in global energy consumption is concerning, with its negative effects on both energy reserves and the environment. The limited and unsustainable nature of fossil fuels makes them a risky energy source. Because of this, there has been a rise in demand for alternatives that are better for the environment. Over the course of millions of years, the decomposition of dead animals and plants results in the formation of fossil fuels such as oil, coal, and natural gas. The world uses over 11 billion tons of oil each year as a fossil fuel. It is important to keep in mind that the global population is increasing; thus, our consumption of oil is also increasing. As a result, there is a chance that we might run out of oil reserves by the year 2052. If we only rely on natural gas and coal, all fossil fuels might be depleted by 2088. While fossil fuels are essential for powering our homes, vehicles, and electricity production, it is important to note that the process of burning them releases carbon dioxide into the atmosphere. This contributes to 65% of greenhouse gases that cause global warming. It is important to recognize the impact of our actions as we continue to burn fossil fuels. The rise in heat-trapping gases is a cause for concern, especially as the levels of atmospheric carbon dioxide have reached their highest point in 3 million years. Considering the disruptive effects of mining techniques on surrounding ecosystems is crucial. The consequences can be severe, including surface failures and wilted vegetation, as well as the diversion of natural water sources and the endangerment of dependent life forms in underground mining tunnels. Let us strive to be mindful of our impact on the environment and work toward sustainable solutions for the benefit of all living beings.

Renewable Hydrogen
ISBN: 978-0-323-95379-5
https://doi.org/10.1016/B978-0-323-95379-5.00002-X

Chapter 4

Metal Carbides and Metal Nitrides Composites for Supercapacitor Applications

Anuj Garg,[1] Tim Tim Mashangva,[1] Upasna Bagri,[2] Ajit Sharma,[2] Deepak Kumar,*[,2] and Mukesh Kumar*[,1]

[1]Department of Physics and Chemistry, Lovely Professional University, Phagwara 144411, India

[2]Department of Chemistry, Lovely Professional University, Phagwara 144411, India

***Email: deepak.sharma99967@gmail.com (D.K.)**

***Email: mukesh.kumar@lpu.co.in (M.K.)**

Supercapacitors have shown a great futuristic opportunity in energy storage devices and can have various applications in multiple fields. Increased efficiency and energy storage technologies have been the subject of extensive research. MXene has high conductivity, excellent chemical reactivity, mechanical properties/flexibility, chemical stability and various other properties making it a suitable candidate for supercapacitor applications. MXene has shown pseudocapacitance which is thermodynamically stable and has faradaic reactions. It has been also observed that MXene has a layered structure and its composites with carbon or polymers to fabricate a hybrid supercapacitor. Various MXene composites have been synthesized and they have achieved a high capacitance with various other properties such as cyclicity and retentivity.

Introduction

For energy extraction, nonrenewable energy sources have been our only source from the beginning of the modern age and it's been depleting at an exponential rate now. So, renewable energy sources are gaining popularity as a more eco-friendly approach. Still, the lack of all-time accessibility and variation in user energy intake is a disadvantage for them. That's why storing energy and using it in a time of need has a lot of applications and scientists are showing interest in them. The increase in population, heavy machinery, and the popularity of wireless devices also require new energy storage methods. As the need for renewable energy is increasing, the necessity for electrochemical energy storage devices has been established (*1*, *2*).

Mahapatra and Singh; Age of MXenes, Volume 3. Applications in Energy Storage: Batteries and Supercapacitors
ACS Symposium Series; American Chemical Society: Washington, DC, 0.

RESEARCH ARTICLE | SEPTEMBER 08 2023

Photo-catalytic detoxification of chlorpyrifos pesticide from the aquatic environment using g-C_3N_4 doped with GO nano-composite

Sahima Tabasum; Suman Rani; Ashima Thakur; Monika Sindhu; Karan Singh Maan; Upasana; Vijay Patel; Sarika; Azad Qayoom Malik; Pratima Gajbhiye; Deepak Kumar; Ajit Kumar Sharma

+ Author & Article Information

AIP Conf. Proc. 2800, 020079 (2023)

https://doi.org/10.1063/5.0163717

Chlorpyrifos insecticide is one of the most extensively used organophosphorus pesticides due to its low cost and excellent performance in controlling pests in agriculture fields and gardens. The presence of pesticides in the aquatic environment produces a slew of issues for both humans and ecosystems. The purpose of this research is to assess the photocatalytic detoxification of chlorpyrifos in wastewater utilizing g-C_3N_4/GO nanoparticles. The g-C_3N_4/GO nanoparticles were successfully synthesized by using calcinations and hydrothermal methods. Additionally, the photocatalytic detoxification of chlorpyrifos was examined by optimizing several parameters such as catalyst type, irradiation period, catalyst concentrations, and pH. The photocatalytic efficiency of g-C_3N_4/GO nanoparticles was determined by using a UV–visible spectrophotometer. According to the findings of this study, the photo detoxification effectiveness of chlorpyrifos pesticides rises with increasing illumination time, and detoxification of chlorpyrifos by using a photo-catalyst was strongly influenced by the operational parameters.

RESEARCH ARTICLE | SEPTEMBER 08 2023

Synthesis and characteristic study of La/ZnO nanocomposites via hydrothermal route for pesticide degradation from agriculture aquatic waste

Suman Rani; Sahima Tabasum; Ashima Thakur; Rohit Patra; Monika Sindhu; Karan Singh Maan; Upasana; Pratima Gajbhiye; Deepak Kumar; Ajit Kumar Sharma

+ Author & Article Information

AIP Conf. Proc. 2800, 020179 (2023)

https://doi.org/10.1063/5.0164232

In the agriculture field, the production yield is often less than the farmer's expected value because a few parts of the crops are damaged by pests and insects. Chemical pesticides have wide applications in the agriculture field. Through the agricultural run-off, these pesticides contaminate the water sources. So, there is a need for highly efficient La-doped ZnO photocatalytic material for pesticide degradation. Photocatalytic material was synthesized via a hydrothermal route. Zn $(NO)_3.6H_2O$ and La $(NO_3)_3.6HM_2O$ was used as zinc and lanthanum precursor in ethanol. Surface Morphology and dopant composition were analyzed by SEM-EDX images which confirmed the hybrid of the metal doping process.

References

1) Tara, N., Siddiqui, S. I., Rathi, G., Chaudhry, S. A., Inamuddin, & Asiri, A. M. (2020). Nano-engineered adsorbent for the removal of dyes from water: A review. *Current Analytical Chemistry*, *16*(1), 14-40.

2) Nidheesh, P. V., Zhou, M., & Oturan, M. A. (2018). An overview on the removal of synthetic dyes from water by electrochemical advanced oxidation processes. *Chemosphere*, *197*, 210-227.

3) Rosegrant, M. W., & Cline, S. A. (2003). Global food security: challenges and policies. *Science*, *302*(5652), 1917-1919.

4) Lapworth, D. J., Baran, N., Stuart, M. E., & Ward, R. S. (2012). Emerging organic contaminants in groundwater: a review of sources, fate and occurrence. *Environmental pollution*, *163*, 287-303.

5) Abdel-Shafy, H. I., & Aly, R. O. (2002). Water issue in Egypt: Resources, pollution and protection endeavors. *Central European Journal of Occupational and Environmental Medicine*, *8*(1), 3-21.

6) Wang, Q., & Yang, Z. (2016). Industrial water pollution, water environment treatment, and health risks in China. *Environmental pollution*, *218*, 358-365.

7) Kurunthachalam, S. K. (2013). *Indian waters: past and Present. Hydrol Current Res S 10: 001*.

8) Kant, A. (2021). *Composite Water Management Index (CWMI). NITI Aayog*.

9) Shogren, J. (2013). *Encyclopedia of energy, natural resource, and environmental economics*. Newnes.

10) Wilkinson, J. L., Boxall, A. B., Kolpin, D. W., Leung, K. M., Lai, R. W., Galbán-Malagón, C., ... & Teta, C. (2022). Pharmaceutical pollution of the world's rivers. *Proceedings of the National Academy of Sciences*, *119*(8), e2113947119.

11) Chen, L., Wang, L., Wu, X., & Ding, X. (2017). A process-level water conservation and pollution control performance evaluation tool of cleaner production technology in textile industry. *Journal of cleaner production*, *143*, 1137-1143.

12) Uhlenbrook, S. (2019). The United Nations world water development report 2019: leaving no one behind.

13) Martin, J. M., Saaristo, M., Bertram, M. G., Lewis, P. J., Coggan, T. L., Clarke, B. O., & Wong, B. B. (2017). The psychoactive pollutant fluoxetine compromises antipredator behaviour in fish. *Environmental Pollution*, *222*, 592-599.

14) Ankley, G. T., Brooks, B. W., Huggett, D. B., & Sumpter, A. J. P. (2007). Repeating history: pharmaceuticals in the environment.

15) Murray-Smith, R. J., Coombe, V. T., Grönlund, M. H., Waern, F., & Baird, J. A. (2012). Managing emissions of active pharmaceutical ingredients from manufacturing facilities: an environmental quality standard approach. *Integrated environmental assessment and management*, *8*(2), 320-330.

16) Karthikeyan, K. G., & Meyer, M. T. (2006). Occurrence of antibiotics in wastewater treatment facilities in Wisconsin, USA. *Science of the total environment*, *361*(1-3), 196-207.

17) Carvalho, I. T., & Santos, L. (2016). Antibiotics in the aquatic environments: a review of the European scenario. *Environment international*, *94*, 736-757.

18) Cleuvers, M. (2004). Mixture toxicity of the anti-inflammatory drugs diclofenac, ibuprofen, naproxen, and acetylsalicylic acid. *Ecotoxicology and environmental safety*, *59*(3), 309-315.

19) Daughton, C. G., & Ternes, T. A. (1999). Pharmaceuticals and personal care products in the environment: agents of subtle change?. *Environmental health perspectives*, *107*(suppl 6), 907-938.
20) Zwiener, C., & Frimmel, F. H. (2003). Short-term tests with a pilot sewage plant and biofilm reactors for the biological degradation of the pharmaceutical compounds clofibric acid, ibuprofen, and diclofenac. *Science of the Total Environment*, *309*(1-3), 201-211.
21) Heberer, T. (2002). Tracking persistent pharmaceutical residues from municipal sewage to drinking water. *Journal of hydrology*, *266*(3-4), 175-189.
22) Wilkinson, J. L., Boxall, A. B., Kolpin, D. W., Leung, K. M., Lai, R. W., Galbán-Malagón, C., ... & Teta, C. (2022). Pharmaceutical pollution of the world's rivers. *Proceedings of the National Academy of Sciences*, *119*(8), e2113947119.
23) Escudero, J., Muñoz, J. L., Morera-Herreras, T., Hernandez, R., Medrano, J., Domingo-Echaburu, S., ... & Lertxundi, U. (2021). Antipsychotics as environmental pollutants: An underrated threat?. *Science of the Total Environment*, *769*, 144634.
24) Sawant, S. A., Patankar, U. R., Kasale, A. S., & Tawade, S. S. (2021). Pharmaceutical pollution: impact on environmental sustainability and management. *World J. Pharm. Res*, *10*(11), 694-719.
25) Kümmerer, K. (2010). Pharmaceuticals in the environment. *Annual review of environment and resources*, *35*(1), 57-75.
26) Sumpter, J. P. (1995). Feminized responses in fish to environmental estrogens. *Toxicology letters*, *82*, 737-742.
27) Organisation for Economic Co-Operation and Development (OECD). (2020). *Pharmaceutical Residues in Freshwater: Hazards and Policy Responses*. IWA Publishing.
28) Yadav, A., Rene, E. R., Mandal, M. K., & Dubey, K. K. (2021). Threat and sustainable technological solution for antineoplastic drugs pollution: Review on a persisting global issue. *Chemosphere*, *263*, 128285.
29) Pereira, A., Silva, L., Laranjeiro, C., & Pena, A. (2021). Assessment of human pharmaceuticals in drinking water catchments, tap and drinking fountain waters. *Applied Sciences*, *11*(15), 7062.
30) Halling-Sørensen, B. N. N. S., Nielsen, S. N., Lanzky, P. F., Ingerslev, F., Lützhøft, H. H., & Jørgensen, S. E. (1998). Occurrence, fate and effects of pharmaceutical substances in the environment-A review. *Chemosphere*, *36*(2), 357-393.
31) Talib, A., & Randhir, T. O. (2016). Managing emerging contaminants: status, impacts, and watershed-wide strategies. *Exposure and Health*, *8*(1), 143-158.
32) Du, J., Huang, W., Pan, Y., Xu, S., Li, H., & Liu, Q. (2024). Fluoroquinolone antibiotics in the aquatic environment: environmental distribution, the research status and eco-toxicity. *Drug and Chemical Toxicology*, *47*(6), 1325-1340.
33) Segura, P. A., François, M., Gagnon, C., & Sauvé, S. (2009). Review of the occurrence of anti-infectives in contaminated wastewaters and natural and drinking waters. *Environmental health perspectives*, *117*(5), 675-684.
34) Aus der Beek, T., Weber, F. A., Bergmann, A., Hickmann, S., Ebert, I., Hein, A., & Küster, A. (2016). Pharmaceuticals in the environment—Global occurrences and perspectives. *Environmental toxicology and chemistry*, *35*(4), 823-835.

35) Kümmerer, K. (2009). The presence of pharmaceuticals in the environment due to human use–present knowledge and future challenges. *Journal of environmental management*, *90*(8), 2354-2366.
36) Nikolaou, A., Meric, S., & Fatta, D. (2007). Occurrence patterns of pharmaceuticals in water and wastewater environments. *Analytical and bioanalytical chemistry*, *387*(4), 1225-1234.
37) Rizzo, L., Manaia, C., Merlin, C., Schwartz, T., Dagot, C., Ploy, M. C., ... & Fatta-Kassinos, D. (2013). Urban wastewater treatment plants as hotspots for antibiotic resistant bacteria and genes spread into the environment: a review. *Science of the total environment*, *447*, 345-360.
38) Zhao, L.; Ji, Y.; Yao, J.; Long, S.; Li, D.; Yang, Y. Quantifying the fate and risk assessment of different antibiotics during wastewater treatment using a Monte Carlo simulation. J. Clean. Prod. 2017, 168, 626–631.
39) He, F.; Cai, W.; Lin, J.; Yu, B.; Owens, G.; Chen, Z. Reducing the impact of antibiotics in wastewaters: Increased removal of mitoxantrone from wastewater by biosynthesized manganese nanoparticles. J. Clean. Prod. 2021, 293, 126207.
40) Lu, D.; Xu, S.; Ma, J. Adsorption and desorption behaviors of antibiotic CIP on functionalized spherical MCM-41 for water treatment. J. Clean. Prod. 2020, 264, 121644.
41) Hu, Y.; Shen, Y.; Wang, J. Pretreatment of antibiotic fermentation residues by combined ultrasound and alkali for enhancing biohydrogen production. J. Clean. Prod. 2020, 268, 122190.
42) Singh, R.; Singh, A.P.; Kumar, S.; Giri, B.S.; Kim, K.-H. Antibiotic resistance in major rivers in the world: A systematic review on occurrence, emergence, and management strategies. J. Clean. Prod. 2019, 234, 1484–1505.
43) Xu, R.; Zhang, Y.; Xiong, W.; Sun, W.; Fan, Q.; Yang, Z. Metagenomic approach reveals the fate of antibiotic resistance genes in a temperature-raising anaerobic digester treating municipal sewage sludge. J. Clean. Prod. 2020, 277, 123504.
44) Nannapaneni, R.; Story, R.; Wiggins, K.C.; Johnson, M.G. Concurrent Quantitation of Total Campylobacter and Total CiprofloxacinResistant Campylobacter Loads in Rinses from Retail Raw Chicken Carcasses from 2001 to 2003 by Direct Plating at 42 ◦C. Appl. Environ. Microbiol. 2005, 71, 4510–4515.
45) Wang, C.; Gao, S.; Zhu, J.; Xia, X.; Wang, M.; Xiong, Y. Enhanced activation of peroxydisulfate by strontium modified BiFeO3perovskite for ciprofloxacin degradation. J. Environ. Sci. 2021, 99, 249–259.
46) Giri, A.S.; Golder, A.K. Ciprofloxacin degradation in photo-Fenton and photo-catalytic processes: Degradation mechanisms and iron chelation. J. Environ. Sci. 2019, 80, 82–92.
47) Cai, Y.; He, J. Degradation of ciprofloxacin by the Mn cycle system (MnCS): Construction, characterization and bacterial analysis. Environ. Res. 2021, 195, 110860.
48) Carabineiro, S.; Thavorn-Amornsri, T.; Pereira, M.; Figueiredo, J. Adsorption of ciprofloxacin on surface-modified carbon materials. Water Res. 2011, 45, 4583–4591.
49) Fick, J., Söderström, H., Lindberg, R. H., Phan, C., Tysklind, M., & Larsson, D. J. (2009). Contamination of surface, ground, and drinking water from pharmaceutical production. *Environmental Toxicology and Chemistry*, *28*(12), 2522-2527.

50) Richardson, S. D. (2008). Environmental mass spectrometry: emerging contaminants and current issues. *Analytical chemistry*, *80*(12), 4373-4402.
51) Strolin Benedetti, M., Plisnier, M., Kaise, J., Maier, L., Baltes, E., Arendt, C., & McCracken, N. (2001). Absorption, distribution, metabolism and excretion of [14C] levocetirizine, the R enantiomer of cetirizine, in healthy volunteers. *European journal of clinical pharmacology*, *57*(8), 571-582.
52) Kosonen, J., & Kronberg, L. (2009). The occurrence of antihistamines in sewage waters and in recipient rivers. *Environmental Science and Pollution Research*, *16*(5), 555-564.
53) A. Bahlmanna, J.J. Carvalhoa, M.G. Wellera, U. Panneb, R.J. Schneidera, Immunoassays as high-throughput tools: monitoring spatial and temporal variations of carbamazepine, caffeine and cetirizine in surface and wastewaters, Chemosphere 89 (11) (2012) 1278–1286.
54) C. Harman, M. Reid, K.V. Thomas, In situ calibration of a passive sampling device for selected illicit drugs and their metabolites in wastewater, and subsequent year-long assessment of community drug usage, Environ. Sci. Technol. 45 (2011) 5676–5682.
55) E. Souri, A. Hatami, N.S. Ravari, F. Alvandifar, M.B. Tehrani, Validating a stability indicating HPLC method for kinetic study of Cetirizine degradation in acidic and oxidative conditions, Iran. J. Pharm. Res. 12 (2) (2013) 287–294
56) Parfitt, K., & Martindale, W. (1999). The complete drug reference. *Pharmaceutical Press, London*, *31*, 51.
57) Tzanetos, D. B., Fahrenholz, J. M., Scott, T., & Buchholz, K. (2011). Comparison of the sedating effects of levocetirizine and cetirizine: a randomized, double-blind, placebo-controlled trial. *Annals of Allergy, Asthma & Immunology*, *107*(6), 517-522.
58) Yamaguchi, T., Hashizume, T., Matsuda, M., Sakashita, M., Fujii, T., Sekine, Y., ... & Uematsu, T. (1994). Pharmacokinetics of the H1-receptor antagonist ebastine and its active metabolite carebastine in healthy subjects. *Arzneimittel-forschung*, *44*(1), 59-64.
59) Oluwole, A. O., Omotola, E. O., & Olatunji, O. S. (2020). Pharmaceuticals and personal care products in water and wastewater: a review of treatment processes and use of photocatalyst immobilized on functionalized carbon in AOP degradation. *BMC chemistry*, *14*(1), 62.
60) Wang, K., Zhuang, T., Su, Z., Chi, M., & Wang, H. (2021). Antibiotic residues in wastewaters from sewage treatment plants and pharmaceutical industries: Occurrence, removal and environmental impacts. *Science of the Total Environment*, *788*, 147811.
61) Ashton, D., Hilton, M., & Thomas, K. V. (2004). Investigating the environmental transport of human pharmaceuticals to streams in the United Kingdom. *Science of the total environment*, *333*(1-3), 167-184.
62) Boxall, A. B., Collins, R., Wilkinson, J. L., Swan, C., Bouzas-Monroy, A., Jones, J., ... & Pearson, C. (2024). Pharmaceutical pollution of the English national parks. *Environmental Toxicology and Chemistry*, *43*(11), 2422-2435.
63) Burch, K. D., Han, B., Pichtel, J., & Zubkov, T. (2019). Removal efficiency of commonly prescribed antibiotics via tertiary wastewater treatment. *Environmental Science and Pollution Research*, *26*(7), 6301-6310.

64) Shamshad, J., & Rehman, R. U. (2025). Innovative approaches to sustainable wastewater treatment: a comprehensive exploration of conventional and emerging technologies. *Environmental Science: Advances*.
65) Patel, M., Kumar, R., Kishor, K., Mlsna, T., Pittman Jr, C. U., & Mohan, D. (2019). Pharmaceuticals of emerging concern in aquatic systems: chemistry, occurrence, effects, and removal methods. *Chemical reviews*, *119*(6), 3510-3673.
66) Ngqwala, N. P., & Muchesa, P. (2020). Occurrence of pharmaceuticals in aquatic environments: A review and potential impacts in South Africa. *South African Journal of Science*, *116*(7-8), 1-7.
67) Walters, E., McClellan, K., & Halden, R. U. (2010). Occurrence and loss over three years of 72 pharmaceuticals and personal care products from biosolids–soil mixtures in outdoor mesocosms. *Water research*, *44*(20), 6011-6020.
68) Lam, M. W., Young, C. J., Brain, R. A., Johnson, D. J., Hanson, M. A., Wilson, C. J., ... & Mabury, S. A. (2004). Aquatic persistence of eight pharmaceuticals in a microcosm study. *Environmental toxicology and chemistry*, *23*(6), 1431-1440.
69) Janecko, N., Pokludova, L., Blahova, J., Svobodova, Z., & Literak, I. (2016). Implications of fluoroquinolone contamination for the aquatic environment—A review. *Environmental Toxicology and Chemistry*, *35*(11), 2647-2656.
70) Aziz, K. H. H., Mustafa, F. S., Karim, M. A., & Hama, S. (2025). Pharmaceutical pollution in the aquatic environment: advanced oxidation processes as efficient treatment approaches: a review. *Materials Advances*.
71) You, J., Guo, Y., Guo, R., & Liu, X. (2019). A review of visible light-active photocatalysts for water disinfection: Features and prospects. *Chemical engineering journal*, *373*, 624-641.
72) Liu, Q., & Wu, L. Z. (2017). Recent advances in visible-light-driven organic reactions. *National Science Review*, *4*(3), 359-380.
73) Nosaka, Y., & Nosaka, A. Y. (2017). Generation and detection of reactive oxygen species in photocatalysis. *Chemical reviews*, *117*(17), 11302-11336.
74) Hu, C., Huang, H., Chen, F., Zhang, Y., Yu, H., & Ma, T. (2020). Coupling piezocatalysis and photocatalysis in Bi4NbO8X (X= Cl, Br) polar single crystals. *Advanced Functional Materials*, *30*(7), 1908168.
75) Zhang, P., Wang, T., Chang, X., & Gong, J. (2016). Effective charge carrier utilization in photocatalytic conversions. *Accounts of chemical research*, *49*(5), 911-921.
76) Dabrowska, D., Kot-Wasik, A., & Namieśnik, J. (2005). Pathways and analytical tools in degradation studies of organic pollutants. *Critical Reviews in Analytical Chemistry*, *35*(2), 155-176.
77) Clifford, D., Subramonian, S., & Sorg, T. J. (1986). Water treatment processes. III. Removing dissolved inorganic contaminants from water. *Environmental science & technology*, *20*(11), 1072-1080.
78) Kusumlata, Ambade, B., Kumar, A., & Gautam, S. (2024). Sustainable solutions: reviewing the future of textile dye contaminant removal with emerging biological treatments. *Limnological Review*, *24*(2), 126-149.
79) Oturan, M. A., & Aaron, J. J. (2014). Advanced oxidation processes in water/wastewater treatment: principles and applications. A review. *Critical reviews in environmental science and technology*, *44*(23), 2577-2641.

80) Tong, H., Ouyang, S., Bi, Y., Umezawa, N., Oshikiri, M., & Ye, J. (2012). Nano-photocatalytic materials: possibilities and challenges. *Advanced materials*, *24*(2), 229-251.
81) Klementova, S., Kahoun, D., Doubkova, L., Frejlachova, K., Dusakova, M., & Zlamal, M. (2017). Catalytic photodegradation of pharmaceuticals–homogeneous and heterogeneous photocatalysis. *Photochemical & Photobiological Sciences*, *16*(1), 67-71.
82) Akpotu, S. O., Oseghe, E. O., Ayanda, O. S., Skelton, A. A., Msagati, T. A., & Ofomaja, A. E. (2019). Photocatalysis and biodegradation of pharmaceuticals in wastewater: effect of abiotic and biotic factors. *Clean Technologies and Environmental Policy*, *21*(9), 1701-1721.
83) Kudo, A., & Miseki, Y. (2009). Heterogeneous photocatalyst materials for water splitting. *Chemical Society Reviews*, *38*(1), 253-278.
84) Khan, M. M., Adil, S. F., & Al-Mayouf, A. (2015). Metal oxides as photocatalysts. *Journal of Saudi chemical society*, *19*(5), 462-464.
85) Zhang, H., Chen, G., & Bahnemann, D. W. (2009). Photoelectrocatalytic materials for environmental applications. *Journal of Materials Chemistry*, *19*(29), 5089-5121.
86) Huang, X., Yin, Z., Wu, S., Qi, X., He, Q., Zhang, Q., ... & Zhang, H. (2011). Graphene-based materials: synthesis, characterization, properties, and applications. *small*, *7*(14), 1876-1902.
87) Chakraborty, T. (2010). Graphene, Nobel Prize and all that jazz. *arXiv preprint arXiv:1011.0444*.
88) Lazăr, A. I., Aghasoleimani, K., Semertsidou, A., Vyas, J., Roșca, A. L., Ficai, D., & Ficai, A. (2023). Graphene-related nanomaterials for biomedical applications. *Nanomaterials*, *13*(6), 1092.
89) Bhimanapati, G. R., Lin, Z., Meunier, V., Jung, Y., Cha, J., Das, S., ... & Robinson, J. A. (2015). Recent advances in two-dimensional materials beyond graphene. *ACS nano*, *9*(12), 11509-11539.
90) Anasori, B., & Gogotsi, Y. (2019). Introduction to 2D transition metal carbides and nitrides (MXenes). In *2D Metal Carbides and Nitrides (MXenes) Structure, Properties and Applications* (pp. 3-12). Cham: Springer International Publishing.
91) Barsoum, M. W., & Radovic, M. (2011). Elastic and mechanical properties of the MAX phases. *Annual review of materials research*, *41*(1), 195-227.
92) Zhang, X., Xu, J., Wang, H., Zhang, J., Yan, H., Pan, B., ... & Xie, Y. (2013). Ultrathin nanosheets of MAX phases with enhanced thermal and mechanical properties in polymeric compositions: Ti3Si0. 75Al0. 25C2. *Angewandte Chemie*, *125*(16), 4457-4461.
93) Higashi, M., Momono, S., Kishida, K., Okamoto, N. L., & Inui, H. (2018). Anisotropic plastic deformation of single crystals of the MAX phase compound Ti3SiC2 investigated by micropillar compression. *Acta Materialia*, *161*, 161-170.
94) Naguib, M., Mashtalir, O., Carle, J., Presser, V., Lu, J., Hultman, L., ... & Barsoum, M. W. (2012). Two-dimensional transition metal carbides. *ACS nano*, *6*(2), 1322-1331.
95) Ganesan, S., Padmapriya, G., Omoikhoje, I., Tharudini, J., & De Zoysa, S. (2023). *Biochar: its characteristics application and utilization of on environment. Basic Sci Sustain Dev 2: 115–124*.

96) Liu, W. J., Jiang, H., & Yu, H. Q. (2015). Development of biochar-based functional materials: toward a sustainable platform carbon material. *Chemical reviews*, *115*(22), 12251-12285.
97) Wan, Y. C., Chen, Y., Cui, Z. X., Ding, H., Gao, S. F., Han, Z., & Gao, J. K. (2019). A promising form-stable phase change material prepared using cost effective pinecone biochar as the matrix of palmitic acid for thermal energy storage. *Scientific Reports*, *9*(1), 11535.
98) De Jesús Báez, L. R., Rosas, A. S., Mahale, P., & Mallouk, T. E. (2023). Chelation-based route to aluminum-free layered transition metal carbides (MXenes). *ACS omega*, *8*(44), 41969-41976.
99) Zeng, M., Chen, Y., Zhang, E., Li, J., Mendes, R. G., Sang, X., ... & Fu, L. (2019). Molecular scaffold growth of two-dimensional, strong interlayer-bonding-layered materials. *CCS Chemistry*, *1*(1), 117-127.
100) Amani, A. M., Vafa, E., Mirzae, M., Abbasi, M., Vaez, A., Najdian, A., ... & Guaman, L. P. (2025). Mxenes as a versatile nanoplatform: synthesis and emerging biomedical applications. *Journal of Industrial and Engineering Chemistry*, *149*, 275-312.
101) Hantanasirisakul, K., & Gogotsi, Y. (2023). Electronic and optical properties of 2D transition metal carbides and nitrides (MXenes). *MXenes*, 135-205.
102) Qamar, M. A., & Ali, S. K. (2025). Functionalized MXenes for Enhanced Visible-Light Photocatalysis: A Focus on Surface Termination Engineering and Composite Design. *Inorganics*, *13*(2), 45.
103) Teja, Y. N., & Sakar, M. (2023). Comprehensive Insights into the Family of Atomically Thin 2D-Materials for Diverse Photocatalytic Applications. *Small*, *19*(46), 2303980.
104) Sun, M., Chu, S., Sun, Z., Jiao, X., Wang, L., Li, Z., & Jiang, L. (2024). A review of etching methods and applications of two-dimensional MXenes. *Nanotechnology*, *35*(38), 382003.
105) Naguib, M., Kurtoglu, M., Presser, V., Lu, J., Niu, J., Heon, M., ... & Barsoum, M. W. (2023). Two-dimensional nanocrystals produced by exfoliation of Ti3AlC2. In *MXenes* (pp. 15-29). Jenny Stanford Publishing.
106) Wu, Q., Xue, Y., Chao, S., Wu, F., Li, L., Javed, M. S., & Zhang, W. (2022). Moiré superlattice mxene nanosheets constructed from twisted hexagon-Ti3AlC2 by microwave-assisted lewis molten salt etching: implications for structural stability in electrochemical energy storage. *ACS Applied Nano Materials*, *6*(1), 677-684.
107) Murali, G., Reddy Modigunta, J. K., Park, Y. H., Lee, J. H., Rawal, J., Lee, S. Y., ... & Park, S. J. (2022). A review on MXene synthesis, stability, and photocatalytic applications. *ACS nano*, *16*(9), 13370-13429.
108) Mahabari, K., Mohili, R. D., Patel, M., Jadhav, A. H., Lee, K., & Chaudhari, N. K. (2024). HF-free microwave-assisted synthesis of MXene as an electrocatalyst for hydrogen evolution in alkaline media. *Nanoscale Advances*, *6*(21), 5388-5397.
109) Zhan, X., Si, C., Zhou, J., & Sun, Z. (2020). MXene and MXene-based composites: synthesis, properties and environment-related applications. *Nanoscale Horizons*, *5*(2), 235-258.
110) Hai, N. T. T., Tu, V. V., Long, P. H., Hien, D. T., Huong, N. T. T., Quynh, P. H., ... & Thang, P. Q. (2023). Improvement of photocatalytic degradation and

adsorption of ciprofloxacin by bismuth oxyiodide. *Chemical Engineering & Technology*, *46*(11), 2404-2411.
111) Iravani, S., & Varma, R. S. (2022). MXene-based photocatalysts in degradation of organic and pharmaceutical pollutants. *Molecules*, *27*(20), 6939.
112) Munien, C., Tetteh, E. K., & Rathilall, S. (2025). Assessing the efficacy of semiconductor photocatalysts by utilizing photocatalytic parameters for wastewater treatment–a kinetic study. *Water Practice & Technology*, *20*(8), 1681-1703.
113) Centers for Disease Control and Prevention (CDC. (1999). Control of infectious diseases. *MMWR. Morbidity and mortality weekly report*, *48*(29), 621-629.
114) World Health Organization. (2023). *Noncommunicable diseases and mental health in small island developing states*. World Health Organization.
115) Size, P. M. (2024). Share & Industry Analysis. *By Component, By Enterprise Type, By Application, By Vertical, and Regional Forecast*, *2032*.
116) Aitken, M., & Kleinrock, M. (2021). The Global Use of Medicines 2022: Outlook to 2026. *IQVIA Institute Report*.
117) Indicators, O. E. C. D. (2023, November). *Health at a Glance 2023*.
118) Verlicchi, P., Al Aukidy, M., & Zambello, E. (2012). Occurrence of pharmaceutical compounds in urban wastewater: removal, mass load and environmental risk after a secondary treatment—a review. *Science of the total environment*, *429*, 123-155.
119) Ashiwaju, B. I., Uzougbo, C. G., & Orikpete, O. F. (2023). Environmental impact of pharmaceuticals: A comprehensive review. *Matrix Science Pharma*, *7*(3), 85-94.
120) Oaks, J. L., Gilbert, M., Virani, M. Z., Watson, R. T., Meteyer, C. U., Rideout, B. A., ... & Ahmed Khan, A. (2004). Diclofenac residues as the cause of vulture population decline in Pakistan. *Nature*, *427*(6975), 630-633.
121) Yang, C., Tan, Q., Li, Q., Zhou, J., Fan, J., Li, B., ... & Lv, K. (2020). 2D/2D Ti3C2 MXene/g-C3N4 nanosheets heterojunction for high efficient CO2 reduction photocatalyst: Dual effects of urea. *Applied Catalysis B: Environmental*, *268*, 118738.
122) Zuccato, E., Calamari, D., Natangelo, M., & Fanelli, R. (2000). Presence of therapeutic drugs in the environment. *The lancet*, *355*(9217), 1789-1790.
123) Gauba, P., & Saxena, A. (2023). Ciprofloxacin properties, impacts, and remediation. *CABI Reviews*, (2023).
124) Lübbert, C., Baars, C., Dayakar, A., Lippmann, N., Rodloff, A. C., Kinzig, M., & Sörgel, F. (2017). Environmental pollution with antimicrobial agents from bulk drug manufacturing industries in Hyderabad, South India, is associated with dissemination of extended-spectrum beta-lactamase and carbapenemase-producing pathogens. *Infection*, *45*(4), 479-491.
125) Almeida, Â., Calisto, V., Esteves, V. I., Schneider, R. J., Soares, A. M., Figueira, E., & Freitas, R. (2017). Ecotoxicity of the antihistaminic drug cetirizine to Ruditapes philippinarum clams. *Science of the Total Environment*, *601*, 793-801.
126) Kumar, D., & James, T. C. (2021). *Pharmaceutical Trade: India's Growth Trajectories*. RIS, Research and Information System for Developing Countries.
127) Klein, E. Y., Van Boeckel, T. P., Martinez, E. M., Pant, S., Gandra, S., Levin, S. A., ... & Laxminarayan, R. (2018). Global increase and geographic convergence in antibiotic consumption between 2000 and 2015. *Proceedings of the National Academy of Sciences*, *115*(15), E3463-E3470.

128) Cherian, J. J., Rahi, M., Singh, S., Reddy, S. E., Gupta, Y. K., Katoch, V. M., ... & Bhargava, B. (2021). India's road to independence in manufacturing active pharmaceutical ingredients: focus on essential medicines. *Economies*, *9*(2), 71.
129) Larsson, D. J., de Pedro, C., & Paxeus, N. (2007). Effluent from drug manufactures contains extremely high levels of pharmaceuticals. *Journal of hazardous materials*, *148*(3), 751-755.
130) Fick, J., Söderström, H., Lindberg, R. H., Phan, C., Tysklind, M., & Larsson, D. J. (2009). Contamination of surface, ground, and drinking water from pharmaceutical production. *Environmental Toxicology and Chemistry*, *28*(12), 2522-2527.
131) Laxminarayan, R., & Chaudhury, R. R. (2016). Antibiotic resistance in India: drivers and opportunities for action. *PLoS medicine*, *13*(3), e1001974.
132) Wilkinson, J. L., Boxall, A. B., Kolpin, D. W., Leung, K. M., Lai, R. W., Galbán-Malagón, C., ... & Teta, C. (2022). Pharmaceutical pollution of the world's rivers. *Proceedings of the National Academy of Sciences*, *119*(8), e2113947119.
133) Kotwani, A., & Holloway, K. (2014). Antibiotic prescribing practice for acute, uncomplicated respiratory tract infections in primary care settings in N ew D elhi, I ndia. *Tropical Medicine & International Health*, *19*(7), 761-768.
134) Vora, A., Gupta, A., Ojha, A., Pandey, P., Marwaha, M. S., Kadam, S., & Singh, S. (2021). India's Pharma and Medical Devices Strategies: An Assessment of The Production Linked Incentive (PLI) Scheme. *International Journal of Information Research and Review*, *8*(3), 7208-7219.
135) Ghosh, A. (2020). Prisoners with drug use disorders during covid-19 pandemic: Caught between a rock and a hard place. *Asian journal of psychiatry*, *54*, 102332.
136) Bhattacharya, D. Indian Pharmaceutical Industry and Environmental Sustainability: An Exposition.
137) Hanchang, S. H. I. (2009). Industrial wastewater-types, amounts and effects. *Point sources of pollution: Local effects and their control*, *2*, 191.
138) Mukherjee, J., Lodh, B. K., Sharma, R., Mahata, N., Shah, M. P., Mandal, S., ... & Bhunia, B. (2023). Advanced oxidation process for the treatment of industrial wastewater: A review on strategies, mechanisms, bottlenecks and prospects. *Chemosphere*, *345*, 140473.
139) Patel, M., Kumar, R., Kishor, K., Mlsna, T., Pittman Jr, C. U., & Mohan, D. (2019). Pharmaceuticals of emerging concern in aquatic systems: chemistry, occurrence, effects, and removal methods. *Chemical reviews*, *119*(6), 3510-3673.
140) Daughton, C. G., & Ternes, T. A. (1999). Pharmaceuticals and personal care products in the environment: agents of subtle change?. *Environmental health perspectives*, *107*(suppl 6), 907-938.
141) Connor, R., United Nations Economic and Social Commission for Western Asia, Economic and Social Commission for Asia and the Pacific, & United Nations Economic Commission for Latin America and the Caribbean. (2017). The united nations world water development report 2017. wastewater: the untapped resource.
142) Singh, M. V. P., & Shankar, K. R. (2024). Next-generation hybrid technologies for the treatment of pharmaceutical industry effluents. *Journal of Environmental Management*, *353*, 120197.

143) Luo, Y., Guo, W., Ngo, H. H., Nghiem, L. D., Hai, F. I., Zhang, J., ... & Wang, X. C. (2014). A review on the occurrence of micropollutants in the aquatic environment and their fate and removal during wastewater treatment. *Science of the total environment*, *473*, 619-641.
144) Larsson, D. J., de Pedro, C., & Paxeus, N. (2007). Effluent from drug manufactures contains extremely high levels of pharmaceuticals. *Journal of hazardous materials*, *148*(3), 751-755.
145) Yuan, J., Huang, S., Yuan, H., Fu, F., & Zhang, Y. (2021). Effects of chloramphenicol on the bacterial community structure and simultaneous nitrification and denitrification performance in a sequencing biofilm batch reactor. *Journal of Water Process Engineering*, *42*, 102095.
146) Milić, N., Milanović, M., Letić, N. G., Sekulić, M. T., Radonić, J., Mihajlović, I., & Miloradov, M. V. (2013). Occurrence of antibiotics as emerging contaminant substances in aquatic environment. *International journal of environmental health research*, *23*(4), 296-310.
147) Bhuyan, A., & Ahmaruzzaman, M. (2023). Recent advances in new generation nanocomposite materials for adsorption of pharmaceuticals from aqueous environment. *Environmental Science and Pollution Research*, *30*(14), 39377-39417.
148) Michael, I., Rizzo, L., McArdell, C. S., Manaia, C. M., Merlin, C., Schwartz, T., ... & Fatta-Kassinos, D. J. W. R. (2013). Urban wastewater treatment plants as hotspots for the release of antibiotics in the environment: a review. *Water research*, *47*(3), 957-995.
149) Bhattacharyya, P., Parmar, P. R., Basak, S., Dubey, K. K., Sutradhar, S., Bandyopadhyay, D., & Chakrabarti, S. (2023). Metal organic framework–derived recyclable magnetic coral Co@ Co3O4/C for adsorptive removal of antibiotics from wastewater. *Environmental Science and Pollution Research*, *30*(17), 50520-50536.
150) Serrano, D., Suárez, S., Lema, J. M., & Omil, F. (2011). Removal of persistent pharmaceutical micropollutants from sewage by addition of PAC in a sequential membrane bioreactor. *Water Research*, *45*(16), 5323-5333.
151) Ioannidou, O., & Zabaniotou, A. (2007). Agricultural residues as precursors for activated carbon production—A review. *Renewable and sustainable energy reviews*, *11*(9), 1966-2005.
152) Rivera-Utrilla, J., Prados-Joya, G., Sánchez-Polo, M., Ferro-García, M. A., & Bautista-Toledo, I. (2009). Removal of nitroimidazole antibiotics from aqueous solution by adsorption/bioadsorption on activated carbon. *Journal of hazardous materials*, *170*(1), 298-305.
153) Tsai, Y. L., Chang, P. H., Gao, Z. Y., Xu, X. Y., Chen, Y. H., Wang, Z. H., ... & Jiang, W. T. (2016). Amitriptyline removal using palygorskite clay. *Chemosphere*, *155*, 292-299.
154) Behera, S. K., Oh, S. Y., & Park, H. S. (2012). Sorptive removal of ibuprofen from water using selected soil minerals and activated carbon. *International journal of environmental science and technology*, *9*(1), 85-94.
155) Tzereme, A., Christodoulou, E., Kyzas, G. Z., Kostoglou, M., Bikiaris, D. N., & Lambropoulou, D. A. (2019). Chitosan grafted adsorbents for diclofenac pharmaceutical compound removal from single-component aqueous solutions and mixtures. *Polymers*, *11*(3), 497.

156) Su, R., Zhang, G., Wang, P., Li, S., Ravenelle, R. M., & Crittenden, J. C. (2015). Treatment of antibiotic pharmaceutical wastewater using a rotating biological contactor. *Journal of Chemistry*, *2015*(1), 705275.
157) Hassard, F., Biddle, J., Cartmell, E., Jefferson, B., Tyrrel, S., & Stephenson, T. (2015). Rotating biological contactors for wastewater treatment–a review. *Process Safety and Environmental Protection*, *94*, 285-306.
158) Ryan, C. C., Tan, D. T., & Arnold, W. A. (2011). Direct and indirect photolysis of sulfamethoxazole and trimethoprim in wastewater treatment plant effluent. *Water research*, *45*(3), 1280-1286.
159) Huber, M. M., GÖbel, A., Joss, A., Hermann, N., LÖffler, D., McArdell, C. S., ... & von Gunten, U. (2005). Oxidation of pharmaceuticals during ozonation of municipal wastewater effluents: a pilot study. *Environmental science & technology*, *39*(11), 4290-4299.
160) Ternes, T. A., Stüber, J., Herrmann, N., McDowell, D., Ried, A., Kampmann, M., & Teiser, B. (2003). Ozonation: a tool for removal of pharmaceuticals, contrast media and musk fragrances from wastewater?. *Water research*, *37*(8), 1976-1982.
161) Sardrood, B. P., Goltapeh, E. M., & Varma, A. (2012). An introduction to bioremediation. In *Fungi as bioremediators* (pp. 3-27). Berlin, Heidelberg: Springer Berlin Heidelberg.
162) Shemer, H., Kunukcu, Y. K., & Linden, K. G. (2006). Degradation of the pharmaceutical metronidazole via UV, Fenton and photo-Fenton processes. *Chemosphere*, *63*(2), 269-276.
163) Andreozzi, R., Raffaele, M., & Nicklas, P. (2003). Pharmaceuticals in STP effluents and their solar photodegradation in aquatic environment. *Chemosphere*, *50*(10), 1319-1330.
164) Sharma, M., Mandal, M. K., Pandey, S., Kumar, R., & Dubey, K. K. (2022). Visible-light-driven photocatalytic degradation of tetracycline using heterostructured Cu2O–TiO2 nanotubes, kinetics, and toxicity evaluation of degraded products on cell lines. *ACS omega*, *7*(37), 33572-33586.
165) Brillas, E., Sirés, I., Arias, C., Cabot, P. L., Centellas, F., Rodríguez, R. M., & Garrido, J. A. (2005). Mineralization of paracetamol in aqueous medium by anodic oxidation with a boron-doped diamond electrode. *Chemosphere*, *58*(4), 399-406.
166) Yadav, A., Rene, E. R., Mandal, M. K., & Dubey, K. K. (2022). Biodegradation of cyclophosphamide and etoposide by white rot fungi and their degradation kinetics. *Bioresource Technology*, *346*, 126355.
167) Madukasi, E. I., Dai, X., He, C., & Zhou, J. (2010). Potentials of phototrophic bacteria in treating pharmaceutical wastewater. *International Journal of Environmental Science & Technology*, *7*(1), 165-174.
168) Koopaei, N. N., & Abdollahi, M. (2017). Health risks associated with the pharmaceuticals in wastewater.
169) Lakhani, S., Acharya, D., Sakariya, R., Sharma, D., Patel, P., Shah, M., & Prajapati, M. (2022). A comprehensive study of bioremediation for pharmaceutical wastewater treatment. *Cleaner Chemical Engineering*, *4*, 100073.
170) Azubuike, C. C., Chikere, C. B., & Okpokwasili, G. C. (2016). Bioremediation techniques–classification based on site of application: principles, advantages, limitations and prospects. *World Journal of Microbiology and Biotechnology*, *32*(11), 180.

171) Arijit Nath, A. N., Sudip Chakraborty, S. C., & Chiranjib Bhattacharjee, C. B. (2014). Bioadsorbtion of industrial dyes from aqueous solution onto water hyacinth (Eichornia crassipes): equilibrium, kinetic, and sorption mechanism study.
172) Rivera-Utrilla, J., Sánchez-Polo, M., Ferro-García, M. Á., Prados-Joya, G., & Ocampo-Pérez, R. (2013). Pharmaceuticals as emerging contaminants and their removal from water. A review. *Chemosphere*, *93*(7), 1268-1287.
173) Aus der Beek, T., Weber, F. A., Bergmann, A., Hickmann, S., Ebert, I., Hein, A., & Küster, A. (2016). Pharmaceuticals in the environment—Global occurrences and perspectives. *Environmental toxicology and chemistry*, *35*(4), 823-835.
174) Adetunji, C. O., Michael, O. S., Varma, A., Oloke, J. K., Kadiri, O., Akram, M., ... & Olisaka, F. N. (2022). Recent advances in the application of biotechnology for improving the production of secondary metabolites from quinoa. *Biology and Biotechnology of Quinoa: Super Grain for Food Security*, 373-396.
175) Qu, X., Brame, J., Li, Q., & Alvarez, P. J. (2013). Nanotechnology for a safe and sustainable water supply: enabling integrated water treatment and reuse. *Accounts of chemical research*, *46*(3), 834-843.
176) Zhang, Y., Chen, Y., Wang, C., & Wei, Y. (2014). Immobilization of 5-aminopyridine-2-tetrazole on cross-linked polystyrene for the preparation of a new adsorbent to remove heavy metal ions from aqueous solution. *Journal of Hazardous Materials*, *276*, 129-137.
177) Gligorovski, S., Strekowski, R., Barbati, S., & Vione, D. (2015). Environmental implications of hydroxyl radicals (• OH). *Chemical reviews*, *115*(24), 13051-13092.
178) Barrera-Díaz, C., Canizares, P., Fernández, F. J., Natividad, R., & Rodrigo, M. A. (2014). Electrochemical advanced oxidation processes: an overview of the current applications to actual industrial effluents. *Journal of the Mexican chemical society*, *58*(3), 256-275.
179) Deng, Y., & Zhao, R. (2015). Advanced oxidation processes (AOPs) in wastewater treatment. *Current pollution reports*, *1*(3), 167-176.
180) Kamat, P. V. (2017). A conversation with akira Fujishima. *ACS Energy Letters*, *2*(7), 1586-1587.
181) Herrmann, J. M., & Puzenat, E. (2015). Photocatalytic engineering. *Green Process Engineering: From Concepts to Industrial Applications*, 364.
182) Marcelino, R. B., & Amorim, C. C. (2019). Towards visible-light photocatalysis for environmental applications: band-gap engineering versus photons absorption—a review. *Environmental Science and Pollution Research*, *26*(5), 4155-4170.
183) Guo, K., Wu, Z., Chen, C., & Fang, J. (2022). UV/chlorine process: an efficient advanced oxidation process with multiple radicals and functions in water treatment. *Accounts of Chemical Research*, *55*(3), 286-297.
184) Chang, J. S., & Chong, M. N. (2021). Photoactive nanomaterials: applications in wastewater treatment and their environmental fate. *Heterogeneous Photocatalysis: From Fundamentals to Applications in Energy Conversion and Depollution*, 331-349.
185) Ahmed, S. N., & Haider, W. (2018). Heterogeneous photocatalysis and its potential applications in water and wastewater treatment: a review. *Nanotechnology*, *29*(34), 342001.

186) Saafie, N., Zulfiqar, M., Samsudin, M. F. R., & Sufian, S. (2022). Current scenario of MXene-based nanomaterials for wastewater remediation: a review. *Chemistry*, *4*(4), 1576-1608.
187) Chen, X., Li, C., Grätzel, M., Kostecki, R., & Mao, S. S. (2012). Nanomaterials for renewable energy production and storage. *Chemical Society Reviews*, *41*(23), 7909-7937.
188) Liu, Z., Feng, L., Song, W., Moussavi, G., & Giannakis, S. Multipurpose CeO2-BiFeO3 heterojunction photocatalyst enables synchronous removal of chemical contaminants, antibiotic-resistant bacteria, and resistance genes. *Available at SSRN 5624377*.
189) Wang, Z., Li, C., & Domen, K. (2019). Recent developments in heterogeneous photocatalysts for solar-driven overall water splitting. *Chemical Society Reviews*, *48*(7), 2109-2125.
190) Hagiwara, H., Watanabe, M., Ida, S., & Ishihara, T. (2017). Overall water splitting on dye-modified inorganic semiconductor photocatalysts. *Journal of the Japan Petroleum Institute*, *60*(1), 10-18.
191) Zhao, S., Chen, S., Yu, H., & Quan, X. (2012). g-C3N4/TiO2 hybrid photocatalyst with wide absorption wavelength range and effective photogenerated charge separation. *Separation and Purification Technology*, *99*, 50-54.
192) Johar, M. A., Afzal, R. A., Alazba, A. A., & Manzoor, U. (2015). Photocatalysis and bandgap engineering using ZnO nanocomposites. *Advances in Materials Science and Engineering*, *2015*(1), 934587.
193) Zhu, S., & Wang, D. (2017). Photocatalysis: basic principles, diverse forms of implementations and emerging scientific opportunities. *Advanced Energy Materials*, *7*(23), 1700841.
194) Marschall, R. (2014). Semiconductor composites: strategies for enhancing charge carrier separation to improve photocatalytic activity. *Advanced Functional Materials*, *24*(17), 2421-2440.
195) Dong, H., Chen, G., Sun, J., Feng, Y., Li, C., & Lv, C. (2014). Stability, durability and regeneration ability of a novel Ag-based photocatalyst, Ag 2 Nb 4 O 11. *Chemical Communications*, *50*(50), 6596-6599.
196) Nair, V., Muñoz-Batista, M. J., Fernández-García, M., Luque, R., & Colmenares, J. C. (2019). Thermo-photocatalysis: environmental and energy applications. *ChemSusChem*, *12*(10), 2098-2116.
197) Chong, M. N., Cho, Y. J., Poh, P. E., & Jin, B. (2015). Evaluation of Titanium dioxide photocatalytic technology for the treatment of reactive Black 5 dye in synthetic and real greywater effluents. *Journal of Cleaner Production*, *89*, 196-202.
198) Zou, Y., Li, S., Zheng, D., Feng, J., Wang, S., Hou, Y., & Zhang, G. (2024). Extended light absorption and accelerated charge migration in ultrathin twisted carbon nitride nanoplates for efficient solar hydrogen production. *Science China Chemistry*, *67*(7), 2215-2223.
199) Rekab, K., Lepeytre, C., Dunand, M., Dappozze, F., Herrmann, J. M., & Guillard, C. (2014). H2O2 and/or photocatalysis under UV-C irradiation for the removal of EDTA, a chelating agent present in nuclear waste waters. *Applied Catalysis A: General*, *488*, 103-110.

200) Chen, H. M., Chen, C. K., Liu, R. S., Zhang, L., Zhang, J., & Wilkinson, D. P. (2012). Nano-architecture and material designs for water splitting photoelectrodes. *Chemical Society Reviews*, *41*(17), 5654-5671.
201) Shan, C., Zhang, Y., Zhao, Q., Fu, K., Zheng, Y., Han, R., ... & Liu, Q. (2022). Acid etching-induced in situ growth of λ-MnO2 over CoMn spinel for low-temperature volatile organic compound oxidation. *Environmental Science & Technology*, *56*(14), 10381-10390.
202) Kołodziejczak-Radzimska, A., & Jesionowski, T. (2014). Zinc oxide—from synthesis to application: a review. *Materials*, *7*(4), 2833-2881.
203) Ye, R. P., Lin, L., Li, Q., Zhou, Z., Wang, T., Russell, C. K., ... & Fan, M. (2018). Recent progress in improving the stability of copper-based catalysts for hydrogenation of carbon–oxygen bonds. *Catalysis Science & Technology*, *8*(14), 3428-3449.
204) Su, H., Chen, R., Tang, S., Zheng, X., Li, J., Yin, Z., ... & Dong, N. (2024). Two heads are better than one: A multi-agent system has the potential to improve scientific idea generation.
205) Zhang, L., Chen, Y., Yu, L., Tao, X., Tang, L., Ye, L., ... & Jin, H. (2024). Efficient sulfur atom-doped three-dimensional porous MXene-assisted sodium ion batteries. *Dalton Transactions*, *53*(15), 6583-6591.
206) Li, J., Yin, D., & Qin, Y. (2023). Carbon materials: structures, properties, synthesis and applications. *Manufacturing Review*, *10*, 13.
207) Novoselov, K. S., Fal′ ko, V. I., Colombo, L., Gellert, P. R., Schwab, M. G., & Kim, K. (2012). A roadmap for graphene. *nature*, *490*(7419), 192-200.
208) Naguib, M., Kurtoglu, M., Presser, V., Lu, J., Niu, J., Heon, M., ... & Barsoum, M. W. (2023). Two-dimensional nanocrystals produced by exfoliation of Ti3AlC2. In *MXenes* (pp. 15-29). Jenny Stanford Publishing.
209) Rasool, K., Helal, M., Ali, A., Ren, C. E., Gogotsi, Y., & Mahmoud, K. A. (2016). Antibacterial activity of Ti3C2T x MXene. *ACS nano*, *10*(3), 3674-3684.
210) Yen, J. Z., Chang, C. B., Jhang, K. S., & Tuan, H. Y. (2023). Excellent Metal Phosphide Electrode for Potassium Ion Hybrid Capacitors: The Case of Carbon Nanotube-Wrapped AgP2. *ACS Applied Energy Materials*, *6*(2), 822-831.
211) Silva, D. H., Facure, M. H., Netto, G. B., Correa, D. S., & Siqueira, J. P. (2025, May). Ultrafast terahertz spectroscopy of Ti3C2Tx MXenes with different thickness. In *CLEO: Science and Innovations* (p. JPS100_161). Optica Publishing Group.
212) Gogotsi, Y., & Anasori, B. (2023). The rise of MXenes. In *MXenes* (pp. 3-11). Jenny Stanford Publishing.
213) Pouramini, Z., Mousavi, S. M., Babapoor, A., Hashemi, S. A., Pynadathu Rumjit, N., Garg, S., ... & Chiang, W. H. (2023). Recent advances in MXene-based nanocomposites for wastewater purification and water treatment: a review. *Water*, *15*(7), 1267.
214) Seling, T., Songsart-Power, M., Shringi, A., Paudyal, J., Yan, F., & Limbu, T. B. (2025). $Ti_3C_2T_x$ MXene-Based Hybrid Photocatalysts in Organic Dye Degradation: A Review
215) Tang, Q., Zhou, Z., & Shen, P. (2012). Are MXenes promising anode materials for Li ion batteries? Computational studies on electronic properties and Li storage capability of Ti3C2 and Ti3C2X2 (X= F, OH) monolayer. *Journal of the American Chemical Society*, *134*(40), 16909-16916.

216) Zhao, J., Ali, A. B., Kadhum, A. A. H., Lin, H., Abdelhameed, A. S., Alanazi, A. M., ... & Atamurotov, F. (2025). Boosting photocatalytic H2O2 production and non-biodegradable ofloxacin removal via a novel Ti3C2 MXene nanosheet-supported BiVO4/InVO4 Z-scheme heterojunction: Optimization and mechanism insights. *Journal of Water Process Engineering*, *74*, 107722.
217) Fatima, S., Anwar, M., Almalki, A. S., Alhadhrami, A., Warsi, M. F., & El-Bahy, Z. M. (2024). Fabrication of rare earth (Tb+ 3) and alkaline earth metal (Mg+ 2) Co-doped CdAl2O4@ MXene composite: A unique approach to tune bandgap energy through quantum confinement effect for photocatalytic applications. *Ceramics International*, *50*(17), 29201-29212.
218) Shanmugam, V., Sanjeevamuthu, S., Jeyaperumal, K. S., & Vairamuthu, R. (2019). Fabrication of heterostructured vanadium modified g-C3N4/TiO2 hybrid photocatalyst for improved photocatalytic performance under visible light exposure and antibacterial activities. *Journal of Industrial and Engineering Chemistry*, *76*, 318-332.
219) Chen, L. X., Chen, Z. W., Jiang, M., Lu, Z., Gao, C., Cai, G., & Singh, C. V. (2021). Insights on the dual role of two-dimensional materials as catalysts and supports for energy and environmental catalysis. *Journal of Materials Chemistry A*, *9*(4), 2018-2042.
220) Ghidiu, M., Lukatskaya, M. R., Zhao, M. Q., Gogotsi, Y., & Barsoum, M. W. (2023). Conductive two-dimensional titanium carbide 'clay'with high volumetric capacitance. In *MXenes* (pp. 379-399). Jenny Stanford Publishing.
221) Murali, G., Reddy Modigunta, J. K., Park, Y. H., Lee, J. H., Rawal, J., Lee, S. Y., ... & Park, S. J. (2022). A review on MXene synthesis, stability, and photocatalytic applications. *ACS nano*, *16*(9), 13370-13429.
222) Chen, L., Wakeel, M., Haq, T. U., Chen, C., & Ren, X. (2022). Insight into UV-induced simultaneous photocatalytic degradation of Ti3C2Tx MXene and reduction of U (VI). *Journal of Hazardous Materials*, *430*, 128377.
223) Chen, T., He, P., Liu, T., Zhou, L., Li, M., Yu, K., ... & Zhu, W. (2022). MXene-derived 3D defect-rich TiO2@ Reduced graphene oxide aerogel with ultrafast carrier separation for photo-assisted uranium extraction: a combined batch, X-ray absorption spectroscopy, and density functional theory calculations. *Inorganic Chemistry*, *61*(32), 12759-12771.
224) Ramesh, G. V., Reddy, N. M., Prasad, M. D., Saritha, D., & Ramesh, K. (2021). 2D Nanomaterials for Photocatalysis and Photoelectrocatalysis. *2D Functional Nanomaterials: Synthesis, Characterization and Applications*, 383-411.
225) Xia, F., Lao, J., Yu, R., Sang, X., Luo, J., Li, Y., & Wu, J. (2019). Ambient oxidation of Ti 3 C 2 MXene initialized by atomic defects. *Nanoscale*, *11*(48), 23330-23337.
226) Huyan, W., Yao, J., Tao, J., Yang, F., Tao, X., Yao, Z., ... & Jiao, Z. (2022). MXene@ C heterogeneous nanocomposites with the 2D-0D structure for ultra-light and broadband electromagnetic wave absorption. *Carbon*, *197*, 444-454.
227) Gao, Y., Liu, Y., & Zou, D. (2023). Microwave-assisted synthesis and environmental remediation: a review. *Environmental Chemistry Letters*, *21*(4), 2399-2416.

228) Zhan, X., Si, C., Zhou, J., & Sun, Z. (2020). MXene and MXene-based composites: synthesis, properties and environment-related applications. *Nanoscale Horizons*, *5*(2), 235-258.
229) Wei, C., Xi, B., Wang, P., Wang, Z., An, X., Tian, K., ... & Xiong, S. (2023). In Situ Growth Engineering on 2D MXenes for Next-Generation Rechargeable Batteries. *Advanced Energy and Sustainability Research*, *4*(11), 2300103.
230) Malaki, M., & Varma, R. S. (2020). Mechanotribological aspects of MXene-reinforced nanocomposites. *Advanced Materials*, *32*(38), 2003154.
231) Yu, M., Liang, H., Zhan, R., Xu, L., & Niu, J. (2021). Sm-doped g-C3N4/Ti3C2 MXene heterojunction for visible-light photocatalytic degradation of ciprofloxacin. *Chinese Chemical Letters*, *32*(7), 2155-2158.
232) Hannan, F. I., Ayyaz, A., Zhang, N., Chen, W., Zhang, K., Huang, Q., ... & Zhou, W. (2017). Environmental Science. *Science*, *4*(9).
233) Gorrepati, V. (2019). The effect of acetaminophen (analgesic) and diphenhydramine (antihistamine) on nociception response of Caenorhabditis elegans, heart rate of Eisenia fetida, and mortality of both E. fetida and C. elegans. *Journal of the South Carolina Academy of Science*, *16*(2), 3.
234) Majumdar, A., & Pal, A. (2020). Recent advancements in visible-light-assisted photocatalytic removal of aqueous pharmaceutical pollutants. *Clean Technologies and Environmental Policy*, *22*(1), 11-42.
235) Rubesh Ashok Kumar, S. (2025). Semiconductor Metal Oxide Incorporated MXene Nanomaterials for Photocatalytic Application. *Doctoral dissertation,* L*ovely professional university*. http://hdl.handle.net/10603/647762
236) Mashtalir, O., Naguib, M., Mochalin, V. N., Dall'Agnese, Y., Heon, M., Barsoum, M. W., & Gogotsi, Y. (2013). Intercalation and delamination of layered carbides and carbonitrides. *Nature communications*, *4*(1), 1716.
237) Numan, A., Rafique, S., Khalid, M., Zaharin, H. A., Radwan, A., Mokri, N. A., ... & Walvekar, R. (2022). Microwave-assisted rapid MAX phase etching and delamination: A paradigm shift in MXene synthesis. *Materials Chemistry and Physics*, *288*, 126429.
238) Waris, M. H., Muzaffar, N., Mumtaz, M. A., Afzal, A. M., Iqbal, M. W., Mumtaz, S., ... & Munnaf, S. A. (2025). High performance lanthanum-doped nickel cobalt ferrites on titanium carbide MXene electrode material for superior hybrid device and precision creatinine sensing. *Applied Physics A*, *131*(3), 220.
239) Liang, J., Han, Y., Chen, H., Zhang, Y., & Gao, X. (2025). Layered Ti3C2Tx MXene heterostructured with V2O5 nanoparticles for enhanced room temperature ammonia sensing. *Journal of Alloys and Compounds*, *1010*, 177798.
240) Cullity, B. D. (1986). *Elements of X-ray Diffraction*. Hsin Yueh.
241) Smith, A. L. (1979). Applied infrared spectroscopy. Fundamentals, techniques and analytical problem solving. *Applied infrared spectroscopy. Fundamentals*.
242) Griffiths, P. R. (1983). Fourier transform infrared spectrometry. *Science*, *222*(4621), 297-302.
243) Reimer, L. (2000). Scanning electron microscopy: physics of image formation and microanalysis. *Measurement Science and Technology*, *11*(12), 1826-1826.
244) Goldstein, J. I., Newbury, D. E., Michael, J. R., Ritchie, N. W., Scott, J. H. J., & Joy, D. C. (2017). *Scanning electron microscopy and X-ray microanalysis*. springer.

245) Carter, D. B. W. C. B. (2009). *Transmission electron microscopy A textbook for materials science*.
246) Hunter, R. J. (2013). *Zeta potential in colloid science: principles and applications* (Vol. 2). Academic press.
247) Delgado, Á. V., González-Caballero, F., Hunter, R. J., Koopal, L. K., & Lyklema, J. (2007). Measurement and interpretation of electrokinetic phenomena. *Journal of colloid and interface science*, *309*(2), 194-224.
248) Kubelka, P. (1931). Ein beitrag zur optik der farbanstriche. *Z. tech. Phys*, *12*, 593-601.
249) Tauc, J. (1968). Optical properties and electronic structure of amorphous Ge and Si. *Materials research bulletin*, *3*(1), 37-46.
250) Wang, Y., Liu, X. H., Wang, Q., Quick, M., Kovalenko, S. A., Chen, Q. Y., ... & Pinna, N. (2020). Insights into charge transfer at an atomically precise nanocluster/semiconductor interface. *Angewandte Chemie*, *132*(20), 7822-7828.
251) Wang, J. (2008). Electrochemical glucose biosensors. *Chemical reviews*, *108*(2), 814-825.
252) Macdonald, J. R., Johnson, W. B., Raistrick, I. D., Franceschetti, D. R., Wagner, N., McKubre, M. C. H., ... & Eisenberg, R. S. (2018). *Impedance spectroscopy: theory, experiment, and applications* (pp. 424-458). John Wiley & Sons.
253) Bard, A. J., Faulkner, L. R., & White, H. S. (2022). *Electrochemical methods: fundamentals and applications*. John Wiley & Sons.
254) Fujishima, A., & Honda, K. (1972). Electrochemical photolysis of water at a semiconductor electrode. *nature*, *238*(5358), 37-38.
255) Herrmann, J. M. (1999). Heterogeneous photocatalysis: fundamentals and applications to the removal of various types of aqueous pollutants. *Catalysis today*, *53*(1), 115-129.
256) He, S., Chen, Y., Li, X., Zeng, L., & Zhu, M. (2022). Heterogeneous photocatalytic activation of persulfate for the removal of organic contaminants in water: a critical review. *Acs Es&T Engineering*, *2*(4), 527-546.
257) Mod, B., Baskar, A. V., Bahadur, R., Tavakkoli, E., Van Zwieten, L., Singh, G., & Vinu, A. (2024). From cane to nano: advanced nanomaterials derived from sugarcane products with insights into their synthesis and applications. *Science and Technology of Advanced Materials*, *25*(1), 2393568.
258) Kuang, P., Low, J., Cheng, B., Yu, J., & Fan, J. (2020). MXene-based photocatalysts. *Journal of materials science & technology*, *56*, 18-44.
259) Alam, M. S., Chowdhury, M. A., Kowser, M. A., Islam, M. S., Islam, M. M., & Khandaker, T. (2024). Advances of MAX phases: Synthesis, characterizations and challenges. *Engineering Reports*, *6*(8), e12911.
260) Vijayaraghavan, K. (2019). Recent advancements in biochar preparation, feedstocks, modification, characterization and future applications. *Environmental Technology Reviews*, *8*(1), 47-64.
261) Yang, H., Yan, R., Chen, H., Zheng, C., Lee, D. H., & Liang, D. T. (2006). In-depth investigation of biomass pyrolysis based on three major components: hemicellulose, cellulose and lignin. *Energy & fuels*, *20*(1), 388-393.
262) Liu, Y., He, Z., & Uchimiya, M. (2015). Comparison of biochar formation from various agricultural by-products using FTIR spectroscopy. *Modern Applied Science*, *9*(4), 246.

263) Suman, S., Yadav, A. M., Jain, T., & SK, A. A. (2021, May). Study in the changes on the functional groups present in biomass during pyrolysis process. In *IOP Conference Series: Materials Science and Engineering* (Vol. 1146, No. 1, p. 012023). IOP Publishing.
264) Ray, A., Banerjee, A., & Dubey, A. (2020). Characterization of biochars from various agricultural by-products using FTIR spectroscopy, SEM focused with image processing. *International Journal of Agriculture, Environment and Biotechnology*, *13*(4), 423-430.
265) Kumar, H., Patel, M., & Mohan, D. (2019). Simplified batch and fixed-bed design system for efficient and sustainable fluoride removal from water using slow pyrolyzed okra stem and black gram straw biochars. *ACS omega*, *4*(22), 19513-19525.
266) Gezahegn, S. (2020). *Wood and Bamboo Biochars and Their Application in Soils and Biocomposites*. University of Toronto (Canada).
267) Béguerie, T., Weiss-Hortala, E., Lyczko, N., & Nzihou, A. (2023). The mechanisms of calcium-catalyzed graphenization of cellulose and lignin biochars uncovered. *Scientific Reports*, *13*(1), 11390.
268) Zheng, Q. F., Wang, Z. M., Chen, B. G., Liu, G. F., & Zhao, J. (2016). Analysis of XRD Spectral Structure and Carbonization of the Biochar Preparation. *Guang pu xue yu Guang pu fen xi= Guang pu*, *36*(10), 3355-3359.
269) Mobarak, M. B., Pinky, N. S., Mustafi, S., Chowdhury, F., Nahar, A., Akhtar, U. S., ... & Alam, M. A. (2024). Unveiling the reactor effect: a comprehensive characterization of biochar derived from rubber seed shell via pyrolysis and in-house reactor. *RSC advances*, *14*(41), 29848-29859.
270) Keiluweit, M., Nico, P. S., Johnson, M. G., & Kleber, M. (2010). Dynamic molecular structure of plant biomass-derived black carbon (biochar). *Environmental science & technology*, *44*(4), 1247-1253.
271) Li, M., Lu, J., Luo, K., Li, Y., Chang, K., Chen, K., ... & Huang, Q. (2019). Element replacement approach by reaction with Lewis acidic molten salts to synthesize nanolaminated MAX phases and MXenes. *Journal of the American Chemical Society*, *141*(11), 4730-4737.
272) Mahmood, M., Rasheed, A., Ayman, I., Rasheed, T., Munir, S., Ajmal, S., ... & Shahid, M. (2021). Synthesis of ultrathin MnO2 nanowire-intercalated 2D-MXenes for high-performance hybrid supercapacitors. *Energy & Fuels*, *35*(4), 3469-3478.
273) Jin, X., Yue, S., Zhang, J., Qian, L., & Guo, X. (2024). Three-dimensional vanadium and nitrogen dual-doped Ti3C2 film with ultra-high specific capacitance and high volumetric energy density for zinc-ion hybrid capacitors. *Nanomaterials*, *14*(6), 490.
274) Liu, M., Su, B., Tang, Y., Jiang, X., & Yu, A. (2017). Recent advances in nanostructured vanadium oxides and composites for energy conversion. *Advanced Energy Materials*, *7*(23), 1700885.
275) Raj, S. M. M., Sundramoorthy, A. K., Atchudan, R., Ganapathy, D., & Khosla, A. (2022). recent trends on the synthesis and different characterization tools for MXenes and their emerging applications. *Journal of the Electrochemical Society*, *169*(7), 077501.
276) Shao, H., Luo, S., Descamps-Mandine, A., Ge, K., Lin, Z., Taberna, P. L., ... & Simon, P. (2023). Synthesis of MAX phase nanofibers and nanoflakes and the resulting MXenes. *Advanced Science*, *10*(1), 2205509.

277) Kalyva, M. (2017). Fate of pharmaceuticals in the environment-A review.
278) Martínez, C., Fernández, M. I., Santaballa, J. A., & Faria, J. (2011). *Applied Catalysis B: Environmental*, *107*(1-2), 110-118.
279) Haddad, F. A., Moussavi, G., & Moradi, M. (2019). *Journal of water process engineering*, *27*, 120-125.
280) Song, Z., Dong, X., Wang, N., Zhu, L., Luo, Z., Fang, J., & Xiong, C. (2017). *Chemical Engineering Journal*, *317*, 925-934.
281) Zhang, X., Jia, X., Xu, R., Lu, X., Liu, H., & Niu, Y. (2022). *Journal of Alloys*
282) Gao, L., Li, C., Huang, W., Mei, S., Lin, H., Ou, Q., ... & Zhang, H. (2020). *Chemistry of Materials*, *32*(5), 1703-1747.
283) Ihsanullah, I. (2022). *Journal of Environmental Chemical Engineering*, *10*(3), 107381.
284) Akbari, M., Rasouli, J., Rasouli, K., Ghaedi, S., Mohammadi, M., Rajabi, H., & Sabbaghi, S. (2024). MXene-based composite photocatalysts for efficient degradation of antibiotics in wastewater. *Scientific reports*, *14*(1), 31498.
285) Gandara, M., Palley, B. F., Rakočević, L., Mladenovic, D., Popovic-Bijelic, A., Sljukic, B., & Gonçalves, E. S. (2024). Electrochemical Performance of Niobium MXenes with Lanthanum. *ACS applied materials & interfaces*, *16*(39), 52277-52289.
286) Chen, F. F., & Zhu, Y. J. (2024). Highly Efficient Rapid Preparation of Inorganic Nanostructured Materials by Microwave Heating.
287) Yao, Y., Chen, C., & Bi, X. (2019). Preparation of Zn-Eu Co-doped TiO2 Photocatalyst by Microwave Hydrothermal Method and Its Photocatalytic Activity.
288) Machado, A. E. H., Santos, L. D., Borges, K. A., Batista, P. S., Paiva, V. A. B., Müller Jr, P. S., ... & França, M. D. (2012). Potential applications for solar photocatalysis: from environmental remediation to energy conversion. *Solar radiation*, *19*, 339-378.
289) Sun, S., Wang, M., Chang, X., Jiang, Y., Zhang, D., Wang, D., ... & Lei, Y. (2020). *Sensors and Actuators B: Chemical*, *304*, 127274.
290) Numan, A., Rafique, S., Khalid, M., Zaharin, H. A., Radwan, A., Mokri, N. A., ... & Walvekar, R. (2022). *Materials Chemistry and Physics*, *288*, 126429.
291) Shameem, A., Devendran, P., Murugan, A., Siva, V., & Bahadur, S. A. (2023). *Journal of Physics and Chemistry of Solids*, *179*, 111392.
292) Barakat, M. A., Schaeffer, H., Hayes, G., & Ismat-Shah, S. (2005). *Applied Catalysis B: Environmental*, *57*(1), 23-30.
293) Numan, A., Rafique, S., Khalid, M., Zaharin, H. A., Radwan, A., Mokri, N. A., ... & Walvekar, R. (2022). *Materials Chemistry and Physics*, *288*, 126429.
294) Munir, S., Rasheed, A., Rasheed, T., Ayman, I., Ajmal, S., Rehman, A., ... & Warsi, M. F. (2020). *ACS omega*, *5*(41), 26845-26854.
295) Ghidiu, M., Lukatskaya, M. R., Zhao, M. Q., Gogotsi, Y., & Barsoum, M. W. (2014). *Nature*, *516*(7529), 78-81.
296) Wang, X., & Zhou, Y. (2002). *Journal of Materials Chemistry*, *12*(3), 455-460.
297) Khan, J., Ahmad, R. T. M., Yu, Q., Liu, H., Khan, U., & Liu, B. (2023). *Science and Technology of Advanced Materials*, *24*(1), 2242262.
298) Iqbal, M., Fatheema, J., Noor, Q., Rani, M., Mumtaz, M., Zheng, R. K., ... & Rizwan, S. (2020). *Materials Today Chemistry*, *16*, 100271.
299) Shi, C., Beidaghi, M., Naguib, M., Mashtalir, O., Gogotsi, Y., & Billinge, S. J. (2014). *Physical review letters*, *112*(12), 125501.

300) Alhabeb, M., Maleski, K., Anasori, B., Lelyukh, P., Clark, L., Sin, S., & Gogotsi, Y. (2017). *Chemistry of Materials*, *29*(18), 7633-7644.
301) Naguib, M., Mochalin, V. N., Barsoum, M. W., & Gogotsi, Y. (2014). *Advanced materials*, *26*(7), 992-1005.
302) Barsoum, M. W. (2000). *Progress in solid state chemistry*, *28*(1-4), 201-281.
303) Majhi, S. M., Ali, A., Greish, Y. E., El-Maghraby, H. F., & Mahmoud, S. T. (2023). *Scientific reports*, *13*(1), 3114.
304) Spiridon, I., Teaca, C. A., & Bodirlau, R. (2011). *BioResources*, *6*(1), 400-413.
305) Zhang, R. Z., Cui, H. L., & Li, X. H. (2019). *Physica B: Condensed Matter*, *561*, 90-96.
306) Yu, Y., Sun, H., Lu, Q., Sun, J., Zhang, P., Zeng, L., ... & Liu, P. (2023). *Journal of Nanobiotechnology*, *21*(1), 193.
307) Feng, Y., Zhang, M., Yan, H., Zhang, Y., Guo, R., & Wang, H. (2022). *Ceramics International*, *48*(7), 9518-9526.
308) Sun, L., Li, M., Gu, J., Li, Y., Liu, J., Li, Y., & Li, M. (2023). *Chemical Engineering Journal*, *469*, 144014.
309) Shafique, R., Rani, M., Batool, K., Alothman, A. A., Mushab, M. S. S., Shah, A. A., ... & Arshad, M. (2023). *journal of materials research and technology*, *24*, 2668-2677.
310) Pogorielov, M., Smyrnova, K., Kyrylenko, S., Gogotsi, O., Zahorodna, V., & Pogrebnjak, A. (2021). *Nanomaterials*, *11*(12), 3412.
311) Zhang, H., Xu, P., Du, G., Chen, Z., Oh, K., Pan, D., & Jiao, Z. (2011). *Nano Research*, *4*, 274-283.
312) Lokhande, P. E., Rednam, U., Kadam, V., Jagtap, C., Kumar, D., & Aepuru, R. (2025). Microwave assisted synthesis of Ti 3 C 2-MXene for supercapacitor application. *Chemical Communications*, *61*(10), 2111-2114.
313) Nandiyanto, A. B. D., Ragadhita, R., & Fiandini, M. (2023). *Indonesian Journal of Science and Technology*, *8*(1), 113-126.
314) Klug, H. P., & Alexander, L. E. (1974). *X-Ray Diffraction Procedure for Polycrystalline and Amorphous Materials*.
315) Usman, M. R., Prasasti, A., Islamiah, S., Firdaus, A. N., Marita, A. W., Fajriyah, S., & Yanti, E. F. (2020). *Jurnal Kimia Valensi*, *6*(1), 82-89.
316) Budarz, J. F., Cooper, E. M., Gardner, C., Hodzic, E., Ferguson, P. L., Gunsch, C. K., & Wiesner, M. R. (2019). *Journal of hazardous materials*, *372*, 61-68.
317) Krishnasamy Lakshmi, K. L., Krishna Kadirvelu, K. K., & Mohan, P. S. (2019).
318) Farhadian, M., & Kazemzad, M. (2016). Photocatalytic degradation of malachite green by magnetic photocatalyst. *Synthesis and Reactivity in Inorganic, Metal-Organic, and Nano-Metal Chemistry*, *46*(3), 458-463.
319) Ayu, D. G., Gea, S., Andriayani, Telaumbanua, D. J., Piliang, A. F. R., Harahap, M., ... & Tok, A. I. Y. (2023). Photocatalytic degradation of methylene blue using N-doped ZnO/carbon dot (N-ZnO/CD) nanocomposites derived from organic soybean. *ACS omega*, *8*(17), 14965-14984.
320) Sayed, M., Khan, J. A., Shah, L. A., Shah, N. S., Shah, F., Khan, H. M., ... & Arandiyan, H. (2018). Solar light responsive poly (vinyl alcohol)-assisted hydrothermal synthesis of immobilized TiO2/Ti film with the addition of

peroxymonosulfate for photocatalytic degradation of ciprofloxacin in aqueous media: a mechanistic approach. *The Journal of Physical Chemistry C*, *122*(1), 406-421.
321) Marschall, R. (2014). Semiconductor composites: strategies for enhancing charge carrier separation to improve photocatalytic activity. *Advanced Functional Materials*, *24*(17), 2421-2440.
322) Peng, J., Chen, X., Ong, W. J., Zhao, X., & Li, N. (2019). Surface and heterointerface engineering of 2D MXenes and their nanocomposites: insights into electro-and photocatalysis. *Chem*, *5*(1), 18-50.
323) Batterjee, M. G., Nabi, A., Kamli, M. R., Alzahrani, K. A., Danish, E. Y., & Malik, M. A. (2022). Green hydrothermal synthesis of zinc oxide nanoparticles for UV-light-induced photocatalytic degradation of ciprofloxacin antibiotic in an aqueous environment. *Catalysts*, *12*(11), 1347.
324) Siddique, I. M. (2024). Exploring functional groups and molecular structures: a comprehensive analysis using FTIR spectroscopy. *development*, *1*(2).
325) Tan, H. L., Abdi, F. F., & Ng, Y. H. (2019). *Chemical Society Reviews*, *48*(5), 1255-1271.
326) Sarma, B., Deb, S. K., & Sarma, B. K. (2016, October). In *Journal of physics: conference series* (Vol. 765, No. 1, p. 012023). IOP Publishing.
327) Liqiang, J., Yichun, Q., Baiqi, W., Shudan, L., Baojiang, J., Libin, Y., ... & Jiazhong, S. (2006). *Solar Energy Materials and Solar Cells*, *90*(12), 1773-1787.
328) Metcalfe, C. D. (2013). *Environmental Toxicology & Chemistry*, *32*(8).
329) Strolin Benedetti, M., Plisnier, M., Kaise, J., Maier, L., Baltes, E., Arendt, C., & McCracken, N. (2001). *European journal of clinical pharmacology*, *57*, 571-582.
330) Lu, D., Zhao, B., Fang, P., Zhai, S., Li, D., Chen, Z., ... & Qi, N. (2015). *Applied Surface Science*, *359*, 435-448.
331) Mane, A. A., & Moholkar, A. V. (2017). *Applied Surface Science*, *416*, 511-520.
332) Jayaraj, S. K., Sadishkumar, V., Arun, T., & Thangadurai, P. (2018). *Materials Science in Semiconductor Processing*, *85*, 122-133.
333) Tahir, T., Chaudhary, K., Warsi, M. F., Saif, M. S., Alsafari, I. A., Shakir, I., ... & Zulfiqar, S. (2022). *Ceramics International*, *48*(2), 1969-1980.
334) Zhang, T., Pan, L., Tang, H., Du, F., Guo, Y., Qiu, T., & Yang, J. (2017). *Journal of alloys and compounds*, *695*, 818-826
335) Numan, A., Rafique, S., Khalid, M., Zaharin, H. A., Radwan, A., Mokri, N. A., ... & Walvekar, R. (2022). *Materials Chemistry and Physics*, *288*, 126429.
336) Wu, Q., Wang, Y., Li, P., Chen, S., & Wu, F. (2021). *Applied Physics A*, *127*, 1-11.
337) Vlăduț, C. M., Mocioiu, O. C., Preda, S., Pandele-Cusu, J., Bratan, V., Trusca, R., & Zaharescu, M. (2022). *Gels*, *8*(12), 811.
338) Satishkumar, P., Isloor, A. M., Rao, L. N., & Farnood, R. (2024). *ACS omega*, *9*(24), 25766-25778.
339) Ahmad, H., Kahar, N. A., Ramli, R., Yusoff, N., Reduan, S. A., Ismail, M. F., ... & Yasin, M. (2021). *Optical Fiber Technology*, *67*, 102683.
340) Sui, J., Chen, X., Li, Y., Peng, W., Zhang, F., & Fan, X. (2021). *RSC advances*, *11*(26), 16065-16082.

341) Feng, Y. P., Shen, L., Yang, M., Wang, A., Zeng, M., Wu, Q., ... & Chang, C. R. (2017). *Wiley Interdisciplinary Reviews: Computational Molecular Science*, *7*(5), e1313.
342) Rozmysłowska, A., Wojciechowski, T., Ziemkowska, W., Chlubny, L., Olszyna, A., Poźniak, S., ... & Jastrzębska, A. M. (2018). *International Journal of Electrochemical Science*, *13*(11), 10837-10847
343) Chand, H., Sharma, M., & Krishnan, V. (2022). *Separation and Purification Technology*, *292*, 121032.
344) Nasikhudin, Diantoro, M., Kusumaatmaja, A., & Triyana, K. (2018, April). In *Journal of Physics: Conference Series* (Vol. 1011, p. 012069). IOP Publishing.
345) Ye, Y., Steigerwald, J. M., Bang, H., Jones, V., Dennehy, K., & Ray, J. R. (2023). *Journal of Materials Chemistry A*, *11*(31), 16803-16814.
346) Tahir, T., Alhashmialameer, D., Zulfiqar, S., Atia, A. M., Warsi, M. F., Chaudhary, K., & El Refay, H. M. (2022). *Ceramics International*, *48*(17), 24840-24849.
347) Sijuade, A. A., Eze, V. O., Arnett, N. Y., & Okoli, O. I. (2023). *Nanotechnology*, *34*(25), 252001.
348) Cao, K., Ge, X., Li, S., Tian, Z., Cui, S., Guo, G., ... & Li, W. (2025). *RSC advances*, *15*(22), 17089-17101.
349) Li, J., Ju, X., Feng, X., Zhang, Y., Huang, G., Ma, D., ... & Shi, J. W. (2025). *Journal of Colloid and Interface Science*, *690*, 137284.
350) Du, H., Zhang, A., Zhang, Q., Sun, Y., Zhu, H., Wang, H., ... & Chen, G. (2025). *Separation and Purification Technology*, *359*, 130597.
351) Khan, S. S., Steffy, J. P., Alfagham, A. T., & Elgorban, A. M. (2025). *Journal of Water Process Engineering*, *71*, 107174.
352) Sre, V. V., Okla, M. K., Janani, B., Abdel-Maksoud, M. A., Al-Amri, S. S., Alaraidh, I. A., ... & Khan, S. S. (2024). *Journal of Water Process Engineering*, *59*, 104957.
353) Xu, R., Xue, Z., Yang, D., Li, X., Nie, H., Guo, Y., ... & Gu, J. (2025). *Advanced Functional Materials*, 2423205.
354) Tian, G., Li, Z., Liao, D., Zhang, C., Peng, H. J., Liu, X., ... & Wei, F. (2025). *Nature Sustainability*, 1-12.
355) Steffy, J. P., Syed, A., Kamaraj, C., Naveenkumar, S., Thomas, A. M., Elgorban, A. M., ... & Khan, S. S. (2025). *Sustainable Materials and Technologies*, *43*, e01185.
356) Jiteshwaran, T., Steffy, J. P., Janani, B., Syed, A., Elgorban, A. M., Abid, I., ... & Khan, S. S. (2025). *Journal of Water Process Engineering*, *71*, 107336.
357) Yang, C., Yao, Q., Li, L., Xiao, X., Lu, L., Liu, C., ... & Yuan, H. (2025). *Applied Catalysis B: Environment and Energy*, *366*, 125056.
358) Pagliara, A., Testa, B., Carrupt, P. A., Jolliet, P., Morin, C., Morin, D., ... & Rihoux, J. P. (1998). *Journal of medicinal chemistry*, *41*(6), 853-863.
359) Hussein-Al-Ali, S. H., Al-Qubaisi, M., Hussein, M. Z., Ismail, M., Zainal, Z., & Hakim, M. N. (2012). *International Journal of Molecular Sciences*, *13*(5), 5899-5916.
360) Fujishima, A., Rao, T. N., & Tryk, D. A. (2000). *Journal of photochemistry and photobiology C: Photochemistry reviews*, *1*(1), 1-21.

361) Rajeshwari, M. R., Subhiksha, V., Alahmadi, T. A., Ansari, M. J., Sillanpää, M., & Khan, S. S. (2024). *Journal of Alloys and Compounds*, *989*, 174283.
362) Sabariselvan, L., Syed, A., Steffy, J. P., Elgorban, A. M., Abid, I., Wong, L. S., & Khan, S. S. (2025). *Journal of Water Process Engineering*, *69*, 106761.
363) Kumar, S., Park, H. M., Singh, T., Kumar, M., & Seo, Y. (2023).*International Journal of Energy Research*, *2023*(1), 5275439.
364) Prasad, K. S., Shivamallu, C., Shruthi, G., & Prasad, M. (2018). *ChemistrySelect*, *3*(13), 3860-3865
365) Janani, B., Sre, V. V., Syed, A., Elgorban, A. M., Abid, I., Wong, L. S., & Khan, S. S. (2024). *Journal of Water Process Engineering*, *66*, 105986.
366) Swetha, S., Alahmadi, T. A., Ansari, M. J., & Khan, S. S. (2024). *Journal of Cleaner Production*, *449*, 141656
367) Bhardwaj, D., Sangwan, S., Shivashankar, S. A., & Umarji, A. M. (2022).. *Bulletin of Materials Science*, *45*(3), 135.
368) Tahir, T., Chaudhary, K., Warsi, M. F., Saif, M. S., Alsafari, I. A., Shakir, I., ... & Zulfiqar, S. (2022). *Ceramics International*, *48*(2), 1969-1980.
369) Dawood, S., Sen, T. K., & Phan, C. (2017). *Bioresource Technology*, *246*, 76-81.
370) Li, Y., Wang, F., Miao, Y., Mai, Y., Li, H., Chen, X., & Chen, J. (2020). *Bioresource technology*, *307*, 123165.
371) Yakout, S. M. (2015). *Bioremediation Journal*, *19*(2), 171-182.
372) Wu, W., Yang, M., Feng, Q., McGrouther, K., Wang, H., Lu, H., & Chen, Y. (2012). *Biomass and bioenergy*, *47*, 268-276.
373) Antil, B., Elkasabi, Y., Strahan, G. D., & Vander Wal, R. L. (2025). *Carbon*, *232*, 119770.
374) Kim, P., Johnson, A., Edmunds, C. W., Radosevich, M., Vogt, F., Rials, T. G., & Labbé, N. (2011). *Energy & fuels*, *25*(10), 4693-4703.
375) Khan, J., Ahmad, R. T. M., Yu, Q., Liu, H., Khan, U., & Liu, B. (2023). *Science and Technology of Advanced Materials*, *24*(1), 2242262.
376) Jahan, N., Hussain, S., Rahman, H. U., Manzoor, I., Pandey, S., Habib, K., ... & Upadhyay, C. (2021). *Journal of Multidisciplinary Applied Natural Science*, *1*(1).
377) Ridley, P., Gallano, C., Andris, R., Shuck, C. E., Gogotsi, Y., & Pomerantseva, E. (2020). *ACS Applied Energy Materials*, *3*(11), 10892-10901.
378) Xu, C., Rangaiah, G. P., & Zhao, X. S. (2014). *Industrial & Engineering Chemistry Research*, *53*(38), 14641-14649.
379) Herrmann, J. M. (1999). *Catalysis today*, *53*(1), 115-129.
380) Zhang, Y., Qu, M., Li, J., Ren, L., Wang, F., Wang, J., ... & Cheng, F. (2024). *Journal of Environmental Chemical Engineering*, *12*(6), 114571.
381) Arshad, A. H., Riaz, S., Hussain, M. D., Kumar, O. P., Ahmad, K., Najam, T., ... & Nazir, M. A. (2025). *Environmental Technology Reviews*, *14*(1), 142-190.
382) Li, Y., Wang, H., Pan, T., Zhong, T., Jiang, J., Wei, L., & Jin, P. (2024). *Coatings*, *14*(8), 1044.
383) Ghidiu, M., Naguib, M., & Barsoum, M. W. (2019). Cham: Springer International Publishing.
384) Karthikeyan, S., Parthibavarman, M., Mohammed, M. K., Mohammed, S. H., Selvapandiyan, M., & Srisuvetha, V. T. (2022). *Chemistry Africa*, *5*(5), 1427-1432.